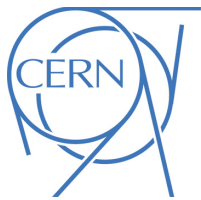


EUROPEAN ORGANISATION FOR NUCLEAR RESEARCH (CERN)



Submitted to: JHEP



CERN-EP-2016-087
3rd June 2016

Measurement of the angular coefficients in Z-boson events using electron and muon pairs from data taken at $\sqrt{s} = 8$ TeV with the ATLAS detector

The ATLAS Collaboration

Abstract

The angular distributions of Drell–Yan charged lepton pairs in the vicinity of the Z-boson mass peak probe the underlying QCD dynamics of Z-boson production. This paper presents a measurement of the complete set of angular coefficients A_{0-7} describing these distributions in the Z-boson Collins–Soper frame. The data analysed correspond to 20.3 fb^{-1} of pp collisions at $\sqrt{s} = 8$ TeV, collected by the ATLAS detector at the CERN LHC. The measurements are compared to the most precise fixed-order calculations currently available ($O(\alpha_s^2)$) and with theoretical predictions embedded in Monte Carlo generators. The measurements are precise enough to probe QCD corrections beyond the formal accuracy of these calculations and to provide discrimination between different parton-shower models. A significant deviation from the $O(\alpha_s^2)$ predictions is observed for $A_0 - A_2$. Evidence is found for non-zero $A_{5,6,7}$, consistent with expectations.

1. Introduction

The angular distributions of charged lepton pairs produced in hadron–hadron collisions via the Drell–Yan neutral current process provide a portal to precise measurements of the production dynamics through spin correlation effects between the initial-state partons and the final-state leptons mediated by a spin-1 intermediate state, predominantly the Z boson. In the Z -boson rest frame, a plane spanned by the directions of the incoming protons can be defined, e.g. using the Collins–Soper (CS) reference frame [1]. The lepton polar and azimuthal angular variables, denoted by $\cos \theta$ and ϕ in the following formalism, are defined in this reference frame. The spin correlations are described by a set of nine helicity density matrix elements, which can be calculated within the context of the parton model using perturbative quantum chromodynamics (QCD). The theoretical formalism is elaborated in Refs. [2–5].

The full five-dimensional differential cross-section describing the kinematics of the two Born-level leptons from the Z -boson decay can be decomposed as a sum of nine harmonic polynomials, which depend on $\cos \theta$ and ϕ , multiplied by corresponding helicity cross-sections that depend on the Z -boson transverse momentum (p_T^Z), rapidity (y^Z), and invariant mass (m^Z). It is a standard convention to factorise out the unpolarised cross-section, denoted in the literature by σ^{U+L} , and to present the five-dimensional differential cross-section as an expansion into nine harmonic polynomials $P_i(\cos \theta, \phi)$ and dimensionless angular coefficients $A_{0-7}(p_T^Z, y^Z, m^Z)$, which represent ratios of helicity cross-sections with respect to the unpolarised one, σ^{U+L} , as explained in detail in Appendix A:

$$\frac{d\sigma}{dp_T^Z dy^Z dm^Z d\cos \theta d\phi} = \frac{3}{16\pi} \frac{d\sigma^{U+L}}{dp_T^Z dy^Z dm^Z} \left\{ \begin{aligned} & (1 + \cos^2 \theta) + \frac{1}{2} A_0(1 - 3 \cos^2 \theta) + A_1 \sin 2\theta \cos \phi \\ & + \frac{1}{2} A_2 \sin^2 \theta \cos 2\phi + A_3 \sin \theta \cos \phi + A_4 \cos \theta \\ & + A_5 \sin^2 \theta \sin 2\phi + A_6 \sin 2\theta \sin \phi + A_7 \sin \theta \sin \phi \end{aligned} \right\}. \quad (1)$$

The dependence of the differential cross-section on $\cos \theta$ and ϕ is thus completely manifest analytically. In contrast, the dependence on p_T^Z , y^Z , and m^Z is entirely contained in the A_i coefficients and σ^{U+L} . Therefore, all hadronic dynamics from the production mechanism are described implicitly within the structure of the A_i coefficients, and are factorised from the decay kinematics in the Z -boson rest frame. This allows the measurement precision to be essentially insensitive to all uncertainties in QCD, quantum electrodynamics (QED), and electroweak (EW) effects related to Z -boson production and decay. In particular, EW corrections that couple the initial-state quarks to the final-state leptons have a negligible impact (below 0.05%) at the Z -boson pole. This has been shown for the LEP precision measurements [6, 7], when calculating the interference between initial-state and final-state QED radiation.

When integrating over $\cos \theta$ or ϕ , the information about the A_1 and A_6 coefficients is lost, so both angles must be explicitly used to extract the full set of eight coefficients. Integrating Eq. (1) over $\cos \theta$ yields:

$$\frac{d\sigma}{dp_T^Z dy^Z dm^Z d\phi} = \frac{1}{2\pi} \frac{d\sigma^{U+L}}{dp_T^Z dy^Z dm^Z} \left\{ 1 + \frac{1}{4} A_2 \cos 2\phi + \frac{3\pi}{16} A_3 \cos \phi + \frac{1}{2} A_5 \sin 2\phi + \frac{3\pi}{16} A_7 \sin \phi \right\}, \quad (2)$$

while integrating over ϕ yields:

$$\frac{d\sigma}{dp_T^Z dy^Z dm^Z d\cos\theta} = \frac{3}{8} \frac{d\sigma^{U+L}}{dp_T^Z dy^Z dm^Z} \left\{ (1 + \cos^2\theta) + \frac{1}{2} A_0(1 - 3\cos^2\theta) + A_4 \cos\theta \right\}. \quad (3)$$

At leading order (LO) in QCD, only the annihilation diagram $q\bar{q} \rightarrow Z$ is present and only A_4 is non-zero. At next-to-leading order (NLO) in QCD ($\mathcal{O}(\alpha_s)$), A_{0-3} also become non-zero. The Lam–Tung relation [8–10], which predicts that $A_0 - A_2 = 0$ due to the spin-1 of the gluon in the $qg \rightarrow Zq$ and $q\bar{q} \rightarrow Zg$ diagrams, is expected to hold up to $\mathcal{O}(\alpha_s)$, but can be violated at higher orders. The coefficients $A_{5,6,7}$ are expected to become non-zero, while remaining small, only at next-to-next-to-leading order (NNLO) in QCD ($\mathcal{O}(\alpha_s^2)$), because they arise from gluon loops that are included in the calculations [11, 12]. The coefficients A_3 and A_4 depend on the product of vector and axial couplings to quarks and leptons, and are sensitive to the Weinberg angle $\sin^2\theta_W$. The explicit formulae for these dependences can be found in Appendix A.

The full set of coefficients has been calculated for the first time at $\mathcal{O}(\alpha_s^2)$ in Refs. [2–5]. More recent discussions of these angular coefficients may be found in Ref. [13], where the predictions in the NNLOPS scheme of the PowHEG [14–17] event generator are shown for Z -boson production, and in Ref. [18], where the coefficients are explored in the context of W -boson production, for which the same formalism holds.

The CDF Collaboration at the Tevatron published [19] a measurement of some of the angular coefficients of lepton pairs produced near the Z -boson mass pole, using 2.1 fb^{-1} of proton–anti-proton collision data at a centre-of-mass energy $\sqrt{s} = 1.96 \text{ TeV}$. Since the measurement was performed only in projections of $\cos\theta$ and ϕ , the coefficients A_1 and A_6 were inaccessible. They further assumed A_5 and A_7 to be zero since the sensitivity to these coefficients was beyond the precision of the measurements; the coefficients $A_{0,2,3,4}$ were measured as a function of p_T^Z . These measurements were later used by CDF [20] to infer an indirect measurement of $\sin^2\theta_W$, or equivalently, the W -boson mass in the on-shell scheme, from the average A_4 coefficient. These first measurements of the angular coefficients demonstrated the potential of this not-yet-fully explored experimental avenue for investigating hard QCD and EW physics.

Measurements of the W -boson angular coefficients at the LHC were published by both ATLAS [21] and CMS [22]. More recently, a measurement of the Z -boson angular coefficients with $Z \rightarrow \mu\mu$ decays was published by CMS [23], where the first five coefficients were measured with 19.7 fb^{-1} of proton–proton (pp) collision data at $\sqrt{s} = 8 \text{ TeV}$. The measurement was performed in two y^Z bins, $0 < |y^Z| < 1$ and $1 < |y^Z| < 2.1$, each with eight bins in p_T^Z up to 300 GeV. The violation of the Lam–Tung relation was observed, as predicted by QCD calculations beyond NLO.

This paper presents an inclusive measurement of the full set of eight A_i coefficients using charged lepton pairs (electrons or muons), denoted hereafter by ℓ . The measurement is performed in the Z -boson invariant mass window of 80–100 GeV, as a function of p_T^Z , and also in three bins of y^Z . These results are based on 20.3 fb^{-1} of pp collision data collected at $\sqrt{s} = 8 \text{ TeV}$ by the ATLAS experiment [24] at the LHC. With the measurement techniques developed for this analysis, the complete set of coefficients is extracted with fine granularity over 23 bins of p_T^Z up to 600 GeV. The measurements, performed in the CS reference frame [1], are first presented as a function of p_T^Z , integrating over y^Z . Further measurements divided into three bins of y^Z are also presented: $0 < |y^Z| < 1$, $1 < |y^Z| < 2$, and $2 < |y^Z| < 3.5$. The $Z/\gamma^* \rightarrow e^+e^-$ and $Z/\gamma^* \rightarrow \mu^+\mu^-$ channels where both leptons fall within the pseudorapidity range $|\eta| < 2.4$ (hereafter referred to as the central–central or ee_{CC} and $\mu\mu_{CC}$ channels) are used for the y^Z -integrated measurement and the first two y^Z bins. The $Z/\gamma^* \rightarrow e^+e^-$ channel where one of the electrons instead falls in the region

$|\eta| > 2.5$ (referred to hereafter as the central-forward or ee_{CF} channel) is used to extend the measurement to the high- y^Z region encompassed by the third y^Z bin. In this case, however, because of the fewer events available for the measurement itself and to evaluate the backgrounds (see Section 4), the measurement is only performed for p_T^Z up to 100 GeV using projections of $\cos \theta$ and ϕ , making A_1 and A_6 inaccessible in the $2 < |y^Z| < 3.5$ bin.

The high granularity and precision of the specific measurements presented in this paper provide a stringent test of the most precise perturbative QCD predictions for Z -boson production in pp collisions and of Monte Carlo (MC) event generators used to simulate Z -boson production. This paper is organised as follows. Section 2 summarises the theoretical formalism used to extract the angular coefficients and presents the fixed-order QCD predictions for their variations as a function of p_T^Z . Section 3 describes briefly the ATLAS detector and the data and MC samples used in the analysis, while Section 4 presents the data analysis and background estimates for each of the three channels considered. Section 5 describes the fit methodology used to extract the angular coefficients in the full phase space as a function of p_T^Z and Section 6 gives an overview of the statistical and systematic uncertainties of the measurements. Sections 7 and 8 present the results and compare them to various predictions from theoretical calculations and MC event generators, and Section 9 summarises and concludes the paper.

2. Theoretical predictions

The differential cross-section in Eq. (1) is written for pure Z bosons, although it also holds for the contribution from γ^* and its interference with the Z boson. The tight invariant mass window of 80–100 GeV is chosen to minimise the γ^* contribution, although the predicted A_i coefficients presented in this paper are effective coefficients, containing this small contribution from γ^* . This contribution is not accounted for explicitly in the detailed formalism described in Appendix A, which is presented for simplicity for pure Z -boson production. Throughout this paper, the leptons from Z -boson decays are defined at the Born level, i.e. before final-state QED radiation, when discussing theoretical calculations or predictions at the event-generator level.

The p_T^Z and y^Z dependence of the coefficients varies strongly with the choice of spin quantisation axis in the Z -boson rest frame (z -axis). In the CS reference frame adopted for this paper, the z -axis is defined in the Z -boson rest frame as the external bisector of the angle between the momenta of the two protons, as depicted in Fig. 1. The positive direction of the z -axis is defined by the direction of positive longitudinal Z -boson momentum in the laboratory frame. To complete the coordinate system, the y -axis is defined as the normal vector to the plane spanned by the two incoming proton momenta and the x -axis is chosen to define a right-handed Cartesian coordinate system with the other two axes. Polar and azimuthal angles are calculated with respect to the negatively charged lepton and are labelled θ_{CS} and ϕ_{CS} , respectively. In the case where $p_T^Z = 0$, the direction of the y -axis and the definition of ϕ_{CS} are arbitrary. Historically, there has been an ambiguity in the definition of the sign of the ϕ_{CS} angle in the CS frame: this paper adopts the recent convention followed by Refs. [13, 23], whereby the coefficients A_1 and A_3 are positive.

The coefficients are not explicitly used as input to the theoretical calculations nor in the MC event generators. They can, however, be extracted from the shapes of the angular distributions with the method proposed in Ref. [3], owing to the orthogonality of the P_i polynomials. The weighted average of the angular distributions with respect to any specific polynomial isolates an average reference value or moment

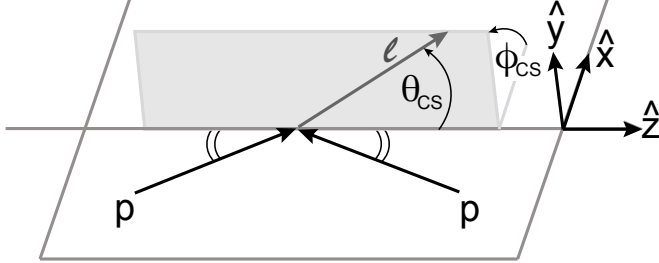


Figure 1: Sketch of the Collins-Soper reference frame, in which the angles θ_{CS} and ϕ_{CS} are defined with respect to the negatively charged lepton ℓ (see text). The notations \hat{x} , \hat{y} and \hat{z} denote the unit vectors along the corresponding axes in this reference frame.

of its corresponding coefficient. The moment of a polynomial $P(\cos \theta, \phi)$ over a specific range of p_T^Z , y^Z , and m^Z is defined to be:

$$\langle P(\cos \theta, \phi) \rangle = \frac{\int P(\cos \theta, \phi) d\sigma(\cos \theta, \phi) d\cos \theta d\phi}{\int d\sigma(\cos \theta, \phi) d\cos \theta d\phi}. \quad (4)$$

The moment of each harmonic polynomial can thus be expressed as (see Eq. (1)):

$$\begin{aligned} \langle \frac{1}{2}(1 - 3 \cos^2 \theta) \rangle &= \frac{3}{20}(A_0 - \frac{2}{3}); & \langle \sin 2\theta \cos \phi \rangle &= \frac{1}{5}A_1; & \langle \sin^2 \theta \cos 2\phi \rangle &= \frac{1}{10}A_2; \\ \langle \sin \theta \cos \phi \rangle &= \frac{1}{4}A_3; & \langle \cos \theta \rangle &= \frac{1}{4}A_4; & \langle \sin^2 \theta \sin 2\phi \rangle &= \frac{1}{5}A_5; \\ \langle \sin 2\theta \sin \phi \rangle &= \frac{1}{5}A_6; & \langle \sin \theta \sin \phi \rangle &= \frac{1}{4}A_7. \end{aligned} \quad (5)$$

One thus obtains a representation of the effective angular coefficients for Z/γ^* production. These effective angular coefficients display in certain cases a dependence on y^Z , which arises mostly from the fact that the interacting quark direction is unknown on an event-by-event basis. As the method of Ref. [3] relies on integration over the full phase space of the angular distributions, it cannot be applied directly to data, but is used to compute all the theoretical predictions shown in this paper.

The inclusive fixed-order perturbative QCD predictions for Z -boson production at NLO and NNLO were obtained with DYNNLO v1.3 [25]. These inclusive calculations are formally accurate to $\mathcal{O}(\alpha_s^2)$. The Z -boson is produced, however, at non-zero transverse momentum only at $\mathcal{O}(\alpha_s)$, and therefore the calculation of the coefficients as a function of p_T^Z is only NLO. Even though the fixed-order calculations do not provide reliable absolute predictions for the p_T^Z spectrum at low values, they can be used for $p_T^Z > 2.5$ GeV for the angular coefficients. The results were cross-checked with NNLO predictions from FEWZ v3.1.b2 [26–28] and agreement between the two programs was found within uncertainties. The

renormalisation and factorisation scales in the calculations were set to $E_T^Z = \sqrt{(m^Z)^2 + (p_T^Z)^2}$ [29] on an event-by-event basis. The calculations were done using the CT10 NLO or NNLO parton distribution functions (PDFs) [30], depending on the order of the prediction.

The NLO EW corrections affect mostly the leading-order QCD cross-section normalisation in the Z -pole region and have some impact on the p_T^Z distribution, but they do not affect the angular correlations at the Z -boson vertex. The DYNNLO calculation was done at leading order in EW, using the G_μ scheme [31]. This choice determines the value of A_4 at low p_T^Z , and for the purpose of the comparisons presented in this paper, both A_3 and A_4 obtained from DYNNLO are rescaled to the values predicted when using the measured value of $\sin^2 \theta_W^{\text{eff}} = 0.23113$ [32].

The theoretical predictions are shown in Fig. 2 and tabulated in Table 1 for three illustrative p_T^Z bins. The binning in p_T^Z is chosen based on the experimental resolution at low p_T^Z and on the number of events at high p_T^Z and has the following boundaries (in GeV) used consistently throughout the measurement:

$$p_T^{Z,\text{boundary}}[\text{GeV}] = \{0, 2.5, 5.0, 8.0, 11.4, 14.9, 18.5, 22.0, \\ 25.5, 29.0, 32.6, 36.4, 40.4, 44.9, 50.2, 56.4, \\ 63.9, 73.4, 85.4, 105.0, 132.0, 173.0, 253.0, 600.0\}. \quad (6)$$

The predictions show the following general features. The A_0 and A_2 coefficients increase as a function of p_T^Z and the deviations from lowest-order expectations are quite large, even at modest values of $p_T^Z = 20\text{--}50\text{ GeV}$. The A_1 and A_3 coefficients are relatively small even at large p_T^Z , with a maximum value of 0.08. In the limit where $p_T^Z = 0$, all coefficients except A_4 are expected to vanish at NLO. The NNLO corrections are typically small for all coefficients except A_2 , for which the largest correction has a value of -0.08 , in agreement with the original theoretical studies [2]. The theoretical predictions for $A_{5,6,7}$ are not shown because these coefficients are expected to be very small at all values of p_T^Z : they are zero at NLO and the NNLO contribution is large enough to be observable, namely of the order of 0.005 for values of p_T^Z in the range 20–200 GeV.

The statistical uncertainties of the calculations, as well as the factorisation and renormalisation scale and PDF uncertainties, were all considered as sources of theoretical uncertainties. The statistical uncertainties of the NLO and NNLO predictions in absolute units are typically 0.0003 and 0.003, respectively. The larger statistical uncertainties of the NNLO predictions are due to the longer computational time required than for the NLO predictions. The scale uncertainties were estimated by varying the renormalisation and factorisation scales simultaneously up and down by a factor of two. As stated in Ref. [2], the theoretical uncertainties due to the choice of these scales are very small for the angular coefficients because they are ratios of cross-sections. The resulting variations of the coefficients at NNLO were found in most cases to be comparable to the statistical uncertainty. The PDF uncertainties were estimated using the CT10 NNLO eigenvector variations, as obtained from FEWZ and normalised to 68% confidence level. They were found to be small compared to the NNLO statistical uncertainty, namely of the order of 0.001 for A_{0-3} and 0.002 for A_4 .

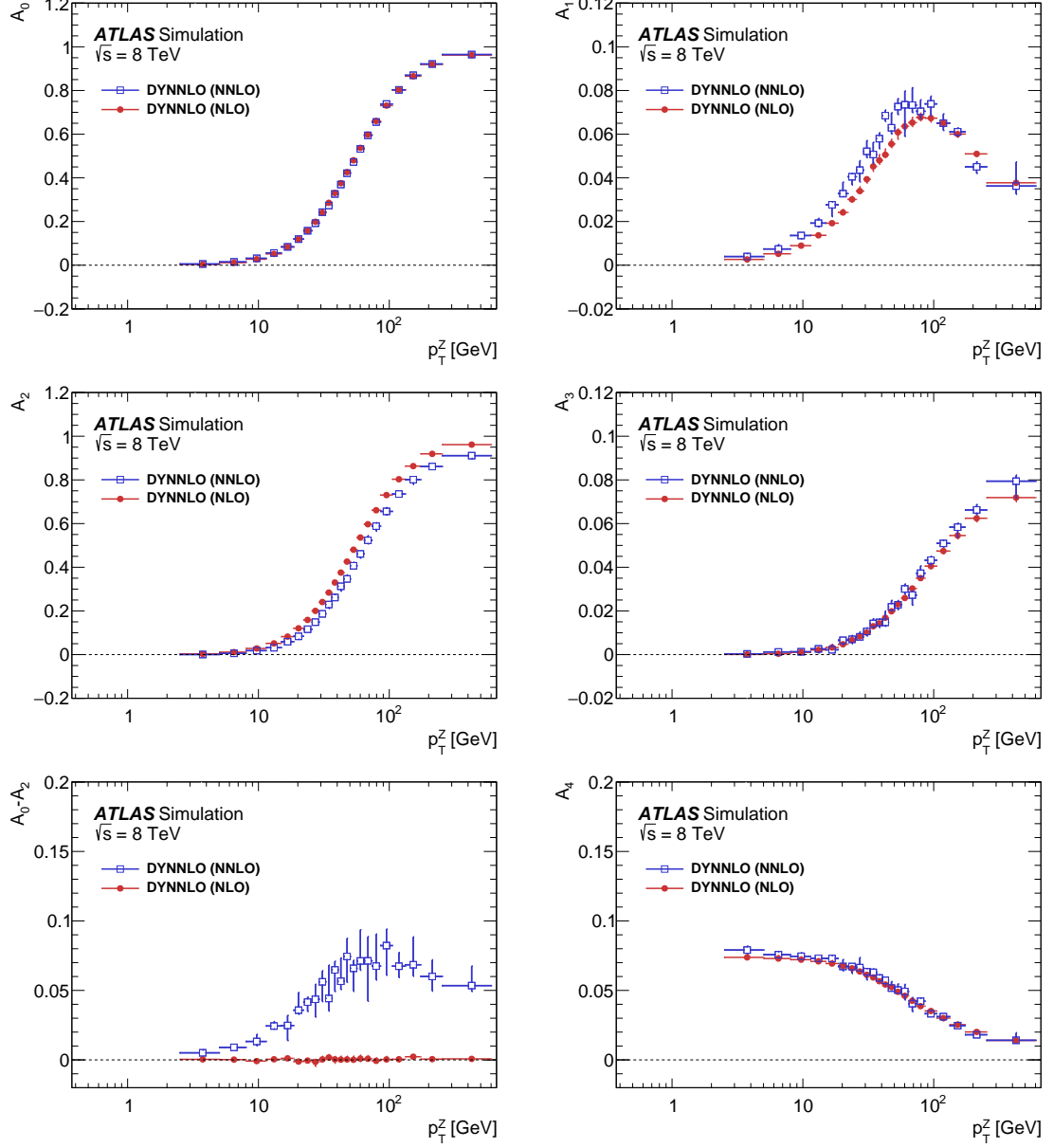


Figure 2: The angular coefficients A_{0-4} and the difference $A_0 - A_2$, shown as a function of p_T^z , as predicted from DYNNNLO calculations at NLO and NNLO in QCD. The NLO predictions for $A_0 - A_2$ are compatible with zero, as expected from the Lam–Tung relation [8–10]. The error bars show the total uncertainty of the predictions, including contributions from statistical uncertainties, QCD scale variations and PDFs. The statistical uncertainties of the NNLO predictions are dominant and an order of magnitude larger than those of the NLO predictions.

Table 1: Summary of predictions from DYNNLO at NLO and NNLO for A_0 , A_2 , $A_0 - A_2$, A_1 , A_3 , A_4 , A_5 , A_6 , and A_7 at low (5–8 GeV), mid (22–25.5 GeV), and high (132–173 GeV) p_T^Z for the y^Z -integrated configuration. The uncertainty represents the sum of statistical and systematic uncertainties.

	$p_T^Z = 5 - 8 \text{ GeV}$		$p_T^Z = 22 - 25.5 \text{ GeV}$		$p_T^Z = 132 - 173 \text{ GeV}$	
	NLO	NNLO	NLO	NNLO	NLO	NNLO
A_0	$0.0115^{+0.0006}_{-0.0003}$	$0.0150^{+0.0006}_{-0.0008}$	$0.1583^{+0.0008}_{-0.0009}$	$0.1577^{+0.0041}_{-0.0018}$	$0.8655^{+0.0008}_{-0.0006}$	$0.8697^{+0.0017}_{-0.0023}$
A_2	$0.0113^{+0.0004}_{-0.0004}$	$0.0060^{+0.0010}_{-0.0017}$	$0.1588^{+0.0014}_{-0.0009}$	$0.1161^{+0.0092}_{-0.0028}$	$0.8632^{+0.0013}_{-0.0009}$	$0.8012^{+0.0073}_{-0.0215}$
$A_0 - A_2$	$0.0002^{+0.0007}_{-0.0005}$	$0.0090^{+0.0014}_{-0.0013}$	$-0.0005^{+0.0016}_{-0.0012}$	$0.0416^{+0.0036}_{-0.0067}$	$0.0023^{+0.0015}_{-0.0011}$	$0.0685^{+0.0200}_{-0.0082}$
A_1	$0.0052^{+0.0004}_{-0.0003}$	$0.0074^{+0.0020}_{-0.0008}$	$0.0301^{+0.0013}_{-0.0013}$	$0.0405^{+0.0014}_{-0.0038}$	$0.0600^{+0.0013}_{-0.0015}$	$0.0611^{+0.0018}_{-0.0023}$
A_3	$0.0004^{+0.0002}_{-0.0001}$	$0.0012^{+0.0003}_{-0.0006}$	$0.0066^{+0.0003}_{-0.0005}$	$0.0070^{+0.0017}_{-0.0020}$	$0.0545^{+0.0003}_{-0.0016}$	$0.0584^{+0.0018}_{-0.0047}$
A_4	$0.0729^{+0.0023}_{-0.0006}$	$0.0757^{+0.0021}_{-0.0025}$	$0.0659^{+0.0019}_{-0.0003}$	$0.0672^{+0.0018}_{-0.0050}$	$0.0253^{+0.0007}_{-0.0002}$	$0.0247^{+0.0024}_{-0.0018}$
A_5	$0.0001^{+0.0002}_{-0.0002}$	$0.0001^{+0.0007}_{-0.0007}$	< 0.0001	$0.0011^{+0.0013}_{-0.0030}$	$-0.0004^{+0.0005}_{-0.0005}$	$0.0044^{+0.0042}_{-0.0026}$
A_6	$-0.0002^{+0.0002}_{-0.0003}$	$0.0013^{+0.0006}_{-0.0005}$	$0.0004^{+0.0006}_{-0.0004}$	$0.0017^{+0.0043}_{-0.0015}$	$0.0003^{+0.0003}_{-0.0006}$	$0.0028^{+0.0017}_{-0.0018}$
A_7	< 0.0001	$0.0014^{+0.0007}_{-0.0004}$	$0.0002^{+0.0003}_{-0.0007}$	$0.0024^{+0.0013}_{-0.0013}$	$0.0003^{+0.0004}_{-0.0007}$	$0.0048^{+0.0027}_{-0.0012}$

3. The ATLAS experiment and its data and Monte Carlo samples

3.1. ATLAS detector

The ATLAS experiment [24] at the LHC is a multi-purpose particle detector with a forward-backward symmetric cylindrical geometry and a near 4π coverage in solid angle.¹ It consists of an inner tracking detector, electromagnetic (EM) and hadronic calorimeters, and a muon spectrometer. The inner tracker provides precision tracking of charged particles in the pseudorapidity range $|\eta| < 2.5$. This region is matched to a high-granularity EM sampling calorimeter covering the pseudorapidity range $|\eta| < 3.2$ and a coarser granularity calorimeter up to $|\eta| = 4.9$. A hadronic calorimeter system covers the entire pseudorapidity range up to $|\eta| = 4.9$. The muon spectrometer provides triggering and tracking capabilities in the range $|\eta| < 2.4$ and $|\eta| < 2.7$, respectively. A first-level trigger is implemented in hardware, followed by two software-based trigger levels that together reduce the accepted event rate to 400 Hz on average. For this paper, a central lepton is one found in the region $|\eta| < 2.4$ (excluding, for electrons, the electromagnetic calorimeter barrel/end-cap transition region $1.37 < |\eta| < 1.52$), while a forward electron is one found in the region $2.5 < |\eta| < 4.9$ (excluding the transition region $3.16 < |\eta| < 3.35$ between the electromagnetic end-cap and forward calorimeters).

¹ ATLAS uses a right-handed coordinate system with its origin at the nominal interaction point (IP) in the centre of the detector and the z -axis along the beam pipe. The x -axis points from the IP to the centre of the LHC ring, and the y -axis points upwards. Cylindrical coordinates (r, ϕ) are used in the transverse plane, ϕ being the azimuthal angle around the z -axis. The pseudorapidity is defined in terms of the polar angle θ as $\eta = -\ln \tan(\theta/2)$. Angular distance is measured in units of $\Delta R \equiv \sqrt{(\Delta\eta)^2 + (\Delta\phi)^2}$.

3.2. Data and Monte Carlo samples

The data were collected by the ATLAS detector in 2012 at a centre-of-mass energy of $\sqrt{s} = 8$ TeV, and correspond to an integrated luminosity of 20.3 fb^{-1} . The mean number of additional pp interactions per bunch crossing (pile-up events) in the data set is approximately 20.

The simulation samples used in the analysis are shown in Table 2. The four event generators used to produce the $Z/\gamma^* \rightarrow \ell\ell$ signal events are listed in Table 2. The baseline PowHEGBox (v1/r2129) sample [14–17], which uses the CT10 NLO set of PDFs [33], is interfaced to PYTHIA 8 (v.8.170) [34] with the AU2 set of tuned parameters [35] to simulate the parton shower, hadronisation and underlying event, and to PHOTOS (v2.154) [36] to simulate QED final-state radiation (FSR) in the Z -boson decay. The alternative signal samples are from PowHEGBox interfaced to HERWIG (v.6.520.2) [37] for the parton shower and hadronisation, JIMMY (v4.31) [38] for the underlying event, and Photos for FSR. The SHERPA (v.1.4.1) [39–42] generator is also used, and has its own implementation of the parton shower, hadronisation, underlying event and FSR, and uses the CT10 NLO PDF set. These alternative samples are used to test the dependence of the analysis on different matrix-element calculations and parton-shower models, as discussed in Section 6. The PowHEG (v2.1) + MiNLO event generator [43] was used for the Z +jet process at NLO to normalise certain reference coefficients for the ee_{CF} analysis, as described in Section 5. The number of events available in the baseline PowHEGBox + PYTHIA 8 signal sample corresponds to approximately 4 (25) times that in the data below (above) $p_T^Z = 105$ GeV.

Backgrounds from EW (diboson and $\gamma\gamma \rightarrow \ell\ell$ production) and top-quark (production of top-quark pairs and of single top quarks) processes are evaluated from the MC samples listed in Table 2. The $W + \text{jets}$ contribution to the background is instead included in the data-driven multijet background estimate, as described in Section 4; W -boson samples listed in Table 2 are thus only used for studies of the background composition.

All of the samples are processed with the GEANT4-based simulation [44] of the ATLAS detector [45]. The effects of additional pp collisions in the same or nearby bunch crossings are simulated by the addition of so-called minimum-bias events generated with PYTHIA 8.

4. Data analysis

4.1. Event selection

As mentioned in Sections 1 and 3, the data are split into three orthogonal channels, namely the ee_{CC} channel with two central electrons, the $\mu\mu_{CC}$ channel with two central muons, and the ee_{CF} channel with one central electron and one forward electron. Selected events are required to be in a data-taking period in which the beams were stable and the detector was functioning well, and to contain a reconstructed primary vertex with at least three tracks with $p_T > 0.4$ GeV.

Candidate ee_{CC} events are obtained using a dielectron trigger requiring two electron candidates with $p_T > 12$ GeV, combined with high- p_T single-electron triggers. Electron candidates are required to have $p_T > 25$ GeV and are reconstructed from clusters of energy in the electromagnetic calorimeter matched to inner detector tracks. The electron candidates must satisfy a set of “medium” selection criteria [50, 51], which have been optimised for the level of pile-up present in the 2012 data. Events are required to contain exactly two electron candidates of opposite charge satisfying the above criteria.

Table 2: MC samples used to estimate the signal and backgrounds in the analysis.

Signature	Generator	PDF	Refs.
$Z/\gamma^* \rightarrow \ell\ell$	POWHEGBOX + PYTHIA 8	CT10 NLO	[14–17, 33, 34]
$Z/\gamma^* \rightarrow \ell\ell$	POWHEGBOX + JIMMY/HERWIG	CT10 NLO	[37]
$Z/\gamma^* \rightarrow \ell\ell$	SHERPA	CT10 NLO	[39–42]
$Z/\gamma^* \rightarrow \ell\ell + \text{jet}$	POWHEG + MiNLO	CT10 NLO	[43]
$W \rightarrow \ell\nu$	POWHEGBOX + PYTHIA 8	CT10 NLO	
$W \rightarrow \ell\nu$	SHERPA	CT10 NLO	
$t\bar{t}$ pair	MC@NLO + JIMMY/HERWIG	CT10 NLO	[38, 46]
Single top quark:			
t channel	ACERMC + PYTHIA 6	CTEQ6L1	[47, 48]
s and Wt channels	MC@NLO + JIMMY/HERWIG	CT10 NLO	
Dibosons	SHERPA	CT10 NLO	
Dibosons	HERWIG	CTEQ6L1	
$\gamma\gamma \rightarrow \ell\ell$	PYTHIA 8	MRST2004QED NLO	[49]

Candidate $\mu\mu_{\text{CC}}$ events are retained for analysis using a dimuon trigger requiring two muon candidates with $p_{\text{T}} > 18$ GeV and 8 GeV, respectively, combined with single high- p_{T} muon triggers. Muon candidates are required to have $p_{\text{T}} > 25$ GeV and are identified as tracks in the inner detector which are matched and combined with track segments in the muon spectrometer [52]. Track-quality and longitudinal and transverse impact-parameter requirements are imposed for muon identification to suppress backgrounds, and to ensure that the muon candidates originate from a common primary pp interaction vertex. Events are required to contain exactly two muon candidates of opposite charge satisfying the above criteria.

Candidate ee_{CF} events are obtained using a single-electron trigger, requiring an isolated central electron candidate with $p_{\text{T}} > 24$ GeV, combined with a looser high- p_{T} single-electron trigger. The central electron candidate is required to have $p_{\text{T}} > 25$ GeV. Because the expected background from multijet events is larger in this channel than in the ee_{CC} channel, the central electron candidate is required to satisfy a set of “tight” selection criteria [50], which are optimised for the level of pile-up observed in the 2012 data. The forward electron candidate is required to have $p_{\text{T}} > 20$ GeV and to satisfy a set of “medium” selection criteria, based only on the shower shapes in the electromagnetic calorimeter [50] since this region is outside the acceptance of the inner tracker. Events are required to contain exactly two electron candidates satisfying the above criteria.

Since this analysis is focused on the Z -boson pole region, the lepton pair is required to have an invariant mass ($m^{\ell\ell}$) within a narrow window around the Z -boson mass, $80 < m^{\ell\ell} < 100$ GeV. Events are selected for y^Z -integrated measurements without any requirements on the rapidity of the lepton pair ($y^{\ell\ell}$). For the y^Z -binned measurements, events are selected in three bins of rapidity: $|y^{\ell\ell}| < 1.0$, $1.0 < |y^{\ell\ell}| < 2.0$, and $2.0 < |y^{\ell\ell}| < 3.5$. Events are also required to have a dilepton transverse momentum ($p_{\text{T}}^{\ell\ell}$) less than the value of 600 (100) GeV used for the highest bin in the ee_{CC} and $\mu\mu_{\text{CC}}$ (ee_{CF}) channels. The variables $m^{\ell\ell}$, $y^{\ell\ell}$, and $p_{\text{T}}^{\ell\ell}$, which are defined using reconstructed lepton pairs, are to be distinguished from the variables m^Z , y^Z , and p_{T}^Z , which are defined using lepton pairs at the Born level, as described in Section 2.

The simulated events are required to satisfy the same selection criteria, after applying small corrections to account for the differences between data and simulation in terms of reconstruction, identification and trigger efficiencies and of energy scale and resolution for electrons and muons [50–53]. All simulated

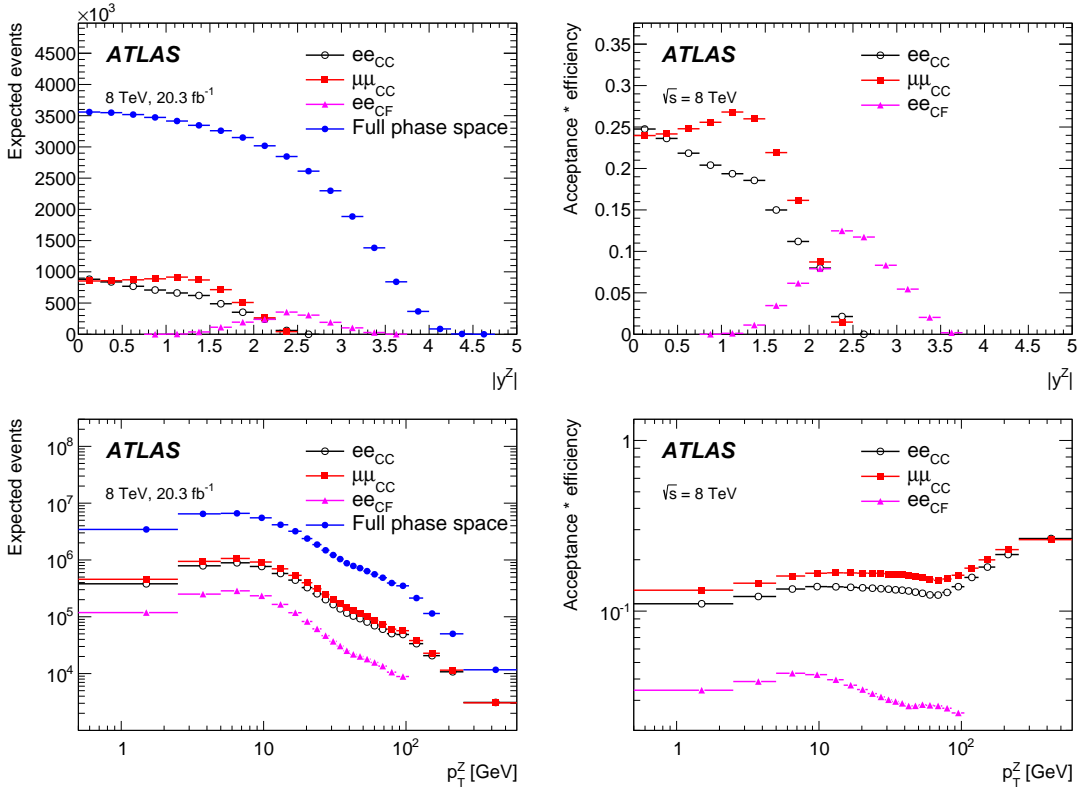


Figure 3: Comparison of the expected yields (left) and acceptance times efficiency of selected events (right) as a function of y^Z (top) and p_T^Z (bottom), for the ee_{CC} , $\mu\mu_{CC}$, and ee_{CF} events. Also shown are the expected yields at the event generator level over the full phase space considered for the measurement, which corresponds to all events with a dilepton mass in the chosen window, $80 < m^Z < 100$ GeV.

events are reweighted to match the distributions observed in data for the level of pile-up and for the primary vertex longitudinal position.

Figure 3 illustrates the different ranges in p_T^Z and y^Z expected to be covered by the three channels along with their acceptance times selection efficiencies, which is defined as the ratio of the number of selected events to the number in the full phase space. The difference in shape between the ee_{CC} and $\mu\mu_{CC}$ channels arises from the lower reconstruction and identification efficiency for central electrons at high values of $|\eta|$ and from the lower trigger and reconstruction efficiency for muons at low values of $|\eta|$. The central–central and central–forward channels overlap in the region $1.5 < |y^Z| < 2.5$.

4.2. Backgrounds

In the Z-boson pole region, the backgrounds from other processes are small, below the half-percent level for the ee_{CC} and $\mu\mu_{CC}$ channels and at the level of 2% for the ee_{CF} channel. The backgrounds from prompt isolated lepton pairs are estimated using simulated samples, as described in Section 3, and consist predominantly of lepton pairs from top-quark processes and from diboson production with a smaller contribution from $Z \rightarrow \tau\tau$ decays. The other background source arises from events in which at least one of the lepton candidates is not a prompt isolated lepton but rather a lepton from heavy-flavour hadron

Table 3: For each of the three channels, yield of events observed in data and expected background yields (multijets, top+electroweak, and total) corresponding to the 2012 data set and an integrated luminosity of 20.3 fb^{-1} . The uncertainties quoted include both the statistical and systematic components (see text).

Channel	Observed	Expected background		
		Multijets (from data)	Top+electroweak (from MC)	Total
ee_{CC}	5.5×10^6	6000 ± 3000	13000 ± 3000	19000 ± 4000
$\mu\mu_{\text{CC}}$	7.0×10^6	9000 ± 4000	19000 ± 4000	28000 ± 6000
ee_{CF}	1.5×10^6	28000 ± 14000	1000 ± 200	29000 ± 14000

decay (beauty or charm) or a fake lepton in the case of electron candidates (these may arise from charged hadrons or from photon conversions within a hadronic jet). This background consists of events containing two such leptons (multijets) or one such lepton ($W + \text{jets}$ or top-quark pairs) and is estimated from data using the lepton isolation as a discriminating variable, a procedure described for example in Ref. [50] for electrons. For the central–central channels, the background determination is carried out in the full two-dimensional space of $(\cos \theta_{\text{CS}}, \phi_{\text{CS}})$ and in each bin of $p_T^{\ell\ell}$. In the case of the central–forward channel, the multijet background, which is by far the dominant one, is estimated separately for each projection in $\cos \theta_{\text{CS}}$ and ϕ_{CS} because of the limited amount of data. This is the main reason why the angular coefficients in the central–forward channel are extracted only in projections, as described in Section 1.

Figure 4 shows the angular distributions, $\cos \theta_{\text{CS}}$ and ϕ_{CS} , for the three channels for the data, the Z -boson signal MC sample, and the main sources of background discussed above. The total background in the central–central events is below 0.5% and its uncertainty is dominated by the large uncertainty in the multijet background of approximately 50%. The uncertainty in the top+electroweak background is taken conservatively to be 20%. In the case of the central–forward electron pairs, the top+electroweak background is so small compared to the much larger multijet background that it is neglected for simplicity in the fit procedure described in Section 5. Table 3 summarises the observed yields of events in data for each channel, integrated over all values of $p_T^{\ell\ell}$, together with the expected background yields with their total uncertainties from multijet events and from top+electroweak sources. More details of the treatment of the background uncertainties are discussed in Section 6.

There are also signal events that are considered as background to the measurement because they are present in the data only due to the finite resolution of the measurements, which leads to migrations in mass and rapidity. These are denoted “Non-fiducial Z ” events and can be divided into four categories: the dominant fraction consists of events that have m^Z at the generator level outside the chosen $m^{\ell\ell}$ mass window but pass event selection, while another contribution arises from events that do not belong to the y^Z bin considered for the measurement at generator level. The latter contribution is sizeable only in the ee_{CF} channel. Other negligible sources of this type of background arise from events for which the central electron has the wrong assigned charge in the ee_{CF} channel or both central electrons have the wrong assigned charge in the ee_{CC} channel, or for which p_T^Z at the generator level is larger than 600 GeV. These backgrounds are all included as a small component of the signal MC sample in Fig. 4. Their contributions amount to one percent or less for the ee_{CC} and $\mu\mu_{\text{CC}}$ channels, increasing to almost 8% for the ee_{CF} channel because of the much larger migrations in energy measurements in the case of forward electrons. For the $2 < |y^Z| < 3.5$ bin in the ee_{CF} channel, the y^Z migration contributes 2% to the non-fiducial Z background. The fractional contribution of all backgrounds to the total sample is shown explicitly for each channel as a function of $p_T^{\ell\ell}$ in Fig. 5 together with the respective contributions of the multijet and

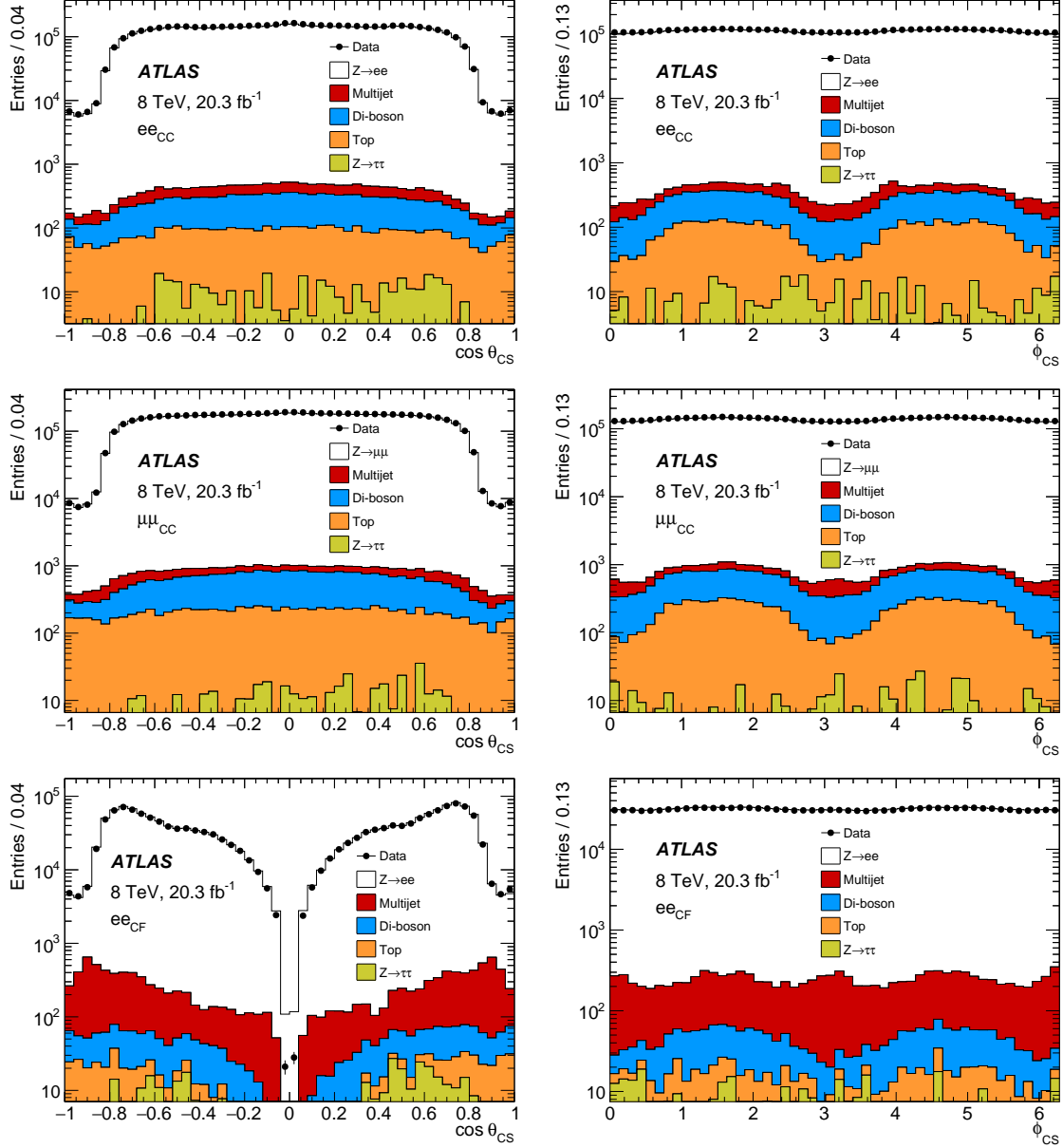


Figure 4: The $\cos \theta_{CS}$ (left) and ϕ_{CS} (right) angular distributions, averaged over all Z -boson p_T , for the ee_{CC} (top), $\mu\mu_{CC}$ (middle) and ee_{CF} (bottom) channels. The distributions are shown separately for the different background sources contributing to each channel. The multijet background is determined from data, as explained in the text.

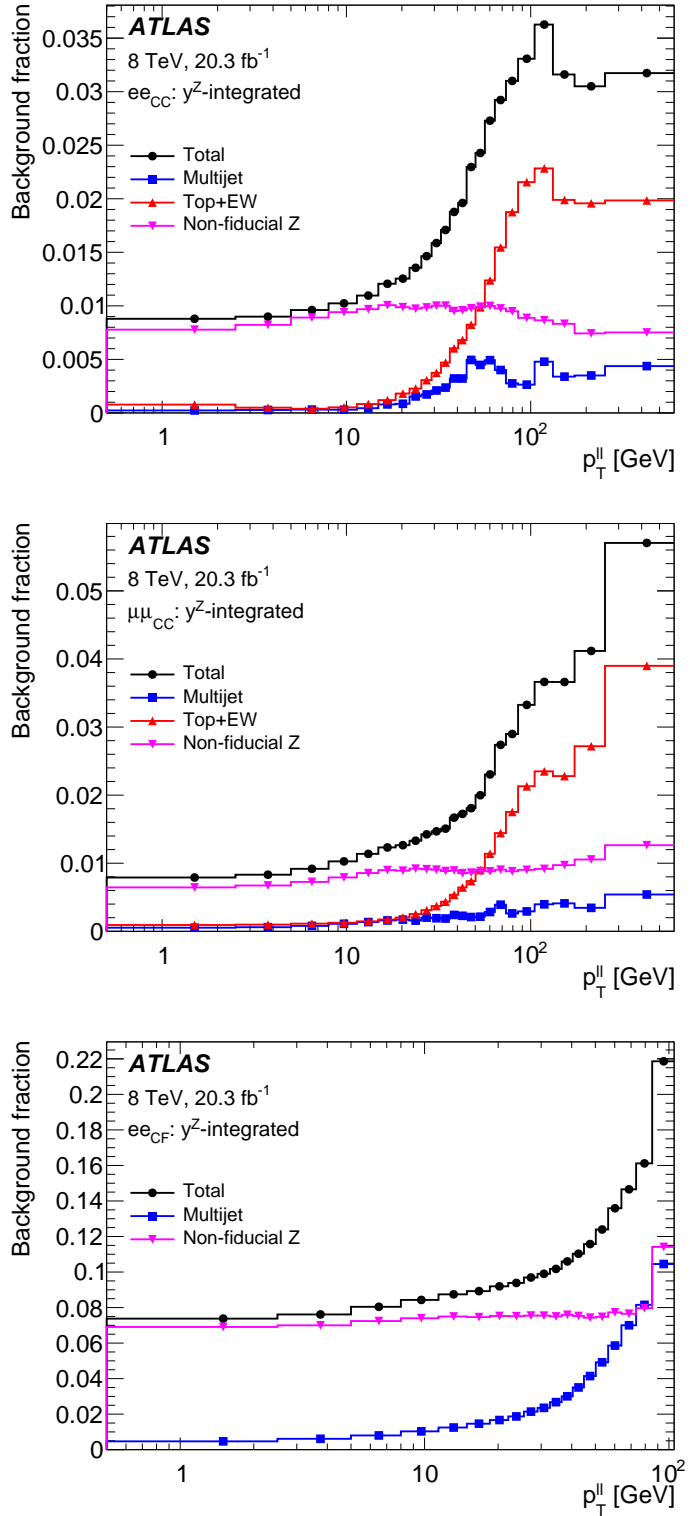


Figure 5: Fractional background contributions as a function of $p_T^{\ell\ell}$, for the ee_{CC} (top), $\mu\mu_{CC}$ (middle) and ee_{CF} (bottom) channels. The distributions are shown separately for the relevant background contributions to each channel together with the summed total background fraction. The label ‘Non-fiducial Z’ refers to signal events which are generated outside the phase space used to extract the angular coefficients (see text).

top+electroweak backgrounds. The sum of all these backgrounds is also shown and templates of their angular distributions are used in the fit to extract the angular coefficients, as described in Section 5.

4.3. Angular distributions

The measurement of the angular coefficients is performed in fine bins of p_T^Z and for a fixed dilepton mass window on the same sample as that used to extract from data the small corrections applied to the lepton efficiencies and calibration. The analysis is thus largely insensitive to the shape of the distribution of p_T^Z , and also to any residual differences in the modelling of the shape of the dilepton mass distribution. It is, however, important to verify qualitatively the level of agreement between data and MC simulation for the $\cos \theta_{\text{CS}}$ and ϕ_{CS} angular distributions before extracting the results of the measurement. This is shown for the three channels separately in Fig. 6, together with the ratio of the observed data to the sum of predicted events. The data and MC distributions are not normalised to each other, resulting in normalisation differences at the level of a few percent. The measurement of the angular coefficients is, however, independent of the normalisation between data and simulation in each bin of p_T^Z . The differences in shape in the angular distributions reflect the mismodelling of the angular coefficients in the simulation (see Section 7).

5. Coefficient measurement methodology

The coefficients are extracted from the data by fitting templates of the P_i polynomial terms, defined in Eq. (1), to the reconstructed angular distributions. Each template is normalised by free parameters for its corresponding coefficient A_i , as well as an additional common parameter representing the unpolarised cross-section. All of these parameters are defined independently in each bin of p_T^Z . The polynomial $P_8 = 1 + \cos^2 \theta_{\text{CS}}$ in Eq. (1) is only normalised by the parameter for the unpolarised cross-section.

In the absence of selections for the final-state leptons, the angular distributions in the gauge-boson rest frame are determined by the gauge-boson polarisation. In the presence of selection criteria for the leptons, the distributions are sculpted by kinematic effects, and can no longer be described by the sum of the nine P_i polynomials as in Eq. (1). Templates of the P_i terms are constructed in a way to account for this, which requires fully simulated signal MC to model the acceptance, efficiency, and migration of events. This process is described in Section 5.1. Section 5.2 then describes the likelihood that is built out of the templates and maximised to obtain the measured coefficients. The methodology for obtaining uncertainties in the measured parameters is also covered there. The procedure for combining multiple channels is covered in Section 5.3, along with alternative coefficient parameterisations used in various tests of measurement results from different channels.

5.1. Templates

To build the templates of the P_i polynomials, the reference coefficients A_i^{ref} for the signal MC sample are first calculated with the moments method, as described in Section 2 and Eq. (5). These are obtained in each of the 23 p_T^Z bins in Eq. (6), and also in each of the three y^Z bins for the y^Z -binned measurements. The information about the angular coefficients in the simulation is then available through the corresponding functional form of Eq. (1). Next, the MC event weights are divided by the value of this function

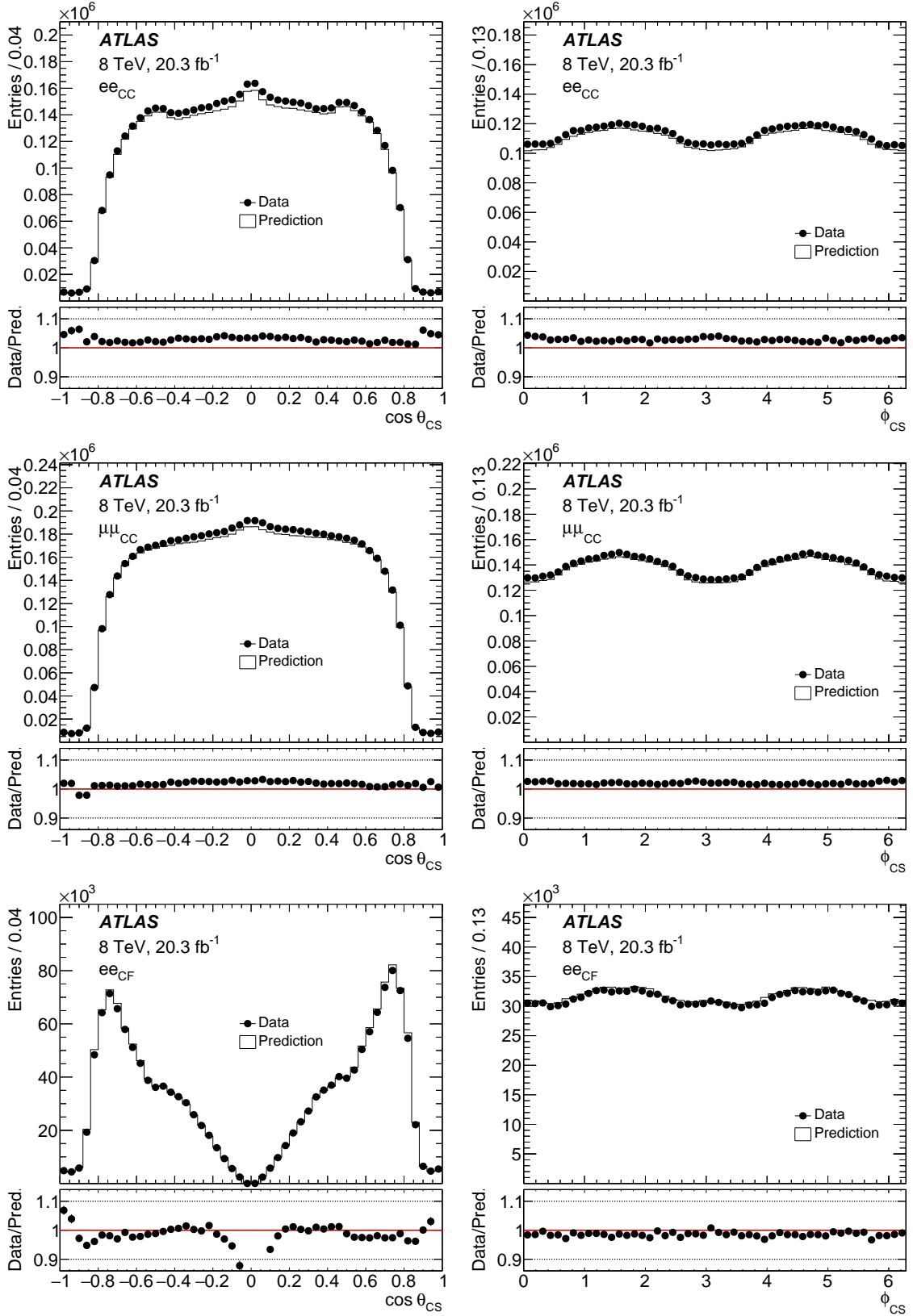


Figure 6: The $\cos \theta_{\text{CS}}$ (left) and ϕ_{CS} (right) angular distributions, averaged over all $p_T^{\ell\ell}$, for the ee_{CC} (top), $\mu\mu_{\text{CC}}$ (middle) and ee_{CF} (bottom) channels. In the panels showing the ratios of the data to the summed signal+background predictions, the uncertainty bars on the points are only statistical.

on an event-by-event basis. When the MC events are weighted in this way, the angular distributions in the full phase space at the event generator level are flat. Effectively, all information about the Z-boson polarisation is removed from the MC sample, so that further weighting the events by any of the P_i terms yields the shape of the polynomial itself, and if selection requirements are applied, this yields the shape of the selection efficiency. The selection requirements, corrections, and event weights mentioned in Section 4 are then applied. Nine separate template histograms for each p_T^Z and y^Z bin j at generator level are finally obtained after weighting by each of the P_i terms. The templates t_{ij} are thus three-dimensional distributions in the measured $\cos\theta_{\text{CS}}$, ϕ_{CS} , and $p_T^{\ell\ell}$ variables, and are constructed for each p_T^Z and y^Z bin. Eight bins in $\cos\theta_{\text{CS}}$ and ϕ_{CS} are used, while the binning for the reconstructed $p_T^{\ell\ell}$ is the same as for the 23 bins defined in Eq. (6). By construction, the sum of all signal templates normalised by their reference coefficients and unpolarised cross-sections agrees exactly with the three-dimensional reconstructed distribution expected for signal MC events. Examples of templates projected onto each of the dimensions $\cos\theta_{\text{CS}}$ and ϕ_{CS} for the y^Z -integrated ee_{CC} channel in three illustrative p_T^Z ranges, along with their corresponding polynomial shapes, are shown in Fig. 7. The polynomials P_1 and P_6 are not shown as they integrate to zero in the full phase space in either projection (see Section 5.2). The effect of the acceptance on the polynomial shape depends on p_T^Z because of the event selection, as can be seen from the difference between the template polynomial shapes in each corresponding p_T^Z bin. This is particularly visible in the P_8 polynomial, which is uniform in ϕ_{CS} , and therefore reflects exactly the acceptance shape in the templated polynomials. In Appendix B, two-dimensional versions of Fig. 7 are given for all nine polynomials in Figs. 21 – 23. These two-dimensional views are required for P_1 and P_6 , as discussed above.

Templates T_B are also built for each of the multijet, top+electroweak, and non-fiducial Z-boson backgrounds discussed in Section 4.2. These are normalised by their respective cross-sections times luminosity, or data-driven estimates in the case of the multijet background. The templates for the projection measurements in the ee_{CF} channel are integrated over either the $\cos\theta_{\text{CS}}$ or ϕ_{CS} axis at the end of the process.

Templates corresponding to variations of the systematic uncertainties in the detector response as well as in the theoretical modelling are built in the same way, after varying the relevant source of systematic uncertainty by ± 1 standard deviation (σ). If such a variation changes the A_i^{ref} coefficients in the MC prediction, for example in the case of PDF or parton shower uncertainties, the varied A_i^{ref} coefficients are used as such in the weighting procedure. In this way, the theoretical uncertainties on the predictions are not directly propagated to the uncertainties on the measured A_i coefficients. However, they may affect indirectly the measurements through their impact on the acceptance, selection efficiency, and migration modelling.

5.2. Likelihood

A likelihood is built from the nominal templates and the varied templates reflecting the systematic uncertainties. A set of nuisance parameters (NPs) $\theta = \{\beta, \gamma\}$ is used to interpolate between them. These are constrained by auxiliary probability density functions and come in two categories: β and γ . The first category β are the NPs representing experimental and theoretical uncertainties. Each β^m in the set $\beta = \{\beta^1, \dots, \beta^M\}$ are constrained by unit Gaussian probability density functions $G(0|\beta^m, 1)$ and linearly interpolate between the nominal and varied templates. These are defined to have a nominal value of zero, with $\beta^m = \pm 1$ corresponding to $\pm 1\sigma$ for the systematic uncertainty under consideration. The total number of β^m is $M = 171$ for the $ee_{\text{CC}} + \mu\mu_{\text{CC}}$ channel and $M = 105$ for the ee_{CF} channel. The second category γ are NPs that handle systematic uncertainties from the limited size of the MC samples. For

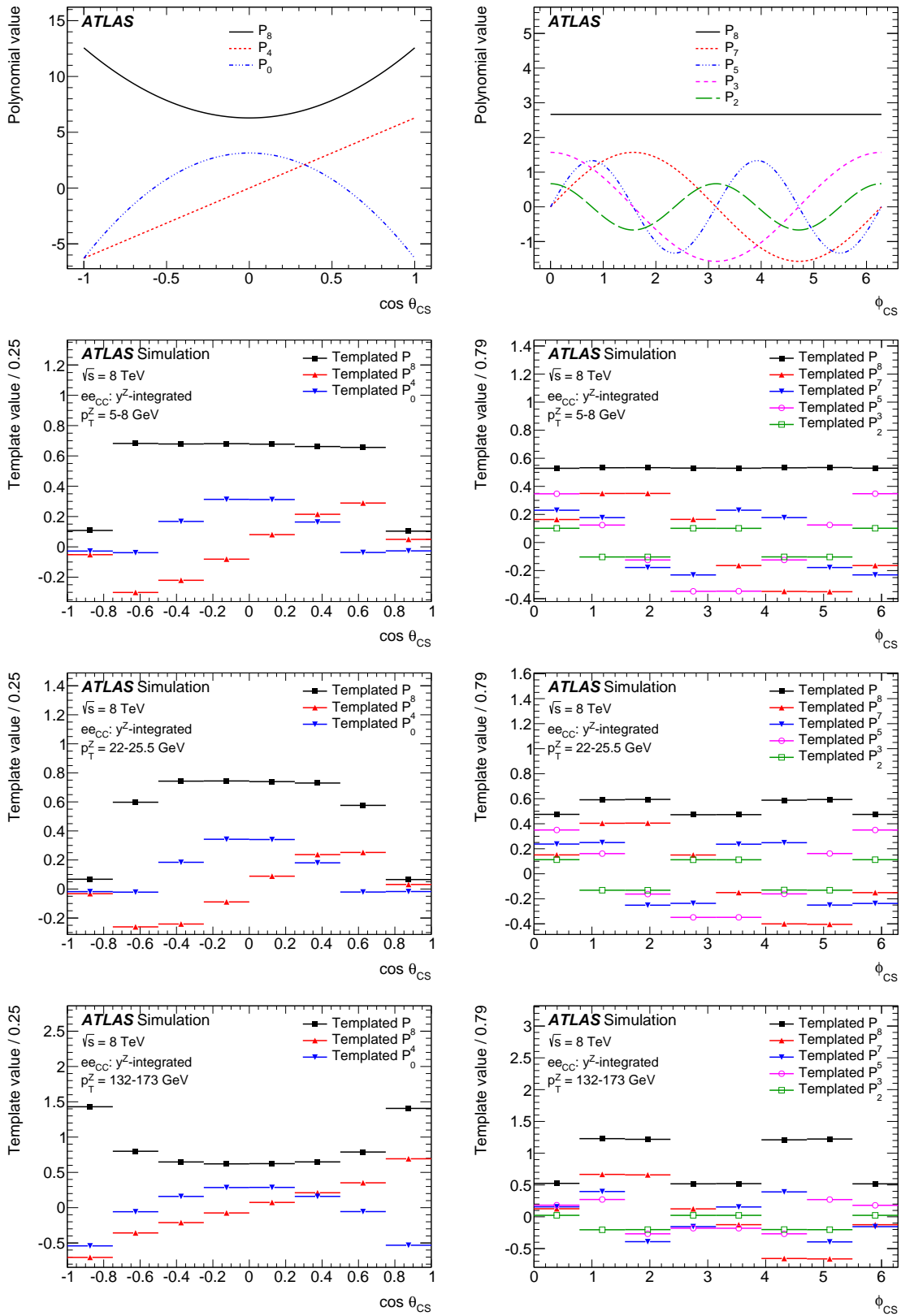


Figure 7: Shapes of polynomials $P_{0,4,8}$ as a function of $\cos \theta_{\text{CS}}$ (top left) and $P_{2,3,5,7,8}$ as a function of ϕ_{CS} (top right). Shown below are the templated polynomials for the y^Z -integrated ee_{CC} events at low ($5-8 \text{ GeV}$), medium ($22-25.5 \text{ GeV}$), and high ($132-173 \text{ GeV}$) values of p_T^Z projected onto each of the dimensions $\cos \theta_{\text{CS}}$ and ϕ_{CS} . The $p_T^{\ell\ell}$ dimension that normally enters through migrations is also integrated over. The differences between the polynomials and the templates reflect the acceptance shape after event selection.

each bin n in the reconstructed $\cos \theta_{\text{CS}}$, ϕ_{CS} , and $p_T^{\ell\ell}$ distribution, γ^n in the set $\gamma = \{\gamma^1, \dots, \gamma^{N_{\text{bins}}}\}$, where $N_{\text{bins}} = 8 \times 8 \times 23$ is the total number of bins in the reconstructed distribution, has a nominal value of one and normalises the expected events in bin n of the templates. They are constrained by Poisson probability density functions $P(N_{\text{eff}}^n | \gamma^n N_{\text{eff}}^n)$, where N_{eff}^n is the effective number of MC events in bin n . The meaning of “effective” here refers to corrections applied for non-uniform event weights. When all signal and background templates are summed over with their respective normalisations, the expected events N_{exp}^n in each bin n can be written as:

$$N_{\text{exp}}^n(A, \sigma, \theta) = \left\{ \sum_{j=1}^{23} \sigma_j \times L \times \left[t_{8j}^n(\beta) + \sum_{i=0}^7 A_{ij} \times t_{ij}^n(\beta) \right] + \sum_B^{\text{bkgs}} T_B^n(\beta) \right\} \times \gamma^n, \quad (7)$$

where:

- A_{ij} : Coefficient parameter for p_T^Z bin j
- A : Set of all A_{ij}
- σ_j : Signal cross-section parameter
- σ : Set of all σ_j
- θ : Set of all NPs
- β : Set of all Gaussian-constrained NPs
- γ^n : Poisson-constrained NP
- t_{ij} : P_i template
- T_B : Background templates
- L : Integrated luminosity constant.

The summation over the index j takes into account the contribution of all p_T^Z bins at generator level in each reconstructed $p_T^{\ell\ell}$ bin. This is necessary to account for migrations in $p_T^{\ell\ell}$. The likelihood is the product of Poisson probabilities across all N_{bins} bins and of auxiliary constraints for each nuisance parameter β_m :

$$\mathcal{L}(A, \sigma, \theta | N_{\text{obs}}) = \prod_n^{N_{\text{bins}}} \left\{ P(N_{\text{obs}}^n | N_{\text{exp}}^n(A, \sigma, \theta)) P(N_{\text{eff}}^n | \gamma^n N_{\text{eff}}^n) \right\} \times \prod_m^M G(0 | \beta^m, 1). \quad (8)$$

Unlike in the ee_{CC} and $\mu\mu_{\text{CC}}$ channels that use both angular variables simultaneously, the ee_{CF} measurements are performed in projections (see Eq. (2) and Eq. (3)), and therefore the A_1 and A_6 coefficients are not measured in this channel. The P_i polynomials that normally integrate to zero when projecting onto one angular variable in full phase space may, however, not integrate to zero if their shape is distorted by the event selection. The residual shape is not sufficient to properly constrain their corresponding A_i , and therefore an external constraint is applied to them. For the A_i that are largely independent of y^Z (A_0 and A_2), the constraints are taken from the independent y^Z -integrated measurements in the combined $ee_{\text{CC}} + \mu\mu_{\text{CC}}$ channel. For the y^Z -dependent coefficients A_1 , A_3 , and A_4 , which are inaccessible to the $ee_{\text{CC}} + \mu\mu_{\text{CC}}$ channels in the y^Z bin in which ee_{CF} is used, predictions from PowHEG + MiNLO [43] are used.

The migration of events between $p_T^{\ell\ell}$ bins leads to anti-correlations between A_i in neighbouring bins which enhance the effects of statistical fluctuations. To mitigate this effect and aid in resolving underlying structure in the A_i spectra, the A_i spectra are regularised by multiplying the unregularised likelihood by a Gaussian penalty term, which is a function of the significance of higher-order derivatives of the A_i with respect to p_T^Z . The covariance terms between the A_{ij} coefficients are taken into account and computed first with the unregularised likelihood. This has parallels with, for example, regularised Bayesian unfolding, where additional information is added through the prior probability of unfolded parameter values [54, 55]. As is the case there, the choice of penalty term (or in the Bayesian case, the choice of added information) must be one that leads to a sound result with minimal bias. See Appendix C for more details.

The uncertainties in the parameters are obtained through a likelihood scan. For each parameter of interest A_{ij} , a likelihood ratio is constructed as

$$\Lambda(A_{ij}) = \frac{\mathcal{L}(A_{ij}, \hat{A}(A_{ij}), \hat{\theta}(A_{ij}))}{\mathcal{L}(\hat{A}, \hat{\theta})}. \quad (9)$$

In the denominator, the likelihood is maximised unconditionally across all parameters of interest and NPs. In the numerator, the likelihood is maximised for a specific value of a single A_{ij} . The maximum likelihood estimators for the other parameters of interest \hat{A} and NPs $\hat{\theta}$ are in general a function of A_{ij} , hence the explicit dependence is shown in the numerator. The MINUIT package is used to perform numerical minimisation [56] of $-2 \log \Lambda(A_{ij})$, and a two-sided test statistic is built from the likelihood ratio:

$$q_{A_{ij}} = -2 \log \Lambda(A_{ij}). \quad (10)$$

This is asymptotically distributed as a χ^2 with one degree of freedom [57]. In this case, the $\pm 1\sigma$ confidence interval of A_{ij} is defined by the condition $q_{A_{ij}^\pm} = 1$, where $A_{ij}^\pm \equiv \hat{A}_{ij} \pm \sigma^\pm$.

5.3. Combinations and alternative parameterisations

When applicable, multiple channels are combined through a simple likelihood multiplication. Each likelihood can be decomposed into three types of terms: those that contain the observed data in each channel, denoted $\mathcal{L}_i(A, \sigma, \theta)$, the auxiliary terms that constrain the nuisance parameters θ , denoted $\mathcal{A}_i(\theta_i)$, and the auxiliary term that imposes the regularisation, $\mathcal{A}_{\text{reg}}(A)$. There are a total of M^{cb} NPs, corresponding to the total number of unique NPs, including the total number of bins, across all combined channels. With this notation the combined likelihood can be written as:

$$\mathcal{L}_{\text{cb}}(A, \sigma, \theta) = \left\{ \prod_i^{\text{channels}} \mathcal{L}_i(A, \sigma, \theta) \right\} \left\{ \prod_i^{M^{\text{cb}}} \mathcal{A}_i(\theta_i) \right\} \mathcal{A}_{\text{reg}}(A). \quad (11)$$

There are several instances in which a combination of two channels is performed. Within these combinations, the compatibility of the channels is assessed. The measurements in the first two y^Z bins and the y^Z -integrated configuration are obtained from a combination of the ee_{CC} and $\mu\mu_{\text{CC}}$ channels. The y^Z -integrated $\mu\mu_{\text{CC}}$ and ee_{CF} channels are also combined in order to assess the compatibility of the high y^Z region probed by the ee_{CF} channel and the lower rapidity region probed by the central–central channels.

The compatibility of channels is assessed through a reparameterisation of the likelihood into parameters that represent the difference between the coefficients in two different channels. For coefficients A_{ij}^a and A_{ij}^b in respective channels a and b , difference parameters $\Delta A_{ij} \equiv A_{ij}^a - A_{ij}^b$ are defined that effectively represent the difference between the measured coefficients in the two channels. Substitutions are made in the form of $A_{ij}^a \rightarrow \Delta A_{ij} + A_{ij}^b$. These new parameters are measured with the same methodology as described in Section 5.2. Similar reparameterisations are also done to measure the difference between the A_0 and A_2 coefficients. These reparameterisations have the advantage that the correlations between the new parameters are automatically taken into account.

6. Measurement uncertainties

Several sources of statistical and systematic uncertainty play a role in the precision of the measurements presented in this paper. In particular, some of the systematic uncertainties impact the template-building procedure described in Section 5.1. For this reason, templates are rebuilt after each variation accounting for a systematic uncertainty, and the difference in shape between the varied and nominal templates is used to evaluate the resulting uncertainty.

A description of the expected statistical uncertainties (both in data in Section 6.1 and in simulation in Section 6.2) and systematic uncertainties (experimental in Section 6.3, theoretical in Section 6.4, and those related to the methodology in Section 6.5) associated with the measurement of the A_i coefficients is given in this section. These uncertainties are summarised in Section 6.6 in three illustrative p_T^Z bins for the ee_{CC} , $\mu\mu_{CC}$ (and their combination), and ee_{CF} channels. The evolution of the uncertainty breakdown as a function of p_T^Z is illustrated there as well.

6.1. Uncertainties from data sample size

Although the harmonic polynomials are completely orthogonal in the full phase space, resolution and acceptance effects lead to some non-zero correlation between them. Furthermore, the angular distributions in a bin of reconstructed $p_T^{\ell\ell}$ have contributions spanning several generator-level p_T^Z bins. This leads to correlations between the measured coefficients which increase their statistical uncertainties. The amount of available data is the largest source of uncertainty, although the resolution and binning in the angular variables also play a role. A discussion of the categorisation of this uncertainty may be found in Appendix D.

6.2. Uncertainties from Monte Carlo sample size

Statistical uncertainties from the simulated MC samples are treated as uncorrelated between each bin of the three-dimensional ($p_T^{\ell\ell}$, $\cos\theta_{CS}$, ϕ_{CS}) distribution. Although the events used to build each template are the same, they receive a different weight from the different polynomials, and are therefore only partially correlated. It was verified that assuming that the templates are fully correlated yields slightly more conservative uncertainties, but central values identical to those obtained using the fully correct treatment. For simplicity, this assumption is used for this uncertainty.

6.3. Experimental systematic uncertainties

Experimental systematic uncertainties affect the migration and efficiency model of the detector simulation, impacting the variables used to construct the templates and the event weights applied to the simulation.

Lepton-related systematic uncertainties: Scale factors correcting the lepton reconstruction, identification, and trigger efficiencies to those observed in data [50–52] are applied to the simulation as event weights. The statistical uncertainties of the scale factors tend to be naturally uncorrelated in the kinematic bins in which they are measured, while the systematic uncertainties tend to be correlated across these bins. Lepton calibration (electron energy scale and resolution as well as muon momentum scale and resolution) [52, 53] and their associated uncertainties are derived from data-driven methods and applied to the simulation. Whereas the charge misidentification rate for muons is negligible, the probability for the electron charge to be misidentified can be significant for central electrons at high $|\eta|$, due to bremsstrahlung in the inner detector and the subsequent conversion of the photon. This uncertainty is a potential issue in particular for the ee_{CF} channel, where the measured charge of the central electron sets the charge of the forward electron (where no charge determination is possible). Measurements of the per-electron charge misidentification rate using same-charge electron pairs have been done in data and compared to that in simulation; the systematic uncertainty coming from this correction has a negligible impact on the measurement.

Background-related systematic uncertainties: Uncertainties in the multijet background estimate come from two sources. The first source is the statistical uncertainty in the normalisation of the background in each bin of reconstructed $p_T^{\ell\ell}$. The second is the systematic uncertainty of the overall background normalisation, which is evaluated using alternative criteria to define the multijet background templates. These uncertainties are applied to all three channels and treated as uncorrelated amongst them. In addition, a 20% systematic uncertainty uncorrelated across $p_T^{\ell\ell}$ bins but correlated across the ee_{CC} and $\mu\mu_{\text{CC}}$ channels is applied to the estimation of the top+electroweak background.

Other experimental systematic uncertainties: Several other potential sources of experimental systematic uncertainty are considered, such as event pileup or possible detector misalignments which might affect the muon momentum measurement, and are found to contribute negligibly to the overall measurement uncertainties. The uncertainty in the integrated luminosity is $\pm 2.8\%$. It is derived following the same methodology as that detailed in Ref. [58]. It only enters (negligibly) in the scaling of the background contributions evaluated from the Monte Carlo samples.

6.4. Theoretical systematic uncertainties

Theoretical systematic uncertainties due to QCD renormalisation/factorisation scale, PDFs, parton-shower modelling, generator modelling, and QED/EW corrections are considered. They are evaluated using either event weights, for example through PDF reweighting, or templates built from alternative Monte Carlo samples. The templates built after each variation accounting for a systematic uncertainty have their own set of reference coefficients so that each variation starts from isotropic angular distributions. This procedure is done so that uncertainties in the simulation predictions for the coefficients propagate minimally to the uncertainties in the measurement; rather, uncertainties in the measurement are due to the theoretical uncertainty of the migration and acceptance modelling. A small fraction of the acceptance can, however, be attributed to the behaviour of coefficients outside the accessible y^Z range. In this specific

case, the theoretical predictions used for the coefficients can have a small influence on the uncertainties in the measured coefficients.

QCD scale: These systematic uncertainties only affect the predictions over the small region of phase space where no measurements are available. They are evaluated by varying the factorisation and renormalisation scale of the predicted coefficients in the region $|y^Z| > 3.5$ (see Fig. 3). The changes induced in the templates due to the variation in acceptance are used to assess the impact of this uncertainty, which is found to be negligible.

PDF: These systematic uncertainties are computed with the 52 CT10 eigenvectors representing 26 independent sources. The CT10 uncertainties are provided at 90% CL, and are therefore rescaled by a factor of 1.64 to bring them to 68% CL variations. Events are also reweighted using the NNPDF2.3 [59] and MSTW [60] PDFs and are treated as independent systematics. These two-point variations are symmetrised in the procedure.

Parton showers: The POWHEG + HERWIG samples are used to compute an alternative set of templates. The shape difference between these and the templates obtained from the baseline POWHEG + PYTHIA 8 samples are used to evaluate the underlying event and parton shower uncertainty.

Event generator: These systematic uncertainties are evaluated through the reweighting of the rapidity distribution of the nominal POWHEG + PYTHIA 8 MC sample to that from SHERPA, which corresponds approximately to a 5% slope per unit of $|y^Z|$. An alternative set of signal templates is built from this variation, using the new set of reference coefficients averaged over rapidity after the reweighting.

QED/EW corrections: The impact of the QED FSR corrections on the measurements is accounted for by the uncertainties in the lepton efficiencies and scales. The contribution of the EW corrections to the calculation of the Z-boson decay angular distributions in Eq. (1) is estimated to be negligible around the Z-pole mass, based on the extensive and detailed work done at LEP in this area [6, 7, 61], as discussed in Section 1.

The PDF uncertainties were found to be the only non-negligible source of theoretical systematic uncertainty in the measured A_i coefficients, and are in particular the dominant source of uncertainty in the measurement of A_0 at low p_T^Z .

6.5. Systematic uncertainties related to the methodology

Systematic uncertainties related to the template building, fitting, and regularisation methodology are considered. These could manifest through sensitivity to the p_T^Z shape in the simulation, the particular shape of the A_i coefficient being fitted, or possible biases caused by the regularisation scheme.

$p_T^{\ell\ell}$ shape: The sensitivity to the shape of the $p_T^{\ell\ell}$ spectrum is tested in two different ways. First, the shape of the $p_T^{\ell\ell}$ spectrum in simulation is reweighted with a polynomial function so that it approximately reproduces the reconstructed spectrum in data. The impact of this procedure is expected to be small, since the signal is normalised to the data in fine bins of p_T^Z . Second, the $p_T^{\ell\ell}$ shape within each $p_T^{\ell\ell}$ bin is reweighted to that of the data. Since the binning is fine enough that the $p_T^{\ell\ell}$ shape does not vary too rapidly within one bin, the impact of this is also small.

A_i shape: Closure tests are performed by fitting to pseudo-data corresponding to various sets of reference A_i^{ref} coefficients to ensure that the fitted A_i coefficients can reproduce the reference. The A_i^{ref} coefficients are obtained from POWHEG + PYTHIA 8, from SHERPA 1.4, or are all set to zero.

Regularisation: The potential bias induced by the regularisation is evaluated with pseudo-experiments. A sixth-order polynomial is fit to the PowHEGBox + PYTHIA 8 set of A_i^{ref} coefficients to obtain a continuous reference spectrum y_{ij} . Pseudo-data are randomised around the expected distribution obtained from this fit using a Poisson distribution for each bin. The difference between y_{ij} and the expectation value $E[A_{ij}]$ of the distribution of fitted and regularised A_{ij} is an estimate of the potential bias in the regularised A_{ij} . The envelope of $|E[A_{ij}] - y_{ij}|$ is symmetrised and taken to be the bias uncertainty. (See Appendix C for more details.)

The effect of p_T^Z reweighting and closure of A_i spectra were found to be negligible. The only non-negligible source of uncertainty in the methodology was found to be the regularisation bias, which can have a size approaching the statistical uncertainty of A_0 and A_2 .

6.6. Summary of uncertainties

Tables 4–7 show the uncertainties in each measured coefficient in three representative p_T^Z bins, along with the impact of each category of systematics. The theoretical uncertainties are dominated by the PDF uncertainties, which in a few cases are larger than the statistical uncertainties. The experimental uncertainties are dominated by the lepton uncertainties and are the leading source of systematic uncertainty for low values of p_T^Z for the A_2 coefficient. The large uncertainties assigned to the multijet background estimates and their shape have a negligible impact on this measurement.

The dominant uncertainty in the measurements of the A_i coefficients is in most cases the statistical uncertainty, even in the most populated bins at low p_T^Z , which contain hundreds of thousands of events. The exception is the A_0 coefficient where PDF and electron efficiency uncertainties dominate for p_T^Z values below 80 GeV. The next largest uncertainty is due to the signal MC statistical uncertainty. This is reflected in Fig. 8, which shows the uncertainty evolution versus p_T^Z for $A_0 - A_2$, including a breakdown of the systematic uncertainties for both the unregularised and regularised measurements. The evolution versus p_T^Z of the total, statistical, and systematic uncertainties is shown for all other coefficients in Fig. 9 for the regularised measurement.

7. Results

This section presents the full set of experimental results. The compatibility between channels is assessed in Section 7.1. The measured A_i coefficients are then shown in Section 7.2. A test is also performed to check for non-zero values of the $A_{5,6,7}$ coefficients. Several cross-checks are presented in Section 7.3, including a test of the validity of the nine-term decomposition, probing for the presence of higher-order P_i polynomial terms.

7.1. Compatibility between channels

Given that a complex fitting procedure based on reconstructed observables is used, the compatibility between different channels is assessed with a strict quantitative test. The likelihood is parameterised in terms of $\Delta A_{ij} \equiv A_{ij}^{\mu\mu} - A_{ij}^{ee}$ for coefficient index i and p_T^Z bin j , as described in Section 5.3. The compatibility of the ΔA_{ij} with zero can be quantified via a χ^2 test taking into account all systematic

Table 4: Summary of regularised uncertainties expected for A_0 , A_2 , and $A_0 - A_2$ at low (5–8 GeV), mid (22–22.5 GeV), and high (132–173 GeV) p_T^Z for the y^Z -integrated configuration. The total systematic uncertainty is shown with the breakdown into its underlying components. Entries marked with “-” indicate that the uncertainty is below 0.0001.

$p_T^Z = 5\text{--}8 \text{ GeV}$									
Coefficient	A_0			A_2			$A_0 - A_2$		
Channel	ee	$\mu\mu$	$ee+\mu\mu$	ee	$\mu\mu$	$ee+\mu\mu$	ee	$\mu\mu$	$ee+\mu\mu$
Total	0.0114	0.0123	0.0083	0.0061	0.0045	0.0036	0.0102	0.0107	0.0076
Data Stat.	0.0034	0.0029	0.0022	0.0039	0.0034	0.0025	0.0050	0.0043	0.0033
Syst.	0.0109	0.0120	0.0081	0.0047	0.0029	0.0026	0.0089	0.0098	0.0068
MC Stat.	0.0017	0.0015	0.0011	0.0020	0.0018	0.0013	-	0.0023	0.0017
Lepton	0.0065	0.0006	0.0014	0.0036	0.0021	0.0017	0.0072	0.0021	0.0022
Bkg.	0.0004	0.0003	0.0002	0.0002	0.0001	0.0001	-	-	0.0006
Theory	0.0054	0.0100	0.0042	0.0006	0.0005	0.0005	0.0046	-	0.0041
Method.	0.0016	0.0016	0.0016	0.0013	0.0013	0.0013	0.0001	0.0001	0.0001
$p_T^Z = 22\text{--}25.5 \text{ GeV}$									
Coefficient	A_0			A_2			$A_0 - A_2$		
Channel	ee	$\mu\mu$	$ee+\mu\mu$	ee	$\mu\mu$	$ee+\mu\mu$	ee	$\mu\mu$	$ee+\mu\mu$
Total	0.0101	0.0120	0.0080	0.0067	0.0050	0.0041	0.0102	0.0111	0.0077
Data Stat.	0.0049	0.0043	0.0033	0.0047	0.0043	0.0031	0.0064	0.0060	0.0045
Syst.	0.0089	0.0112	0.0073	0.0047	0.0027	0.0026	0.0079	0.0094	0.0063
MC Stat.	0.0023	0.0021	0.0015	0.0022	0.0020	0.0015	0.0039	0.0035	0.0025
Lepton	0.0050	0.0005	0.0013	0.0037	0.0003	0.0013	0.0064	0.0009	0.0019
Bkg.	0.0005	0.0003	0.0002	0.0003	0.0002	0.0002	-	-	0.0006
Theory	0.0047	0.0092	0.0038	0.0003	0.0003	0.0002	0.0043	0.0097	0.0039
Method.	0.0021	0.0021	0.0021	0.0016	0.0016	0.0016	0.0003	0.0003	0.0003
$p_T^Z = 132\text{--}173 \text{ GeV}$									
Coefficient	A_0			A_2			$A_0 - A_2$		
Channel	ee	$\mu\mu$	$ee+\mu\mu$	ee	$\mu\mu$	$ee+\mu\mu$	ee	$\mu\mu$	$ee+\mu\mu$
Total	0.0143	0.0143	0.0110	0.0400	0.0380	0.0294	0.0326	0.0367	0.0227
Data Stat.	0.0113	0.0104	0.0077	0.0324	0.0289	0.0214	0.0295	0.0304	0.0196
Syst.	0.0087	0.0092	0.0079	0.0229	0.0239	0.0202	0.0139	0.0206	0.0116
MC Stat.	0.0029	0.0060	0.0032	0.0085	0.0167	0.0092	0.0091	0.0181	0.0100
Lepton	0.0031	0.0006	0.0012	0.0095	0.0026	0.0040	0.0076	-	0.0043
Bkg.	0.0006	0.0009	0.0006	0.0020	0.0033	0.0020	-	-	0.0009
Theory	0.0008	0.0015	0.0010	0.0009	0.0021	0.0016	0.0024	0.0047	0.0026
Method.	0.0067	0.0067	0.0067	0.0172	0.0172	0.0172	0.0067	0.0067	0.0067

Table 5: Summary of regularised uncertainties expected for A_1 , A_3 and A_4 at low (5–8 GeV), mid (22–25.5 GeV), and high (132–173 GeV) p_T^Z for the y^Z -integrated configuration. The total systematic uncertainty is shown with the breakdown into its underlying components. Entries marked with “-” indicate that the uncertainty is below 0.0001.

$p_T^Z = 5\text{--}8 \text{ GeV}$									
Coefficient	A_1			A_3			A_4		
Channel	ee	$\mu\mu$	$ee+\mu\mu$	ee	$\mu\mu$	$ee+\mu\mu$	ee	$\mu\mu$	$ee+\mu\mu$
Total	0.0032	0.0027	0.0023	0.0018	0.0016	0.0012	0.0034	0.0030	0.0024
Data Stat.	0.0024	0.0021	0.0016	0.0016	0.0015	0.0011	0.0023	0.0020	0.0015
Syst.	0.0021	0.0018	0.0017	0.0008	0.0007	0.0006	0.0025	0.0022	0.0019
MC Stat.	0.0012	0.0010	0.0008	0.0008	0.0007	0.0006	0.0011	0.0010	0.0008
Lepton	0.0015	0.0018	0.0012	0.0002	0.0002	0.0001	0.0002	-	0.0001
Bkg.	0.0002	0.0001	0.0001	-	0.0001	-	0.0001	-	0.0001
Theory	0.0003	0.0003	0.0003	0.0001	0.0001	0.0001	0.0020	0.0018	0.0017
Method.	0.0006	0.0006	0.0006	0.0001	0.0001	0.0001	0.0002	0.0002	0.0002
$p_T^Z = 22\text{--}25.5 \text{ GeV}$									
Coefficient	A_1			A_3			A_4		
Channel	ee	$\mu\mu$	$ee+\mu\mu$	ee	$\mu\mu$	$ee+\mu\mu$	ee	$\mu\mu$	$ee+\mu\mu$
Total	0.0042	0.0038	0.0027	0.0023	0.0021	0.0016	0.0039	0.0035	0.0026
Data Stat.	0.0033	0.0029	0.0022	0.0021	0.0019	0.0014	0.0032	0.0028	0.0021
Syst.	0.0026	0.0025	0.0016	0.0010	0.0009	0.0007	0.0022	0.0020	0.0015
MC Stat.	0.0016	0.0014	0.0011	0.0010	0.0009	0.0007	0.0016	0.0014	0.0010
Lepton	0.0011	0.0009	0.0007	0.0003	-	0.0001	0.0003	0.0001	0.0002
Bkg.	-	-	-	0.0001	-	0.0001	0.0001	0.0001	0.0001
Theory	0.0010	0.0014	0.0005	0.0003	0.0002	0.0002	0.0013	0.0012	0.0012
Method.	0.0007	0.0007	0.0007	0.0001	0.0001	0.0001	0.0003	0.0003	0.0003
$p_T^Z = 132\text{--}173 \text{ GeV}$									
Coefficient	A_1			A_3			A_4		
Channel	ee	$\mu\mu$	$ee+\mu\mu$	ee	$\mu\mu$	$ee+\mu\mu$	ee	$\mu\mu$	$ee+\mu\mu$
Total	0.0127	0.0129	0.0092	0.0113	0.0118	0.0081	0.0074	0.0079	0.0054
Data Stat.	0.0113	0.0106	0.0078	0.0108	0.0102	0.0074	0.0071	0.0068	0.0049
Syst.	0.0054	0.0070	0.0049	0.0033	0.0059	0.0034	0.0022	0.0040	0.0022
MC Stat.	0.0035	0.0060	0.0034	0.0032	0.0059	0.0033	0.0021	0.0037	0.0022
Lepton	0.0025	-	0.0007	0.0011	0.0015	0.0007	0.0004	0.0004	0.0002
Bkg.	0.0006	-	-	0.0006	0.0011	0.0003	0.0002	0.0003	0.0001
Theory	0.0010	0.0010	0.0007	-	-	0.0005	0.0004	0.0004	0.0004
Method.	0.0031	0.0031	0.0031	0.0004	0.0004	0.0004	0.0005	0.0005	0.0005

Table 6: Summary of regularised uncertainties expected for A_5 , A_6 and A_7 at low (5–8 GeV), mid (22–25.5 GeV), and high (132–173 GeV) p_T^Z for the y^Z -integrated configuration. The total systematic uncertainty is shown with the breakdown into its underlying components. Entries marked with “-” indicate that the uncertainty is below 0.0001.

$p_T^Z = 5\text{--}8 \text{ GeV}$									
Coefficient	A_5			A_6			A_7		
Channel	ee	$\mu\mu$	$ee+\mu\mu$	ee	$\mu\mu$	$ee+\mu\mu$	ee	$\mu\mu$	$ee+\mu\mu$
Total	0.0021	0.0019	0.0015	0.0022	0.0019	0.0015	0.0015	0.0014	0.0010
Data Stat.	0.0018	0.0017	0.0013	0.0019	0.0017	0.0013	0.0014	0.0012	0.0009
Syst.	0.0010	0.0009	0.0007	0.0011	0.0009	0.0007	0.0007	0.0006	0.0005
MC Stat.	0.0009	0.0008	0.0006	0.0010	0.0009	0.0007	0.0007	0.0006	0.0005
Lepton	0.0003	-	0.0001	0.0001	0.0001	0.0001	0.0001	-	0.0001
Bkg.	0.0001	-	-	0.0001	-	-	-	-	-
Theory	0.0002	0.0001	-	0.0004	0.0004	0.0004	0.0002	0.0002	0.0002
Method.	0.0003	0.0003	0.0003	0.0002	0.0002	0.0002	0.0001	0.0001	0.0001
$p_T^Z = 22\text{--}25.5 \text{ GeV}$									
Coefficient	A_5			A_6			A_7		
Channel	ee	$\mu\mu$	$ee+\mu\mu$	ee	$\mu\mu$	$ee+\mu\mu$	ee	$\mu\mu$	$ee+\mu\mu$
Total	0.0026	0.0023	0.0018	0.0028	0.0025	0.0019	0.0020	0.0018	0.0014
Data Stat.	0.0023	0.0021	0.0015	0.0025	0.0022	0.0017	0.0018	0.0016	0.0012
Syst.	0.0012	0.0011	0.0009	0.0013	0.0012	0.0009	0.0009	0.0008	0.0006
MC Stat.	0.0011	0.0010	0.0008	0.0012	0.0011	0.0008	0.0009	0.0008	0.0006
Lepton	-	-	0.0001	0.0002	0.0001	0.0001	0.0001	0.0001	0.0001
Bkg.	-	-	-	0.0001	0.0001	0.0001	0.0001	0.0001	0.0001
Theory	0.0001	0.0001	-	0.0002	0.0001	0.0001	0.0002	0.0001	0.0001
Method.	0.0004	0.0004	0.0004	0.0002	0.0002	0.0002	0.0001	0.0001	0.0001
$p_T^Z = 132\text{--}173 \text{ GeV}$									
Coefficient	A_5			A_6			A_7		
Channel	ee	$\mu\mu$	$ee+\mu\mu$	ee	$\mu\mu$	$ee+\mu\mu$	ee	$\mu\mu$	$ee+\mu\mu$
Total	0.0092	0.0097	0.0069	0.0076	0.0081	0.0056	0.0066	0.0071	0.0048
Data Stat.	0.0087	0.0083	0.0060	0.0072	0.0070	0.0050	0.0063	0.0061	0.0044
Syst.	0.0034	0.0052	0.0034	0.0023	0.0041	0.0024	0.0018	0.0035	0.0020
MC Stat.	0.0024	0.0046	0.0027	0.0020	0.0039	0.0022	0.0018	0.0035	0.0019
Lepton	0.0013	-	0.0008	0.0006	0.0003	0.0004	0.0005	0.0004	0.0003
Bkg.	0.0004	0.0007	-	0.0004	0.0003	0.0002	0.0003	0.0002	0.0002
Theory	0.0002	0.0008	0.0005	0.0004	0.0003	0.0002	0.0003	0.0003	0.0002
Method.	0.0022	0.0022	0.0022	0.0008	0.0008	0.0008	0.0002	0.0002	0.0002

Table 7: Summary of regularised uncertainties expected for the coefficients at low (5–8 GeV), mid (22–25.5 GeV), and high (73.4–85.4 GeV) p_T^Z for the $2 < |y^Z| < 3.5$ configuration. The total systematic uncertainty is shown with the breakdown into its underlying components. Entries marked with “–” indicate that the uncertainty is below 0.0001.

$p_T^Z = 5\text{--}8 \text{ GeV}$						
Coefficient	A_0	A_2	A_3	A_4	A_5	A_7
Total	0.0377	0.0657	0.0190	0.0097	0.0161	0.0064
Data Stat.	0.0169	0.0569	0.0183	0.0090	0.0152	0.0059
Syst.	0.0337	0.0328	0.0054	0.0036	0.0053	0.0026
Lepton	0.0282	0.0263	0.0014	0.0015	0.0021	0.0005
MC Stat.	0.0059	0.0150	0.0047	0.0032	0.0049	0.0026
Bkg.	0.0047	0.0202	0.0010	0.0006	0.0007	0.0002
Theory	0.0121	0.0032	0.0008	0.0012	-	0.0002
Method.	0.0008	0.0002	0.0006	0.0002	0.0007	0.0001
$p_T^Z = 22\text{--}25.5 \text{ GeV}$						
Coefficient	A_0	A_2	A_3	A_4	A_5	A_7
Total	0.0395	0.0724	0.0225	0.0148	0.0193	0.0107
Data Stat.	0.0257	0.0660	0.0216	0.0140	0.0183	0.0101
Syst.	0.0300	0.0299	0.0063	0.0048	0.0061	0.0035
Lepton	0.0264	0.0203	0.0024	0.0015	0.0014	0.0006
MC Stat.	0.0083	0.0165	0.0057	0.0045	0.0057	0.0035
Bkg.	0.0062	0.0190	0.0015	0.0006	0.0007	0.0004
Theory	0.0089	0.0023	0.0002	0.0013	0.0003	0.0004
Method.	0.0007	0.0011	0.0005	0.0003	0.0002	0.0002
$p_T^Z = 73.4\text{--}85.4 \text{ GeV}$						
Coefficient	A_0	A_2	A_3	A_4	A_5	A_7
Total	0.0425	0.1242	0.0383	0.0211	0.0355	0.0233
Data Stat.	0.0296	0.0991	0.0345	0.0192	0.0323	0.0214
Syst.	0.0304	0.0747	0.0167	0.0089	0.0146	0.0094
Lepton	0.0149	0.0399	0.0034	0.0026	0.0015	0.0017
MC Stat.	0.0125	0.0417	0.0145	0.0083	0.0136	0.0090
Bkg.	0.0301	0.0343	0.0053	0.0018	0.0038	0.0008
Theory	0.0033	0.0069	0.0008	0.0006	0.0009	0.0009
Method.	0.0014	0.0041	0.0012	0.0008	0.0012	0.0004

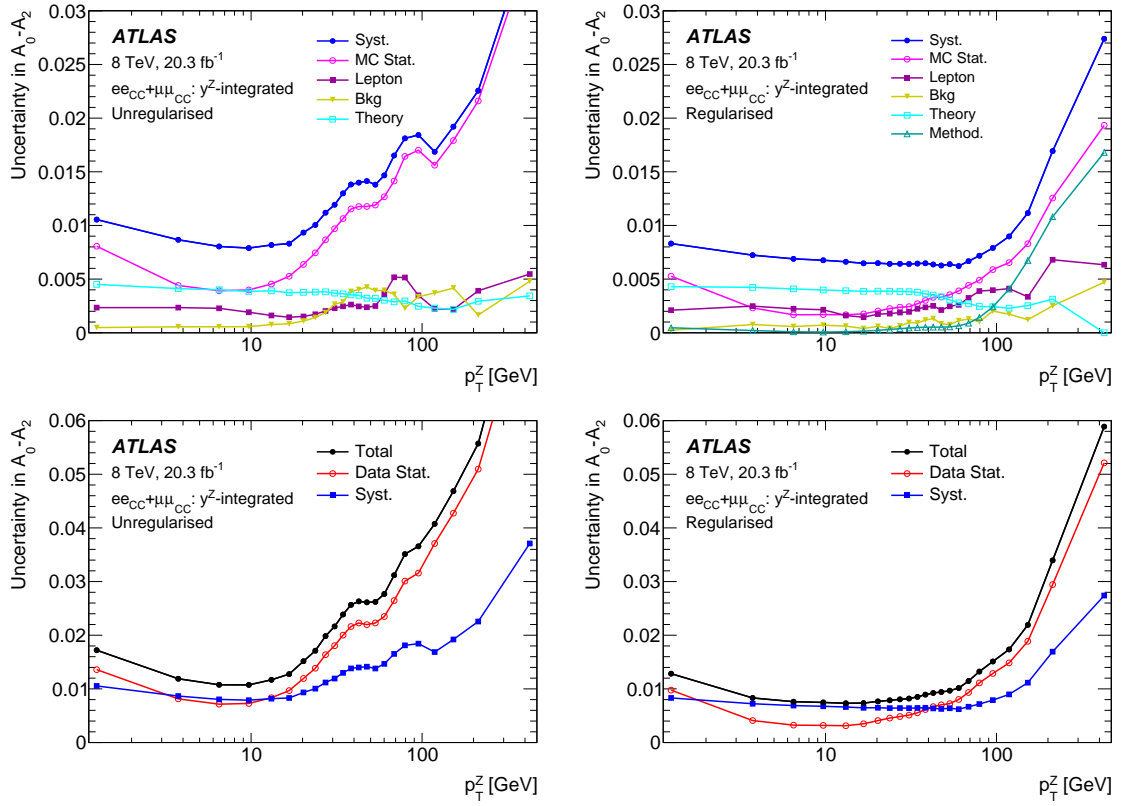


Figure 8: Uncertainty breakdown for $A_0 - A_2$ as a function of p_T^Z in the y^Z -integrated $ee_{CC} + \mu\mu_{CC}$ measurement: the systematic uncertainty (top) and the total uncertainty (bottom). The left column shows the unregularised version, while the right column shows the regularised one.

uncertainty correlations. The χ^2 values are first computed for each coefficient i and across all p_T^Z bins j , then for all coefficients and p_T^Z bins simultaneously. This test is done in the y^Z -integrated case for the differences between the measurements extracted from the $\mu\mu_{CC}$ and ee_{CC} events and from the $\mu\mu_{CC}$ and ee_{CF} events, as well as in the first two y^Z bins for the $\mu\mu_{CC}$ and ee_{CC} events. The χ^2 values are tabulated in Table 8 and indicate almost all the differences are compatible with zero.

The ΔA_{ij} spectra are shown in Fig. 10 for the y^Z -integrated ee_{CC} and $\mu\mu_{CC}$ channels. The regularised and unregularised spectra are overlayed. Visually, it appears that these results are compatible with zero. In some cases, the unregularised ΔA_{ij} show alternating fluctuations above and below zero due to anti-correlations between neighbouring p_T^Z bins. These are smoothed out in the regularised results, which come at the expense of larger bin-to-bin correlations.

7.2. Results in the individual and combined channels

The measurements represent the full set of y^Z -integrated coefficients, including the difference $A_0 - A_2$, as a function of p_T^Z , as well as the y^Z -dependent coefficients as a function of p_T^Z in the available y^Z bins. The combination of the ee_{CC} and $\mu\mu_{CC}$ channels is used for the y^Z -integrated measurements and the measurements in the first two y^Z bins, while the ee_{CF} channel is used for the measurements in the

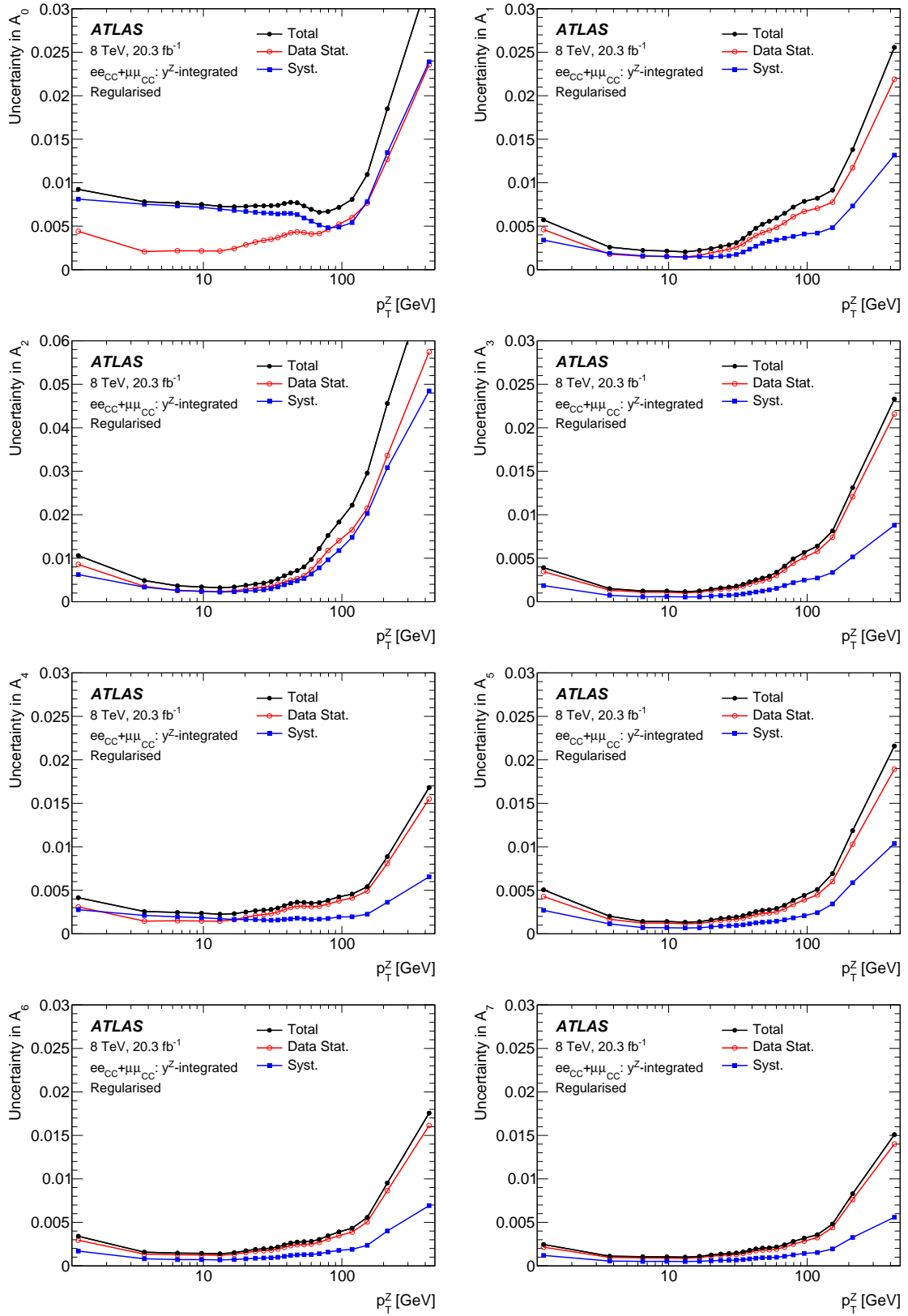


Figure 9: The total uncertainty as a function of p_T^Z along with a breakdown into statistical and systematic components for all coefficients in the regularised $ee_{CC} + \mu\mu_{CC}$ measurement.

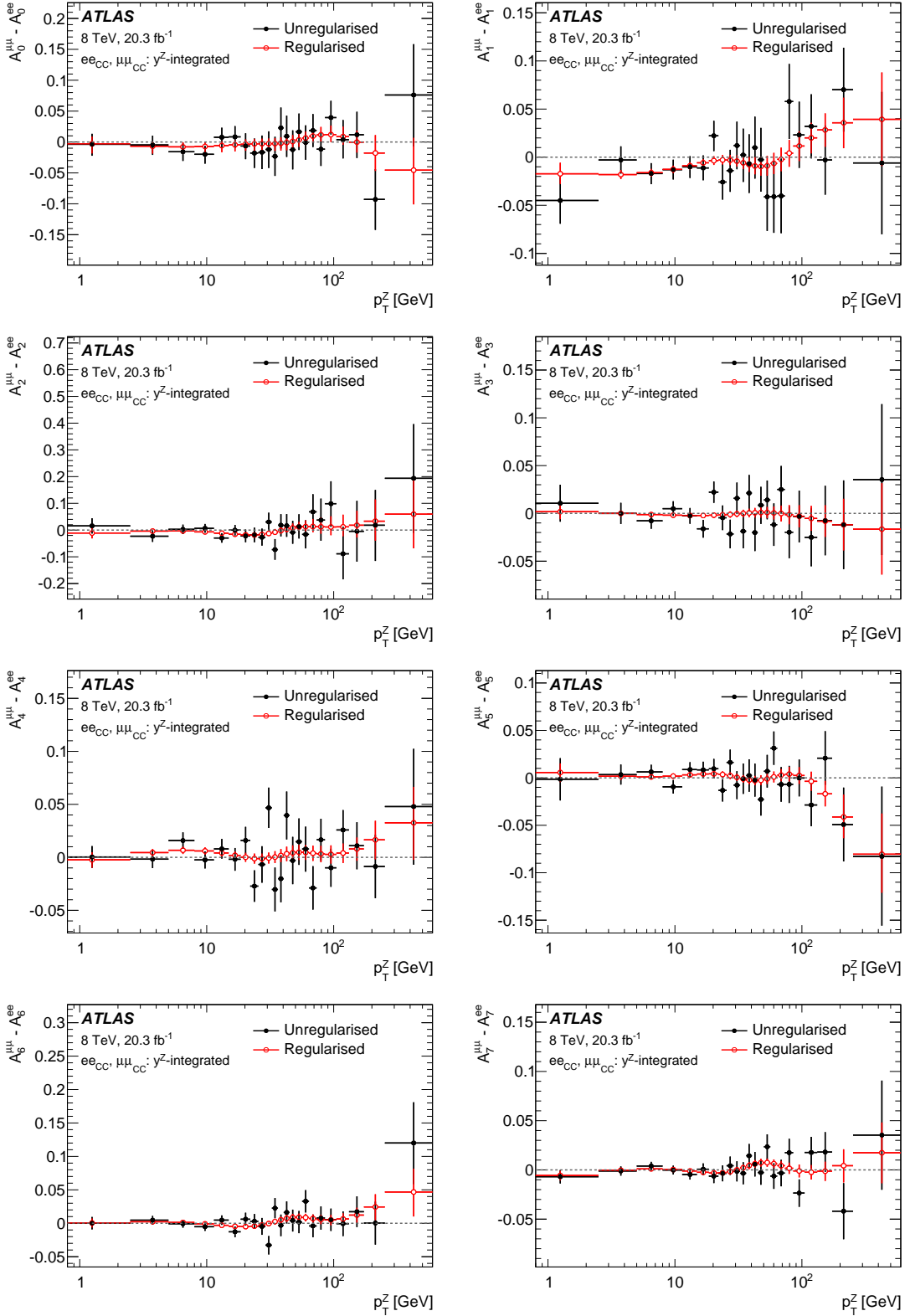


Figure 10: Differences between the measured angular coefficients in the $\mu\mu_{CC}$ and ee_{CC} channels, shown as a function of p_T^Z from top left to bottom right, for all measured coefficients in the y^Z -integrated configuration. The full (open) circles represent the measured differences before (after) regularisation. The error bars represent the total uncertainty in the measurements.

Table 8: Tabulation of the compatibility of the measured ΔA_i with zero reported as χ^2 per degree of freedom (N_{DoF}), where ΔA_i represents the difference between the A_i coefficient extracted from the $\mu\mu_{\text{CC}}$ and ee_{CC} events (left) and from the $\mu\mu_{\text{CC}}$ and ee_{CF} events (right). For the ee_{CC} versus $\mu\mu_{\text{CC}}$ tests, the number of degrees of freedom is 23 for the tests of the individual coefficients and 184 for the tests of all coefficients simultaneously. Likewise, for the ee_{CF} versus $\mu\mu_{\text{CC}}$ tests, there are 19 degrees of freedom for the tests of the individual coefficients, 38 for the simultaneous test in the $\cos \theta_{\text{CS}}$ projection, and 76 for the simultaneous test in the ϕ_{CS} projection. The comparisons are not performed for the A_1 and A_6 coefficients between the $\mu\mu_{\text{CC}}$ and ee_{CF} channels (see Section 5.2).

A_i	χ^2/N_{DoF} for $\mu\mu_{\text{CC}}$ versus ee_{CC}			χ^2/N_{DoF} for $\mu\mu_{\text{CC}}$ versus ee_{CF}	
	y^Z -integrated	$0 < y^Z < 1$	$1 < y^Z < 2$	y^Z -integrated ($\cos \theta_{\text{CS}}$ -proj.)	y^Z -integrated (ϕ_{CS} -proj.)
0	15.4 / 23	25.0 / 23	9.8 / 23	18.9 / 19	-
1	32.9 / 23	24.9 / 23	28.2 / 23	-	-
2	17.0 / 23	22.7 / 23	19.4 / 23	-	35.0 / 19
3	15.8 / 23	20.9 / 23	19.5 / 23	-	16.9 / 19
4	27.2 / 23	31.1 / 23	23.4 / 23	15.1 / 19	-
5	20.0 / 23	23.1 / 23	18.4 / 23	-	17.9 / 19
6	21.9 / 23	17.7 / 23	27.6 / 23	-	-
7	18.3 / 23	22.9 / 23	18.1 / 23	-	27.4 / 19
All	173.1 / 184	190 / 184	166.1 / 184	33.8 / 38	94.5 / 76

last y^Z bin. A summary of these measurements is tabulated in Tables 9–10 for three representative p_T^Z bins. Figure 11 shows the y^Z -integrated measurements for all A_i and overlays of the y^Z -dependent A_i in each accessible y^Z bin. The A_1 and A_6 measurements are missing from the third y^Z bin since they are inaccessible in the projections used in the ee_{CF} channel (see Section 5.2). Also, a measurement of $A_0 - A_2$ is missing in this bin since A_0 and A_2 are accessible in different projections. Complete tables can be found in Appendix F along with additional figures in y^Z bins. Similarly to the regularised ΔA_{ij} measurements, there is a large degree of correlation from bin to bin. This, coupled with statistical fluctuations, can lead to correlated deviations in the spectra, for example near $p_T^Z = 40$ GeV for A_4 in the $2 < |y^Z| < 3.5$ bin, and for A_1 in the $0 < |y^Z| < 1$ bin. Visually, the coefficients $A_{5,6,7}$ all show a trend towards non-zero positive values in the region with p_T^Z around 100 GeV.

7.3. Cross-checks

Several cross-checks are performed to ensure that the fit is of good quality and that the underlying theoretical assumptions are valid to the extent of the precision of the analysis.

The signal MC distributions are reweighted to the full set of measured parameters. An event-by-event weight is calculated as a ratio using the right-hand side of Eq. (1): the numerator uses the measured parameters, and the denominator uses the reference values in the MC simulation. Distributions are obtained after applying this reweighting; the $\cos \theta_{\text{CS}}$ and ϕ_{CS} distributions integrated in y^Z are shown in Fig. 12, along with their bin-by-bin pulls, obtained by combining the statistical and systematic uncertainties. Overall, the data and MC simulation agree well. One observes significant pulls near $\cos \theta_{\text{CS}} = 0$ for the ee_{CF} channel, but the number of events in this region is very small and its impact on the coefficient measurements is negligible.

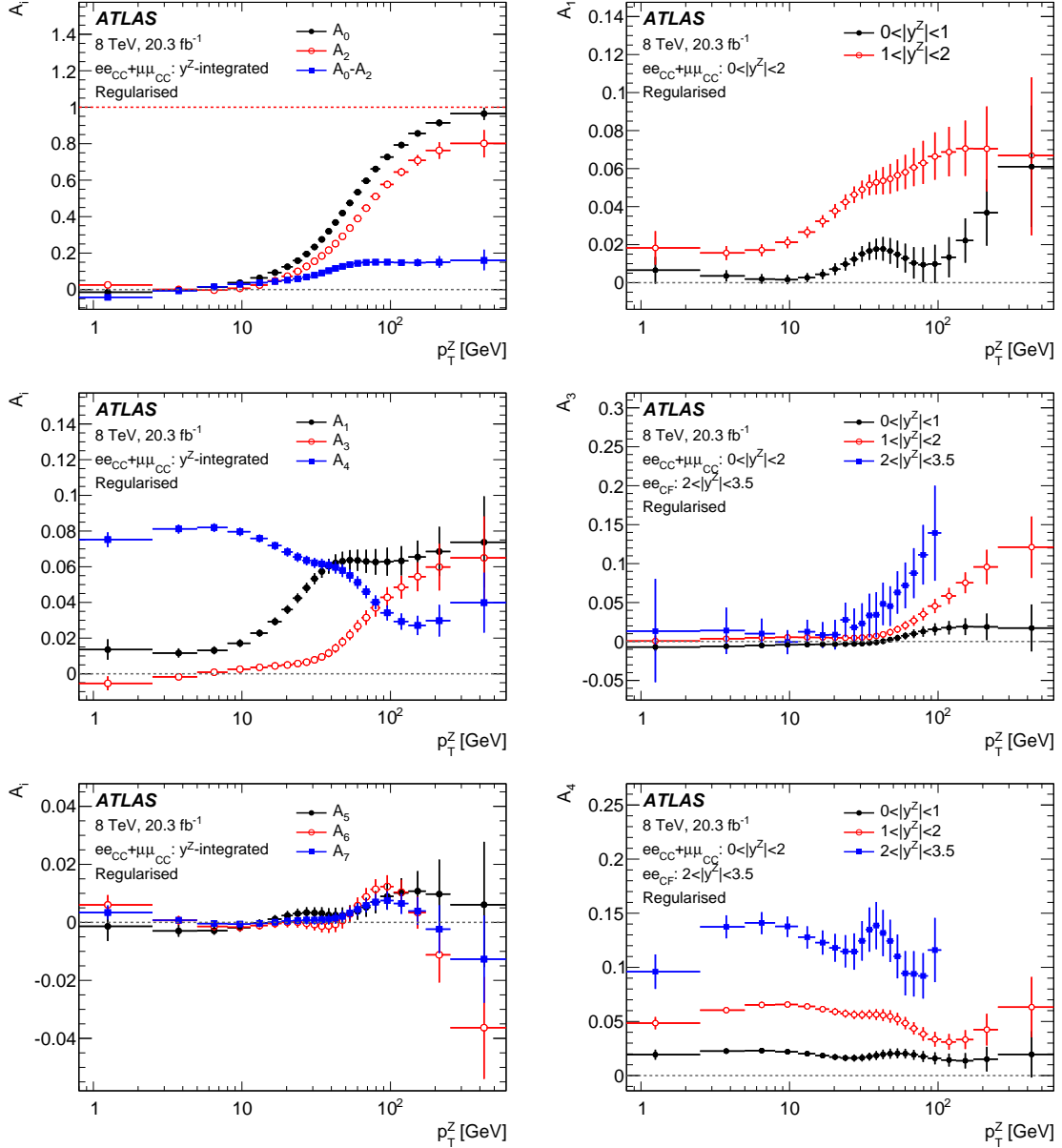


Figure 11: Measurements of the angular coefficients in the y^Z -integrated and y^Z -binned configurations versus p_T^Z . Among the y^Z -integrated configurations, are shown $A_{0,2}$ and $A_0 - A_2$ (top left), $A_{1,3,4}$ (middle left), and $A_{5,6,7}$ (bottom left). The y^Z -binned A_i are overlayed in each accessible y^Z bin for A_1 (top right), A_3 (middle right), and A_4 (bottom right). The error bars represent the total uncertainty in the measurements.

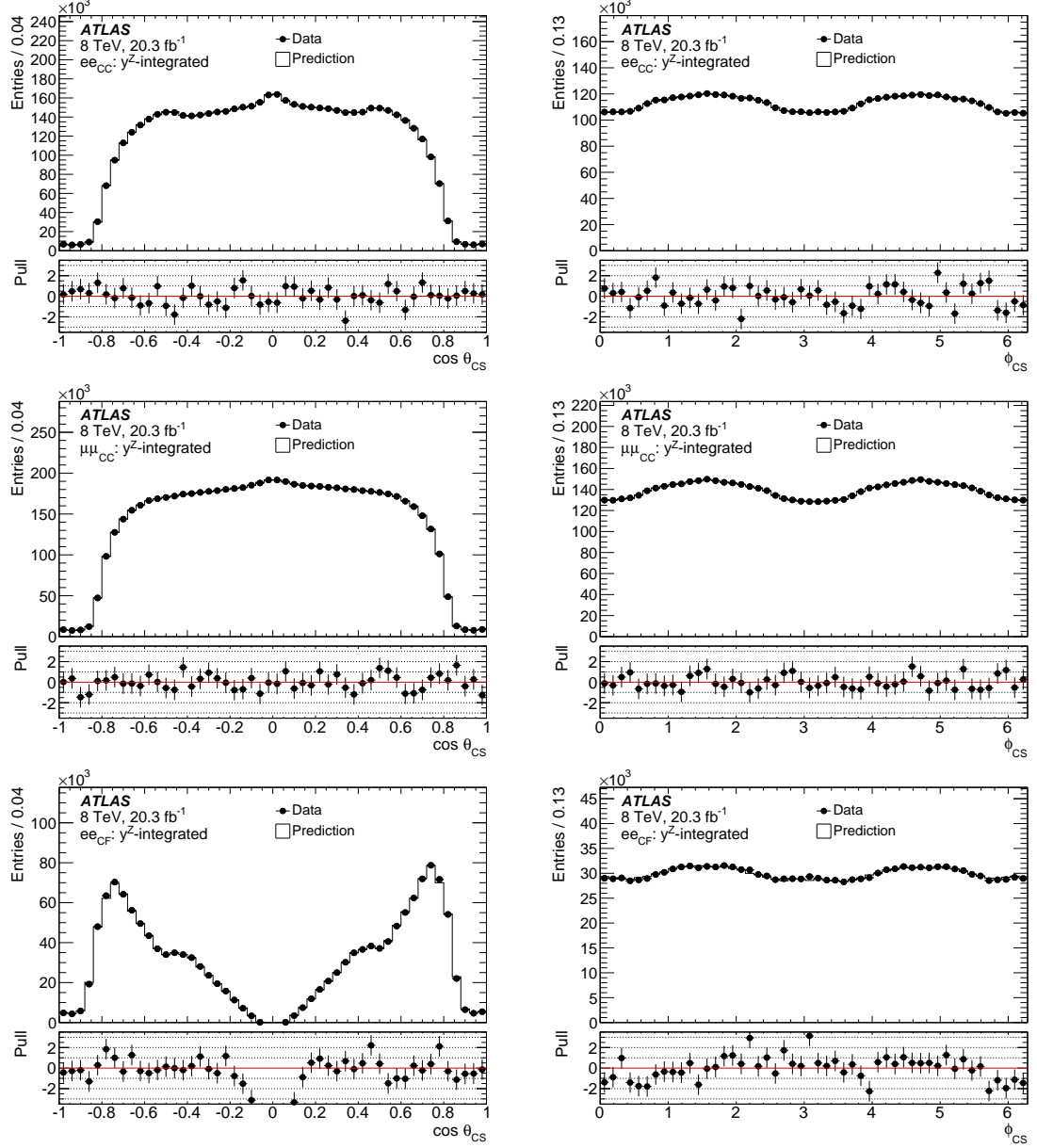


Figure 12: Reweighted $\cos \theta_{CS}$ (left) and ϕ_{CS} (right) distribution integrated over y^Z in the ee_{CC} (top), $\mu\mu_{CC}$ (middle), and ee_{CF} (bottom) channels and the corresponding pulls of the distributions after reweighting them predictions to data. The pulls are computed using the full statistical and systematic uncertainties. Two points in the bottom-left pull plot near $\cos \theta_{CS} = 0$ fall below the range shown, but the number of events in these two bins is very small.

Table 9: Summary of the measured coefficients in the $ee_{\text{CC}} + \mu\mu_{\text{CC}}$ y^Z -integrated channel at low (5–8 GeV), mid (22–25.5 GeV), and high (132–173 GeV) p_T^Z . The uncertainties are given as $\pm(\text{stat.}) \pm (\text{syst.})$.

$ y^Z $ -integrated measurements			
p_T^Z range [GeV]	A_0	A_2	$A_0 - A_2$
5.0–8.0	$0.015 \pm 0.002 \pm 0.007$	$-0.003 \pm 0.003 \pm 0.003$	$0.018 \pm 0.003 \pm 0.007$
22.0–25.5	$0.159 \pm 0.003 \pm 0.007$	$0.100 \pm 0.003 \pm 0.003$	$0.059 \pm 0.005 \pm 0.006$
132–173	$0.856 \pm 0.008 \pm 0.008$	$0.708 \pm 0.022 \pm 0.020$	$0.148 \pm 0.019 \pm 0.011$
p_T^Z range [GeV]	A_1	A_3	A_4
5.0–8.0	$0.013 \pm 0.002 \pm 0.002$	$0.001 \pm 0.001 \pm 0.001$	$0.082 \pm 0.001 \pm 0.002$
22.0–25.5	$0.042 \pm 0.002 \pm 0.002$	$0.006 \pm 0.001 \pm 0.001$	$0.065 \pm 0.002 \pm 0.002$
132–173	$0.065 \pm 0.008 \pm 0.005$	$0.054 \pm 0.007 \pm 0.003$	$0.027 \pm 0.005 \pm 0.002$
p_T^Z range [GeV]	A_5	A_6	A_7
5.0–8.0	$-0.002 \pm 0.001 \pm 0.001$	$-0.001 \pm 0.001 \pm 0.001$	$0.000 \pm 0.001 \pm 0.001$
22.0–25.5	$0.003 \pm 0.002 \pm 0.001$	$0.000 \pm 0.002 \pm 0.001$	$0.001 \pm 0.001 \pm 0.001$
132–173	$0.011 \pm 0.006 \pm 0.003$	$0.003 \pm 0.005 \pm 0.002$	$0.004 \pm 0.004 \pm 0.002$

After reweighting the signal MC events to the measured parameters, the global fit quality is evaluated by computing the χ^2 of the data with respect to the sum of expected events in each bin used in the likelihood fit. This test takes into account data statistical and MC statistical uncertainties, but not other systematic effects. The resulting χ^2 values for all channels are consistent with expectations across all y^Z configurations.

The best-fit values of each nuisance parameter along with their post-fit constraints are checked. Most parameters have a fit value close to zero with a constraint close to unity. It was also checked that the regularisation procedure does not significantly change the best-fit value or post-fit constraint of the nuisance parameters.

Finally, the degree to which the data follow the nine- P_i polynomial decomposition is tested by checking for the presence of higher-order P_i in the data. The original nine P_i are up to second order in spherical harmonics. The template-building methodology described in Section 5.1 is extended to have more than nine P_i by using third- and fourth-order spherical harmonics, corresponding to 16 additional P_i . One additional P_i template is fitted at a time. The higher-order coefficients are found to be compatible with zero using a χ^2 test as in Section 7.1, leading to the conclusion that any possible breaking of the nine P_i polynomial decomposition is beyond the sensitivity of the analysis.

8. Comparisons with theory

In this section, the measurements are compared to the most precise fixed-order calculations currently available. They probe the dynamics of perturbative QCD, including the presence of higher-order corrections, and explore the effects from the $V-A$ structure of Z -boson couplings. These comparisons are made with both the y^Z -integrated and y^Z -binned measurements. For the y^Z -integrated measurements and for the $0 < |y^Z| < 1$ and $1 < |y^Z| < 2$ bins, the combined ee_{CC} and $\mu\mu_{\text{CC}}$ measurements are used, while the ee_{CF} measurements are used for the $2 < |y^Z| < 3.5$ bin. In all cases, the regularised uncertainties described

Table 10: Summary of the measured coefficients in the $ee_{\text{CC}} + \mu\mu_{\text{CC}}$ channel for the two bins $0 < |y^Z| < 1$ and $1 < |y^Z| < 2$ and in the ee_{CF} channel for the $2 < |y^Z| < 3.5$ bin at low (5–8 GeV), mid (22–25.5 GeV), and high (132–173 GeV) p_T^Z . The uncertainties are given as $\pm(\text{stat.}) \pm (\text{syst.})$.

$ y^Z $ -binned measurements			
A_1			
p_T^Z range [GeV]	$0 < y^Z < 1$	$1 < y^Z < 2$	$2 < y^Z < 3.5$
5.0–8.0	$0.002 \pm 0.002 \pm 0.001$	$0.017 \pm 0.002 \pm 0.002$	
22.0–25.5	$0.010 \pm 0.003 \pm 0.002$	$0.042 \pm 0.003 \pm 0.002$	
132–173	$0.022 \pm 0.010 \pm 0.006$	$0.071 \pm 0.013 \pm 0.007$	
A_3			
p_T^Z range [GeV]	$0 < y^Z < 1$	$1 < y^Z < 2$	$2 < y^Z < 3.5$
5.0–8.0	$-0.005 \pm 0.001 \pm 0.001$	$0.005 \pm 0.002 \pm 0.001$	$0.005 \pm 0.002 \pm 0.001$
22.0–25.5	$-0.003 \pm 0.002 \pm 0.001$	$0.005 \pm 0.002 \pm 0.001$	$0.005 \pm 0.002 \pm 0.001$
132–173	$0.019 \pm 0.010 \pm 0.004$	$0.075 \pm 0.012 \pm 0.006$	
A_4			
p_T^Z range [GeV]	$0 < y^Z < 1$	$1 < y^Z < 2$	$2 < y^Z < 3.5$
5.0–8.0	$0.023 \pm 0.002 \pm 0.001$	$0.065 \pm 0.002 \pm 0.001$	$0.065 \pm 0.002 \pm 0.001$
22.0–25.5	$0.016 \pm 0.003 \pm 0.001$	$0.057 \pm 0.003 \pm 0.002$	$0.057 \pm 0.003 \pm 0.002$
132–173	$0.014 \pm 0.006 \pm 0.003$	$0.033 \pm 0.008 \pm 0.004$	

in Section 5 are used for the data. The measurements are also compared to various event generators, in particular to probe different parton-shower models and event-generator implementations.

The overlays of the y^Z -integrated measurements are shown in Figs. 13–15 for all coefficients. The calculations from DYNNLO are shown at NNLO for $p_T^Z > 2.5$ GeV with their uncertainties computed as a sum in quadrature of statistical, QCD scale, and PDF uncertainties, as described in Section 2. The Powheg + MiNLO predictions, which are shown only including statistical uncertainties, were obtained using the $Z + \text{jet}$ process at NLO [43] over the full p_T^Z range. Owing to numerical issues in the phase-space integration, the Powheg + MiNLO results show fluctuations beyond their statistical uncertainties. The formal accuracy of both calculations is the same, namely $O(\alpha_s)$ for the predictions of the A_i coefficients as a function of p_T^Z . The left-hand plots in these figures illustrate the behaviour of each coefficient as a function of p_T^Z , while the right-hand plots, in which the data measurements are used as a reference, show to which extent the various theoretical predictions agree with the data. In the very first p_T^Z bin, ϕ_{CS} has poor resolution and therefore suffers from larger measurement uncertainties. This is reflected in the deviation from the prediction in A_2 , for example, which is derived primarily from ϕ_{CS} .

The predictions from the DYNNLO and Powheg + MiNLO calculations agree with the data within uncertainties for most coefficients. The striking exception is the A_2 coefficient, which rises more slowly as p_T^Z increases in the data than in the calculations. The data confirm that the Lam–Tung relation ($A_0 - A_2 = 0$) does not hold at $O(\alpha_s^2)$. For $p_T^Z > 50$ GeV, significant deviations from zero, almost a factor of two larger than those predicted by the calculations, are observed. Since the impact of the PDF uncertainties on the calculations is very small, these deviations must be due to higher-order QCD effects.

In the case of the $A_{5,6,7}$ coefficients, the trend towards non-zero values at high p_T^Z discussed in Section 7 is also compatible with that from the predictions, although it is at the limit of the sensitivity for both

the data and the calculations. As shown in Fig. 15 and also in Table 1, the predictions from DYNNLO suggest that the values of the $A_{5,6,7}$ coefficients should be at the level of 0.005 at high values of p_T^Z . A test is performed to quantify the significance of the deviation from zero (see Appendix E). A signed χ^2 test statistic is defined based on the tail probability of each individual measurement, taking into account the correlations between the parameters in bins of p_T^Z . An ensemble test is performed to compute the observed and expected significance of all three coefficients together, where pseudo-data from DYNNLO is used for the expected value. This test gives an observed (expected) significance of 3.0 (3.2) standard deviations.

The measurements of the A_1 , A_3 , and A_4 coefficients in the three y^Z bins (only the first two bins are available for the A_1 coefficient) are compared to the predictions in Figs. 16–18. Overall, the predictions and the data agree for all three y^Z bins. These coefficients are the only ones that display any significant y^Z dependence and it is interesting to note that, for high values of p_T^Z , the A_1 and A_3 coefficients increase as y^Z increases. As explained in Section 1 and detailed in Appendix A, at low values of p_T^Z , the measured value of the A_4 coefficient can be directly related to the Weinberg angle $\sin^2 \theta_W$ [62]. The strong dependence of the value of the A_4 coefficient on $|y^Z|$ is, however, mostly a consequence of the approximation made for the interacting quark direction in the CS reference frame on an event-by-event basis. The impact of this approximation decreases at higher values of $|y^Z|$, and, as a result, the measured and expected values of the A_4 coefficient increase, as can be seen in Figs. 16 – 18.

The effect of the parton-shower modelling and matching scheme on the reference angular coefficients is explored in Fig. 19, which shows a comparison of the measurements of A_0 , A_1 , A_2 , and $A_0 - A_2$ with DYNNLO at NLO and NNLO, PowHEGBox (without parton shower), and with the same process in PowHEGBox with the parton shower simulated with PYTHIA 8 (POWHEGBOX + PYTHIA 8) and HERWIG (POWHEGBOX + HERWIG). The predictions from DYNNLO at NLO and PowHEGBox without parton shower, which are formally at the same level of accuracy, agree for A_1 and A_2 . For the A_2 coefficient, which is the most sensitive one to higher-order corrections, adding the parton-shower simulation to the PowHEGBox Z-boson production process brings the predictions closer to DYNNLO at NNLO. This is consistent with the assumption that the parton-shower model emulates higher-order effects, although the discrepancy between the measurements and the parton-shower models is larger than that with DYNNLO at NNLO. The A_0 coefficient has an unexpected offset of -0.025 at low values of p_T^Z in the PowHEGBox implementation. This effect is also reflected in the predictions for $A_0 - A_2$ and has been corrected in the more recent version of PowHEGBox (v2.1) used in this paper for the $Z +$ jet predictions with POWHEG + MiNLO [14–17]. The predictions from DYNNLO at NLO and NNLO agree well with the data measurements for the A_0 coefficient, but overestimate the rise of the A_2 coefficient at higher values of p_T^Z , as discussed above. Finally, it is interesting to note that, whereas the agreement between PYTHIA 8 and HERWIG is good for most of the coefficients, the A_1 coefficient displays significant differences between the two predictions over most of the p_T^Z range. Although this might be ascribed to differences between the parton-shower model and matching schemes at intermediate values of p_T^Z , it is somewhat surprising to observe large differences for the highest values of p_T^Z .

Figure 20 shows a comparison of the measurements of A_0 , A_2 and $A_0 - A_2$ with SHERPA 1.4 (up to five jets at LO) and SHERPA 2.1 [39–42]. The effect of simulating SHERPA 2.1 events (up to two jets at NLO and up to five jets at LO for higher jet multiplicities) is explicitly shown. None of the configurations correctly predict the behaviour of A_0 or A_2 . The SHERPA 2.1 version follows the data more closely than the SHERPA 1.4 version. In addition, in all versions except SHERPA 2.1 with two jets, significant higher-order polynomial behaviour was found to be present. This is probably due to the matrix-element matching scheme used in the event generator for the calculation of the $Z + n$ -jet process for $n > 2$.

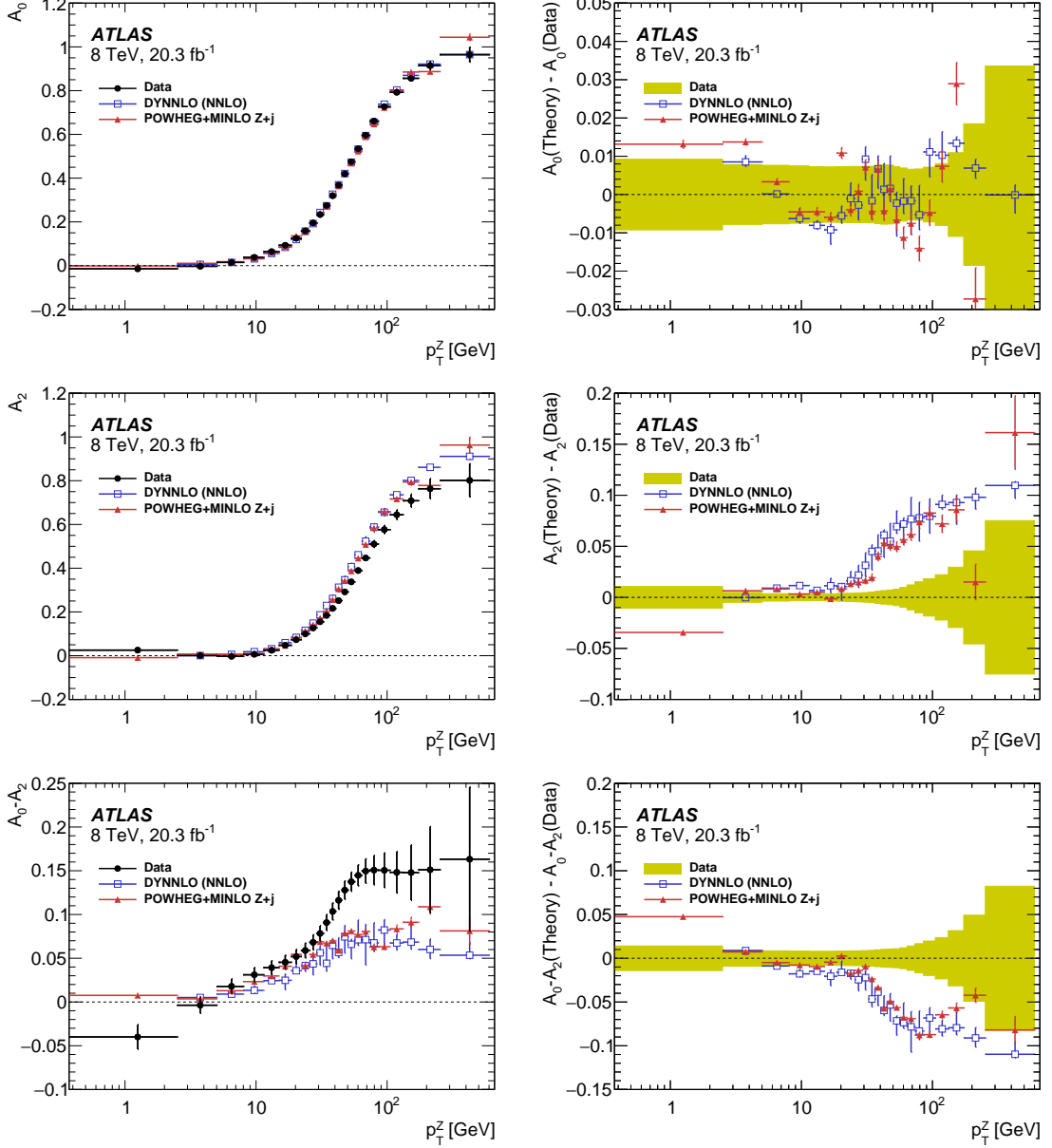


Figure 13: Distributions of the angular coefficients A_0 (top), A_2 (middle) and $A_0 - A_2$ (bottom) as a function of p_T^Z . The results from the y^Z -integrated measurements are compared to the DYNNLO and Powheg MiNLO predictions (left). The differences between the two calculations and the data are also shown (right), with the shaded band around zero representing the total uncertainty in the measurements. The error bars for the calculations show the total uncertainty for DYNNLO, but only the statistical uncertainties for Powheg MiNLO (see text).

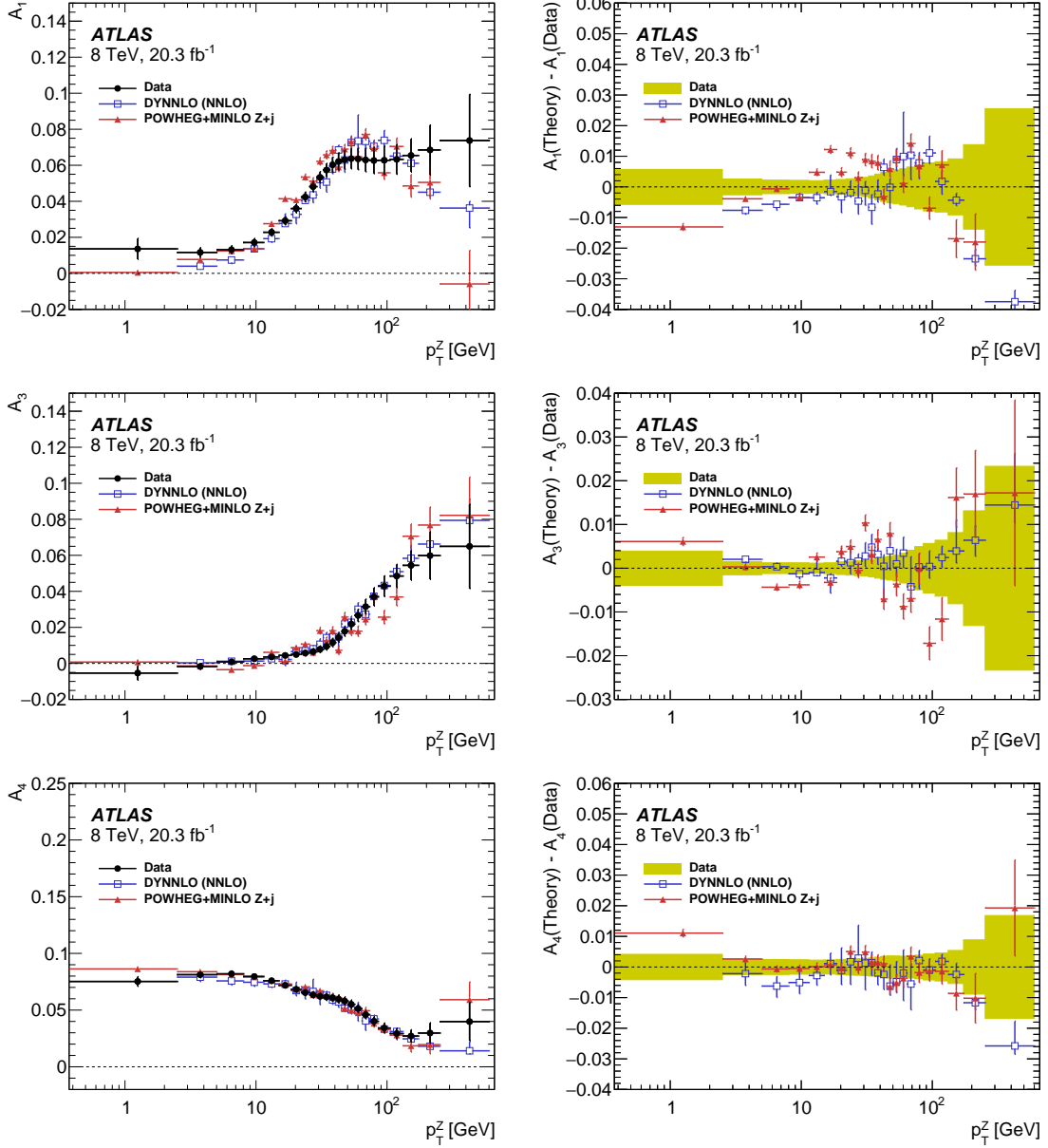


Figure 14: Distributions of the angular coefficients A_1 (top), A_3 (middle) and A_4 (bottom) as a function of p_T^Z . The results from the y^Z -integrated measurements are compared to the DYNNLO and Powheg MiNLO predictions (left). The differences between the two calculations and the data are also shown (right), with the shaded band around zero representing the total uncertainty in the measurements. The error bars for the calculations show the total uncertainty for DYNNLO, but only the statistical uncertainties for Powheg MiNLO (see text).

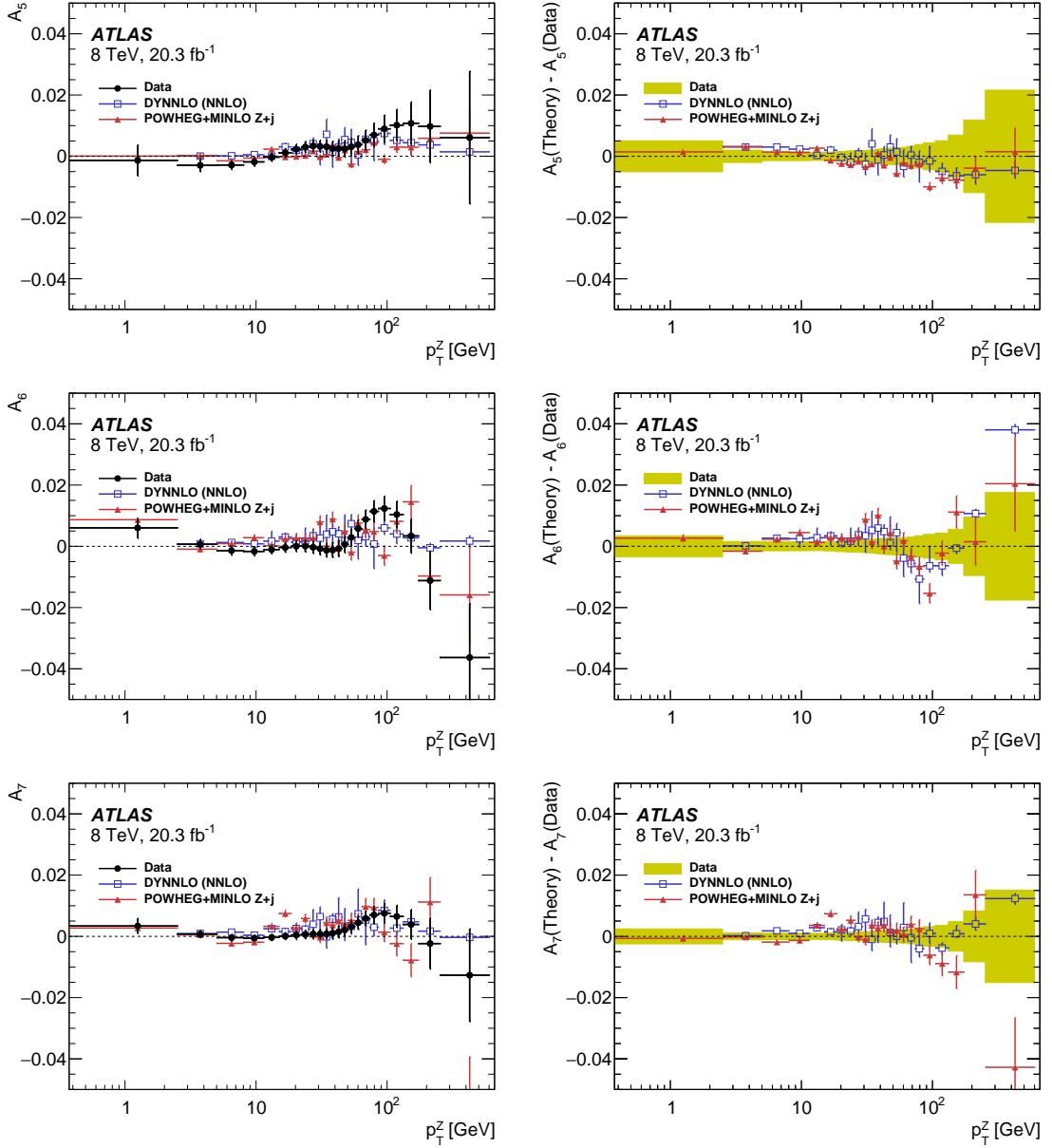


Figure 15: Distributions of the angular coefficients A_5 (top), A_6 (middle) and A_7 (bottom) as a function of p_T^Z . The results from the y^Z -integrated measurements are compared to the DYNNLO and Powheg MiNLO predictions (left). The differences between the two calculations and the data are also shown (right), with the shaded band around zero representing the total uncertainty in the measurements. The error bars for the calculations show the total uncertainty for DYNNLO, but only the statistical uncertainties for Powheg MiNLO (see text).

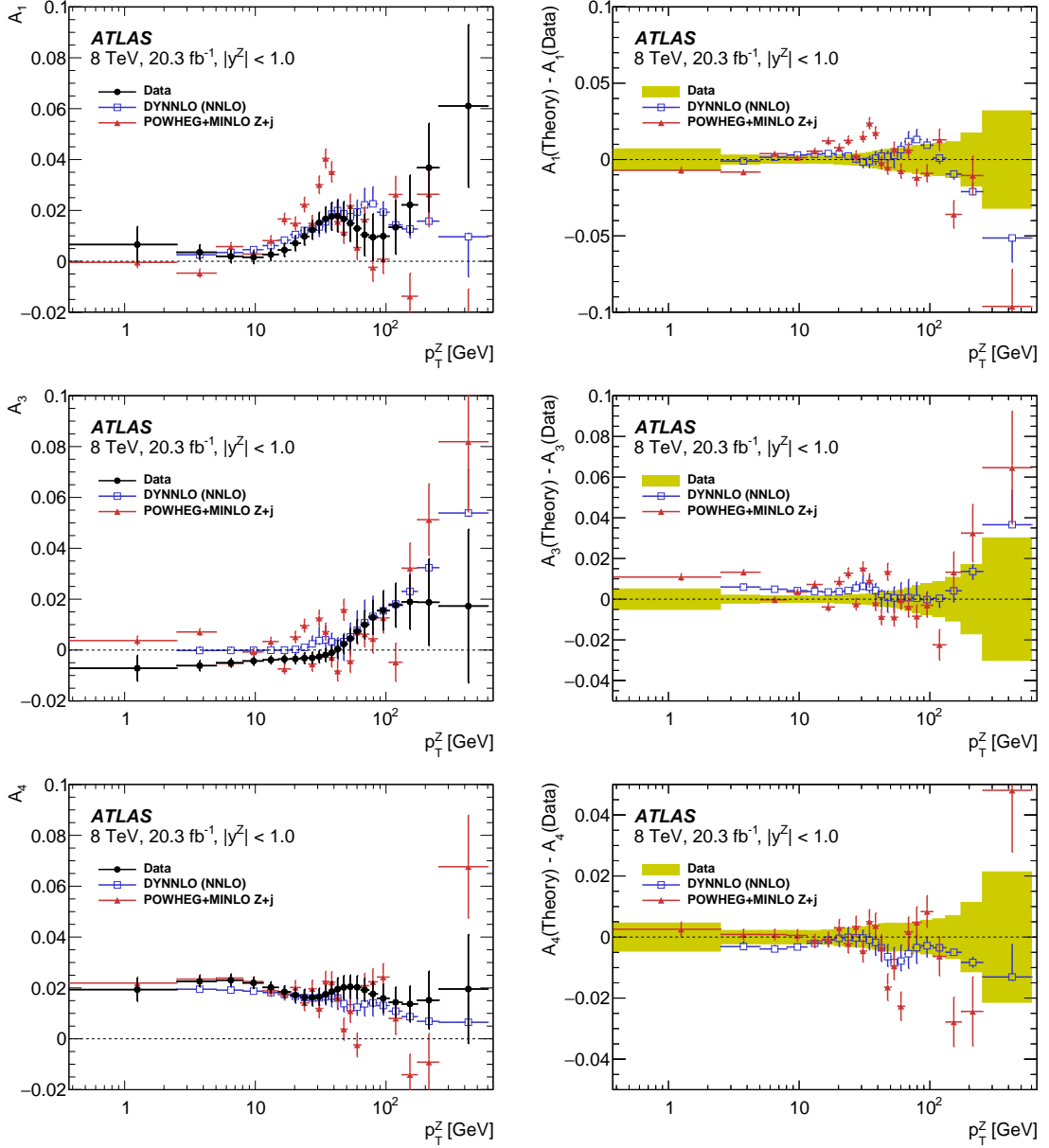


Figure 16: Distributions of the angular coefficients A_1 (top), A_3 (middle) and A_4 (bottom) as a function of p_T^Z for $0 < |y^Z| < 1$. The results from the measurements are compared to the DYNNLO and Powheg MiNLO predictions (left). The differences between the two calculations and the data are also shown (right), with the shaded band around zero representing the total uncertainty in the measurements. The error bars for the calculations show the total uncertainty for DYNNLO, but only the statistical uncertainties for Powheg MiNLO (see text).

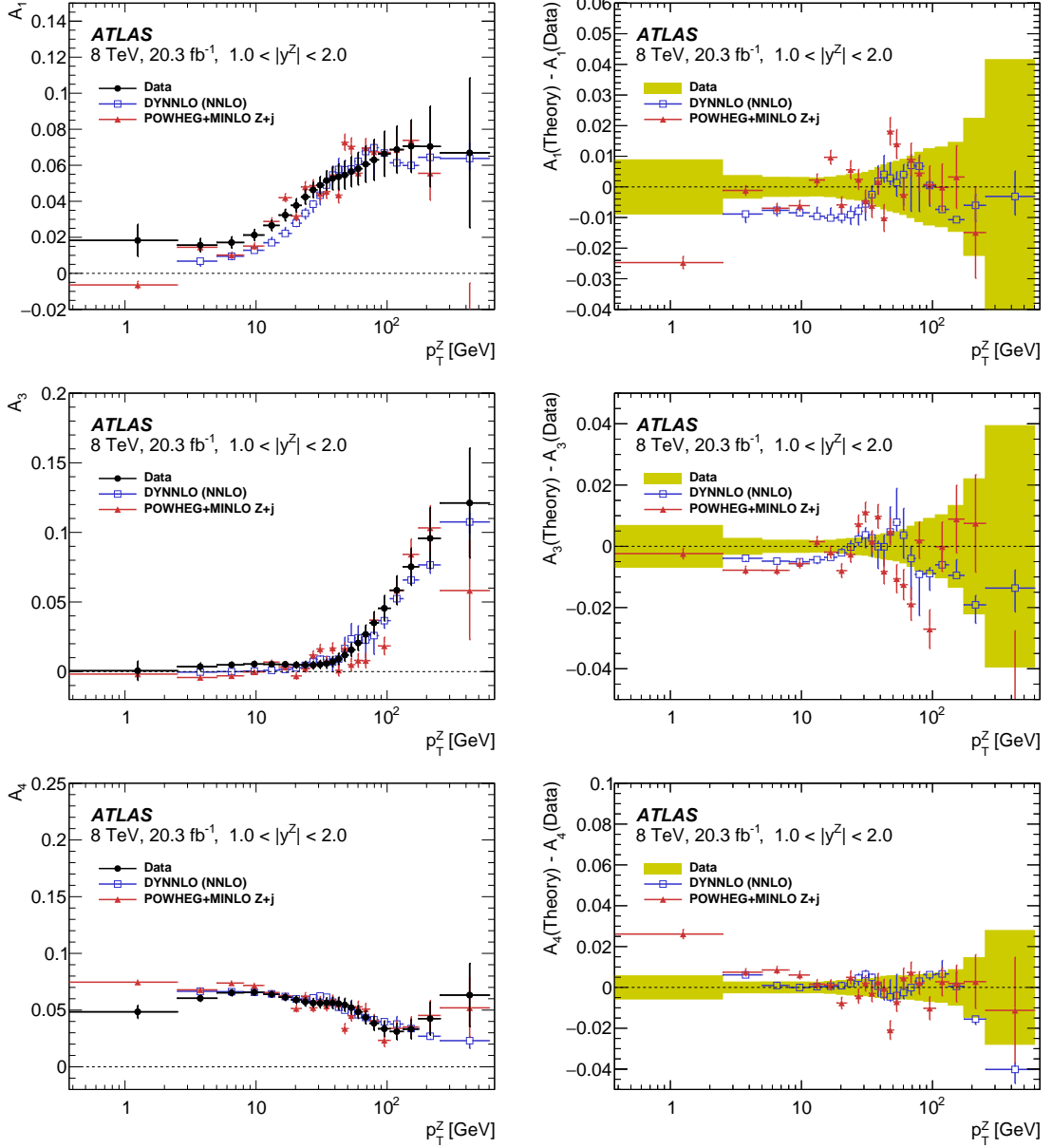


Figure 17: Distributions of the angular coefficients A_1 (top), A_3 (middle) and A_4 (bottom) as a function of p_T^Z for $1 < |y^Z| < 2$. The results from the measurements are compared to the DYNNLO and Powheg MiNLO predictions (left). The differences between the two calculations and the data are also shown (right), with the shaded band around zero representing the total uncertainty in the measurements. The error bars for the calculations show the total uncertainty for DYNNLO, but only the statistical uncertainties for Powheg MiNLO (see text).

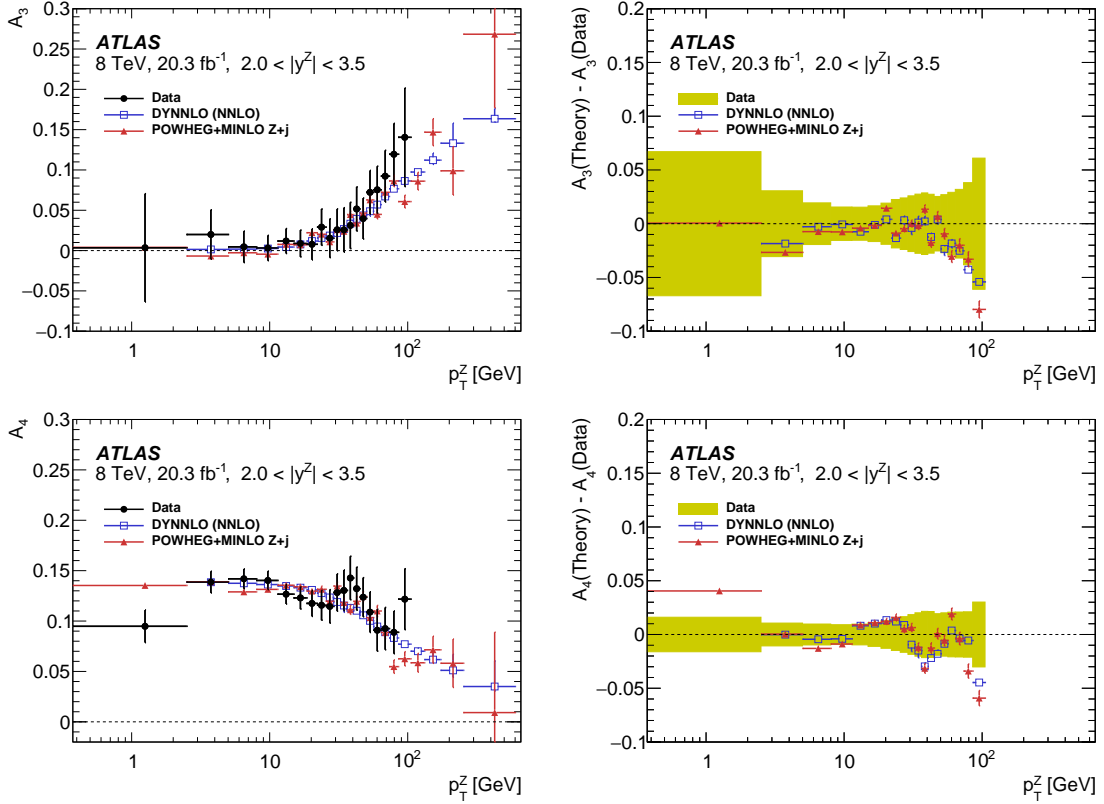


Figure 18: Distributions of the angular coefficients A_3 (top) and A_4 (bottom) as a function of p_T^Z for $2 < |y^Z| < 3.5$. The results from the measurements are compared to the DYNNNLO and Powheg MiNLO predictions (left). The differences between the two calculations and the data are also shown (right), with the shaded band around zero representing the total uncertainty in the measurements. The error bars for the calculations show the total uncertainty for DYNNNLO, but only the statistical uncertainties for Powheg MiNLO (see text).

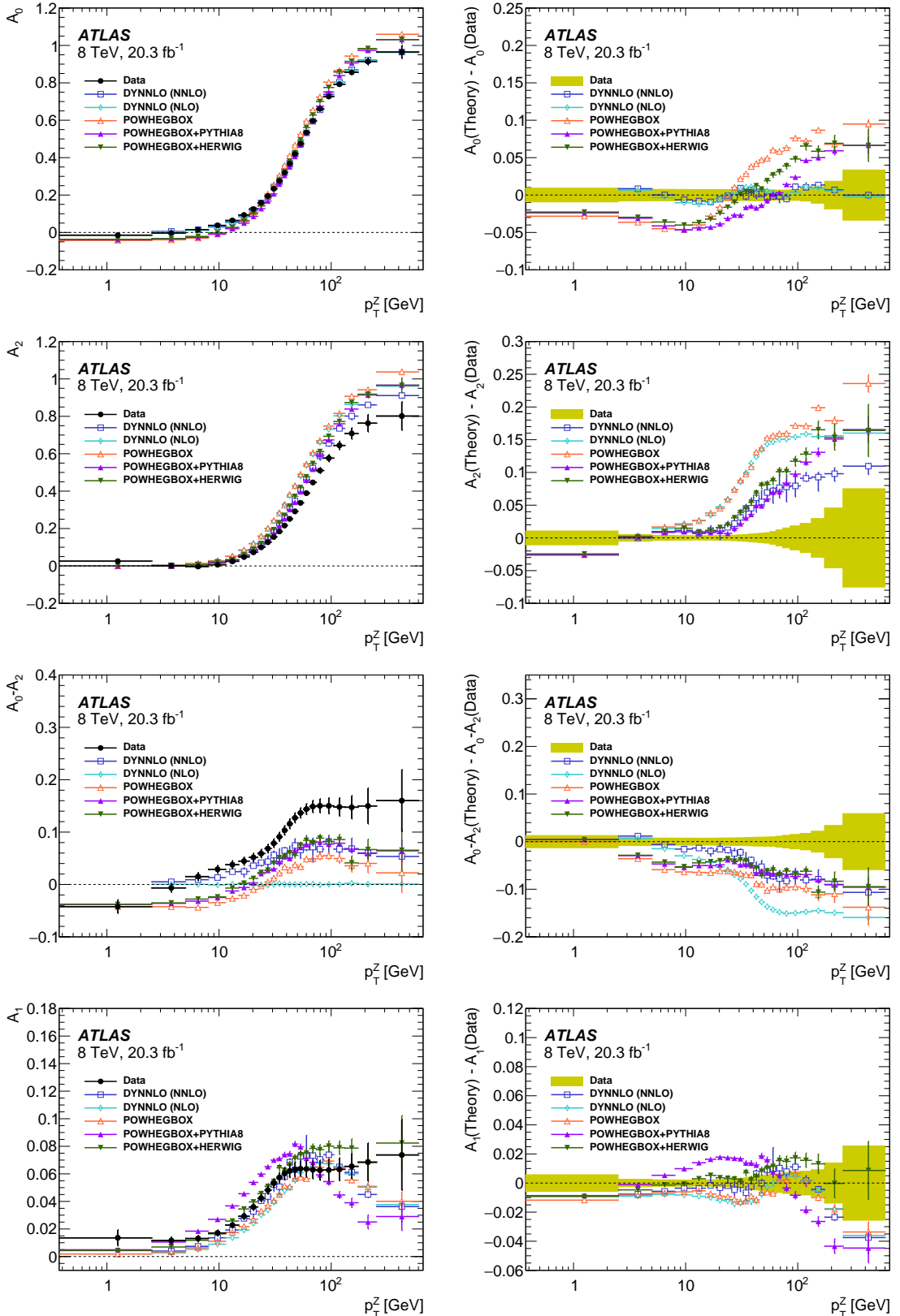


Figure 19: Distributions of the angular coefficients A_0 , A_2 , $A_0 - A_2$ and A_1 (from top to bottom) as a function of p_T^z . The results from the y^Z -integrated measurements are compared to the DYNNLO predictions at NLO and at NNLO, as well as to those from PowhegBox + Pythia8 and PowhegBox + Herwig (left). The differences between the calculations and the data are also shown (right), with the shaded band around zero representing the total uncertainty in the measurements. The error bars for the calculations show the total uncertainty for DYNNLO, but only the statistical uncertainties for PowhegBox.

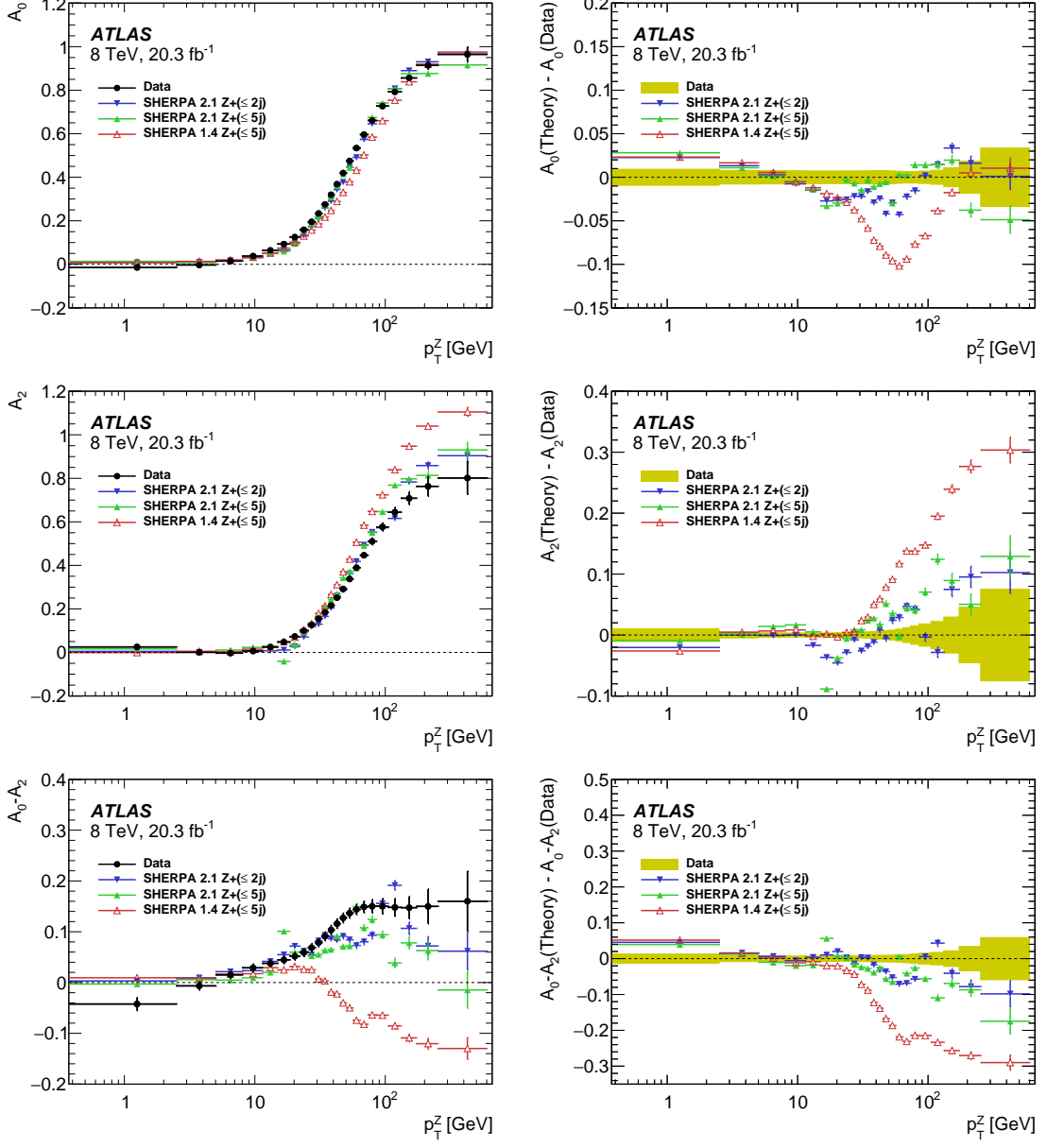


Figure 20: Distributions of the angular coefficients A_0 (top), A_2 (middle) and $A_0 - A_2$ (bottom) as a function of p_T^Z . The results from the y^Z -integrated measurements are compared to various predictions from the SHERPA event generator (left). The differences between the calculations and the data are also shown (right), with the shaded band around zero representing the total uncertainty in the measurements. The error bars for the SHERPA predictions represent only the statistical uncertainties.

9. Summary

This paper presents a precise set of measurements of the Z-boson production dynamics in the Z-boson pole region, through the angular distributions of the leptons. The data analysed correspond to 20.3 fb^{-1} of pp collisions at $\sqrt{s} = 8 \text{ TeV}$, collected by the ATLAS detector at the CERN LHC. The measurements are obtained as a function of p_T^Z , integrated over y^Z and in bins of y^Z , covering almost the full range of y^Z spanned by Z-boson production at $\sqrt{s} = 8 \text{ TeV}$. This is made possible by exploiting the decomposition of the production cross-section into nine terms, where in each term the angular coefficients that encapsulate the production dynamics are factorised from the decay dynamics described by angular polynomials. Templates of the nine polynomials folded to the detector level are fitted to the data to extract the angular coefficients in the full phase space of the Z boson.

Over most of the phase space, the measurements that are obtained from samples of electron and muon pairs covering respectively the ranges $0 < |y^Z| < 3.5$ and $0 < |y^Z| < 2.5$ are limited only by statistical uncertainties in the data. These uncertainties are small and range from 0.002 at low p_T^Z to 0.008 at $p_T^Z = 150 \text{ GeV}$. The experimental systematic uncertainties are much smaller in almost all cases. The theory systematic uncertainties are minimised through the template-building procedure, such that the PDF uncertainties, which are the dominant source of theoretical uncertainties, are below 0.004 in all cases.

The measurements, when compared to theoretical calculations and to predictions from MC generators, are precise enough to probe QCD corrections beyond the formal accuracy of the calculations. A significant deviation from the $\mathcal{O}(\alpha_s^2)$ predictions from DYNNLO is observed for $A_0 - A_2$, indicating that higher-order QCD corrections are required to describe the data. Evidence at the 3σ level is found for non-zero $A_{5,6,7}$ coefficients, consistent with expectations from DYNNLO at $\mathcal{O}(\alpha_s^2)$. The measurements also provide discrimination between various event generators, in particular in terms of the related implementation of different parton-shower models.

The measurements of the A_i coefficients, in particular through the correlation of the angular distributions with the lepton transverse momentum distributions, are thus an important ingredient to the next steps in precision measurements of electroweak parameters at the LHC, both for the effective weak mixing angle $\sin^2 \theta_W$ and for the W-boson mass.

Acknowledgements

We thank CERN for the very successful operation of the LHC, as well as the support staff from our institutions without whom ATLAS could not be operated efficiently.

We acknowledge the support of ANPCyT, Argentina; YerPhI, Armenia; ARC, Australia; BMWFW and FWF, Austria; ANAS, Azerbaijan; SSTC, Belarus; CNPq and FAPESP, Brazil; NSERC, NRC and CFI, Canada; CERN; CONICYT, Chile; CAS, MOST and NSFC, China; COLCIENCIAS, Colombia; MSMT CR, MPO CR and VSC CR, Czech Republic; DNRF and DNSRC, Denmark; IN2P3-CNRS, CEA-DSM/IRFU, France; GNSF, Georgia; BMBF, HGF, and MPG, Germany; GSRT, Greece; RGC, Hong Kong SAR, China; ISF, I-CORE and Benoziyo Center, Israel; INFN, Italy; MEXT and JSPS, Japan; CNRST, Morocco; FOM and NWO, Netherlands; RCN, Norway; MNiSW and NCN, Poland; FCT, Portugal; MNE/IFA, Romania; MES of Russia and NRC KI, Russian Federation; JINR; MESTD, Serbia; MSSR, Slovakia; ARRS and MIZŠ, Slovenia; DST/NRF, South Africa; MINECO, Spain; SRC and Wallenberg Foundation, Sweden; SERI, SNSF and Cantons of Bern and Geneva, Switzerland; MOST, Taiwan; TAEK, Turkey; STFC, United Kingdom; DOE and NSF, United States of America. In addition, individual groups and members have received support from BCKDF, the Canada Council, CANARIE, CRC, Compute Canada, FQRNT, and the Ontario Innovation Trust, Canada; EPLANET, ERC, FP7, Horizon 2020 and Marie Skłodowska-Curie Actions, European Union; Investissements d’Avenir Labex and Idex, ANR, Région Auvergne and Fondation Partager le Savoir, France; DFG and AvH Foundation, Germany; Herakleitos, Thales and Aristeia programmes co-financed by EU-ESF and the Greek NSRF; BSF, GIF and Minerva, Israel; BRF, Norway; Generalitat de Catalunya, Generalitat Valenciana, Spain; the Royal Society and Leverhulme Trust, United Kingdom.

The crucial computing support from all WLCG partners is acknowledged gratefully, in particular from CERN and the ATLAS Tier-1 facilities at TRIUMF (Canada), NDGF (Denmark, Norway, Sweden), CC-IN2P3 (France), KIT/GridKA (Germany), INFN-CNAF (Italy), NL-T1 (Netherlands), PIC (Spain), ASGC (Taiwan), RAL (UK) and BNL (USA) and in the Tier-2 facilities worldwide.

Appendix

A. Theoretical formalism

Following the notation in Ref. [3], the lepton–hadron correlations in the $pp \rightarrow Z \rightarrow \ell\ell$ process are described by the contraction of the lepton tensor $L_{\mu\nu}$ with the parton-level hadron tensor $H^{\mu\nu}$. The tensor $L_{\mu\nu}$ acts as an analyser of the structure of $H^{\mu\nu}$, which carries effective information about the polarisation of the Z boson mediating the interaction. The angular dependence can be elucidated by introducing nine helicity density matrix elements

$$H_{mm'} = \epsilon_\mu^*(m) H^{\mu\nu} \epsilon_\nu(m') \quad (12)$$

where $m, m' = +, 0, -$ and

$$\epsilon_\mu(\pm) = \frac{1}{\sqrt{2}}(0; \pm 1, -i, 0), \quad \epsilon_\mu(0) = (0; 0, 0, 1) \quad (13)$$

are the polarisation vectors for the Z boson, defined with respect to its rest frame. The angular dependence of the differential cross-section can be written as:

$$\frac{d\sigma}{dp_T^Z dy^Z dm^Z d\cos\theta d\phi} = \sum_{\alpha \in M} g^\alpha(\theta, \phi) \frac{3}{16\pi} \frac{d\sigma^\alpha}{dp_T^Z dy^Z dm^Z}, \quad M = \{U + L, L, T, I, P, A, 7, 8, 9\}, \quad (14)$$

where the $g^\alpha(\theta, \phi)$ are second-order harmonic polynomials, multiplied by normalisation constants. The helicity cross-sections σ^α are linear combinations of the helicity density matrix elements $H_{mm'}$:

$$\begin{aligned} \sigma^{U+L} &\propto H_{00} + H_{++} + H_{--} \\ \sigma^L &\propto H_{00} \\ \sigma^T &\propto 1/2(H_{+-} + H_{-+}) \\ \sigma^I &\propto 1/4(H_{+0} + H_{0+} - H_{-0} - H_{0-}) \\ \sigma^P &\propto H_{++} - H_{--} \\ \sigma^A &\propto 1/4(H_{+0} + H_{0+} + H_{-0} + H_{0-}) \\ \sigma^7 &\propto -i/2(H_{+-} - H_{-+}) \\ \sigma^8 &\propto -i/4(H_{+0} - H_{0+} + H_{-0} - H_{0-}) \\ \sigma^9 &\propto -i/4(H_{+0} - H_{0+} - H_{-0} + H_{0-}). \end{aligned} \quad (15)$$

The unpolarised cross-section is denoted historically by σ^{U+L} , whereas $\sigma^{L,T,I,P,A,7,8,9}$ characterise the Z -boson polarisation. Respectively, these are the contributions to the Z -boson cross-section from longitudinally and transversely polarised states, transverse-longitudinal interference, etc., as described in Ref. [2].

The individual helicity cross-sections depend on the coupling coefficients of the Z boson as follows:

$$\begin{aligned} \sigma^{U+L,L,T,I} &\propto (v_\ell^2 + a_\ell^2)(v_\ell^2 + a_q^2) \\ \sigma^{P,A} &\propto v_\ell a_\ell v_q a_q \\ \sigma^{7,8} &\propto (v_\ell^2 + a_\ell^2)(v_q a_q) \\ \sigma^9 &\propto v_\ell a_\ell (v_q^2 + a_q^2), \end{aligned}$$

where $v_q(v_\ell)$ and $a_q(a_\ell)$ denote the vector and axial-vector coupling of the Z boson to the quarks (leptons). The cross-sections $\sigma^{U+L,L,T,I,9}$ receive contributions from the parity-conserving component of the hadron tensor, while the others, $\sigma^{P,A,7,8}$, are proportional to the parity-violating component of $H^{\mu\nu}$. However, the angular polynomials $g^{P,A,9}(\theta, \phi)$ are parity-violating as well, so contributions to the angular distributions from $\sigma^{U+L,L,T,I,P,A}$ are parity-conserving.

It is standard notation to factorise out the unpolarised cross-section, and to present the five-dimensional differential cross-section as an expansion in harmonic polynomials $P_i(\cos\theta, \phi)$ and dimensionless angular coefficients A_{0-7} , which represent ratios of helicity cross-sections with respect to the unpolarised one, as follows:

$$\begin{aligned}
A_0 &= 2d\sigma^L/d\sigma^{U+L} \\
A_1 &= 2\sqrt{2}d\sigma^I/d\sigma^{U+L} \\
A_2 &= 4d\sigma^T/d\sigma^{U+L} \\
A_3 &= 4\sqrt{2}d\sigma^A/d\sigma^{U+L} \\
A_4 &= 2d\sigma^P/d\sigma^{U+L} \\
A_5 &= 2d\sigma^7/d\sigma^{U+L} \\
A_6 &= 2\sqrt{2}d\sigma^8/d\sigma^{U+L} \\
A_7 &= 4\sqrt{2}d\sigma^9/d\sigma^{U+L}.
\end{aligned} \tag{16}$$

This leads to Eq. (1), as discussed in Section 1.

B. Additional Templates

To expand upon the one-dimensional templates shown in Section 5, the two-dimensional versions are shown here. The dimension corresponding to migrations in $p_T^{\ell\ell}$ is integrated over. Figures 21–23 show each analytical polynomial for each corresponding coefficient along with the templated versions in three representative p_T^Z bins after acceptance and selection requirements. The differences between the analytical polynomials and their templates reflect primarily the effect of the acceptance shape in the angular variables, and to a lesser extent resolution effects.

C. Regularisation

The migration of events between p_T^Z bins leads to anti-correlations between the measured A_i in neighbouring p_T^Z bins which enhance the effects of statistical fluctuations. To mitigate this effect and aid in resolving the underlying structure of the A_i spectra, the A_i coefficients are regularised by imposing a Gaussian penalty term on the significance of their higher-order derivatives with respect to p_T^Z . This penalty multiplies the likelihood in Eq. (8).

The exact derivative order is chosen based on the expected reduction in statistical uncertainties of the measurement and the potential bias that the regularisation scheme may introduce. The smaller statistical uncertainties come with increased positive correlation between neighbouring coefficients. The n^{th} derivative of A_{ij} is defined as:

$$A_{ij}^{(n)} = \begin{cases} A_{i,j}^{(n-1)} - A_{i,j-1}^{(n-1)}, & n \text{ odd} \\ A_{i,j+1}^{(n-1)} - A_{i,j}^{(n-1)}, & n \text{ even}, \end{cases} \tag{17}$$

where $A_{ij}^{(0)} \equiv A_{ij}$. The derivatives are staggered between even and odd orders in order to create a derivative definition more symmetric around each p_T^Z bin.

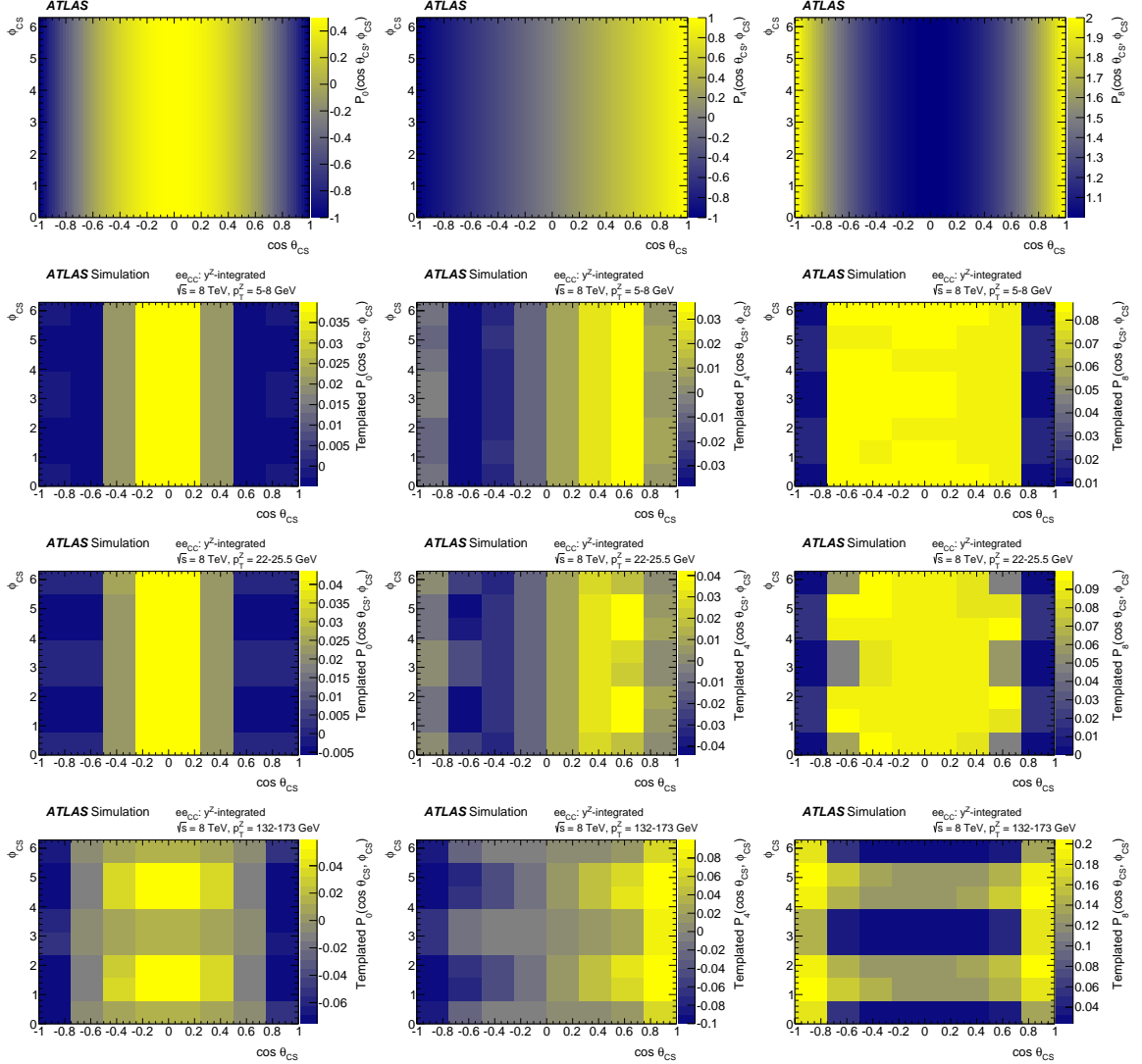


Figure 21: Shapes of the polynomials $P_{0,4,8}$ as a function of $\cos \theta_{\text{CS}}$ and ϕ_{CS} (top). Below these are the templated polynomials for the y^Z -integrated ee_{CC} events at low ($5-8$ GeV), medium ($22-25.5$ GeV), and high ($132-173$ GeV) values of p_T^Z .

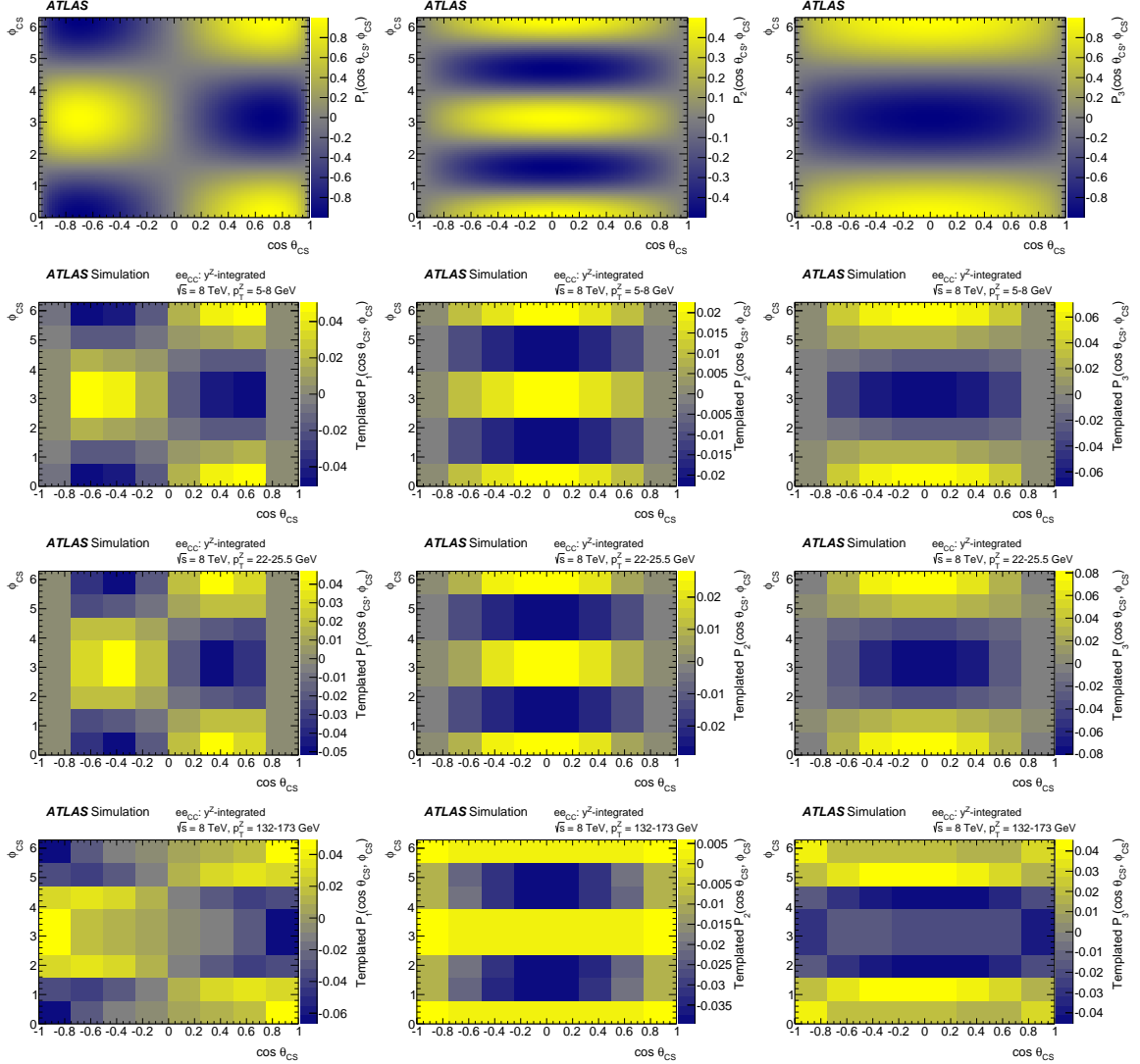


Figure 22: Shapes of the polynomials $P_{1,2,3}$ as a function of $\cos \theta_{\text{CS}}$ and ϕ_{CS} (top). Below these are the templated polynomials for the y^Z -integrated ee_{CC} events at low ($5-8$ GeV), medium ($22-25.5$ GeV), and high ($132-173$ GeV) values of p_T^Z .

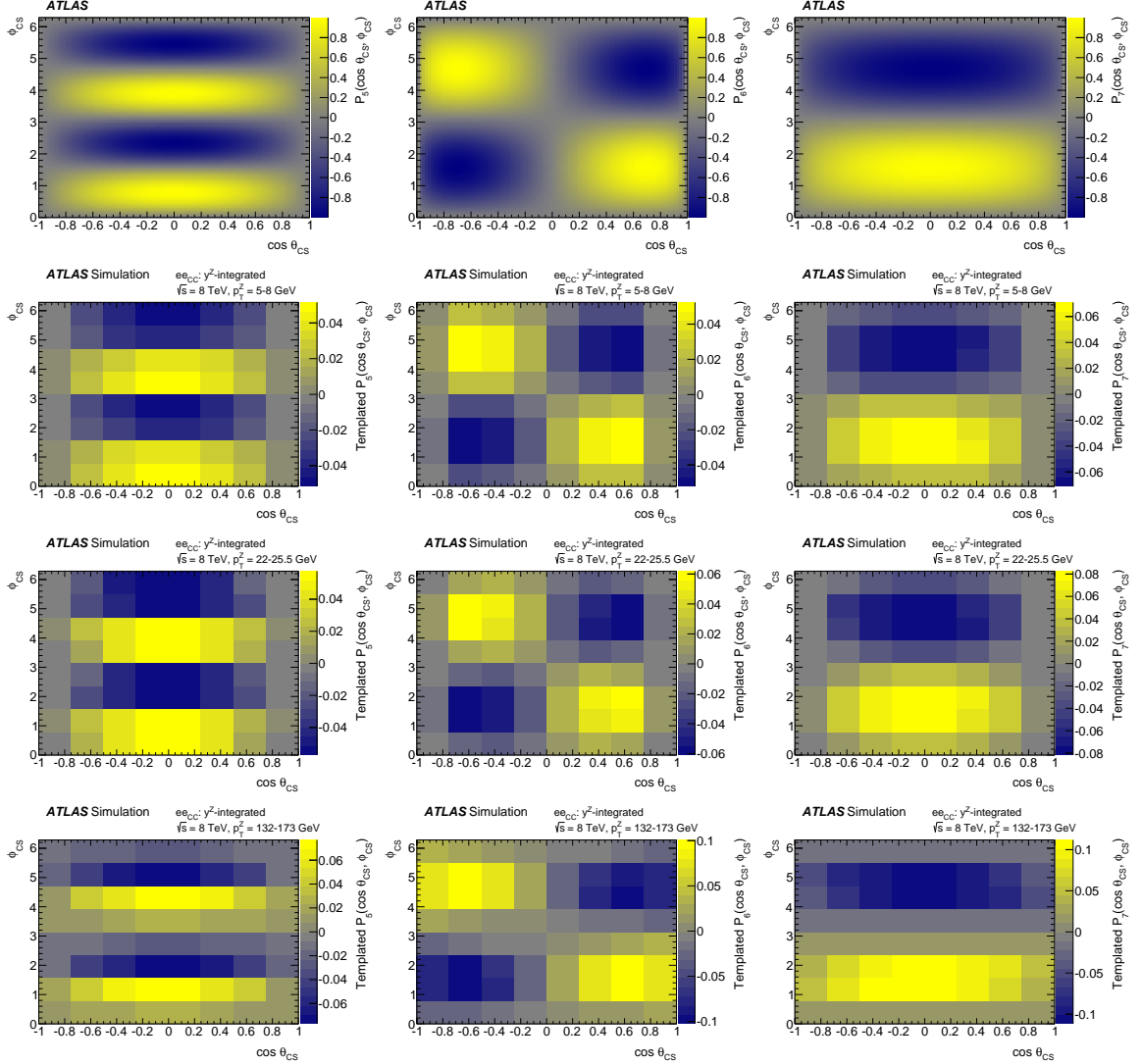


Figure 23: Shapes of the polynomials $P_{5,6,7}$ as a function of $\cos \theta_{\text{CS}}$ and ϕ_{CS} (top). Below these are the templated polynomials for the y^Z -integrated ee_{CC} events at low ($5-8$ GeV), medium ($22-25.5$ GeV), and high ($132-173$ GeV) values of p_T^Z .

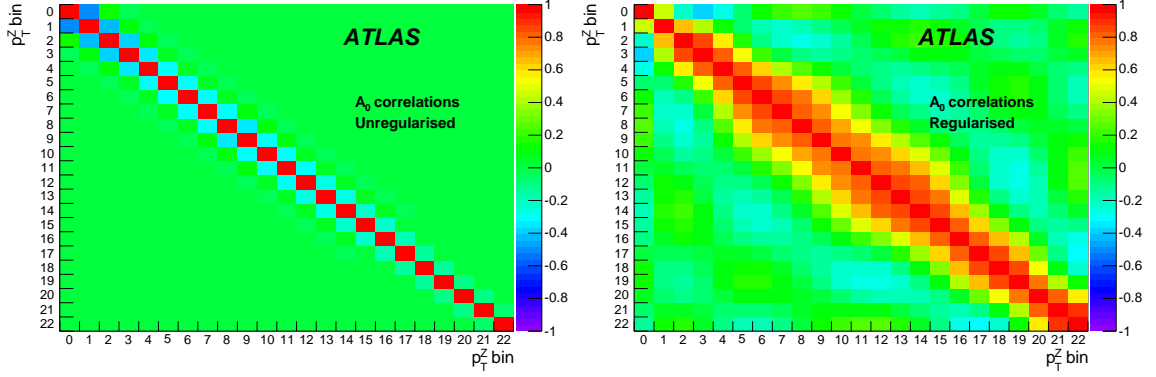


Figure 24: Correlation matrix between the p_T^Z bins of A_0 before (left) and after (right) regularisation.

Since the measurement is determined from the exact likelihood expression for the coefficients, the covariance matrix Σ of the coefficients can be derived based on the second-order partial derivatives of the likelihood [57]. Along with the uncertainties in A_i and A_j , namely $\sigma(A_i)$ and $\sigma(A_j)$, their correlation can be computed as $\rho_{ij} = \Sigma_{ij}/\sigma(A_i)\sigma(A_j)$. This is done based on pseudo-data taken from PowHEG + PYTHIA 8 and is shown in Fig. 24 before and after regularisation.

A Jacobian matrix \mathbf{J} (and its transpose \mathbf{J}^T) is used to transform the covariance matrix of the coefficients to the covariance matrix of their derivatives. A regularisation strength γ is introduced to control the amount by which the derivatives are penalised. The penalty term applied to the likelihood that controls the regularisation is therefore defined as

$$\mathcal{A}(\mathbf{A}_{\text{reg}}) = \exp \left\{ -0.5\gamma \vec{A}^{(n)} (\mathbf{J}\Sigma\mathbf{J}^T)^{-1} \vec{A}^{(n),T} \right\}. \quad (18)$$

In all channels, a regularisation scheme using sixth-order derivatives is used.

In the limit that the regularisation procedure described above has infinite strength, an n^{th} -order derivative regularisation fixes the measured spectrum to be an $(n-1)^{th}$ -order polynomial. This can be seen in Fig. 25, which shows the residual of a fifth-order polynomial fit to the A_0 spectrum regularised with sixth-order derivatives and strength $\gamma = 100$; the fit is nearly perfect (the regularisation strength used in this case is large but not infinite and so there are some small non-zero residuals). Also shown is the residual of a fourth-order polynomial fit to this same spectrum; a fifth-order term can be clearly observed in the residual. The regularisation bias $B[A_{ij}]$ in the coefficients is evaluated using pseudo-experiments based on the difference between the expectation value of the best-fit coefficient $E[A_{ij}]$ and the value of the coefficient y_{ij} used to randomise the data: $B[A_{ij}] = E[A_{ij}] - y_{ij}$. The choice of y_{ij} is derived from a sixth-order polynomial fit to the PowHEG + PYTHIA 8 reference coefficients.

The derived uncertainty due to the regularisation bias in the y^Z -integrated A_0 coefficient in the $ee_{\text{CC}} + \mu\mu_{\text{CC}}$ channel is shown in Fig. 26 for four different regularisation strengths, along with the corresponding statistical uncertainty of the coefficient for each strength. As can be seen, the regularisation uncertainty increases with increasing regularisation strength, while the corresponding statistical uncertainty decreases, as expected. In the limit that the regularisation strength goes to zero, the statistical uncertainty approaches

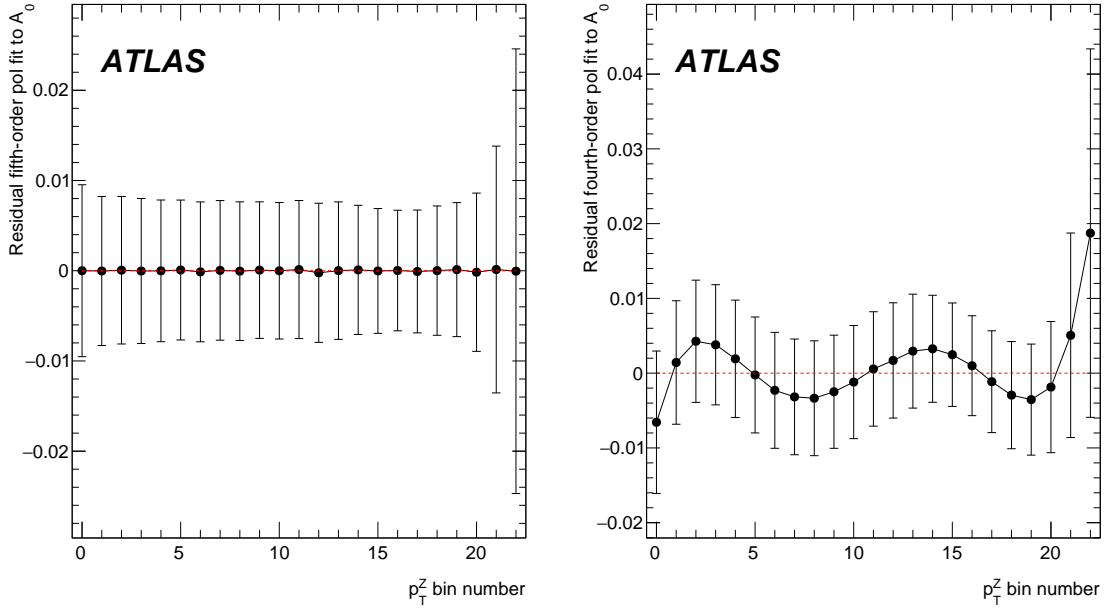


Figure 25: Residuals of a fifth-order (left) and fourth-order (right) polynomial fit to the measured A_0 spectrum in the ee_{CC} y^Z -integrated channel, regularised with sixth-order derivatives.

the unregularised one. Along with the decrease in statistical uncertainty comes an increase in correlation among the measured coefficients of neighbouring p_T^Z bins. The regularisation bias uncertainty appears to plateau between $\gamma = 10$ and $\gamma = 100$, which corresponds to the limit that the spectrum is fixed to a sixth-order polynomial, as described above. Based on these studies, a strength of $\gamma = 100$ is chosen for the ee_{CC} and $\mu\mu_{CC}$ channels, while the scheme in the ee_{CF} channel is based on a strength of $\gamma = 5$.

Overlays of the regularised measurements for the $ee_{CC} + \mu\mu_{CC}$ channel in the y^Z -integrated configuration are shown in Fig. 27 for A_{0-7} and in Fig. 28 for $A_0 - A_2$. In the unregularised results, there are many bin-to-bin fluctuations that enter primarily through anti-correlations between neighbouring measurements. In contrast, the regularised results are largely correlated from bin-to-bin and are much smoother.

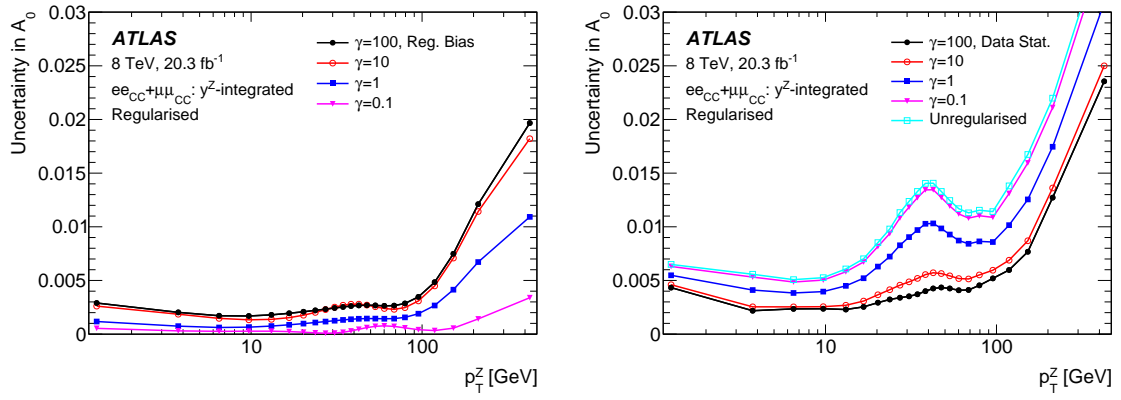


Figure 26: For the $ee_{CC} + \mu\mu_{CC}$ channel, the derived regularisation bias uncertainty in the y^Z -integrated A_0 coefficient for various regularisation strengths (left) along with the corresponding statistical uncertainty of the coefficient (right) versus p_T^Z . The unregularised statistical uncertainty is shown for comparison.

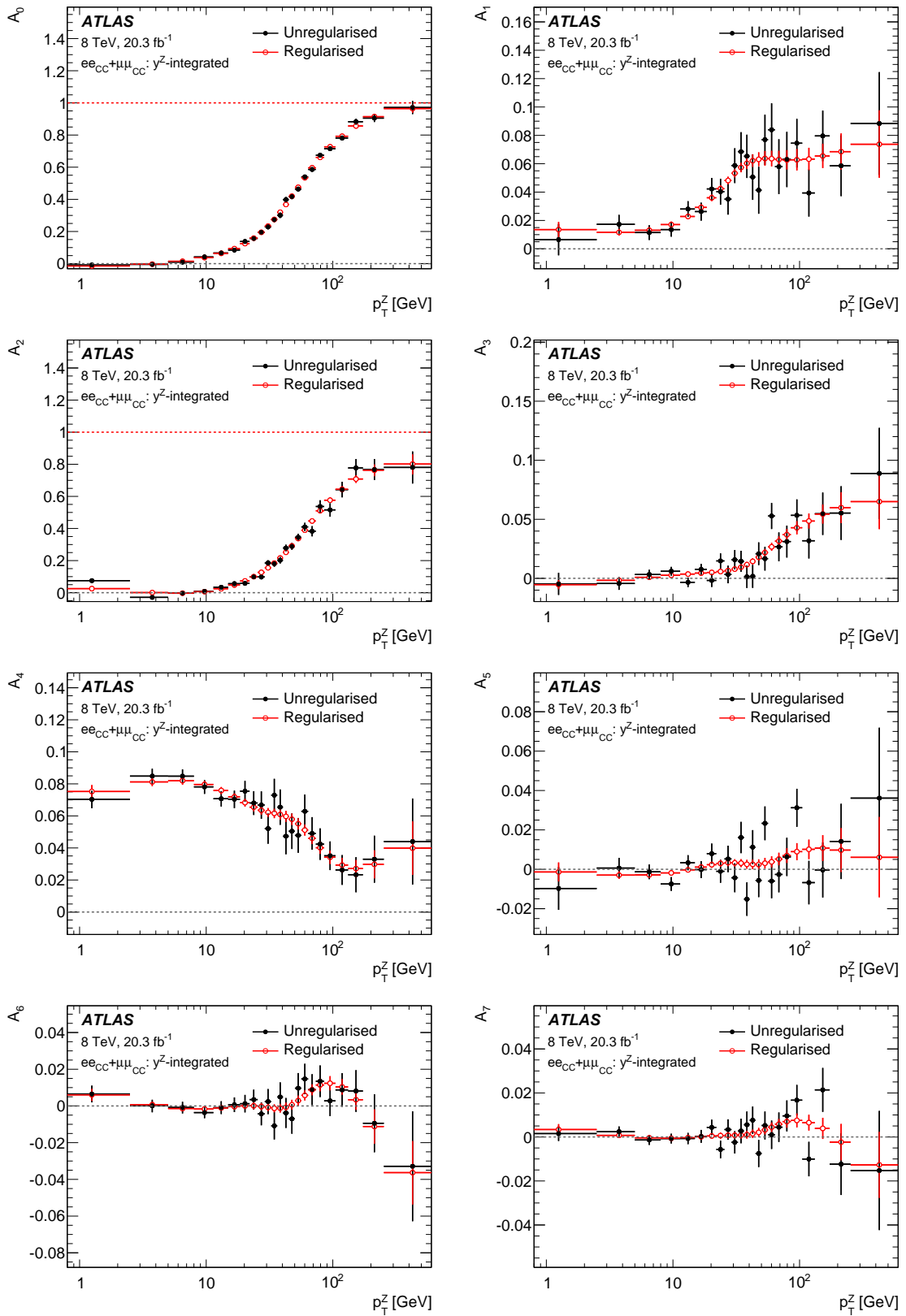


Figure 27: For the $ee_{cc} + \mu\mu_{cc}$ channel in the y^Z -integrated configuration, overlays of regularised with unregularised results are shown for A_{0-7} .

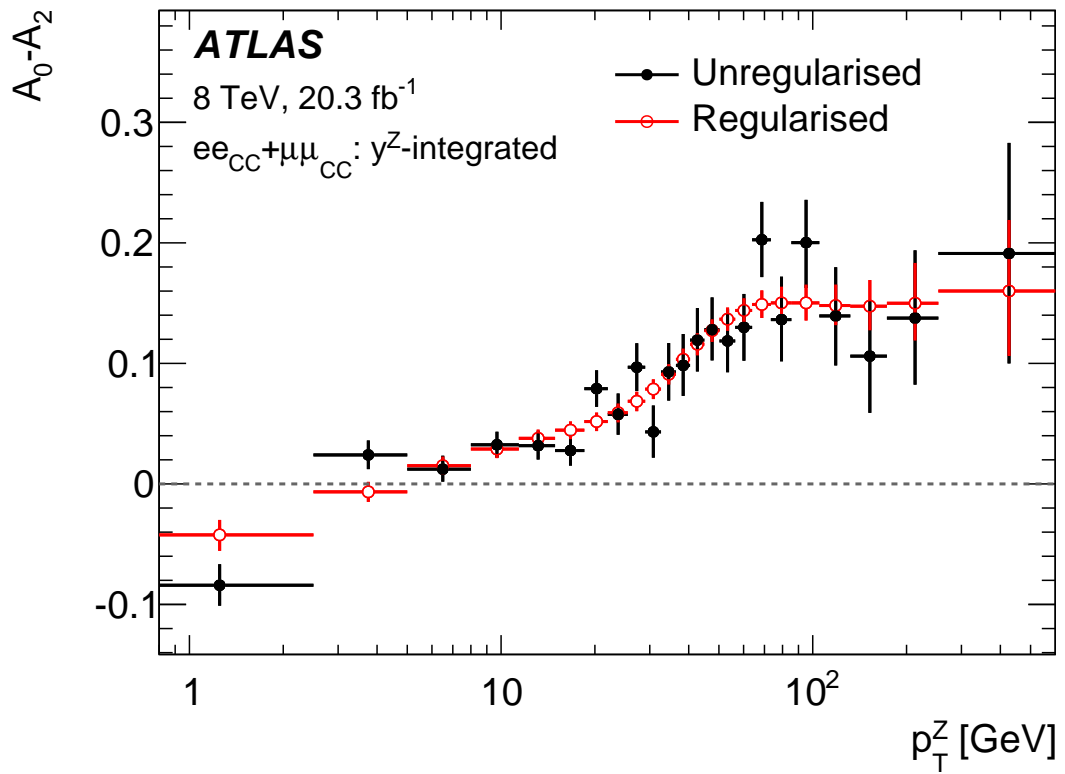


Figure 28: For the $ee_{CC} + \mu\mu_{CC}$ channel in the y^Z -integrated configuration, overlays of regularised with unregularised results are shown for $A_0 - A_2$.

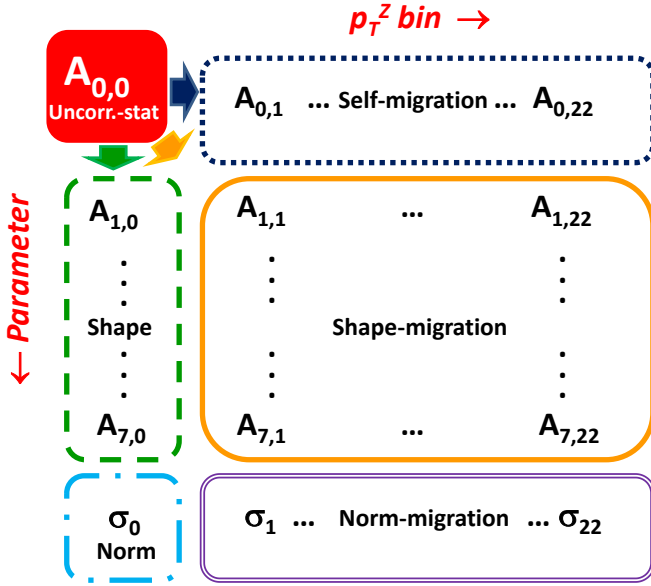


Figure 29: Categorisation of parameters leading to the data statistical uncertainty in the measured coefficients illustrated by the uncertainty categorisation for A_0 in p_T^Z bin 0.

D. Categorisation of statistical uncertainties

The categorisation of statistical uncertainties is illustrated in Fig. 29 for A_0 in p_T^Z bin 0. Uncertainties due to the parameter of interest alone are labelled as “Uncorr.-stat” in the solid red box. Boxes directly below the solid red box represent parameters common to the same p_T^Z bin as the parameter of interest, and are therefore non-migration parameters. The other boxes represent parameters in different p_T^Z bins, and are categorised as migration parameters. The categorisation can be broken down as follows:

- Parameters in the dashed green box are from *different* coefficient numbers but the *same* p_T^Z bin and are labelled as “Shape” parameters.
- Parameters in the dotted blue box are from the *same* coefficient number (A_0) but in a *different* p_T^Z bin and are labelled as “Self-migration” parameters.
- The complements to these two categories are the parameters in the single-lined orange box and are labelled as “Shape-migration”; they are outside of both the chosen p_T^Z bin and coefficient number.

These separations are done as well for the cross-section parameters, and are labelled as “Norm” and “Norm-migration” in the dot-dashed blue and double-lined purple boxes, respectively.

An illustration of this categorisation of the various components of the statistical uncertainty is shown for the $eeCC + \mu\muCC$, y^Z -integrated measurement of the coefficient A_0 in Fig. 30.

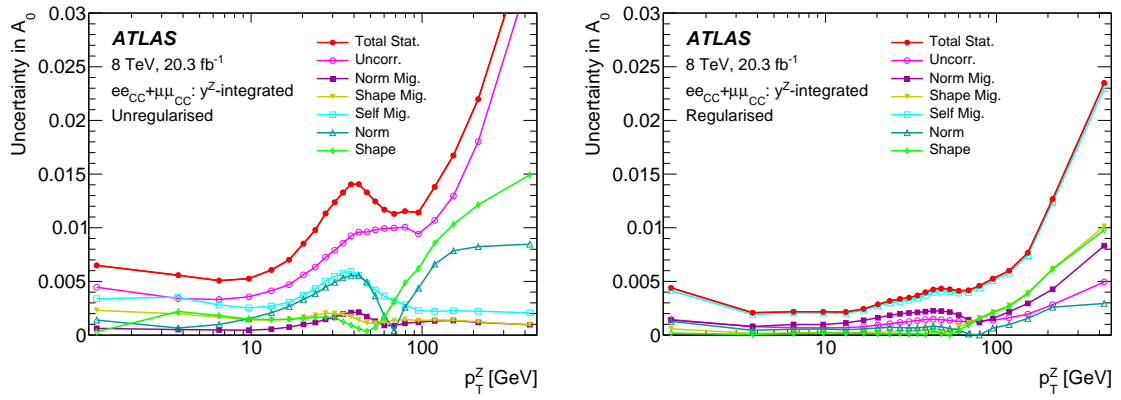


Figure 30: Statistical uncertainty decomposition for the unregularised (left) and regularised (right) measurement of the A_0 coefficient in the $ee_{CC} + \mu\mu_{CC}$ channel for the integrated y^Z configuration.

E. Quantifying $A_{5,6,7}$

The coefficients $A_{5,6,7}$ are expected to be zero at NLO, but are expected to receive NNLO contributions as large as 0.005 at high p_T^Z . The data measurements appear to be consistent with this, although the level at which the data measurements are non-zero should be quantified. A simple method to quantify this would be a standard χ^2 test of the measured spectra with respect to the null hypothesis of zero, but this has several disadvantages. First, the coefficients are expected to be non-zero only at high p_T^Z , and therefore a χ^2 test across the entire spectrum would be diluted by the low p_T^Z bins. Performing the test only for high p_T^Z could improve this locally, although this introduces some model dependence due to the choice of p_T^Z cutoff, as well as introducing a look-elsewhere-effect. Second, a χ^2 test is insensitive to the sign of the measured coefficients in each bin. Finally, it does not optimally account for positive or negative trends in the observation.

A signed covariant test statistic $Q_{\text{signed}}^{\text{cov}}$ based on pseudo-experiments was developed for the purpose of quantifying the observed spectra. This takes into account pair-wise correlations between coefficients in neighbouring p_T^Z bins, as well as correlations between the different coefficients in the same p_T^Z bin. The contribution of each coefficient measurement to the test statistic is signed. Measurements below zero have a negative contribution, while measurements above zero have a positive contribution. $Q_{\text{signed}}^{\text{cov}}$ is computed both on observed data and simulated data based on DYNNNLO predictions at NNLO. The distribution of $Q_{\text{signed}}^{\text{cov}}$ is obtained from ensemble tests under the null hypothesis. A p-value is obtained by integrating this distribution from the observed and simulated values to positive infinity, and converted to a one-sided statistical significance.

To compute $Q_{\text{signed}}^{\text{cov}}$ (for any observed, simulated, or pseudo data), an initial set of pseudo-experiments are used to obtain the distribution of $\hat{A}_{5,6,7}^{\text{pseudo}}$. A fit is first performed to the data under the null hypothesis $A_{5,6,7} = 0$ to obtain $\hat{A}_{0-4}^{\text{null}}$, $\hat{\sigma}^{\text{null}}$, and $\hat{\theta}^{\text{null}}$. Pseudo-data is then generated in each likelihood bin around the expected events $N_{\text{exp}}^n(\hat{A}_{0-4}^{\text{null}}, \hat{\sigma}^{\text{null}}, \hat{\theta}^{\text{null}})$ (see Eq. (7)). A fit is performed to the pseudo-data to obtain $\hat{A}_{5,6,7}^{\text{pseudo}}$.

$Q_{\text{signed}}^{\text{cov}}$ is computed based on $\hat{A}_{5,6,7}$ in any particular dataset in conjunction with the distribution of $\hat{A}_{5,6,7}^{\text{pseudo}}$ from pseudo-data. It includes several components, which are described here. The significance Z_i of the deviation from zero of each of the three $A_{5,6,7}$ coefficients in every p_T^Z bin is computed as depicted in Fig. 31. A weight, $w_{ij} = (\text{sign}(Z_i)Z_i^2 + \text{sign}(Z_j)Z_j^2)/(Z_i^2 + Z_j^2)$, is computed based on the individual Z_i values for every coefficient pair, both in coefficient number and bin in p_T^Z . A weight w_{ij} has the property that $w_{ij} = +1$ or -1 if Z_i and Z_j are both above or below zero, respectively, while it is a weighted difference between them otherwise. The correlation coefficient ρ_{ij} between these pairs is extracted from their two-dimensional distributions. The pair-wise significance Z_{ij} is computed from the tail probability of the measurement being more outward in its quadrant than is observed. An example of this for each quadrant is shown in Fig. 31. $Q_{\text{signed}}^{\text{cov}}$ is defined using these components as follows:

$$Q_{\text{signed}}^{\text{cov}} = \sum_i \text{sign}(Z_i)Z_i^2 + \sum_{i>j} w_{ij}Z_{ij}^2|\rho_{ij}|. \quad (19)$$

The distribution of $Q_{\text{signed}}^{\text{cov}}$ is finally obtained from a second set of pseudo-experiments. The observed value is computed along with the value from the DYNNNLO expectation. The distribution is shown

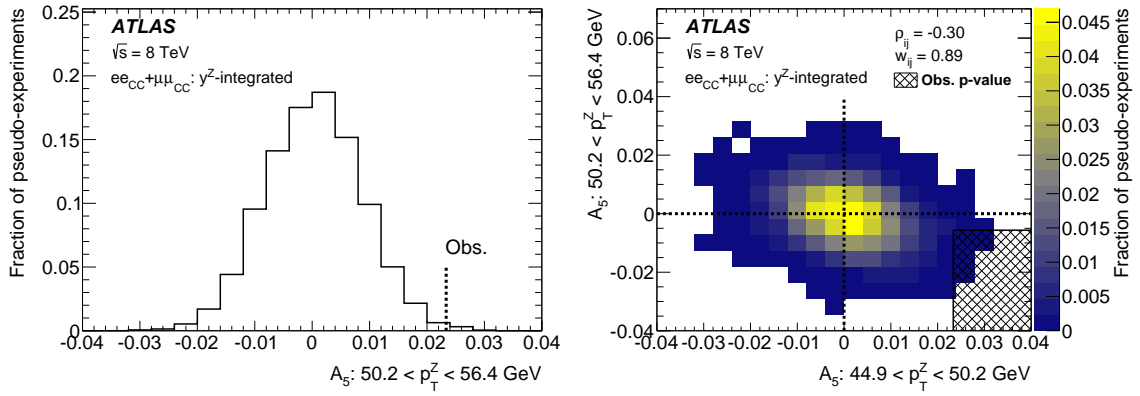


Figure 31: Left: Example of the distribution of the fitted value of A_5 in one p_T^Z bin from pseudo-data along with the observed value represented by a dashed line. The p -value computed as the right-sided tail probability is used to calculate the individual values of Z_i . Right: Two-dimensional distribution of the fitted A_5 from pseudo-data for two neighbouring p_T^Z bins. The upper left corner of the shaded area represents the value measured in the observed data, while the shaded area represents the p -value used to calculate Z_i .

in Fig. 32, with vertical bars representing the observed and expected values. A total of 7800 pseudo-experiments were used in this computation. Integrating from the observed value to the right, the fraction of events in the tail is 0.14%, corresponding to a significance of 3.0σ . Similarly, the expected significance is 3.2σ .

F. Additional results

Results are presented in Tables 11–13 for the y^Z -integrated measurements and in Tables 14–21 in bins of y^Z . Figure 33 shows the coefficients in bins of y^Z . Tables 22–27 show uncertainty breakdowns for the coefficients in the first two y^Z bins.

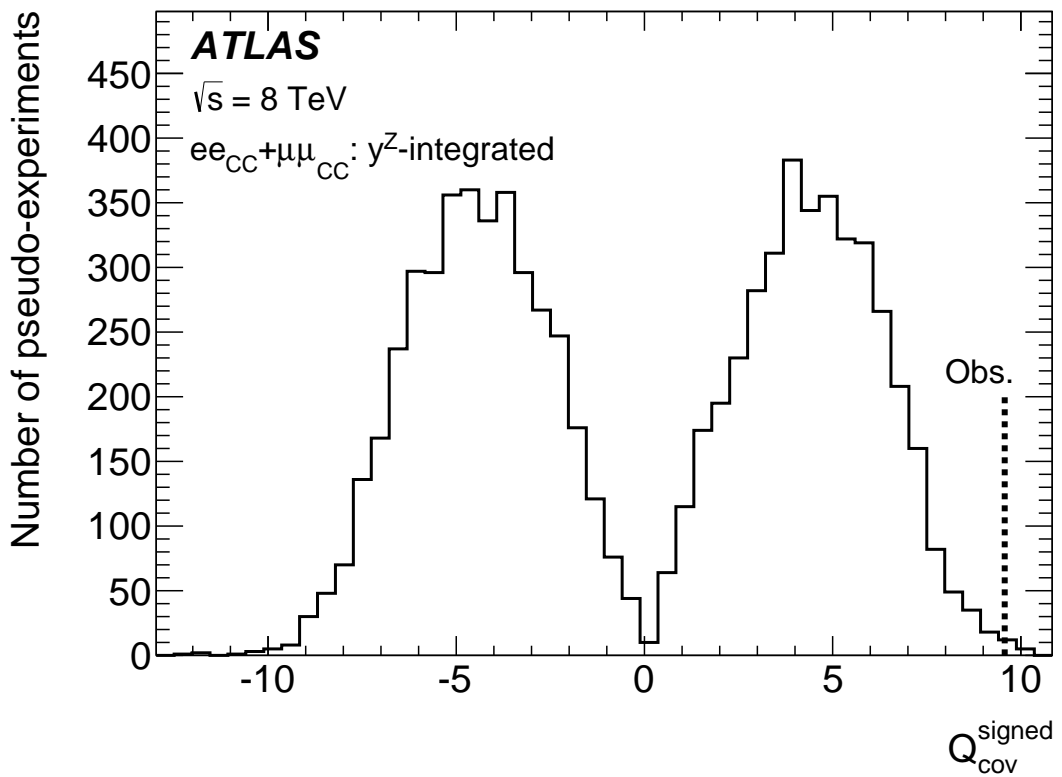


Figure 32: Distribution of the test statistic $Q_{\text{cov}}^{\text{signed}}$ from pseudo-experiments, along with the observed value represented by the vertical dashed line. The area to the right of the dashed line is used to compute the significance of non-zero positive values of the observed $A_{5,6,7}$.

Table 11: Measured angular coefficients A_0 , A_2 and difference $A_0 - A_2$ with uncertainties $\pm \delta_{\text{stat}} \pm \delta_{\text{syst}}$ for the y^Z -integrated measurement.

p_T^Z range [GeV]	y^Z -integrated		
	A_0	A_2	$A_0 - A_2$
0.0 – 2.5	$-0.014 \pm 0.004 \pm 0.008$	$0.025 \pm 0.009 \pm 0.006$	$-0.039 \pm 0.010 \pm 0.008$
2.5 – 5.0	$-0.003 \pm 0.002 \pm 0.008$	$0.001 \pm 0.004 \pm 0.003$	$-0.003 \pm 0.004 \pm 0.007$
5.0 – 8.0	$0.015 \pm 0.002 \pm 0.007$	$-0.003 \pm 0.003 \pm 0.003$	$0.018 \pm 0.003 \pm 0.007$
8.0 – 11.4	$0.038 \pm 0.002 \pm 0.007$	$0.007 \pm 0.002 \pm 0.002$	$0.031 \pm 0.003 \pm 0.007$
11.4 – 14.9	$0.064 \pm 0.002 \pm 0.007$	$0.025 \pm 0.002 \pm 0.002$	$0.039 \pm 0.003 \pm 0.007$
14.9 – 18.5	$0.093 \pm 0.002 \pm 0.007$	$0.048 \pm 0.002 \pm 0.002$	$0.045 \pm 0.003 \pm 0.006$
18.5 – 22.0	$0.125 \pm 0.003 \pm 0.007$	$0.073 \pm 0.003 \pm 0.002$	$0.052 \pm 0.004 \pm 0.006$
22.0 – 25.5	$0.159 \pm 0.003 \pm 0.007$	$0.100 \pm 0.003 \pm 0.003$	$0.059 \pm 0.005 \pm 0.006$
25.5 – 29.0	$0.195 \pm 0.003 \pm 0.007$	$0.127 \pm 0.003 \pm 0.003$	$0.068 \pm 0.005 \pm 0.006$
29.0 – 32.6	$0.234 \pm 0.003 \pm 0.006$	$0.155 \pm 0.004 \pm 0.003$	$0.078 \pm 0.005 \pm 0.006$
32.6 – 36.4	$0.275 \pm 0.004 \pm 0.006$	$0.184 \pm 0.004 \pm 0.003$	$0.091 \pm 0.006 \pm 0.006$
36.4 – 40.4	$0.320 \pm 0.004 \pm 0.006$	$0.216 \pm 0.005 \pm 0.004$	$0.103 \pm 0.006 \pm 0.006$
40.4 – 44.9	$0.368 \pm 0.004 \pm 0.006$	$0.252 \pm 0.005 \pm 0.004$	$0.116 \pm 0.007 \pm 0.006$
44.9 – 50.2	$0.420 \pm 0.004 \pm 0.006$	$0.292 \pm 0.005 \pm 0.005$	$0.128 \pm 0.007 \pm 0.006$
50.2 – 56.4	$0.475 \pm 0.004 \pm 0.006$	$0.337 \pm 0.006 \pm 0.005$	$0.137 \pm 0.007 \pm 0.006$
56.4 – 63.9	$0.534 \pm 0.004 \pm 0.006$	$0.389 \pm 0.007 \pm 0.006$	$0.145 \pm 0.008 \pm 0.006$
63.9 – 73.4	$0.596 \pm 0.004 \pm 0.005$	$0.447 \pm 0.009 \pm 0.008$	$0.150 \pm 0.009 \pm 0.007$
73.4 – 85.4	$0.661 \pm 0.005 \pm 0.005$	$0.510 \pm 0.012 \pm 0.010$	$0.151 \pm 0.011 \pm 0.007$
85.4 – 105	$0.727 \pm 0.005 \pm 0.005$	$0.576 \pm 0.014 \pm 0.012$	$0.151 \pm 0.013 \pm 0.008$
105 – 132	$0.793 \pm 0.006 \pm 0.005$	$0.644 \pm 0.017 \pm 0.015$	$0.148 \pm 0.015 \pm 0.009$
132 – 173	$0.856 \pm 0.008 \pm 0.008$	$0.708 \pm 0.022 \pm 0.020$	$0.148 \pm 0.019 \pm 0.011$
173 – 253	$0.914 \pm 0.013 \pm 0.013$	$0.763 \pm 0.034 \pm 0.031$	$0.151 \pm 0.029 \pm 0.017$
253 – 600	$0.965 \pm 0.024 \pm 0.024$	$0.801 \pm 0.057 \pm 0.048$	$0.163 \pm 0.052 \pm 0.027$

Table 12: Measured angular coefficients A_1 , A_3 and A_4 with uncertainties $\pm\delta_{\text{stat}} \pm \delta_{\text{syst}}$ for the y^Z -integrated measurement.

p_T^Z range [GeV]	y^Z -integrated		
	A_1	A_3	A_4
0.0 – 2.5	$0.014 \pm 0.005 \pm 0.003$	$-0.005 \pm 0.003 \pm 0.002$	$0.075 \pm 0.003 \pm 0.003$
2.5 – 5.0	$0.012 \pm 0.002 \pm 0.002$	$-0.001 \pm 0.001 \pm 0.001$	$0.081 \pm 0.001 \pm 0.002$
5.0 – 8.0	$0.013 \pm 0.002 \pm 0.002$	$0.001 \pm 0.001 \pm 0.001$	$0.082 \pm 0.001 \pm 0.002$
8.0 – 11.4	$0.017 \pm 0.002 \pm 0.002$	$0.003 \pm 0.001 \pm 0.001$	$0.080 \pm 0.001 \pm 0.002$
11.4 – 14.9	$0.023 \pm 0.001 \pm 0.001$	$0.004 \pm 0.001 \pm 0.001$	$0.076 \pm 0.001 \pm 0.002$
14.9 – 18.5	$0.029 \pm 0.002 \pm 0.001$	$0.004 \pm 0.001 \pm 0.001$	$0.072 \pm 0.002 \pm 0.002$
18.5 – 22.0	$0.036 \pm 0.002 \pm 0.001$	$0.005 \pm 0.001 \pm 0.001$	$0.068 \pm 0.002 \pm 0.002$
22.0 – 25.5	$0.042 \pm 0.002 \pm 0.002$	$0.006 \pm 0.001 \pm 0.001$	$0.065 \pm 0.002 \pm 0.002$
25.5 – 29.0	$0.048 \pm 0.002 \pm 0.002$	$0.007 \pm 0.002 \pm 0.001$	$0.064 \pm 0.002 \pm 0.002$
29.0 – 32.6	$0.053 \pm 0.003 \pm 0.002$	$0.008 \pm 0.002 \pm 0.001$	$0.062 \pm 0.002 \pm 0.002$
32.6 – 36.4	$0.057 \pm 0.003 \pm 0.002$	$0.009 \pm 0.002 \pm 0.001$	$0.062 \pm 0.003 \pm 0.002$
36.4 – 40.4	$0.060 \pm 0.003 \pm 0.002$	$0.012 \pm 0.002 \pm 0.001$	$0.061 \pm 0.003 \pm 0.002$
40.4 – 44.9	$0.062 \pm 0.004 \pm 0.003$	$0.014 \pm 0.002 \pm 0.001$	$0.060 \pm 0.003 \pm 0.002$
44.9 – 50.2	$0.063 \pm 0.004 \pm 0.003$	$0.018 \pm 0.002 \pm 0.001$	$0.058 \pm 0.003 \pm 0.002$
50.2 – 56.4	$0.064 \pm 0.005 \pm 0.003$	$0.022 \pm 0.003 \pm 0.001$	$0.055 \pm 0.003 \pm 0.002$
56.4 – 63.9	$0.064 \pm 0.005 \pm 0.003$	$0.027 \pm 0.003 \pm 0.002$	$0.051 \pm 0.003 \pm 0.002$
63.9 – 73.4	$0.063 \pm 0.005 \pm 0.004$	$0.031 \pm 0.004 \pm 0.002$	$0.046 \pm 0.003 \pm 0.002$
73.4 – 85.4	$0.063 \pm 0.006 \pm 0.004$	$0.037 \pm 0.004 \pm 0.002$	$0.040 \pm 0.003 \pm 0.002$
85.4 – 105	$0.063 \pm 0.007 \pm 0.004$	$0.043 \pm 0.005 \pm 0.002$	$0.034 \pm 0.004 \pm 0.002$
105 – 132	$0.063 \pm 0.007 \pm 0.004$	$0.049 \pm 0.006 \pm 0.003$	$0.029 \pm 0.004 \pm 0.002$
132 – 173	$0.065 \pm 0.008 \pm 0.005$	$0.054 \pm 0.007 \pm 0.003$	$0.027 \pm 0.005 \pm 0.002$
173 – 253	$0.069 \pm 0.012 \pm 0.007$	$0.060 \pm 0.012 \pm 0.005$	$0.030 \pm 0.008 \pm 0.004$
253 – 600	$0.074 \pm 0.022 \pm 0.013$	$0.065 \pm 0.022 \pm 0.009$	$0.040 \pm 0.015 \pm 0.007$

Table 13: Measured angular coefficients A_5 , A_6 and A_7 with uncertainties $\pm\delta_{\text{stat}} \pm \delta_{\text{syst}}$ for the y^Z -integrated measurement.

p_T^Z range [GeV]	y^Z -integrated		
	A_5	A_6	A_7
0.0 – 2.5	$-0.001 \pm 0.004 \pm 0.003$	$0.006 \pm 0.003 \pm 0.002$	$0.003 \pm 0.002 \pm 0.001$
2.5 – 5.0	$-0.002 \pm 0.002 \pm 0.001$	$0.001 \pm 0.001 \pm 0.001$	$0.001 \pm 0.001 \pm 0.001$
5.0 – 8.0	$-0.002 \pm 0.001 \pm 0.001$	$-0.001 \pm 0.001 \pm 0.001$	$0.000 \pm 0.001 \pm 0.001$
8.0 – 11.4	$-0.001 \pm 0.001 \pm 0.001$	$-0.001 \pm 0.001 \pm 0.001$	$0.000 \pm 0.001 \pm 0.001$
11.4 – 14.9	$0.000 \pm 0.001 \pm 0.001$	$-0.001 \pm 0.001 \pm 0.001$	$0.000 \pm 0.001 \pm 0.000$
14.9 – 18.5	$0.001 \pm 0.001 \pm 0.001$	$0.000 \pm 0.001 \pm 0.001$	$0.000 \pm 0.001 \pm 0.001$
18.5 – 22.0	$0.002 \pm 0.001 \pm 0.001$	$0.000 \pm 0.002 \pm 0.001$	$0.000 \pm 0.001 \pm 0.001$
22.0 – 25.5	$0.003 \pm 0.002 \pm 0.001$	$0.000 \pm 0.002 \pm 0.001$	$0.001 \pm 0.001 \pm 0.001$
25.5 – 29.0	$0.003 \pm 0.002 \pm 0.001$	$0.000 \pm 0.002 \pm 0.001$	$0.001 \pm 0.001 \pm 0.001$
29.0 – 32.6	$0.003 \pm 0.002 \pm 0.001$	$0.000 \pm 0.002 \pm 0.001$	$0.001 \pm 0.001 \pm 0.001$
32.6 – 36.4	$0.003 \pm 0.002 \pm 0.001$	$-0.001 \pm 0.002 \pm 0.001$	$0.001 \pm 0.001 \pm 0.001$
36.4 – 40.4	$0.003 \pm 0.002 \pm 0.001$	$-0.001 \pm 0.002 \pm 0.001$	$0.001 \pm 0.002 \pm 0.001$
40.4 – 44.9	$0.003 \pm 0.002 \pm 0.001$	$0.000 \pm 0.002 \pm 0.001$	$0.001 \pm 0.002 \pm 0.001$
44.9 – 50.2	$0.002 \pm 0.002 \pm 0.001$	$0.001 \pm 0.002 \pm 0.001$	$0.002 \pm 0.002 \pm 0.001$
50.2 – 56.4	$0.003 \pm 0.002 \pm 0.001$	$0.003 \pm 0.002 \pm 0.001$	$0.003 \pm 0.002 \pm 0.001$
56.4 – 63.9	$0.004 \pm 0.003 \pm 0.001$	$0.006 \pm 0.002 \pm 0.001$	$0.004 \pm 0.002 \pm 0.001$
63.9 – 73.4	$0.005 \pm 0.003 \pm 0.002$	$0.009 \pm 0.003 \pm 0.001$	$0.006 \pm 0.002 \pm 0.001$
73.4 – 85.4	$0.007 \pm 0.003 \pm 0.002$	$0.011 \pm 0.003 \pm 0.002$	$0.007 \pm 0.002 \pm 0.001$
85.4 – 105	$0.009 \pm 0.004 \pm 0.002$	$0.012 \pm 0.003 \pm 0.002$	$0.008 \pm 0.003 \pm 0.001$
105 – 132	$0.010 \pm 0.004 \pm 0.002$	$0.010 \pm 0.004 \pm 0.002$	$0.007 \pm 0.003 \pm 0.002$
132 – 173	$0.011 \pm 0.006 \pm 0.003$	$0.003 \pm 0.005 \pm 0.002$	$0.004 \pm 0.004 \pm 0.002$
173 – 253	$0.010 \pm 0.010 \pm 0.006$	$-0.011 \pm 0.009 \pm 0.004$	$-0.002 \pm 0.008 \pm 0.003$
253 – 600	$0.006 \pm 0.019 \pm 0.010$	$-0.036 \pm 0.016 \pm 0.007$	$-0.012 \pm 0.014 \pm 0.006$

Table 14: The angular coefficient $A_0 \pm \delta_{\text{stat}} \pm \delta_{\text{syst}}$ in bins of y^Z .

p_T^Z range [GeV]	y^Z -binned A_0		
	$0 < y^Z < 1$	$1 < y^Z < 2$	$2 < y^Z < 3.5$
0.0 – 2.5	$0.004 \pm 0.006 \pm 0.005$	$-0.016 \pm 0.008 \pm 0.008$	$0.093 \pm 0.027 \pm 0.044$
2.5 – 5.0	$0.009 \pm 0.003 \pm 0.004$	$-0.001 \pm 0.004 \pm 0.007$	$0.085 \pm 0.019 \pm 0.035$
5.0 – 8.0	$0.022 \pm 0.003 \pm 0.004$	$0.017 \pm 0.004 \pm 0.007$	$0.070 \pm 0.017 \pm 0.033$
8.0 – 11.4	$0.041 \pm 0.003 \pm 0.004$	$0.038 \pm 0.004 \pm 0.007$	$0.069 \pm 0.016 \pm 0.032$
11.4 – 14.9	$0.064 \pm 0.003 \pm 0.004$	$0.061 \pm 0.004 \pm 0.006$	$0.070 \pm 0.017 \pm 0.032$
14.9 – 18.5	$0.091 \pm 0.003 \pm 0.004$	$0.087 \pm 0.004 \pm 0.006$	$0.084 \pm 0.019 \pm 0.031$
18.5 – 22.0	$0.122 \pm 0.004 \pm 0.004$	$0.115 \pm 0.005 \pm 0.006$	$0.115 \pm 0.022 \pm 0.030$
22.0 – 25.5	$0.156 \pm 0.004 \pm 0.004$	$0.147 \pm 0.005 \pm 0.006$	$0.131 \pm 0.026 \pm 0.030$
25.5 – 29.0	$0.193 \pm 0.004 \pm 0.004$	$0.181 \pm 0.006 \pm 0.006$	$0.172 \pm 0.029 \pm 0.029$
29.0 – 32.6	$0.232 \pm 0.005 \pm 0.005$	$0.219 \pm 0.006 \pm 0.006$	$0.203 \pm 0.031 \pm 0.030$
32.6 – 36.4	$0.275 \pm 0.005 \pm 0.005$	$0.260 \pm 0.006 \pm 0.006$	$0.240 \pm 0.034 \pm 0.029$
36.4 – 40.4	$0.320 \pm 0.005 \pm 0.005$	$0.305 \pm 0.007 \pm 0.006$	$0.277 \pm 0.036 \pm 0.030$
40.4 – 44.9	$0.369 \pm 0.005 \pm 0.005$	$0.355 \pm 0.007 \pm 0.006$	$0.316 \pm 0.035 \pm 0.030$
44.9 – 50.2	$0.421 \pm 0.006 \pm 0.005$	$0.408 \pm 0.008 \pm 0.006$	$0.362 \pm 0.030 \pm 0.029$
50.2 – 56.4	$0.476 \pm 0.005 \pm 0.005$	$0.464 \pm 0.007 \pm 0.006$	$0.417 \pm 0.030 \pm 0.030$
56.4 – 63.9	$0.534 \pm 0.005 \pm 0.004$	$0.524 \pm 0.007 \pm 0.006$	$0.469 \pm 0.029 \pm 0.031$
63.9 – 73.4	$0.595 \pm 0.005 \pm 0.004$	$0.588 \pm 0.007 \pm 0.006$	$0.557 \pm 0.029 \pm 0.031$
73.4 – 85.4	$0.658 \pm 0.006 \pm 0.004$	$0.654 \pm 0.008 \pm 0.006$	$0.652 \pm 0.030 \pm 0.029$
85.4 – 105	$0.722 \pm 0.007 \pm 0.005$	$0.721 \pm 0.009 \pm 0.006$	$0.789 \pm 0.042 \pm 0.049$
105 – 132	$0.786 \pm 0.008 \pm 0.006$	$0.788 \pm 0.010 \pm 0.007$	
132 – 173	$0.849 \pm 0.010 \pm 0.009$	$0.855 \pm 0.012 \pm 0.009$	
173 – 253	$0.909 \pm 0.016 \pm 0.015$	$0.918 \pm 0.021 \pm 0.015$	
253 – 600	$0.963 \pm 0.030 \pm 0.025$	$0.975 \pm 0.039 \pm 0.027$	

Table 15: The angular coefficient $A_1 \pm \delta_{\text{stat}} \pm \delta_{\text{syst}}$ in bins of y^Z . The A_1 measurements are missing from the third y^Z bin since they are inaccessible in the ee_{CF} channel.

p_T^Z range [GeV]	y^Z -binned A_1		
	$0 < y^Z < 1$	$1 < y^Z < 2$	$2 < y^Z < 3.5$
0.0 – 2.5	$0.007 \pm 0.006 \pm 0.004$	$0.018 \pm 0.008 \pm 0.005$	
2.5 – 5.0	$0.004 \pm 0.002 \pm 0.002$	$0.016 \pm 0.003 \pm 0.002$	
5.0 – 8.0	$0.002 \pm 0.002 \pm 0.001$	$0.017 \pm 0.002 \pm 0.002$	
8.0 – 11.4	$0.002 \pm 0.002 \pm 0.001$	$0.021 \pm 0.002 \pm 0.002$	
11.4 – 14.9	$0.003 \pm 0.002 \pm 0.001$	$0.027 \pm 0.002 \pm 0.002$	
14.9 – 18.5	$0.004 \pm 0.002 \pm 0.001$	$0.032 \pm 0.003 \pm 0.002$	
18.5 – 22.0	$0.007 \pm 0.003 \pm 0.002$	$0.038 \pm 0.003 \pm 0.002$	
22.0 – 25.5	$0.010 \pm 0.003 \pm 0.002$	$0.042 \pm 0.003 \pm 0.002$	
25.5 – 29.0	$0.012 \pm 0.003 \pm 0.002$	$0.046 \pm 0.004 \pm 0.002$	
29.0 – 32.6	$0.015 \pm 0.003 \pm 0.002$	$0.049 \pm 0.004 \pm 0.002$	
32.6 – 36.4	$0.017 \pm 0.004 \pm 0.003$	$0.052 \pm 0.005 \pm 0.003$	
36.4 – 40.4	$0.018 \pm 0.005 \pm 0.003$	$0.053 \pm 0.005 \pm 0.003$	
40.4 – 44.9	$0.018 \pm 0.005 \pm 0.003$	$0.054 \pm 0.006 \pm 0.004$	
44.9 – 50.2	$0.017 \pm 0.006 \pm 0.004$	$0.055 \pm 0.007 \pm 0.004$	
50.2 – 56.4	$0.015 \pm 0.006 \pm 0.004$	$0.056 \pm 0.007 \pm 0.004$	
56.4 – 63.9	$0.013 \pm 0.006 \pm 0.004$	$0.058 \pm 0.008 \pm 0.005$	
63.9 – 73.4	$0.010 \pm 0.007 \pm 0.004$	$0.061 \pm 0.009 \pm 0.005$	
73.4 – 85.4	$0.009 \pm 0.008 \pm 0.004$	$0.063 \pm 0.010 \pm 0.006$	
85.4 – 105	$0.010 \pm 0.009 \pm 0.005$	$0.066 \pm 0.011 \pm 0.006$	
105 – 132	$0.013 \pm 0.009 \pm 0.005$	$0.069 \pm 0.011 \pm 0.006$	
132 – 173	$0.022 \pm 0.010 \pm 0.006$	$0.071 \pm 0.013 \pm 0.007$	
173 – 253	$0.037 \pm 0.015 \pm 0.009$	$0.070 \pm 0.019 \pm 0.011$	
253 – 600	$0.061 \pm 0.028 \pm 0.016$	$0.067 \pm 0.037 \pm 0.020$	

Table 16: The angular coefficient $A_2 \pm \delta_{\text{stat}} \pm \delta_{\text{syst}}$ in bins of y^Z .

p_T^Z range [GeV]	y^Z -binned A_2		
	$0 < y^Z < 1$	$1 < y^Z < 2$	$2 < y^Z < 3.5$
0.0 – 2.5	$0.032 \pm 0.011 \pm 0.007$	$0.039 \pm 0.015 \pm 0.011$	$0.198 \pm 0.094 \pm 0.063$
2.5 – 5.0	$0.007 \pm 0.005 \pm 0.003$	$0.010 \pm 0.006 \pm 0.005$	$0.081 \pm 0.071 \pm 0.041$
5.0 – 8.0	$0.003 \pm 0.003 \pm 0.002$	$0.003 \pm 0.004 \pm 0.003$	$0.071 \pm 0.059 \pm 0.035$
8.0 – 11.4	$0.012 \pm 0.003 \pm 0.002$	$0.009 \pm 0.004 \pm 0.002$	$0.070 \pm 0.048 \pm 0.031$
11.4 – 14.9	$0.028 \pm 0.003 \pm 0.002$	$0.025 \pm 0.004 \pm 0.003$	$0.091 \pm 0.047 \pm 0.026$
14.9 – 18.5	$0.050 \pm 0.003 \pm 0.002$	$0.047 \pm 0.004 \pm 0.003$	$0.116 \pm 0.050 \pm 0.026$
18.5 – 22.0	$0.075 \pm 0.004 \pm 0.003$	$0.070 \pm 0.005 \pm 0.004$	$0.151 \pm 0.057 \pm 0.026$
22.0 – 25.5	$0.100 \pm 0.004 \pm 0.003$	$0.097 \pm 0.005 \pm 0.004$	$0.159 \pm 0.066 \pm 0.030$
25.5 – 29.0	$0.127 \pm 0.004 \pm 0.003$	$0.123 \pm 0.005 \pm 0.004$	$0.191 \pm 0.066 \pm 0.030$
29.0 – 32.6	$0.155 \pm 0.005 \pm 0.003$	$0.151 \pm 0.006 \pm 0.004$	$0.187 \pm 0.069 \pm 0.032$
32.6 – 36.4	$0.185 \pm 0.005 \pm 0.004$	$0.179 \pm 0.007 \pm 0.005$	$0.234 \pm 0.071 \pm 0.033$
36.4 – 40.4	$0.216 \pm 0.006 \pm 0.004$	$0.210 \pm 0.007 \pm 0.006$	$0.228 \pm 0.072 \pm 0.036$
40.4 – 44.9	$0.252 \pm 0.007 \pm 0.005$	$0.244 \pm 0.008 \pm 0.006$	$0.312 \pm 0.066 \pm 0.035$
44.9 – 50.2	$0.291 \pm 0.007 \pm 0.005$	$0.283 \pm 0.009 \pm 0.007$	$0.348 \pm 0.060 \pm 0.033$
50.2 – 56.4	$0.335 \pm 0.008 \pm 0.006$	$0.327 \pm 0.010 \pm 0.008$	$0.428 \pm 0.063 \pm 0.040$
56.4 – 63.9	$0.385 \pm 0.010 \pm 0.007$	$0.376 \pm 0.012 \pm 0.009$	$0.433 \pm 0.068 \pm 0.040$
63.9 – 73.4	$0.439 \pm 0.013 \pm 0.009$	$0.432 \pm 0.015 \pm 0.011$	$0.503 \pm 0.076 \pm 0.044$
73.4 – 85.4	$0.499 \pm 0.016 \pm 0.011$	$0.495 \pm 0.019 \pm 0.014$	$0.424 \pm 0.099 \pm 0.075$
85.4 – 105	$0.560 \pm 0.019 \pm 0.013$	$0.562 \pm 0.022 \pm 0.017$	$0.258 \pm 0.159 \pm 0.152$
105 – 132	$0.622 \pm 0.022 \pm 0.016$	$0.634 \pm 0.027 \pm 0.022$	
132 – 173	$0.680 \pm 0.029 \pm 0.020$	$0.706 \pm 0.035 \pm 0.033$	
173 – 253	$0.728 \pm 0.044 \pm 0.029$	$0.774 \pm 0.056 \pm 0.051$	
253 – 600	$0.761 \pm 0.074 \pm 0.046$	$0.831 \pm 0.096 \pm 0.082$	

Table 17: The angular coefficient $A_3 \pm \delta_{\text{stat}} \pm \delta_{\text{syst}}$ in bins of y^Z .

p_T^Z range [GeV]	y^Z -binned A_3		
	$0 < y^Z < 1$	$1 < y^Z < 2$	$2 < y^Z < 3.5$
0.0 – 2.5	$-0.007 \pm 0.004 \pm 0.002$	$0.001 \pm 0.006 \pm 0.003$	$0.004 \pm 0.064 \pm 0.020$
2.5 – 5.0	$-0.006 \pm 0.002 \pm 0.001$	$0.004 \pm 0.002 \pm 0.001$	$0.020 \pm 0.029 \pm 0.009$
5.0 – 8.0	$-0.005 \pm 0.001 \pm 0.001$	$0.005 \pm 0.002 \pm 0.001$	$0.005 \pm 0.019 \pm 0.006$
8.0 – 11.4	$-0.004 \pm 0.001 \pm 0.001$	$0.005 \pm 0.002 \pm 0.001$	$0.003 \pm 0.015 \pm 0.005$
11.4 – 14.9	$-0.003 \pm 0.001 \pm 0.001$	$0.005 \pm 0.002 \pm 0.001$	$0.012 \pm 0.015 \pm 0.004$
14.9 – 18.5	$-0.003 \pm 0.001 \pm 0.001$	$0.005 \pm 0.002 \pm 0.001$	$0.009 \pm 0.016 \pm 0.005$
18.5 – 22.0	$-0.003 \pm 0.002 \pm 0.001$	$0.005 \pm 0.002 \pm 0.001$	$0.008 \pm 0.018 \pm 0.005$
22.0 – 25.5	$-0.003 \pm 0.002 \pm 0.001$	$0.005 \pm 0.002 \pm 0.001$	$0.029 \pm 0.022 \pm 0.006$
25.5 – 29.0	$-0.003 \pm 0.002 \pm 0.001$	$0.005 \pm 0.002 \pm 0.001$	$0.015 \pm 0.023 \pm 0.006$
29.0 – 32.6	$-0.002 \pm 0.002 \pm 0.001$	$0.005 \pm 0.003 \pm 0.001$	$0.026 \pm 0.025 \pm 0.007$
32.6 – 36.4	$-0.001 \pm 0.002 \pm 0.001$	$0.006 \pm 0.003 \pm 0.001$	$0.026 \pm 0.026 \pm 0.008$
36.4 – 40.4	$-0.001 \pm 0.003 \pm 0.001$	$0.007 \pm 0.003 \pm 0.002$	$0.031 \pm 0.027 \pm 0.008$
40.4 – 44.9	$0.000 \pm 0.003 \pm 0.002$	$0.009 \pm 0.004 \pm 0.002$	$0.052 \pm 0.026 \pm 0.008$
44.9 – 50.2	$0.002 \pm 0.003 \pm 0.002$	$0.012 \pm 0.004 \pm 0.002$	$0.040 \pm 0.024 \pm 0.009$
50.2 – 56.4	$0.005 \pm 0.004 \pm 0.002$	$0.016 \pm 0.004 \pm 0.002$	$0.072 \pm 0.025 \pm 0.010$
56.4 – 63.9	$0.007 \pm 0.004 \pm 0.002$	$0.021 \pm 0.005 \pm 0.002$	$0.075 \pm 0.027 \pm 0.012$
63.9 – 73.4	$0.010 \pm 0.005 \pm 0.003$	$0.027 \pm 0.006 \pm 0.003$	$0.092 \pm 0.029 \pm 0.013$
73.4 – 85.4	$0.013 \pm 0.006 \pm 0.003$	$0.035 \pm 0.007 \pm 0.004$	$0.119 \pm 0.034 \pm 0.016$
85.4 – 105	$0.016 \pm 0.007 \pm 0.003$	$0.045 \pm 0.008 \pm 0.004$	$0.140 \pm 0.053 \pm 0.030$
105 – 132	$0.018 \pm 0.008 \pm 0.004$	$0.058 \pm 0.009 \pm 0.004$	
132 – 173	$0.019 \pm 0.010 \pm 0.004$	$0.075 \pm 0.012 \pm 0.006$	
173 – 253	$0.019 \pm 0.016 \pm 0.007$	$0.096 \pm 0.020 \pm 0.009$	
253 – 600	$0.017 \pm 0.028 \pm 0.012$	$0.121 \pm 0.036 \pm 0.016$	

Table 18: The angular coefficient $A_4 \pm \delta_{\text{stat}} \pm \delta_{\text{syst}}$ in bins of y^Z .

p_T^Z range [GeV]	y^Z -binned A_4		
	$0 < y^Z < 1$	$1 < y^Z < 2$	$2 < y^Z < 3.5$
0.0 – 2.5	$0.019 \pm 0.004 \pm 0.002$	$0.048 \pm 0.005 \pm 0.003$	$0.095 \pm 0.014 \pm 0.007$
2.5 – 5.0	$0.023 \pm 0.002 \pm 0.001$	$0.060 \pm 0.002 \pm 0.001$	$0.139 \pm 0.010 \pm 0.004$
5.0 – 8.0	$0.023 \pm 0.002 \pm 0.001$	$0.065 \pm 0.002 \pm 0.001$	$0.142 \pm 0.009 \pm 0.004$
8.0 – 11.4	$0.022 \pm 0.002 \pm 0.001$	$0.066 \pm 0.002 \pm 0.001$	$0.140 \pm 0.008 \pm 0.004$
11.4 – 14.9	$0.020 \pm 0.002 \pm 0.001$	$0.064 \pm 0.002 \pm 0.001$	$0.127 \pm 0.009 \pm 0.004$
14.9 – 18.5	$0.018 \pm 0.002 \pm 0.001$	$0.061 \pm 0.003 \pm 0.001$	$0.123 \pm 0.010 \pm 0.004$
18.5 – 22.0	$0.017 \pm 0.002 \pm 0.001$	$0.059 \pm 0.003 \pm 0.002$	$0.118 \pm 0.012 \pm 0.005$
22.0 – 25.5	$0.016 \pm 0.003 \pm 0.001$	$0.057 \pm 0.003 \pm 0.002$	$0.116 \pm 0.014 \pm 0.005$
25.5 – 29.0	$0.016 \pm 0.003 \pm 0.001$	$0.056 \pm 0.003 \pm 0.002$	$0.115 \pm 0.016 \pm 0.005$
29.0 – 32.6	$0.016 \pm 0.003 \pm 0.001$	$0.056 \pm 0.004 \pm 0.002$	$0.128 \pm 0.017 \pm 0.006$
32.6 – 36.4	$0.018 \pm 0.003 \pm 0.002$	$0.056 \pm 0.004 \pm 0.002$	$0.130 \pm 0.019 \pm 0.006$
36.4 – 40.4	$0.019 \pm 0.004 \pm 0.002$	$0.056 \pm 0.004 \pm 0.002$	$0.143 \pm 0.020 \pm 0.007$
40.4 – 44.9	$0.020 \pm 0.004 \pm 0.002$	$0.056 \pm 0.005 \pm 0.002$	$0.132 \pm 0.020 \pm 0.007$
44.9 – 50.2	$0.020 \pm 0.004 \pm 0.002$	$0.055 \pm 0.005 \pm 0.003$	$0.124 \pm 0.018 \pm 0.007$
50.2 – 56.4	$0.020 \pm 0.004 \pm 0.002$	$0.052 \pm 0.005 \pm 0.003$	$0.109 \pm 0.019 \pm 0.008$
56.4 – 63.9	$0.020 \pm 0.004 \pm 0.002$	$0.048 \pm 0.005 \pm 0.003$	$0.091 \pm 0.019 \pm 0.008$
63.9 – 73.4	$0.019 \pm 0.004 \pm 0.002$	$0.044 \pm 0.005 \pm 0.003$	$0.093 \pm 0.019 \pm 0.009$
73.4 – 85.4	$0.018 \pm 0.004 \pm 0.002$	$0.038 \pm 0.006 \pm 0.003$	$0.089 \pm 0.019 \pm 0.009$
85.4 – 105	$0.016 \pm 0.005 \pm 0.002$	$0.034 \pm 0.006 \pm 0.003$	$0.122 \pm 0.026 \pm 0.015$
105 – 132	$0.014 \pm 0.005 \pm 0.003$	$0.031 \pm 0.007 \pm 0.003$	
132 – 173	$0.014 \pm 0.006 \pm 0.003$	$0.033 \pm 0.008 \pm 0.004$	
173 – 253	$0.015 \pm 0.010 \pm 0.004$	$0.042 \pm 0.013 \pm 0.006$	
253 – 600	$0.020 \pm 0.020 \pm 0.008$	$0.063 \pm 0.026 \pm 0.011$	

Table 19: The angular coefficient $A_5 \pm \delta_{\text{stat}} \pm \delta_{\text{syst}}$ in bins of y^Z .

p_T^Z range [GeV]	y^Z -binned A_5		
	$0 < y^Z < 1$	$1 < y^Z < 2$	$2 < y^Z < 3.5$
0.0 – 2.5	$-0.002 \pm 0.005 \pm 0.003$	$0.000 \pm 0.007 \pm 0.004$	$-0.030 \pm 0.072 \pm 0.025$
2.5 – 5.0	$-0.003 \pm 0.002 \pm 0.001$	$-0.002 \pm 0.003 \pm 0.002$	$0.012 \pm 0.026 \pm 0.009$
5.0 – 8.0	$-0.003 \pm 0.002 \pm 0.001$	$-0.001 \pm 0.002 \pm 0.001$	$0.013 \pm 0.015 \pm 0.005$
8.0 – 11.4	$-0.002 \pm 0.002 \pm 0.001$	$0.000 \pm 0.002 \pm 0.001$	$0.006 \pm 0.013 \pm 0.005$
11.4 – 14.9	$0.000 \pm 0.002 \pm 0.001$	$0.003 \pm 0.002 \pm 0.001$	$0.004 \pm 0.013 \pm 0.005$
14.9 – 18.5	$0.000 \pm 0.002 \pm 0.001$	$0.004 \pm 0.002 \pm 0.001$	$0.000 \pm 0.014 \pm 0.005$
18.5 – 22.0	$0.002 \pm 0.002 \pm 0.001$	$0.005 \pm 0.002 \pm 0.001$	$0.004 \pm 0.016 \pm 0.005$
22.0 – 25.5	$0.003 \pm 0.002 \pm 0.001$	$0.005 \pm 0.002 \pm 0.001$	$0.013 \pm 0.018 \pm 0.006$
25.5 – 29.0	$0.003 \pm 0.002 \pm 0.001$	$0.004 \pm 0.003 \pm 0.001$	$0.012 \pm 0.020 \pm 0.006$
29.0 – 32.6	$0.004 \pm 0.002 \pm 0.001$	$0.003 \pm 0.003 \pm 0.001$	$0.025 \pm 0.022 \pm 0.007$
32.6 – 36.4	$0.004 \pm 0.002 \pm 0.001$	$0.002 \pm 0.003 \pm 0.001$	$0.026 \pm 0.023 \pm 0.008$
36.4 – 40.4	$0.003 \pm 0.003 \pm 0.001$	$0.001 \pm 0.003 \pm 0.002$	$0.041 \pm 0.025 \pm 0.008$
40.4 – 44.9	$0.002 \pm 0.003 \pm 0.002$	$0.001 \pm 0.004 \pm 0.002$	$0.030 \pm 0.025 \pm 0.008$
44.9 – 50.2	$0.002 \pm 0.003 \pm 0.002$	$0.002 \pm 0.004 \pm 0.002$	$0.025 \pm 0.023 \pm 0.009$
50.2 – 56.4	$0.001 \pm 0.003 \pm 0.002$	$0.004 \pm 0.004 \pm 0.002$	$0.002 \pm 0.025 \pm 0.010$
56.4 – 63.9	$0.001 \pm 0.003 \pm 0.002$	$0.006 \pm 0.004 \pm 0.002$	$-0.014 \pm 0.026 \pm 0.011$
63.9 – 73.4	$0.001 \pm 0.004 \pm 0.002$	$0.009 \pm 0.005 \pm 0.002$	$-0.010 \pm 0.028 \pm 0.012$
73.4 – 85.4	$0.003 \pm 0.005 \pm 0.002$	$0.011 \pm 0.005 \pm 0.003$	$-0.052 \pm 0.032 \pm 0.014$
85.4 – 105	$0.006 \pm 0.005 \pm 0.003$	$0.010 \pm 0.006 \pm 0.003$	$0.005 \pm 0.049 \pm 0.026$
105 – 132	$0.011 \pm 0.006 \pm 0.003$	$0.006 \pm 0.007 \pm 0.004$	
132 – 173	$0.018 \pm 0.008 \pm 0.004$	$-0.004 \pm 0.010 \pm 0.005$	
173 – 253	$0.030 \pm 0.014 \pm 0.007$	$-0.023 \pm 0.017 \pm 0.008$	
253 – 600	$0.045 \pm 0.025 \pm 0.012$	$-0.055 \pm 0.031 \pm 0.014$	

Table 20: The angular coefficient $A_6 \pm \delta_{\text{stat}} \pm \delta_{\text{syst}}$ in bins of y^Z . The A_6 measurements are missing from the third y^Z bin since they are inaccessible in the ee_{CF} channel.

p_T^Z range [GeV]	y^Z -binned A_6		
	$0 < y^Z < 1$	$1 < y^Z < 2$	$2 < y^Z < 3.5$
0.0 – 2.5	$0.008 \pm 0.004 \pm 0.003$	$0.003 \pm 0.005 \pm 0.003$	
2.5 – 5.0	$0.000 \pm 0.002 \pm 0.001$	$0.000 \pm 0.002 \pm 0.001$	
5.0 – 8.0	$-0.003 \pm 0.002 \pm 0.001$	$0.000 \pm 0.002 \pm 0.001$	
8.0 – 11.4	$-0.003 \pm 0.002 \pm 0.001$	$0.000 \pm 0.002 \pm 0.001$	
11.4 – 14.9	$-0.002 \pm 0.002 \pm 0.001$	$0.001 \pm 0.002 \pm 0.001$	
14.9 – 18.5	$-0.002 \pm 0.002 \pm 0.001$	$0.002 \pm 0.002 \pm 0.001$	
18.5 – 22.0	$-0.001 \pm 0.002 \pm 0.001$	$0.002 \pm 0.002 \pm 0.001$	
22.0 – 25.5	$-0.001 \pm 0.002 \pm 0.001$	$0.003 \pm 0.003 \pm 0.001$	
25.5 – 29.0	$-0.001 \pm 0.002 \pm 0.002$	$0.003 \pm 0.003 \pm 0.001$	
29.0 – 32.6	$-0.002 \pm 0.002 \pm 0.002$	$0.004 \pm 0.003 \pm 0.001$	
32.6 – 36.4	$-0.003 \pm 0.003 \pm 0.002$	$0.004 \pm 0.003 \pm 0.001$	
36.4 – 40.4	$-0.003 \pm 0.003 \pm 0.002$	$0.005 \pm 0.003 \pm 0.002$	
40.4 – 44.9	$-0.003 \pm 0.003 \pm 0.002$	$0.006 \pm 0.004 \pm 0.002$	
44.9 – 50.2	$-0.002 \pm 0.003 \pm 0.002$	$0.008 \pm 0.004 \pm 0.002$	
50.2 – 56.4	$0.000 \pm 0.003 \pm 0.002$	$0.011 \pm 0.004 \pm 0.002$	
56.4 – 63.9	$0.002 \pm 0.003 \pm 0.002$	$0.013 \pm 0.004 \pm 0.002$	
63.9 – 73.4	$0.005 \pm 0.004 \pm 0.002$	$0.017 \pm 0.004 \pm 0.002$	
73.4 – 85.4	$0.007 \pm 0.004 \pm 0.002$	$0.019 \pm 0.005 \pm 0.002$	
85.4 – 105	$0.008 \pm 0.005 \pm 0.003$	$0.020 \pm 0.005 \pm 0.003$	
105 – 132	$0.006 \pm 0.005 \pm 0.003$	$0.019 \pm 0.006 \pm 0.003$	
132 – 173	$-0.001 \pm 0.007 \pm 0.004$	$0.013 \pm 0.008 \pm 0.004$	
173 – 253	$-0.018 \pm 0.011 \pm 0.007$	$0.002 \pm 0.014 \pm 0.006$	
253 – 600	$-0.047 \pm 0.021 \pm 0.013$	$-0.017 \pm 0.027 \pm 0.011$	

Table 21: The angular coefficient $A_7 \pm \delta_{\text{stat}} \pm \delta_{\text{syst}}$ in bins of y^Z .

p_T^Z range [GeV]	y^Z -binned A_7		
	$0 < y^Z < 1$	$1 < y^Z < 2$	$2 < y^Z < 3.5$
0.0 – 2.5	$0.004 \pm 0.003 \pm 0.002$	$0.001 \pm 0.003 \pm 0.002$	$-0.023 \pm 0.013 \pm 0.007$
2.5 – 5.0	$0.001 \pm 0.001 \pm 0.001$	$0.001 \pm 0.002 \pm 0.001$	$-0.005 \pm 0.006 \pm 0.003$
5.0 – 8.0	$0.000 \pm 0.001 \pm 0.001$	$0.000 \pm 0.001 \pm 0.001$	$-0.004 \pm 0.006 \pm 0.003$
8.0 – 11.4	$0.000 \pm 0.001 \pm 0.001$	$0.000 \pm 0.001 \pm 0.001$	$0.007 \pm 0.006 \pm 0.002$
11.4 – 14.9	$0.001 \pm 0.001 \pm 0.001$	$-0.001 \pm 0.001 \pm 0.001$	$0.006 \pm 0.006 \pm 0.002$
14.9 – 18.5	$0.002 \pm 0.001 \pm 0.001$	$-0.001 \pm 0.001 \pm 0.001$	$0.008 \pm 0.007 \pm 0.003$
18.5 – 22.0	$0.002 \pm 0.002 \pm 0.001$	$-0.001 \pm 0.002 \pm 0.001$	$0.006 \pm 0.009 \pm 0.003$
22.0 – 25.5	$0.002 \pm 0.002 \pm 0.001$	$0.000 \pm 0.002 \pm 0.001$	$0.010 \pm 0.010 \pm 0.004$
25.5 – 29.0	$0.001 \pm 0.002 \pm 0.001$	$0.000 \pm 0.002 \pm 0.001$	$0.005 \pm 0.011 \pm 0.004$
29.0 – 32.6	$0.000 \pm 0.002 \pm 0.001$	$0.001 \pm 0.002 \pm 0.001$	$0.010 \pm 0.013 \pm 0.004$
32.6 – 36.4	$0.000 \pm 0.002 \pm 0.001$	$0.002 \pm 0.002 \pm 0.001$	$0.011 \pm 0.014 \pm 0.005$
36.4 – 40.4	$-0.001 \pm 0.002 \pm 0.001$	$0.004 \pm 0.003 \pm 0.001$	$0.007 \pm 0.016 \pm 0.005$
40.4 – 44.9	$-0.001 \pm 0.002 \pm 0.001$	$0.006 \pm 0.003 \pm 0.002$	$0.011 \pm 0.016 \pm 0.005$
44.9 – 50.2	$-0.001 \pm 0.002 \pm 0.001$	$0.007 \pm 0.003 \pm 0.002$	$0.009 \pm 0.015 \pm 0.006$
50.2 – 56.4	$0.000 \pm 0.003 \pm 0.001$	$0.008 \pm 0.003 \pm 0.002$	$0.005 \pm 0.017 \pm 0.007$
56.4 – 63.9	$0.002 \pm 0.003 \pm 0.001$	$0.009 \pm 0.003 \pm 0.002$	$0.004 \pm 0.018 \pm 0.008$
63.9 – 73.4	$0.004 \pm 0.003 \pm 0.001$	$0.009 \pm 0.003 \pm 0.002$	$0.011 \pm 0.019 \pm 0.008$
73.4 – 85.4	$0.006 \pm 0.003 \pm 0.002$	$0.009 \pm 0.004 \pm 0.002$	$0.006 \pm 0.021 \pm 0.009$
85.4 – 105	$0.007 \pm 0.004 \pm 0.002$	$0.008 \pm 0.004 \pm 0.002$	$-0.005 \pm 0.032 \pm 0.017$
105 – 132	$0.006 \pm 0.004 \pm 0.002$	$0.005 \pm 0.005 \pm 0.003$	
132 – 173	$0.003 \pm 0.006 \pm 0.003$	$0.001 \pm 0.007 \pm 0.004$	
173 – 253	$-0.006 \pm 0.010 \pm 0.004$	$-0.003 \pm 0.013 \pm 0.007$	
253 – 600	$-0.022 \pm 0.018 \pm 0.007$	$-0.010 \pm 0.023 \pm 0.012$	

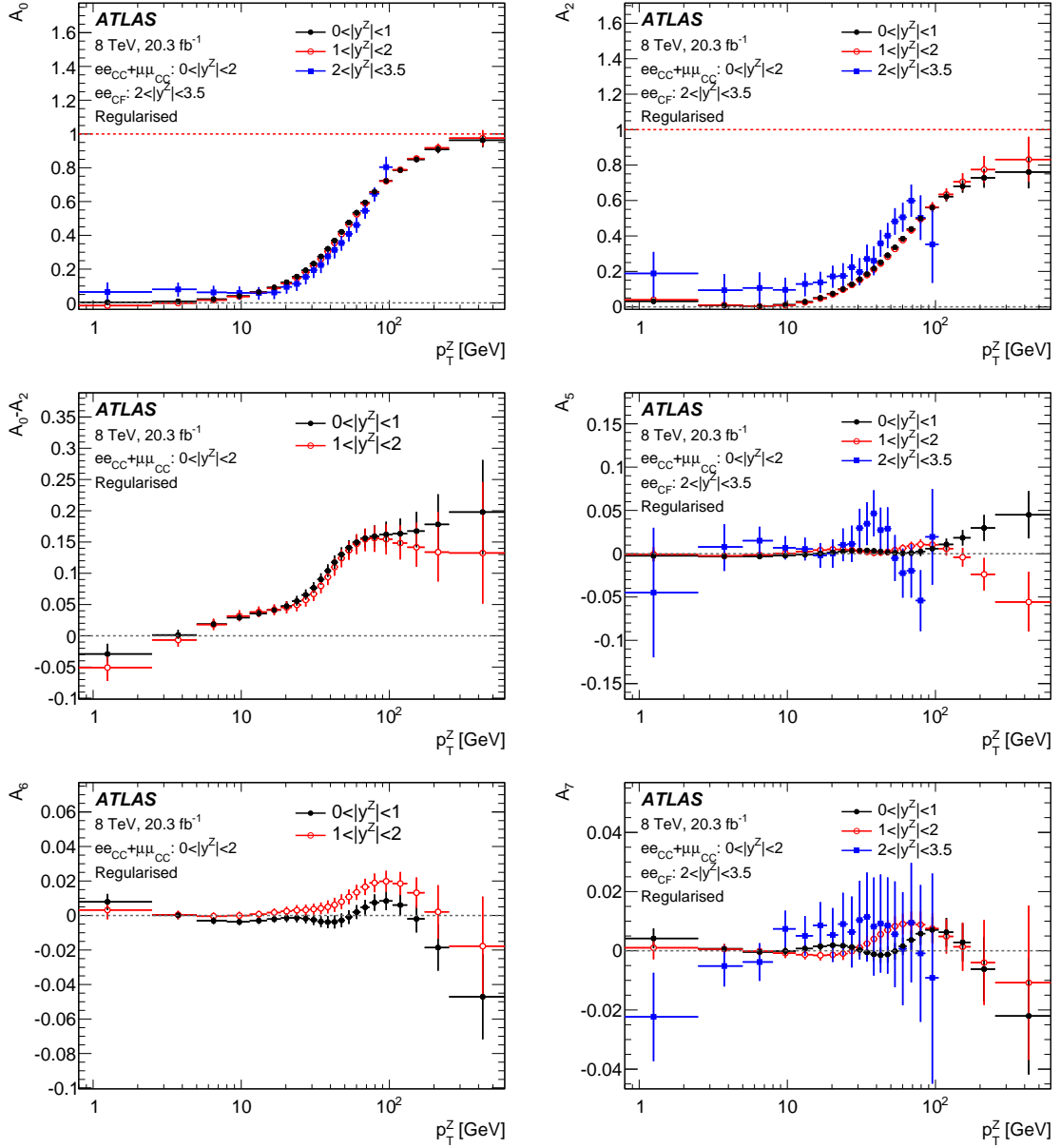


Figure 33: The measured angular coefficients A_0 , A_2 , $A_0 - A_2$, A_5 , A_6 , and A_7 in bins of y^Z .

Table 22: Summary of regularised uncertainties expected for A_0 and A_2 at low (5–8 GeV), mid (22–22.5 GeV), and high (132–173 GeV) p_T^Z for the $0 < |y^Z| < 1$ configuration. The total systematic uncertainty is shown with the breakdown into its underlying components. Entries marked with “-” indicate that the uncertainty is below 0.0001.

$p_T^Z = 5\text{--}8 \text{ GeV}$						
Coefficient	A_0			A_2		
Channel	ee	$\mu\mu$	$ee+\mu\mu$	ee	$\mu\mu$	$ee+\mu\mu$
Total	0.0098	0.0050	0.0053	0.0062	0.0055	0.0042
Data Stat.	0.0043	0.0038	0.0028	0.0049	0.0048	0.0034
Syst.	0.0088	0.0033	0.0045	0.0038	0.0029	0.0024
MC Stat.	0.0023	0.0021	0.0015	0.0025	0.0026	0.0018
Lepton	0.0072	0.0005	0.0017	0.0025	0.0015	0.0014
Bkg	0.0005	0.0003	-	0.0001	0.0002	0.0002
Theory	0.0006	0.0009	0.0006	0.0001	0.0002	0.0002
Method.	0.0020	0.0017	0.0015	0.0009	0.0009	0.0010
$p_T^Z = 22\text{--}25.5 \text{ GeV}$						
Coefficient	A_0			A_2		
Channel	ee	$\mu\mu$	$ee+\mu\mu$	ee	$\mu\mu$	$ee+\mu\mu$
Total	0.0098	0.0067	0.0066	0.0076	0.0068	0.0050
Data Stat.	0.0063	0.0056	0.0042	0.0059	0.0060	0.0042
Syst.	0.0075	0.0036	0.0050	0.0048	0.0032	0.0027
MC Stat.	0.0029	0.0027	0.0020	0.0029	0.0029	0.0021
Lepton	0.0056	0.0001	0.0016	0.0034	0.0003	0.0014
Bkg	0.0005	-	0.0003	0.0003	0.0002	0.0002
Theory	0.0009	0.0008	0.0007	0.0003	0.0003	0.0002
Method.	0.0022	0.0021	0.0024	0.0012	0.0012	0.0010
$p_T^Z = 132\text{--}173 \text{ GeV}$						
Coefficient	A_0			A_2		
Channel	ee	$\mu\mu$	$ee+\mu\mu$	ee	$\mu\mu$	$ee+\mu\mu$
Total	0.0158	0.0176	0.0131	0.0421	0.0474	0.0334
Data Stat.	0.0135	0.0141	0.0098	0.0372	0.0397	0.0272
Syst.	0.0081	0.0104	0.0088	0.0197	0.0259	0.0194
MC Stat.	0.0038	0.0080	0.0041	0.0109	0.0228	0.0116
Lepton	0.0028	0.0006	0.0014	0.0099	0.0033	0.0044
Bkg	0.0003	0.0008	0.0008	0.0023	0.0036	0.0020
Theory	-	0.0007	-	0.0018	0.0025	0.0011
Method.	0.0063	0.0071	0.0075	0.0135	0.0127	0.0148

Table 23: Summary of regularised uncertainties expected for A_0 and A_2 at low (5–8 GeV), mid (22–22.5 GeV), and high (132–173 GeV) p_T^Z for the $1 < |y^Z| < 2$ configuration. The total systematic uncertainty is shown with the breakdown into its underlying components. Entries marked with “-” indicate that the uncertainty is below 0.0001.

$p_T^Z = 5\text{--}8 \text{ GeV}$						
Coefficient	A_0			A_2		
Channel	ee	$\mu\mu$	$ee+\mu\mu$	ee	$\mu\mu$	$ee+\mu\mu$
Total	0.0110	0.0081	0.0079	0.0094	0.0064	0.0058
Data Stat.	0.0058	0.0048	0.0037	0.0070	0.0053	0.0044
Syst.	0.0094	0.0065	0.0070	0.0063	0.0037	0.0039
MC Stat.	0.0029	0.0025	0.0019	0.0034	0.0026	0.0020
Lepton	0.0077	0.0009	0.0019	0.0055	0.0025	0.0023
Bkg	0.0003	0.0004	0.0004	-	0.0001	0.0001
Theory	0.0058	0.0057	0.0047	-	0.0002	0.0001
Method.	0.0013	0.0012	0.0013	0.0025	0.0019	0.0023
$p_T^Z = 22\text{--}25.5 \text{ GeV}$						
Coefficient	A_0			A_2		
Channel	ee	$\mu\mu$	$ee+\mu\mu$	ee	$\mu\mu$	$ee+\mu\mu$
Total	0.0116	0.0095	0.0085	0.0120	0.0080	0.0064
Data Stat.	0.0084	0.0070	0.0054	0.0083	0.0066	0.0051
Syst.	0.0081	0.0065	0.0066	0.0086	0.0045	0.0039
MC Stat.	0.0040	0.0035	0.0026	0.0038	0.0031	0.0024
Lepton	0.0057	0.0005	0.0017	0.0058	0.0005	0.0017
Bkg	-	-	-	0.0005	0.0003	0.0003
Theory	0.0048	0.0051	0.0041	0.0006	0.0004	0.0004
Method.	0.0012	0.0017	0.0016	0.0026	0.0031	0.0025
$p_T^Z = 132\text{--}173 \text{ GeV}$						
Coefficient	A_0			A_2		
Channel	ee	$\mu\mu$	$ee+\mu\mu$	ee	$\mu\mu$	$ee+\mu\mu$
Total	0.0228	0.0201	0.0154	0.0684	0.0588	0.0482
Data Stat.	0.0195	0.0163	0.0124	0.0567	0.0457	0.0354
Syst.	0.0118	0.0117	0.0091	0.0383	0.0371	0.0328
MC Stat.	0.0050	0.0092	0.0054	0.0154	0.0263	0.0160
Lepton	0.0048	0.0010	0.0019	0.0152	0.0048	0.0059
Bkg	-	0.0008	0.0005	0.0038	0.0037	0.0027
Theory	-	0.0013	0.0010	0.0040	0.0037	0.0028
Method.	0.0070	0.0068	0.0068	0.0278	0.0259	0.0276

Table 24: Summary of regularised uncertainties expected for A_1 , A_3 , and A_4 at low (5–8 GeV), mid (22–22.5 GeV), and high (132–173 GeV) p_T^Z for the $0 < |y^Z| < 1$ configuration. The total systematic uncertainty is shown with the breakdown into its underlying components. Entries marked with “-” indicate that the uncertainty is below 0.0001.

$p_T^Z = 5\text{--}8 \text{ GeV}$									
Coefficient	A_1			A_3			A_4		
Channel	ee	$\mu\mu$	$ee+\mu\mu$	ee	$\mu\mu$	$ee+\mu\mu$	ee	$\mu\mu$	$ee+\mu\mu$
Total	0.0042	0.0032	0.0026	0.0024	0.0023	0.0016	0.0033	0.0029	0.0022
Data Stat.	0.0031	0.0027	0.0021	0.0021	0.0021	0.0015	0.0029	0.0026	0.0019
Syst.	0.0028	0.0017	0.0015	0.0011	0.0011	0.0008	0.0015	0.0014	0.0010
MC Stat.	0.0015	0.0014	0.0010	0.0010	0.0010	0.0007	0.0015	0.0014	0.0010
Lepton	0.0019	0.0013	0.0011	0.0004	0.0002	0.0002	0.0003	0.0001	0.0002
Bkg	0.0003	-	0.0001	0.0002	0.0002	0.0001	0.0001	0.0001	0.0001
Theory	0.0004	-	0.0002	0.0002	0.0001	0.0001	0.0002	0.0002	0.0002
Method.	0.0007	0.0008	0.0006	0.0002	0.0001	0.0002	-	0.0001	0.0001
$p_T^Z = 22\text{--}25.5 \text{ GeV}$									
Coefficient	A_1			A_3			A_4		
Channel	ee	$\mu\mu$	$ee+\mu\mu$	ee	$\mu\mu$	$ee+\mu\mu$	ee	$\mu\mu$	$ee+\mu\mu$
Total	0.0051	0.0044	0.0034	0.0031	0.0029	0.0021	0.0046	0.0042	0.0031
Data Stat.	0.0042	0.0039	0.0028	0.0027	0.0026	0.0019	0.0041	0.0037	0.0028
Syst.	0.0027	0.0021	0.0019	0.0014	0.0013	0.0009	0.0020	0.0019	0.0014
MC Stat.	0.0021	0.0019	0.0014	0.0013	0.0013	0.0009	0.0020	0.0019	0.0014
Lepton	0.0014	0.0007	0.0007	0.0002	-	0.0001	0.0003	0.0003	0.0002
Bkg	-	0.0001	0.0001	-	-	-	0.0002	0.0002	0.0001
Theory	-	0.0003	0.0002	-	-	-	0.0002	0.0002	0.0002
Method.	0.0012	0.0008	0.0010	0.0002	0.0002	0.0001	0.0002	0.0002	-
$p_T^Z = 132\text{--}173 \text{ GeV}$									
Coefficient	A_1			A_3			A_4		
Channel	ee	$\mu\mu$	$ee+\mu\mu$	ee	$\mu\mu$	$ee+\mu\mu$	ee	$\mu\mu$	$ee+\mu\mu$
Total	0.0156	0.0168	0.0117	0.0142	0.0162	0.0107	0.0094	0.0107	0.0071
Data Stat.	0.0144	0.0143	0.0101	0.0135	0.0141	0.0098	0.0091	0.0093	0.0065
Syst.	0.0059	0.0089	0.0058	0.0042	0.0081	0.0044	0.0025	0.0053	0.0028
MC Stat.	0.0044	0.0080	0.0044	0.0040	0.0080	0.0042	0.0025	0.0051	0.0027
Lepton	0.0016	0.0015	0.0013	0.0017	0.0004	0.0012	-	0.0006	0.0004
Bkg	0.0002	0.0011	0.0003	0.0011	-	0.0006	-	0.0004	0.0002
Theory	-	0.0011	0.0011	0.0009	-	0.0007	-	0.0004	-
Method.	0.0035	0.0038	0.0036	0.0015	0.0010	0.0010	0.0001	0.0007	0.0004

Table 25: Summary of regularised uncertainties expected for A_1 , A_3 , and A_4 at low (5–8 GeV), mid (22–22.5 GeV), and high (132–173 GeV) p_T^Z for the $1 < |y^Z| < 2$ configuration. The total systematic uncertainty is shown with the breakdown into its underlying components. Entries marked with “-” indicate that the uncertainty is below 0.0001.

$p_T^Z = 5\text{--}8 \text{ GeV}$									
Coefficient	A_1			A_3			A_4		
Channel	ee	$\mu\mu$	$ee+\mu\mu$	ee	$\mu\mu$	$ee+\mu\mu$	ee	$\mu\mu$	$ee+\mu\mu$
Total	0.0046	0.0041	0.0030	0.0033	0.0025	0.0020	0.0041	0.0036	0.0027
Data Stat.	0.0038	0.0032	0.0024	0.0029	0.0023	0.0018	0.0036	0.0031	0.0024
Syst.	0.0026	0.0026	0.0019	0.0015	0.0011	0.0009	0.0019	0.0017	0.0013
MC Stat.	0.0018	0.0016	0.0012	0.0014	0.0011	0.0008	0.0018	0.0016	0.0012
Lepton	0.0017	0.0023	0.0015	0.0001	0.0001	0.0001	0.0004	0.0001	0.0003
Bkg	-	0.0002	0.0002	-	0.0001	0.0001	0.0002	-	0.0001
Theory	0.0007	0.0004	0.0004	-	-	0.0001	0.0005	0.0004	0.0004
Method.	0.0007	0.0007	0.0007	0.0003	0.0003	0.0003	0.0001	0.0003	0.0003
$p_T^Z = 22\text{--}25.5 \text{ GeV}$									
Coefficient	A_1			A_3			A_4		
Channel	ee	$\mu\mu$	$ee+\mu\mu$	ee	$\mu\mu$	$ee+\mu\mu$	ee	$\mu\mu$	$ee+\mu\mu$
Total	0.0064	0.0052	0.0040	0.0042	0.0033	0.0026	0.0057	0.0049	0.0037
Data Stat.	0.0053	0.0044	0.0034	0.0038	0.0029	0.0023	0.0051	0.0044	0.0033
Syst.	0.0035	0.0027	0.0022	0.0018	0.0014	0.0011	0.0026	0.0022	0.0017
MC Stat.	0.0025	0.0021	0.0016	0.0017	0.0014	0.0011	0.0025	0.0022	0.0016
Lepton	0.0016	0.0011	0.0009	0.0005	0.0003	0.0003	0.0005	0.0003	0.0003
Bkg	0.0006	0.0004	0.0003	-	0.0002	0.0002	0.0003	0.0002	0.0001
Theory	0.0015	0.0012	0.0011	0.0002	0.0002	0.0002	0.0004	0.0003	0.0003
Method.	0.0009	0.0010	0.0008	0.0006	0.0003	0.0003	0.0006	0.0004	0.0004
$p_T^Z = 132\text{--}173 \text{ GeV}$									
Coefficient	A_1			A_3			A_4		
Channel	ee	$\mu\mu$	$ee+\mu\mu$	ee	$\mu\mu$	$ee+\mu\mu$	ee	$\mu\mu$	$ee+\mu\mu$
Total	0.0207	0.0197	0.0147	0.0199	0.0182	0.0134	0.0124	0.0122	0.0087
Data Stat.	0.0191	0.0168	0.0127	0.0189	0.0157	0.0121	0.0118	0.0105	0.0078
Syst.	0.0080	0.0103	0.0073	0.0063	0.0092	0.0058	0.0038	0.0061	0.0038
MC Stat.	0.0058	0.0094	0.0057	0.0056	0.0092	0.0055	0.0033	0.0059	0.0035
Lepton	0.0034	-	0.0014	0.0018	0.0025	0.0006	0.0004	0.0003	0.0004
Bkg	0.0011	0.0004	0.0003	0.0007	0.0009	-	0.0004	-	0.0001
Theory	0.0021	0.0016	0.0015	0.0008	0.0009	0.0003	0.0005	0.0003	0.0002
Method.	0.0042	0.0035	0.0040	0.0022	0.0017	0.0013	0.0015	0.0011	0.0014

Table 26: Summary of regularised uncertainties expected for A_5 , A_6 , and A_7 at low (5–8 GeV), mid (22–22.5 GeV), and high (132–173 GeV) p_T^Z for the $0 < |y^Z| < 1$ configuration. The total systematic uncertainty is shown with the breakdown into its underlying components. Entries marked with “-” indicate that the uncertainty is below 0.0001.

$p_T^Z = 5\text{--}8 \text{ GeV}$									
Coefficient	A_5			A_6			A_7		
Channel	ee	$\mu\mu$	$ee+\mu\mu$	ee	$\mu\mu$	$ee+\mu\mu$	ee	$\mu\mu$	$ee+\mu\mu$
Total	0.0027	0.0027	0.0019	0.0029	0.0027	0.0020	0.0020	0.0020	0.0014
Data Stat.	0.0024	0.0024	0.0017	0.0025	0.0023	0.0017	0.0018	0.0018	0.0013
Syst.	0.0013	0.0013	0.0010	0.0015	0.0014	0.0011	0.0010	0.0009	0.0007
MC Stat.	0.0012	0.0013	0.0008	0.0013	0.0012	0.0009	0.0009	0.0009	0.0006
Lepton	0.0002	-	-	0.0002	0.0001	-	0.0002	0.0001	0.0001
Bkg	-	-	-	0.0001	0.0001	-	0.0001	0.0001	-
Theory	0.0002	-	-	-	0.0001	-	0.0001	-	-
Method.	0.0005	0.0002	0.0004	0.0007	0.0007	0.0006	0.0001	-	-
$p_T^Z = 22\text{--}25.5 \text{ GeV}$									
Coefficient	A_5			A_6			A_7		
Channel	ee	$\mu\mu$	$ee+\mu\mu$	ee	$\mu\mu$	$ee+\mu\mu$	ee	$\mu\mu$	$ee+\mu\mu$
Total	0.0033	0.0033	0.0024	0.0037	0.0035	0.0027	0.0026	0.0026	0.0019
Data Stat.	0.0030	0.0029	0.0021	0.0033	0.0030	0.0022	0.0023	0.0023	0.0017
Syst.	0.0015	0.0016	0.0011	0.0019	0.0018	0.0015	0.0012	0.0012	0.0008
MC Stat.	0.0014	0.0015	0.0010	0.0016	0.0015	0.0011	0.0012	0.0012	0.0008
Lepton	0.0002	-	0.0001	0.0003	0.0002	0.0002	0.0002	0.0001	0.0001
Bkg	-	-	-	0.0001	0.0001	0.0001	0.0001	0.0001	0.0001
Theory	-	0.0001	-	0.0002	0.0001	0.0001	0.0001	0.0001	0.0001
Method.	0.0004	0.0005	0.0004	0.0009	0.0009	0.0010	0.0002	0.0001	0.0001
$p_T^Z = 132\text{--}173 \text{ GeV}$									
Coefficient	A_5			A_6			A_7		
Channel	ee	$\mu\mu$	$ee+\mu\mu$	ee	$\mu\mu$	$ee+\mu\mu$	ee	$\mu\mu$	$ee+\mu\mu$
Total	0.0116	0.0138	0.0090	0.0101	0.0117	0.0078	0.0083	0.0099	0.0064
Data Stat.	0.0110	0.0117	0.0080	0.0092	0.0097	0.0066	0.0080	0.0086	0.0059
Syst.	0.0036	0.0073	0.0040	0.0043	0.0066	0.0042	0.0023	0.0049	0.0025
MC Stat.	0.0032	0.0067	0.0033	0.0028	0.0055	0.0028	0.0022	0.0048	0.0024
Lepton	0.0008	-	-	0.0004	0.0005	0.0004	0.0005	0.0004	0.0003
Bkg	-	0.0001	-	-	0.0004	0.0002	0.0004	0.0003	0.0002
Theory	-	0.0004	0.0002	-	0.0004	0.0003	0.0003	0.0005	0.0002
Method.	0.0018	0.0027	0.0019	0.0034	0.0036	0.0030	0.0004	0.0004	0.0003

Table 27: Summary of regularised uncertainties expected for A_5 , A_6 , and A_7 at low (5–8 GeV), mid (22–22.5 GeV), and high (132–173 GeV) p_T^Z for the $1 < |y^Z| < 2$ configuration. The total systematic uncertainty is shown with the breakdown into its underlying components. Entries marked with “-” indicate that the uncertainty is below 0.0001.

$p_T^Z = 5\text{--}8 \text{ GeV}$									
Coefficient	A_5			A_6			A_7		
Channel	ee	$\mu\mu$	$ee+\mu\mu$	ee	$\mu\mu$	$ee+\mu\mu$	ee	$\mu\mu$	$ee+\mu\mu$
Total	0.0037	0.0028	0.0023	0.0034	0.0030	0.0022	0.0026	0.0021	0.0016
Data Stat.	0.0033	0.0025	0.0020	0.0030	0.0026	0.0020	0.0023	0.0018	0.0014
Syst.	0.0017	0.0013	0.0010	0.0016	0.0014	0.0010	0.0012	0.0010	0.0008
MC Stat.	0.0016	0.0013	0.0010	0.0016	0.0014	0.0010	0.0012	0.0009	0.0007
Lepton	0.0006	0.0002	0.0003	0.0003	0.0001	0.0001	0.0002	0.0001	0.0001
Bkg	0.0003	0.0002	0.0001	0.0001	0.0001	0.0001	0.0001	0.0001	-
Theory	0.0003	0.0002	0.0002	0.0001	0.0001	0.0001	0.0001	0.0001	0.0001
Method.	0.0002	0.0002	0.0002	0.0002	0.0001	0.0001	0.0003	0.0004	0.0004
$p_T^Z = 22\text{--}25.5 \text{ GeV}$									
Coefficient	A_5			A_6			A_7		
Channel	ee	$\mu\mu$	$ee+\mu\mu$	ee	$\mu\mu$	$ee+\mu\mu$	ee	$\mu\mu$	$ee+\mu\mu$
Total	0.0044	0.0035	0.0027	0.0046	0.0039	0.0030	0.0034	0.0027	0.0022
Data Stat.	0.0039	0.0031	0.0024	0.0041	0.0035	0.0026	0.0030	0.0024	0.0019
Syst.	0.0020	0.0016	0.0012	0.0021	0.0017	0.0013	0.0016	0.0013	0.0011
MC Stat.	0.0019	0.0015	0.0012	0.0020	0.0017	0.0013	0.0015	0.0012	0.0009
Lepton	0.0004	0.0003	0.0004	0.0005	0.0002	0.0003	0.0003	0.0001	0.0002
Bkg	0.0003	-	0.0002	0.0002	0.0001	0.0001	0.0001	0.0001	0.0001
Theory	0.0001	0.0003	0.0002	0.0002	0.0002	0.0001	0.0002	0.0001	0.0001
Method.	0.0003	0.0002	0.0002	0.0006	-	0.0002	0.0005	0.0004	0.0005
$p_T^Z = 132\text{--}173 \text{ GeV}$									
Coefficient	A_5			A_6			A_7		
Channel	ee	$\mu\mu$	$ee+\mu\mu$	ee	$\mu\mu$	$ee+\mu\mu$	ee	$\mu\mu$	$ee+\mu\mu$
Total	0.0159	0.0145	0.0108	0.0129	0.0122	0.0089	0.0118	0.0109	0.0082
Data Stat.	0.0152	0.0126	0.0097	0.0124	0.0106	0.0081	0.0111	0.0092	0.0072
Syst.	0.0047	0.0073	0.0048	0.0036	0.0061	0.0037	0.0039	0.0058	0.0040
MC Stat.	0.0043	0.0074	0.0045	0.0035	0.0060	0.0036	0.0032	0.0052	0.0032
Lepton	0.0027	0.0013	0.0010	0.0007	0.0006	0.0006	0.0008	0.0006	0.0006
Bkg	0.0019	-	-	0.0006	0.0005	0.0004	0.0007	0.0004	0.0003
Theory	0.0017	-	-	0.0006	0.0005	0.0004	0.0005	0.0004	0.0003
Method.	0.0006	0.0012	0.0016	0.0006	0.0001	0.0003	0.0022	0.0025	0.0022

References

- [1] J. C. Collins and D. E. Soper,
Angular Distribution of Dileptons in High-Energy Hadron Collisions,
Phys. Rev. D **16** (1977) 2219.
- [2] E. Mirkes, *Angular decay distributions of lepton from W-bosons at NLO in hadron colliders*,
Nucl. Phys. B **387** (1992) 3.
- [3] E. Mirkes and J. Ohnemus, *W and Z Polarization Effects in Hadronic Collisions*,
Phys. Rev. D **50** (1994) 5692, arXiv:[9406381 \[hep-ph\]](#).
- [4] E. Mirkes and J. Ohnemus, *Angular distributions of Drell-Yan lepton pairs at the Tevatron: order α_s^2 corrections and Monte Carlo studies.*, *Phys. Rev. D* **51** (1995) 4891,
arXiv:[9412289 \[hep-ph\]](#).
- [5] E. Mirkes and J. Ohnemus,
Polarization effects in Drell-Yan type processes $h_1 + h_2 \rightarrow (W, Z, \gamma^, J/\psi) + X$* (1994),
arXiv:[9408402 \[hep-ph\]](#).
- [6] S. Jadach and Z. Was,
Suppression of QED interference contributions to the charge asymmetry at the Z resonance,
Phys. Lett. B **219** (1989) 103.
- [7] S. Jadach et al., *Initial final state interference in the Z line shape*, *Phys. Lett. B* **465** (1999) 254,
arXiv:[9907547 \[hep-ph\]](#).
- [8] C. Lam and W.-K. Tung,
A Systematic Approach to Inclusive Lepton Pair Production in Hadronic Collisions,
Phys. Rev. D **18** (1978) 2447.
- [9] C. Lam and W.-K. Tung,
Structure Function Relations at Large Transverse Momenta in Lepton Pair Production Processes,
Phys. Lett. B **80** (1979) 228.
- [10] C. Lam and W.-K. Tung,
A Parton Model Relation Sans QCD Modifications in Lepton Pair Productions,
Phys. Rev. D **21** (1980) 2712.
- [11] K. Hagiwara, K. Hikasa and N. Kai,
Time-reversal-odd asymmetry in semi-inclusive lepton production in quantum chromodynamics,
Phys. Rev. D **27** (1983) 84.
- [12] K. Hagiwara, T. Kuruma and Y. Yamada, *Probing the one loop Z g g vertex at hadron colliders*,
Nucl. Phys. B **369** (1992) 171.
- [13] A. Karlberg, E. Re and G. Zanderighi, *NNLOPS accurate Drell-Yan production*,
JHEP **09** (2014) 134, arXiv:[1407.2940 \[hep-ph\]](#).
- [14] P. Nason, *A New method for combining NLO QCD with shower Monte Carlo algorithms*,
JHEP **11** (2004) 040, arXiv:[0409146 \[hep-ph\]](#).
- [15] S. Frixione, P. Nason and C. Oleari,
Matching NLO QCD computations with Parton Shower simulations: the POWHEG method,
JHEP **11** (2007) 070, arXiv:[0709.2092 \[hep-ph\]](#).

- [16] S. Alioli et al., *NLO vector-boson production matched with shower in POWHEG*, **JHEP** **07** (2008) 060, arXiv:[0805.4802 \[hep-ph\]](#).
- [17] S. Alioli et al., *A general framework for implementing NLO calculations in shower Monte Carlo programs: the POWHEG BOX*, **JHEP** **06** (2010) 043, arXiv:[1002.2581 \[hep-ph\]](#).
- [18] Z. Bern et al., *Left-Handed W Bosons at the LHC*, **Phys. Rev. D** **84** (2011) 034008, arXiv:[1103.5445 \[hep-ph\]](#).
- [19] CDF Collaboration, T. Aaltonen et al., *First Measurement of the Angular Coefficients of Drell-Yan e^+e^- pairs in the Z Mass Region from $p\bar{p}$ Collisions at $\sqrt{s} = 1.96$ TeV*, **Phys. Rev. Lett.** **106** (2011) 241801, arXiv:[1103.5699 \[hep-ex\]](#).
- [20] CDF Collaboration, T. Aaltonen et al., *Indirect measurement of $\sin\theta_W^2$ using e^+e^- pairs from γ^*/Z bosons produced in $p\bar{p}$ collisions at a centre-of-momentum energy of 1.96 TeV*, **Phys. Rev. D** **88.7** (2013) 072002, [Erratum: **Phys. Rev.D88,no.7,079905(2013)**], arXiv:[1307.0770 \[hep-ex\]](#).
- [21] ATLAS Collaboration, *Measurement of the polarisation of W bosons produced with large transverse momentum in pp collisions at $\sqrt{s} = 7$ TeV with the ATLAS experiment*, **Eur. Phys. J. C** **72** (2012) 2001, arXiv:[1203.2165 \[hep-ex\]](#).
- [22] CMS Collaboration, *Measurement of the Polarization of W Bosons with Large Transverse Momenta in W+Jets Events at the LHC*, **Phys. Rev. Lett.** **107** (2011) 021802, arXiv:[1104.3829 \[hep-ex\]](#).
- [23] CMS Collaboration, *Angular coefficients of Z bosons produced in pp collisions at $\sqrt{s} = 8$ TeV and decaying to $\mu^+\mu^-$ as a function of transverse momentum and rapidity*, **Phys. Lett. B** **750** (2015) 154, arXiv:[1504.03512 \[hep-ex\]](#).
- [24] ATLAS Collaboration, *The ATLAS Experiment at the CERN Large Hadron Collider*, **JINST** **3** (2008) S08003.
- [25] S. Catani et al., *Vector boson production at hadron colliders: A Fully exclusive QCD calculation at NNLO*, **Phys. Rev. Lett.** **103** (2009) 082001, arXiv:[0903.2120 \[hep-ph\]](#).
- [26] R. Gavin et al., *FEWZ 2.0: A code for hadronic Z production at next-to-next-to-leading order*, **Comput. Phys. Commun.** **182** (2011) 2388, arXiv:[1011.3540 \[hep-ph\]](#).
- [27] R. Gavin et al., *W Physics at the LHC with FEWZ 2.1*, **Comput. Phys. Commun.** **184** (2013) 208, arXiv:[1201.5896 \[hep-ph\]](#).
- [28] Y. Li and F. Petriello, *Combining QCD and electroweak corrections to dilepton production in FEWZ*, **Phys. Rev. D** **86** (2012) 094034, arXiv:[1208.5967 \[hep-ph\]](#).
- [29] ATLAS Collaboration, *Measurement of the Z/ γ^* boson transverse momentum distribution in pp collisions at $\sqrt{s} = 7$ TeV with the ATLAS detector*, **JHEP** **09** (2014) 145, arXiv:[1406.3660 \[hep-ex\]](#).
- [30] J. Gao et al., *CT10 next-to-next-to-leading order global analysis of QCD*, **Phys. Rev. D** **89.3** (2014) 033009, arXiv:[1302.6246 \[hep-ph\]](#).
- [31] S. Dittmaier and M. Kramer, *Electroweak radiative corrections to W-boson production at hadron colliders*, **Phys. Rev. D** **65** (2002) 073007, arXiv:[0109062 \[hep-ph\]](#).

- [32] K. A. Olive et al. (Particle Data Group), *Review of Particle Physics*, Chin. Phys. **C38** (2014).
- [33] H.-L. Lai et al., *New parton distributions for collider physics*, Phys. Rev. D **82** (2010) 074024, arXiv:[1007.2241 \[hep-ph\]](#).
- [34] T. Sjöstrand, S. Mrenna, and P. Skands, *A Brief Introduction to PYTHIA 8.1*, Comput. Phys. Commun. **178** (2008) 852, arXiv:[0710.3820 \[hep-ph\]](#).
- [35] ATLAS Collaboration, *Summary of ATLAS Pythia 8 tunes*, ATL-PHYS-PUB-2012-003, 2012, URL: <https://cds.cern.ch/record/1474107>.
- [36] P. Golonka and Z. Was,
PHOTOS Monte Carlo: A Precision tool for QED corrections in Z and W decays, Eur. Phys. J. C **45** (2006) 97, arXiv:[0506026 \[hep-ph\]](#).
- [37] G. Corcella et al., *HERWIG 6: An Event generator for hadron emission reactions with interfering gluons (including supersymmetric processes)*, JHEP **01** (2001) 010, arXiv:[0011363 \[hep-ph\]](#).
- [38] J. M. Butterworth, J. R. Forshaw and M. Seymour,
Multiparton interactions in photoproduction at HERA, Z. Phys. C **72** (1996) 637, arXiv:[9601371 \[hep-ph\]](#).
- [39] T. Gleisberg, S. Hoeche, F. Krauss et al., *Event generation with SHERPA 1.1*, JHEP **02** (2009) 007, arXiv:[0811.4622 \[hep-ph\]](#).
- [40] S. Hoeche et al., *QCD matrix elements and truncated showers*, JHEP **05** (2009) 053, arXiv:[0903.1219 \[hep-ph\]](#).
- [41] T. Gleisberg and S. Hoeche, *Comix, a new matrix element generator*, JHEP **12** (2008) 039, arXiv:[0808.3674 \[hep-ph\]](#).
- [42] S. Schumann and F. Krauss,
A Parton shower algorithm based on Catani-Seymour dipole factorisation, JHEP **03** (2008) 038, arXiv:[0709.1027 \[hep-ph\]](#).
- [43] K. Hamilton, P. Nason and G. Zanderighi, *MiNLO: Multi-Scale Improved NLO*, JHEP **10** (2012) 155, arXiv:[1206.3572 \[hep-ph\]](#).
- [44] S. Agostinelli et al., *GEANT4: A simulation toolkit*, Nucl. Instrum. Meth. A **506** (2003) 250.
- [45] ATLAS Collaboration, *The ATLAS Simulation Infrastructure*, Eur. Phys. J. C **70** (2010) 823, arXiv:[1005.4568 \[hep-ex\]](#).
- [46] S. Frixione and B. R. Webber, *Matching NLO QCD computations and parton shower simulations*, JHEP **06** (2002) 029, arXiv:[0204244 \[hep-ph\]](#).
- [47] B. P. Kersevan and E. Richter-Was, *The Monte Carlo event generator AcerMC versions 2.0 to 3.8 with interfaces to PYTHIA 6.4, HERWIG 6.5 and ARIADNE 4.1*, Comput. Phys. Commun. **184** (2013) 919, arXiv:[0405247 \[hep-ph\]](#).
- [48] J. Pumplin et al.,
New generation of parton distributions with uncertainties from global QCD analysis, JHEP **07** (2002) 012, arXiv:[0201195 \[hep-ph\]](#).
- [49] A. D. Martin et al., *Parton distributions incorporating QED contributions*, Eur. Phys. J. C **39** (2005) 155, arXiv:[0411040 \[hep-ph\]](#).
- [50] ATLAS Collaboration, *Electron reconstruction and identification efficiency measurements with the ATLAS detector using the 2011 LHC proton-proton collision data*, Eur. Phys. J. C **74** (2014) 2941, arXiv:[1404.2240 \[hep-ex\]](#).

- [51] ATLAS Collaboration, *Electron efficiency measurements with the ATLAS detector using the 2012 LHC proton-proton collision data*, ATLAS-CONF-2014-032, 2014,
URL: <http://cds.cern.ch/record/1706245>.
- [52] ATLAS Collaboration, *Measurement of the muon reconstruction performance of the ATLAS detector using 2011 and 2012 LHC proton-proton collision data*, *Eur. Phys. J. C* **74** (2014) 3130, arXiv:[1407.3935 \[hep-ex\]](https://arxiv.org/abs/1407.3935).
- [53] ATLAS Collaboration, *Electron and photon energy calibration with the ATLAS detector using LHC Run 1 data*, *Eur. Phys. J. C* **74** (2014) 3071, arXiv:[1407.5063 \[hep-ex\]](https://arxiv.org/abs/1407.5063).
- [54] V. Blobel, *An unfolding method for high energy physics experiments* (2002), arXiv:[0208022 \[hep-ex\]](https://arxiv.org/abs/0208022).
- [55] G. Choudalakis, *Fully Bayesian Unfolding* (2012), arXiv:[1201.4612 \[physics.data-an\]](https://arxiv.org/abs/1201.4612).
- [56] F. James and M. Roos, *Minuit: A System for Function Minimization and Analysis of the Parameter Errors and Correlations*, *Comput. Phys. Commun.* **10** (1975) 343.
- [57] G. Cowan et al., *Asymptotic formulae for likelihood-based tests of new physics*, *Eur. Phys. J. C* **71** (2011) 1554, [Erratum: Eur. Phys. J. C 73,2501(2013)], arXiv:[1007.1727 \[physics.data-an\]](https://arxiv.org/abs/1007.1727).
- [58] ATLAS Collaboration, *Improved luminosity determination in pp collisions at $\sqrt{s} = 7$ TeV using the ATLAS detector at the LHC*, *Eur. Phys. J. C* **73** (2013) 2518, arXiv:[1302.4393 \[hep-ex\]](https://arxiv.org/abs/1302.4393).
- [59] R. D. Ball et al., *Parton distributions with LHC data*, *Nucl. Phys. B* **867** (2013) 244, arXiv:[1207.1303 \[hep-ph\]](https://arxiv.org/abs/1207.1303).
- [60] A. D. Martin et al., *Parton distributions for the LHC*, *Eur. Phys. J. C* **63** (2009) 189, arXiv:[0901.0002 \[hep-ph\]](https://arxiv.org/abs/0901.0002).
- [61] Z. Was and S. Jadach, *First- and higher-order non-interference QED radiative corrections to the charge asymmetry at the Z resonance*, *Phys. Rev. D* **41** (1990) 1425.
- [62] ATLAS Collaboration, *Measurement of the forward-backward asymmetry of electron and muon pair-production in pp collisions at $\sqrt{s} = 7$ TeV with the ATLAS detector*, *JHEP* **09** (2015) 049, arXiv:[1503.03709 \[hep-ex\]](https://arxiv.org/abs/1503.03709).

The ATLAS Collaboration

G. Aad⁸⁷, B. Abbott¹¹⁴, J. Abdallah⁶⁵, O. Abdinov¹², B. Abelsoos¹¹⁸, R. Aben¹⁰⁸, O.S. AbouZeid¹³⁸, N.L. Abraham¹⁵⁰, H. Abramowicz¹⁵⁴, H. Abreu¹⁵³, R. Abreu¹¹⁷, Y. Abulaiti^{147a,147b}, B.S. Acharya^{164a,164b,^a}, L. Adamczyk^{40a}, D.L. Adams²⁷, J. Adelman¹⁰⁹, S. Adomeit¹⁰¹, T. Adye¹³², A.A. Affolder⁷⁶, T. Agatonovic-Jovin¹⁴, J. Agricola⁵⁶, J.A. Aguilar-Saavedra^{127a,127f}, S.P. Ahlen²⁴, F. Ahmadov^{67,b}, G. Aielli^{134a,134b}, H. Akerstedt^{147a,147b}, T.P.A. Åkesson⁸³, A.V. Akimov⁹⁷, G.L. Alberghi^{22a,22b}, J. Albert¹⁶⁹, S. Albrand⁵⁷, M.J. Alconada Verzini⁷³, M. Aleksi³², I.N. Aleksandrov⁶⁷, C. Alexa^{28b}, G. Alexander¹⁵⁴, T. Alexopoulos¹⁰, M. Alhroob¹¹⁴, M. Aliev^{75a,75b}, G. Alimonti^{93a}, J. Alison³³, S.P. Alkire³⁷, B.M.M. Allbrooke¹⁵⁰, B.W. Allen¹¹⁷, P.P. Allport¹⁹, A. Aloisio^{105a,105b}, A. Alonso³⁸, F. Alonso⁷³, C. Alpigiani¹³⁹, M. Alstaty⁸⁷, B. Alvarez Gonzalez³², D. Álvarez Piqueras¹⁶⁷, M.G. Alviggi^{105a,105b}, B.T. Amadio¹⁶, K. Amako⁶⁸, Y. Amaral Coutinho^{26a}, C. Amelung²⁵, D. Amidei⁹¹, S.P. Amor Dos Santos^{127a,127c}, A. Amorim^{127a,127b}, S. Amoroso³², G. Amundsen²⁵, C. Anastopoulos¹⁴⁰, L.S. Ansu⁵¹, N. Andari¹⁰⁹, T. Andeen¹¹, C.F. Anders^{60b}, G. Anders³², J.K. Anders⁷⁶, K.J. Anderson³³, A. Andreazza^{93a,93b}, V. Andrei^{60a}, S. Angelidakis⁹, I. Angelozzi¹⁰⁸, P. Anger⁴⁶, A. Angerami³⁷, F. Anghinolfi³², A.V. Anisenkov^{110,c}, N. Anjos¹³, A. Annovi^{125a,125b}, M. Antonelli⁴⁹, A. Antonov⁹⁹, J. Antos^{145b}, F. Anulli^{133a}, M. Aoki⁶⁸, L. Aperio Bella¹⁹, G. Arabidze⁹², Y. Arai⁶⁸, J.P. Araque^{127a}, A.T.H. Arce⁴⁷, F.A. Arduh⁷³, J.-F. Arguin⁹⁶, S. Argyropoulos⁶⁵, M. Arik^{20a}, A.J. Armbruster¹⁴⁴, L.J. Armitage⁷⁸, O. Arnaez³², H. Arnold⁵⁰, M. Arratia³⁰, O. Arslan²³, A. Artamonov⁹⁸, G. Artoni¹²¹, S. Artz⁸⁵, S. Asai¹⁵⁶, N. Asbah⁴⁴, A. Ashkenazi¹⁵⁴, B. Åsman^{147a,147b}, L. Asquith¹⁵⁰, K. Assamagan²⁷, R. Astalos^{145a}, M. Atkinson¹⁶⁶, N.B. Atlay¹⁴², K. Augsten¹²⁹, G. Avolio³², B. Axen¹⁶, M.K. Ayoub¹¹⁸, G. Azuelos^{96,d}, M.A. Baak³², A.E. Baas^{60a}, M.J. Baca¹⁹, H. Bachacou¹³⁷, K. Bachas^{75a,75b}, M. Backes³², M. Backhaus³², P. Bagiacchi^{133a,133b}, P. Bagnaia^{133a,133b}, Y. Bai^{35a}, J.T. Barnes¹³², O.K. Baker¹⁷⁶, E.M. Baldin^{110,c}, P. Balek¹³⁰, T. Balestri¹⁴⁹, F. Balli¹³⁷, W.K. Balunas¹²³, E. Banas⁴¹, Sw. Banerjee^{173,e}, A.A.E. Bannoura¹⁷⁵, L. Barak³², E.L. Barberio⁹⁰, D. Barberis^{52a,52b}, M. Barbero⁸⁷, T. Barillari¹⁰², T. Barklow¹⁴⁴, N. Barlow³⁰, S.L. Barnes⁸⁶, B.M. Barnett¹³², R.M. Barnett¹⁶, Z. Barnovska⁵, A. Baroncelli^{135a}, G. Barone²⁵, A.J. Barr¹²¹, L. Barranco Navarro¹⁶⁷, F. Barreiro⁸⁴, J. Barreiro Guimarães da Costa^{35a}, R. Bartoldus¹⁴⁴, A.E. Barton⁷⁴, P. Bartos^{145a}, A. Basalaev¹²⁴, A. Bassalat¹¹⁸, R.L. Bates⁵⁵, S.J. Batista¹⁵⁹, J.R. Batley³⁰, M. Battaglia¹³⁸, M. Baucé^{133a,133b}, F. Bauer¹³⁷, H.S. Bawa^{144,f}, J.B. Beacham¹¹², M.D. Beattie⁷⁴, T. Beau⁸², P.H. Beauchemin¹⁶², P. Bechtle²³, H.P. Beck^{18,g}, K. Becker¹²¹, M. Becker⁸⁵, M. Beckingham¹⁷⁰, C. Becot¹¹¹, A.J. Beddall^{20e}, A. Beddall^{20b}, V.A. Bednyakov⁶⁷, M. Bedognetti¹⁰⁸, C.P. Bee¹⁴⁹, L.J. Beemster¹⁰⁸, T.A. Beermann³², M. Begel²⁷, J.K. Behr⁴⁴, C. Belanger-Champagne⁸⁹, A.S. Bell⁸⁰, G. Bella¹⁵⁴, L. Bellagamba^{22a}, A. Bellerive³¹, M. Bellomo⁸⁸, K. Belotskiy⁹⁹, O. Beltramello³², N.L. Belyaev⁹⁹, O. Benary¹⁵⁴, D. Benchekroun^{136a}, M. Bender¹⁰¹, K. Bendtz^{147a,147b}, N. Benekos¹⁰, Y. Benhammou¹⁵⁴, E. Benhar Noccioli¹⁷⁶, J. Benitez⁶⁵, D.P. Benjamin⁴⁷, J.R. Bensinger²⁵, S. Bentvelsen¹⁰⁸, L. Beresford¹²¹, M. Beretta⁴⁹, D. Berge¹⁰⁸, E. Bergeaas Kuutmann¹⁶⁵, N. Berger⁵, J. Beringer¹⁶, S. Berlendis⁵⁷, N.R. Bernard⁸⁸, C. Bernius¹¹¹, F.U. Bernlochner²³, T. Berry⁷⁹, P. Berta¹³⁰, C. Bertella⁸⁵, G. Bertoli^{147a,147b}, F. Bertolucci^{125a,125b}, I.A. Bertram⁷⁴, C. Bertsche⁴⁴, D. Bertsche¹¹⁴, G.J. Besjes³⁸, O. Bessidskaia Bylund^{147a,147b}, M. Bessner⁴⁴, N. Besson¹³⁷, C. Betancourt⁵⁰, S. Bethke¹⁰², A.J. Bevan⁷⁸, W. Bhimji¹⁶, R.M. Bianchi¹²⁶, L. Bianchini²⁵, M. Bianco³², O. Biebel¹⁰¹, D. Biedermann¹⁷, R. Bielski⁸⁶, N.V. Biesuz^{125a,125b}, M. Biglietti^{135a}, J. Bilbao De Mendizabal⁵¹, H. Bilonok⁴⁹, M. Bindi⁵⁶, S. Binet¹¹⁸, A. Bingul^{20b}, C. Bini^{133a,133b}, S. Biondi^{22a,22b}, D.M. Bjergaard⁴⁷, C.W. Black¹⁵¹, J.E. Black¹⁴⁴, K.M. Black²⁴, D. Blackburn¹³⁹, R.E. Blair⁶, J.-B. Blanchard¹³⁷, J.E. Blanco⁷⁹, T. Blazek^{145a}, I. Bloch⁴⁴, C. Blocker²⁵, W. Blum^{85,*}, U. Blumenschein⁵⁶, S. Blunier^{34a},

G.J. Bobbink¹⁰⁸, V.S. Bobrovnikov^{110,c}, S.S. Bocchetta⁸³, A. Bocci⁴⁷, C. Bock¹⁰¹, M. Boehler⁵⁰,
 D. Boerner¹⁷⁵, J.A. Bogaerts³², D. Bogavac¹⁴, A.G. Bogdanchikov¹¹⁰, C. Bohm^{147a}, V. Boisvert⁷⁹,
 P. Bokan¹⁴, T. Bold^{40a}, A.S. Boldyrev^{164a,164c}, M. Bomben⁸², M. Bona⁷⁸, M. Boonekamp¹³⁷,
 A. Borisov¹³¹, G. Borissov⁷⁴, J. Bortfeldt¹⁰¹, D. Bortoletto¹²¹, V. Bortolotto^{62a,62b,62c}, K. Bos¹⁰⁸,
 D. Boscherini^{22a}, M. Bosman¹³, J.D. Bossio Sola²⁹, J. Boudreau¹²⁶, J. Bouffard²,
 E.V. Bouhova-Thacker⁷⁴, D. Boumediene³⁶, C. Bourdarios¹¹⁸, S.K. Boutle⁵⁵, A. Boveia³², J. Boyd³²,
 I.R. Boyko⁶⁷, J. Bracinik¹⁹, A. Brandt⁸, G. Brandt⁵⁶, O. Brandt^{60a}, U. Bratzler¹⁵⁷, B. Brau⁸⁸,
 J.E. Brau¹¹⁷, H.M. Braun^{175,*}, W.D. Breaden Madden⁵⁵, K. Brendlinger¹²³, A.J. Brennan⁹⁰,
 L. Brenner¹⁰⁸, R. Brenner¹⁶⁵, S. Bressler¹⁷², T.M. Bristow⁴⁸, D. Britton⁵⁵, D. Britzger⁴⁴, F.M. Brochu³⁰,
 I. Brock²³, R. Brock⁹², G. Brooijmans³⁷, T. Brooks⁷⁹, W.K. Brooks^{34b}, J. Brosamer¹⁶, E. Brost¹¹⁷,
 J.H. Broughton¹⁹, P.A. Bruckman de Renstrom⁴¹, D. Bruncko^{145b}, R. Bruneliere⁵⁰, A. Bruni^{22a},
 G. Bruni^{22a}, BH Brunt³⁰, M. Bruschi^{22a}, N. Bruscino²³, P. Bryant³³, L. Bryngemark⁸³, T. Buanes¹⁵,
 Q. Buat¹⁴³, P. Buchholz¹⁴², A.G. Buckley⁵⁵, I.A. Budagov⁶⁷, F. Buehrer⁵⁰, M.K. Bugge¹²⁰,
 O. Bulekov⁹⁹, D. Bullock⁸, H. Burckhart³², S. Burdin⁷⁶, C.D. Burgard⁵⁰, B. Burghgrave¹⁰⁹, K. Burka⁴¹,
 S. Burke¹³², I. Burmeister⁴⁵, E. Busato³⁶, D. Büscher⁵⁰, V. Büscher⁸⁵, P. Bussey⁵⁵, J.M. Butler²⁴,
 C.M. Buttar⁵⁵, J.M. Butterworth⁸⁰, P. Butti¹⁰⁸, W. Buttlinger²⁷, A. Buzatu⁵⁵, A.R. Buzykaev^{110,c},
 S. Cabrera Urbán¹⁶⁷, D. Caforio¹²⁹, V.M. Cairo^{39a,39b}, O. Cakir^{4a}, N. Calace⁵¹, P. Calafuria¹⁶,
 A. Calandri⁸⁷, G. Calderini⁸², P. Calfayan¹⁰¹, L.P. Caloba^{26a}, D. Calvet³⁶, S. Calvet³⁶, T.P. Calvet⁸⁷,
 R. Camacho Toro³³, S. Camarda³², P. Camarri^{134a,134b}, D. Cameron¹²⁰, R. Caminal Armadans¹⁶⁶,
 C. Camincher⁵⁷, S. Campana³², M. Campanelli⁸⁰, A. Camplani^{93a,93b}, A. Campoverde¹⁴⁹,
 V. Canale^{105a,105b}, A. Canepa^{160a}, M. Cano Bret^{35e}, J. Cantero¹¹⁵, R. Cantrill^{127a}, T. Cao⁴²,
 M.D.M. Capeans Garrido³², I. Caprini^{28b}, M. Caprini^{28b}, M. Capua^{39a,39b}, R. Caputo⁸⁵, R.M. Carbone³⁷,
 R. Cardarelli^{134a}, F. Cardillo⁵⁰, I. Carli¹³⁰, T. Carli³², G. Carlino^{105a}, L. Carminati^{93a,93b}, S. Caron¹⁰⁷,
 E. Carquin^{34b}, G.D. Carrillo-Montoya³², J.R. Carter³⁰, J. Carvalho^{127a,127c}, D. Casadei¹⁹,
 M.P. Casado^{13,h}, M. Casolino¹³, D.W. Casper¹⁶³, E. Castaneda-Miranda^{146a}, R. Castelijn¹⁰⁸,
 A. Castelli¹⁰⁸, V. Castillo Gimenez¹⁶⁷, N.F. Castro^{127a,i}, A. Catinaccio³², J.R. Catmore¹²⁰, A. Cattai³²,
 J. Caudron⁸⁵, V. Cavalieri¹⁶⁶, E. Cavallaro¹³, D. Cavalli^{93a}, M. Cavalli-Sforza¹³, V. Cavasinni^{125a,125b},
 F. Ceradini^{135a,135b}, L. Cerdá Alberich¹⁶⁷, B.C. Cerio⁴⁷, A.S. Cerqueira^{26b}, A. Cerri¹⁵⁰, L. Cerrito⁷⁸,
 F. Cerutti¹⁶, M. Cerv³², A. Cervelli¹⁸, S.A. Cetin^{20d}, A. Chafaq^{136a}, D. Chakraborty¹⁰⁹, S.K. Chan⁵⁹,
 Y.L. Chan^{62a}, P. Chang¹⁶⁶, J.D. Chapman³⁰, D.G. Charlton¹⁹, A. Chatterjee⁵¹, C.C. Chau¹⁵⁹,
 C.A. Chavez Barajas¹⁵⁰, S. Che¹¹², S. Cheatham⁷⁴, A. Chegwidden⁹², S. Chekanov⁶,
 S.V. Chekulaev^{160a}, G.A. Chelkov^{67,j}, M.A. Chelstowska⁹¹, C. Chen⁶⁶, H. Chen²⁷, K. Chen¹⁴⁹,
 S. Chen^{35c}, S. Chen¹⁵⁶, X. Chen^{35f}, Y. Chen⁶⁹, H.C. Cheng⁹¹, H.J. Cheng^{35a}, Y. Cheng³³,
 A. Cheplakov⁶⁷, E. Cheremushkina¹³¹, R. Cherkaoui El Moursli^{136e}, V. Chernyatin^{27,*}, E. Cheu⁷,
 L. Chevalier¹³⁷, V. Chiarella⁴⁹, G. Chiarelli^{125a,125b}, G. Chiodini^{75a}, A.S. Chisholm¹⁹, A. Chitan^{28b},
 M.V. Chizhov⁶⁷, K. Choi⁶³, A.R. Chomont³⁶, S. Chouridou⁹, B.K.B. Chow¹⁰¹, V. Christodoulou⁸⁰,
 D. Chromek-Burckhardt³², J. Chudoba¹²⁸, A.J. Chuinard⁸⁹, J.J. Chwastowski⁴¹, L. Chytka¹¹⁶,
 G. Ciapetti^{133a,133b}, A.K. Ciftci^{4a}, D. Cinca⁵⁵, V. Cindro⁷⁷, I.A. Cioara²³, A. Ciocio¹⁶, F. Cirotto^{105a,105b},
 Z.H. Citron¹⁷², M. Citterio^{93a}, M. Ciubancan^{28b}, A. Clark⁵¹, B.L. Clark⁵⁹, M.R. Clark³⁷, P.J. Clark⁴⁸,
 R.N. Clarke¹⁶, C. Clement^{147a,147b}, Y. Coadou⁸⁷, M. Cobal^{164a,164c}, A. Coccaro⁵¹, J. Cochran⁶⁶,
 L. Coffey²⁵, L. Colasurdo¹⁰⁷, B. Cole³⁷, A.P. Colijn¹⁰⁸, J. Collot⁵⁷, T. Colombo³², G. Compostella¹⁰²,
 P. Conde Muiño^{127a,127b}, E. Coniavitis⁵⁰, S.H. Connell^{146b}, I.A. Connolly⁷⁹, V. Consorti⁵⁰,
 S. Constantinescu^{28b}, G. Conti³², F. Conventi^{105a,k}, M. Cooke¹⁶, B.D. Cooper⁸⁰, A.M. Cooper-Sarkar¹²¹,
 K.J.R. Cormier¹⁵⁹, T. Cornelissen¹⁷⁵, M. Corradi^{133a,133b}, F. Corriveau^{89,l}, A. Corso-Radu¹⁶³,
 A. Cortes-Gonzalez¹³, G. Cortiana¹⁰², G. Costa^{93a}, M.J. Costa¹⁶⁷, D. Costanzo¹⁴⁰, G. Cottin³⁰,
 G. Cowan⁷⁹, B.E. Cox⁸⁶, K. Cranmer¹¹¹, S.J. Crawley⁵⁵, G. Cree³¹, S. Crépé-Renaudin⁵⁷, F. Crescioli⁸²,
 W.A. Cribbs^{147a,147b}, M. Crispin Ortuzar¹²¹, M. Cristinziani²³, V. Croft¹⁰⁷, G. Crosetti^{39a,39b},

T. Cuhadar Donszelmann¹⁴⁰, J. Cummings¹⁷⁶, M. Curatolo⁴⁹, J. Cúth⁸⁵, C. Cuthbert¹⁵¹, H. Czirr¹⁴²,
 P. Czodrowski³, G. D'amen^{22a,22b}, S. D'Auria⁵⁵, M. D'Onofrio⁷⁶,
 M.J. Da Cunha Sargedas De Sousa^{127a,127b}, C. Da Via⁸⁶, W. Dabrowski^{40a}, T. Dado^{145a}, T. Dai⁹¹,
 O. Dale¹⁵, F. Dallaire⁹⁶, C. Dallapiccola⁸⁸, M. Dam³⁸, J.R. Dandoy³³, N.P. Dang⁵⁰, A.C. Daniells¹⁹,
 N.S. Dann⁸⁶, M. Danninger¹⁶⁸, M. Dano Hoffmann¹³⁷, V. Dao⁵⁰, G. Darbo^{52a}, S. Darmora⁸,
 J. Dassoulas³, A. Dattagupta⁶³, W. Davey²³, C. David¹⁶⁹, T. Davidek¹³⁰, M. Davies¹⁵⁴, P. Davison⁸⁰,
 E. Dawe⁹⁰, I. Dawson¹⁴⁰, R.K. Daya-Ishmukhametova⁸⁸, K. De⁸, R. de Asmundis^{105a},
 A. De Benedetti¹¹⁴, S. De Castro^{22a,22b}, S. De Cecco⁸², N. De Groot¹⁰⁷, P. de Jong¹⁰⁸, H. De la Torre⁸⁴,
 F. De Lorenzi⁶⁶, A. De Maria⁵⁶, D. De Pedis^{133a}, A. De Salvo^{133a}, U. De Sanctis¹⁵⁰, A. De Santo¹⁵⁰,
 J.B. De Vivie De Regie¹¹⁸, W.J. Dearnaley⁷⁴, R. Debbe²⁷, C. Debenedetti¹³⁸, D.V. Dedovich⁶⁷,
 N. Dehghanian³, I. Deigaard¹⁰⁸, M. Del Gaudio^{39a,39b}, J. Del Peso⁸⁴, T. Del Prete^{125a,125b},
 D. Delgove¹¹⁸, F. Deliot¹³⁷, C.M. Delitzsch⁵¹, M. Deliyergiyev⁷⁷, A. Dell'Acqua³², L. Dell'Asta²⁴,
 M. Dell'Orso^{125a,125b}, M. Della Pietra^{105a,k}, D. della Volpe⁵¹, M. Delmastro⁵, P.A. Delsart⁵⁷,
 C. Deluca¹⁰⁸, D.A. DeMarco¹⁵⁹, S. Demers¹⁷⁶, M. Demichev⁶⁷, A. Demilly⁸², S.P. Denisov¹³¹,
 D. Denysiuk¹³⁷, D. Derendarz⁴¹, J.E. Derkaoui^{136d}, F. Derue⁸², P. Dervan⁷⁶, K. Desch²³, C. Deterre⁴⁴,
 K. Dette⁴⁵, P.O. Deviveiros³², A. Dewhurst¹³², S. Dhaliwal²⁵, A. Di Ciacio^{134a,134b}, L. Di Ciacio⁵,
 W.K. Di Clemente¹²³, C. Di Donato^{133a,133b}, A. Di Girolamo³², B. Di Girolamo³², B. Di Micco^{135a,135b},
 R. Di Nardo³², A. Di Simone⁵⁰, R. Di Sipio¹⁵⁹, D. Di Valentino³¹, C. Diaconu⁸⁷, M. Diamond¹⁵⁹,
 F.A. Dias⁴⁸, M.A. Diaz^{34a}, E.B. Diehl⁹¹, J. Dietrich¹⁷, S. Diglio⁸⁷, A. Dimitrieva¹⁴, J. Dingfelder²³,
 P. Dita^{28b}, S. Dita^{28b}, F. Dittus³², F. Djama⁸⁷, T. Djobava^{53b}, J.I. Djuvsland^{60a}, M.A.B. do Vale^{26c},
 D. Dobos³², M. Dobre^{28b}, C. Doglioni⁸³, T. Dohmae¹⁵⁶, J. Dolejsi¹³⁰, Z. Dolezal¹³⁰,
 B.A. Dolgoshein^{99,*}, M. Donadelli^{26d}, S. Donati^{125a,125b}, P. Dondero^{122a,122b}, J. Donini³⁶, J. Dopke¹³²,
 A. Doria^{105a}, M.T. Dova⁷³, A.T. Doyle⁵⁵, E. Drechsler⁵⁶, M. Dris¹⁰, Y. Du^{35d}, J. Duarte-Campderros¹⁵⁴,
 E. Duchovni¹⁷², G. Duckeck¹⁰¹, O.A. Ducu^{96,m}, D. Duda¹⁰⁸, A. Dudarev³², L. Duflot¹¹⁸, L. Duguid⁷⁹,
 M. Dührssen³², M. Dumancic¹⁷², M. Dunford^{60a}, H. Duran Yildiz^{4a}, M. Düren⁵⁴, A. Durglishvili^{53b},
 D. Duschinger⁴⁶, B. Dutta⁴⁴, M. Dyndal⁴⁴, C. Eckardt⁴⁴, K.M. Ecker¹⁰², R.C. Edgar⁹¹, N.C. Edwards⁴⁸,
 T. Eifert³², G. Eigen¹⁵, K. Einsweiler¹⁶, T. Ekelof¹⁶⁵, M. El Kacimi^{136c}, V. Ellajosyula⁸⁷, M. Ellert¹⁶⁵,
 S. Elles⁵, F. Ellinghaus¹⁷⁵, A.A. Elliot¹⁶⁹, N. Ellis³², J. Elmsheuser²⁷, M. Elsing³², D. Emeliyanov¹³²,
 Y. Enari¹⁵⁶, O.C. Endner⁸⁵, M. Endo¹¹⁹, J.S. Ennis¹⁷⁰, J. Erdmann⁴⁵, A. Ereditato¹⁸, G. Ernis¹⁷⁵,
 J. Ernst², M. Ernst²⁷, S. Errede¹⁶⁶, E. Ertel⁸⁵, M. Escalier¹¹⁸, H. Esch⁴⁵, C. Escobar¹²⁶, B. Esposito⁴⁹,
 A.I. Etienne¹³⁷, E. Etzion¹⁵⁴, H. Evans⁶³, A. Ezhilov¹²⁴, F. Fabbri^{22a,22b}, L. Fabbri^{22a,22b}, G. Facini³³,
 R.M. Fakhrutdinov¹³¹, S. Falciano^{133a}, R.J. Falla⁸⁰, J. Faltova¹³⁰, Y. Fang^{35a}, M. Fanti^{93a,93b}, A. Farbin⁸,
 A. Farilla^{135a}, C. Farina¹²⁶, T. Farooque¹³, S. Farrell¹⁶, S.M. Farrington¹⁷⁰, P. Farthouat³², F. Fassi^{136e},
 P. Fassnacht³², D. Fassouliotis⁹, M. Fucci Giannelli⁷⁹, A. Favareto^{52a,52b}, W.J. Fawcett¹²¹, L. Fayard¹¹⁸,
 O.L. Fedin^{124,n}, W. Fedorko¹⁶⁸, S. Feigl¹²⁰, L. Feligioni⁸⁷, C. Feng^{35d}, E.J. Feng³², H. Feng⁹¹,
 A.B. Fenyuk¹³¹, L. Feremenga⁸, P. Fernandez Martinez¹⁶⁷, S. Fernandez Perez¹³, J. Ferrando⁵⁵,
 A. Ferrari¹⁶⁵, P. Ferrari¹⁰⁸, R. Ferrari^{122a}, D.E. Ferreira de Lima^{60b}, A. Ferrer¹⁶⁷, D. Ferrere⁵¹,
 C. Ferretti⁹¹, A. Ferretto Parodi^{52a,52b}, F. Fiedler⁸⁵, A. Filipčič⁷⁷, M. Filipuzzi⁴⁴, F. Filthaut¹⁰⁷,
 M. Fincke-Keeler¹⁶⁹, K.D. Finelli¹⁵¹, M.C.N. Fiolhais^{127a,127c}, L. Fiorini¹⁶⁷, A. Firan⁴², A. Fischer²,
 C. Fischer¹³, J. Fischer¹⁷⁵, W.C. Fisher⁹², N. Flaschel⁴⁴, I. Fleck¹⁴², P. Fleischmann⁹¹, G.T. Fletcher¹⁴⁰,
 R.R.M. Fletcher¹²³, T. Flick¹⁷⁵, A. Floderus⁸³, L.R. Flores Castillo^{62a}, M.J. Flowerdew¹⁰²,
 G.T. Forcolin⁸⁶, A. Formica¹³⁷, A. Forti⁸⁶, A.G. Foster¹⁹, D. Fournier¹¹⁸, H. Fox⁷⁴, S. Fracchia¹³,
 P. Francavilla⁸², M. Franchini^{22a,22b}, D. Francis³², L. Franconi¹²⁰, M. Franklin⁵⁹, M. Frate¹⁶³,
 M. Fraternali^{122a,122b}, D. Freeborn⁸⁰, S.M. Fressard-Batraneanu³², F. Friedrich⁴⁶, D. Froidevaux³²,
 J.A. Frost¹²¹, C. Fukunaga¹⁵⁷, E. Fullana Torregrosa⁸⁵, T. Fusayasu¹⁰³, J. Fuster¹⁶⁷, C. Gabaldon⁵⁷,
 O. Gabizon¹⁷⁵, A. Gabrielli^{22a,22b}, A. Gabrielli¹⁶, G.P. Gach^{40a}, S. Gadatsch³², S. Gadomski⁵¹,
 G. Gagliardi^{52a,52b}, L.G. Gagnon⁹⁶, P. Gagnon⁶³, C. Galea¹⁰⁷, B. Galhardo^{127a,127c}, E.J. Gallas¹²¹,

B.J. Gallop¹³², P. Gallus¹²⁹, G. Galster³⁸, K.K. Gan¹¹², J. Gao^{35b,87}, Y. Gao⁴⁸, Y.S. Gao^{144,f},
 F.M. Garay Walls⁴⁸, C. García¹⁶⁷, J.E. García Navarro¹⁶⁷, M. Garcia-Sciveres¹⁶, R.W. Gardner³³,
 N. Garelli¹⁴⁴, V. Garonne¹²⁰, A. Gascon Bravo⁴⁴, C. Gatti⁴⁹, A. Gaudiello^{52a,52b}, G. Gaudio^{122a},
 B. Gaur¹⁴², L. Gauthier⁹⁶, I.L. Gavrilenko⁹⁷, C. Gay¹⁶⁸, G. Gaycken²³, E.N. Gazis¹⁰, Z. Gecse¹⁶⁸,
 C.N.P. Gee¹³², Ch. Geich-Gimbel²³, M.P. Geisler^{60a}, C. Gemme^{52a}, M.H. Genest⁵⁷, C. Geng^{35b,o},
 S. Gentile^{133a,133b}, S. George⁷⁹, D. Gerbaudo¹³, A. Gershon¹⁵⁴, S. Ghasemi¹⁴², H. Ghazlane^{136b},
 M. Ghneimat²³, B. Giacobbe^{22a}, S. Giagu^{133a,133b}, P. Giannetti^{125a,125b}, B. Gibbard²⁷, S.M. Gibson⁷⁹,
 M. Gignac¹⁶⁸, M. Gilchriese¹⁶, T.P.S. Gillam³⁰, D. Gillberg³¹, G. Gilles¹⁷⁵, D.M. Gingrich^{3,d},
 N. Giokaris⁹, M.P. Giordani^{164a,164c}, F.M. Giorgi^{22a}, F.M. Giorgi¹⁷, P.F. Giraud¹³⁷, P. Giromini⁵⁹,
 D. Giugni^{93a}, F. Giuli¹²¹, C. Giuliani¹⁰², M. Giulini^{60b}, B.K. Gjelsten¹²⁰, S. Gkaitatzis¹⁵⁵, I. Gkialas¹⁵⁵,
 E.L. Gkougkousis¹¹⁸, L.K. Gladilin¹⁰⁰, C. Glasman⁸⁴, J. Glatzer³², P.C.F. Glaysher⁴⁸, A. Glazov⁴⁴,
 M. Goblirsch-Kolb¹⁰², J. Godlewski⁴¹, S. Goldfarb⁹¹, T. Golling⁵¹, D. Golubkov¹³¹,
 A. Gomes^{127a,127b,127d}, R. Gonçalo^{127a}, J. Goncalves Pinto Firmino Da Costa¹³⁷, L. Gonella¹⁹,
 A. Gongadze⁶⁷, S. González de la Hoz¹⁶⁷, G. Gonzalez Parra¹³, S. Gonzalez-Sevilla⁵¹, L. Goossens³²,
 P.A. Gorbounov⁹⁸, H.A. Gordon²⁷, I. Gorelov¹⁰⁶, B. Gorini³², E. Gorini^{75a,75b}, A. Gorišek⁷⁷,
 E. Gornicki⁴¹, A.T. Goshaw⁴⁷, C. Gössling⁴⁵, M.I. Gostkin⁶⁷, C.R. Goudet¹¹⁸, D. Goujdami^{136c},
 A.G. Goussiou¹³⁹, N. Govender^{146b,p}, E. Gozani¹⁵³, L. Graber⁵⁶, I. Grabowska-Bold^{40a}, P.O.J. Gradin⁵⁷,
 P. Grafström^{22a,22b}, J. Gramling⁵¹, E. Gramstad¹²⁰, S. Grancagnolo¹⁷, V. Gratchev¹²⁴, H.M. Gray³²,
 E. Graziani^{135a}, Z.D. Greenwood^{81,q}, C. Grefe²³, K. Gregersen⁸⁰, I.M. Gregor⁴⁴, P. Grenier¹⁴⁴,
 K. Grevtsov⁵, J. Griffiths⁸, A.A. Grillo¹³⁸, K. Grimm⁷⁴, S. Grinstein^{13,r}, Ph. Gris³⁶, J.-F. Grivaz¹¹⁸,
 S. Groh⁸⁵, J.P. Grohs⁴⁶, E. Gross¹⁷², J. Grosse-Knetter⁵⁶, G.C. Grossi⁸¹, Z.J. Grout¹⁵⁰, L. Guan⁹¹,
 W. Guan¹⁷³, J. Guenther¹²⁹, F. Guescini⁵¹, D. Guest¹⁶³, O. Gueta¹⁵⁴, E. Guido^{52a,52b}, T. Guillemin⁵,
 S. Guindon², U. Gul⁵⁵, C. Gumpert³², J. Guo^{35e}, Y. Guo^{35b,o}, S. Gupta¹²¹, G. Gustavino^{133a,133b},
 P. Gutierrez¹¹⁴, N.G. Gutierrez Ortiz⁸⁰, C. Gutschow⁴⁶, C. Guyot¹³⁷, C. Gwenlan¹²¹, C.B. Gwilliam⁷⁶,
 A. Haas¹¹¹, C. Haber¹⁶, H.K. Hadavand⁸, N. Haddad^{136e}, A. Hadef⁸⁷, P. Haefner²³, S. Hageböck²³,
 Z. Hajduk⁴¹, H. Hakobyan^{177,*}, M. Haleem⁴⁴, J. Haley¹¹⁵, G. Halladjian⁹², G.D. Hallewell⁸⁷,
 K. Hamacher¹⁷⁵, P. Hamal¹¹⁶, K. Hamano¹⁶⁹, A. Hamilton^{146a}, G.N. Hamity¹⁴⁰, P.G. Hamnett⁴⁴,
 L. Han^{35b}, K. Hanagaki^{68,s}, K. Hanawa¹⁵⁶, M. Hance¹³⁸, B. Haney¹²³, P. Hanke^{60a}, R. Hanna¹³⁷,
 J.B. Hansen³⁸, J.D. Hansen³⁸, M.C. Hansen²³, P.H. Hansen³⁸, K. Hara¹⁶¹, A.S. Hard¹⁷³, T. Harenberg¹⁷⁵,
 F. Hariri¹¹⁸, S. Harkusha⁹⁴, R.D. Harrington⁴⁸, P.F. Harrison¹⁷⁰, F. Hartjes¹⁰⁸, N.M. Hartmann¹⁰¹,
 M. Hasegawa⁶⁹, Y. Hasegawa¹⁴¹, A. Hasib¹¹⁴, S. Hassani¹³⁷, S. Haug¹⁸, R. Hauser⁹², L. Hauswald⁴⁶,
 M. Havranek¹²⁸, C.M. Hawkes¹⁹, R.J. Hawkings³², D. Hayden⁹², C.P. Hays¹²¹, J.M. Hays⁷⁸,
 H.S. Hayward⁷⁶, S.J. Haywood¹³², S.J. Head¹⁹, T. Heck⁸⁵, V. Hedberg⁸³, L. Heelan⁸, S. Heim¹²³,
 T. Heim¹⁶, B. Heinemann¹⁶, J.J. Heinrich¹⁰¹, L. Heinrich¹¹¹, C. Heinz⁵⁴, J. Hejbal¹²⁸, L. Helary²⁴,
 S. Hellman^{147a,147b}, C. Helsens³², J. Henderson¹²¹, R.C.W. Henderson⁷⁴, Y. Heng¹⁷³, S. Henkelmann¹⁶⁸,
 A.M. Henriques Correia³², S. Henrot-Versille¹¹⁸, G.H. Herbert¹⁷, Y. Hernández Jiménez¹⁶⁷, G. Herten⁵⁰,
 R. Hertenberger¹⁰¹, L. Hervas³², G.G. Hesketh⁸⁰, N.P. Hessey¹⁰⁸, J.W. Hetherly⁴², R. Hickling⁷⁸,
 E. Higón-Rodríguez¹⁶⁷, E. Hill¹⁶⁹, J.C. Hill³⁰, K.H. Hiller⁴⁴, S.J. Hillier¹⁹, I. Hincliffe¹⁶, E. Hines¹²³,
 R.R. Hinman¹⁶, M. Hirose¹⁵⁸, D. Hirschbuehl¹⁷⁵, J. Hobbs¹⁴⁹, N. Hod^{160a}, M.C. Hodgkinson¹⁴⁰,
 P. Hodgson¹⁴⁰, A. Hoecker³², M.R. Hoeferkamp¹⁰⁶, F. Hoenig¹⁰¹, M. Hohlfeld⁸⁵, D. Hohn²³,
 T.R. Holmes¹⁶, M. Homann⁴⁵, T.M. Hong¹²⁶, B.H. Hooberman¹⁶⁶, W.H. Hopkins¹¹⁷, Y. Horii¹⁰⁴,
 A.J. Horton¹⁴³, J.-Y. Hostachy⁵⁷, S. Hou¹⁵², A. Hoummada^{136a}, J. Howarth⁴⁴, M. Hrabovsky¹¹⁶,
 I. Hristova¹⁷, J. Hrivnac¹¹⁸, T. Hryna'ova⁵, A. Hrynevich⁹⁵, C. Hsu^{146c}, P.J. Hsu^{152,t}, S.-C. Hsu¹³⁹,
 D. Hu³⁷, Q. Hu^{35b}, Y. Huang⁴⁴, Z. Hubacek¹²⁹, F. Hubaut⁸⁷, F. Huegging²³, T.B. Huffman¹²¹,
 E.W. Hughes³⁷, G. Hughes⁷⁴, M. Huhtinen³², T.A. Hülsing⁸⁵, P. Huo¹⁴⁹, N. Huseynov^{67,b}, J. Huston⁹²,
 J. Huth⁵⁹, G. Iacobucci⁵¹, G. Iakovidis²⁷, I. Ibragimov¹⁴², L. Iconomidou-Fayard¹¹⁸, E. Ideal¹⁷⁶,
 Z. Idrissi^{136e}, P. Iengo³², O. Igonkina^{108,u}, T. Iizawa¹⁷¹, Y. Ikegami⁶⁸, M. Ikeno⁶⁸, Y. Ilchenko^{11,v},

D. Iliadis¹⁵⁵, N. Ilic¹⁴⁴, T. Ince¹⁰², G. Introzzi^{122a,122b}, P. Ioannou^{9,*}, M. Iodice^{135a}, K. Iordanidou³⁷, V. Ippolito⁵⁹, M. Ishino⁷⁰, M. Ishitsuka¹⁵⁸, R. Ishmukhametov¹¹², C. Issever¹²¹, S. Istin^{20a}, F. Ito¹⁶¹, J.M. Iturbe Ponce⁸⁶, R. Iuppa^{134a,134b}, W. Iwanski⁴¹, H. Iwasaki⁶⁸, J.M. Izen⁴³, V. Izzo^{105a}, S. Jabbar³, B. Jackson¹²³, M. Jackson⁷⁶, P. Jackson¹, V. Jain², K.B. Jakobi⁸⁵, K. Jakobs⁵⁰, S. Jakobsen³², T. Jakoubek¹²⁸, D.O. Jamin¹¹⁵, D.K. Jana⁸¹, E. Jansen⁸⁰, R. Jansky⁶⁴, J. Janssen²³, M. Janus⁵⁶, G. Jarlskog⁸³, N. Javadov^{67,b}, T. Javůrek⁵⁰, F. Jeanneau¹³⁷, L. Jeanty¹⁶, J. Jejelava^{53a,w}, G.-Y. Jeng¹⁵¹, D. Jennens⁹⁰, P. Jenni^{50,x}, J. Jentzsch⁴⁵, C. Jeske¹⁷⁰, S. Jézéquel⁵, H. Ji¹⁷³, J. Jia¹⁴⁹, H. Jiang⁶⁶, Y. Jiang^{35b}, S. Jiggins⁸⁰, J. Jimenez Pena¹⁶⁷, S. Jin^{35a}, A. Jinaru^{28b}, O. Jinnouchi¹⁵⁸, P. Johansson¹⁴⁰, K.A. Johns⁷, W.J. Johnson¹³⁹, K. Jon-And^{147a,147b}, G. Jones¹⁷⁰, R.W.L. Jones⁷⁴, S. Jones⁷, T.J. Jones⁷⁶, J. Jongmanns^{60a}, P.M. Jorge^{127a,127b}, J. Jovicevic^{160a}, X. Ju¹⁷³, A. Juste Rozas^{13,r}, M.K. Köhler¹⁷², A. Kaczmarska⁴¹, M. Kado¹¹⁸, H. Kagan¹¹², M. Kagan¹⁴⁴, S.J. Kahn⁸⁷, E. Kajomovitz⁴⁷, C.W. Kalderon¹²¹, A. Kaluza⁸⁵, S. Kama⁴², A. Kamenshchikov¹³¹, N. Kanaya¹⁵⁶, S. Kaneti³⁰, L. Kanjur⁷⁷, V.A. Kantserov⁹⁹, J. Kanzaki⁶⁸, B. Kaplan¹¹¹, L.S. Kaplan¹⁷³, A. Kapliy³³, D. Kar^{146c}, K. Karakostas¹⁰, A. Karamaoun³, N. Karastathis¹⁰, M.J. Kareem⁵⁶, E. Karentzos¹⁰, M. Karnevskiy⁸⁵, S.N. Karpov⁶⁷, Z.M. Karpova⁶⁷, K. Karthik¹¹¹, V. Kartvelishvili⁷⁴, A.N. Karyukhin¹³¹, K. Kasahara¹⁶¹, L. Kashif¹⁷³, R.D. Kass¹¹², A. Kastanas¹⁵, Y. Kataoka¹⁵⁶, C. Kato¹⁵⁶, A. Katre⁵¹, J. Katzy⁴⁴, K. Kawagoe⁷², T. Kawamoto¹⁵⁶, G. Kawamura⁵⁶, S. Kazama¹⁵⁶, V.F. Kazanin^{110,c}, R. Keeler¹⁶⁹, R. Kehoe⁴², J.S. Keller⁴⁴, J.J. Kempster⁷⁹, K. Kentaro¹⁰⁴, H. Keoshkerian¹⁵⁹, O. Kepka¹²⁸, B.P. Kerševan⁷⁷, S. Kersten¹⁷⁵, R.A. Keyes⁸⁹, F. Khalil-zada¹², A. Khanov¹¹⁵, A.G. Kharlamov^{110,c}, T.J. Khoo⁵¹, V. Khovanskiy⁹⁸, E. Khramov⁶⁷, J. Khubua^{53b,y}, S. Kido⁶⁹, H.Y. Kim⁸, S.H. Kim¹⁶¹, Y.K. Kim³³, N. Kimura¹⁵⁵, O.M. Kind¹⁷, B.T. King⁷⁶, M. King¹⁶⁷, S.B. King¹⁶⁸, J. Kirk¹³², A.E. Kiryunin¹⁰², T. Kishimoto⁶⁹, D. Kisielewska^{40a}, F. Kiss⁵⁰, K. Kiuchi¹⁶¹, O. Kivernyk¹³⁷, E. Kladiva^{145b}, M.H. Klein³⁷, M. Klein⁷⁶, U. Klein⁷⁶, K. Kleinknecht⁸⁵, P. Klimek^{147a,147b}, A. Klimentov²⁷, R. Klingenberg⁴⁵, J.A. Klinger¹⁴⁰, T. Klioutchnikova³², E.-E. Kluge^{60a}, P. Kluit¹⁰⁸, S. Kluth¹⁰², J. Knapik⁴¹, E. Knerner⁶⁴, E.B.F.G. Knoops⁸⁷, A. Knue⁵⁵, A. Kobayashi¹⁵⁶, D. Kobayashi¹⁵⁸, T. Kobayashi¹⁵⁶, M. Kobel⁴⁶, M. Kocian¹⁴⁴, P. Kodys¹³⁰, T. Koffeman¹⁰⁸, T. Koi¹⁴⁴, H. Kolanoski¹⁷, M. Kolb^{60b}, I. Koletsou⁵, A.A. Komar^{97,*}, Y. Komori¹⁵⁶, T. Kondo⁶⁸, N. Kondrashova⁴⁴, K. Köneke⁵⁰, A.C. König¹⁰⁷, T. Kono^{68,z}, R. Konoplich^{111,aa}, N. Konstantinidis⁸⁰, R. Kopeliansky⁶³, S. Koperny^{40a}, L. Köpke⁸⁵, A.K. Kopp⁵⁰, K. Korcyl⁴¹, K. Kordas¹⁵⁵, A. Korn⁸⁰, A.A. Korol^{110,c}, I. Korolkov¹³, E.V. Korolkova¹⁴⁰, O. Kortner¹⁰², S. Kortner¹⁰², T. Kosek¹³⁰, V.V. Kostyukhin²³, A. Kotwal⁴⁷, A. Kourkoumeli-Charalampidi¹⁵⁵, C. Kourkoumelis⁹, V. Kouskoura²⁷, A.B. Kowalewska⁴¹, R. Kowalewski¹⁶⁹, T.Z. Kowalski^{40a}, C. Kozakai¹⁵⁶, W. Kozanecki¹³⁷, A.S. Kozhin¹³¹, V.A. Kramarenko¹⁰⁰, G. Kramberger⁷⁷, D. Krasnopervtsev⁹⁹, M.W. Krasny⁸², A. Krasznahorkay³², J.K. Kraus²³, A. Kravchenko²⁷, M. Kretz^{60c}, J. Kretzschmar⁷⁶, K. Kreutzfeldt⁵⁴, P. Krieger¹⁵⁹, K. Krizka³³, K. Kroeninger⁴⁵, H. Kroha¹⁰², J. Kroll¹²³, J. Kroseberg²³, J. Krstic¹⁴, U. Kruchonak⁶⁷, H. Krüger²³, N. Krumnack⁶⁶, A. Kruse¹⁷³, M.C. Kruse⁴⁷, M. Kruskal²⁴, T. Kubota⁹⁰, H. Kucuk⁸⁰, S. Kuday^{4b}, J.T. Kuechler¹⁷⁵, S. Kuehn⁵⁰, A. Kugel^{60c}, F. Kuger¹⁷⁴, A. Kuhl¹³⁸, T. Kuhl⁴⁴, V. Kukhtin⁶⁷, R. Kukla¹³⁷, Y. Kulchitsky⁹⁴, S. Kuleshov^{34b}, M. Kuna^{133a,133b}, T. Kunigo⁷⁰, A. Kupco¹²⁸, H. Kurashige⁶⁹, Y.A. Kurochkin⁹⁴, V. Kus¹²⁸, E.S. Kuwertz¹⁶⁹, M. Kuze¹⁵⁸, J. Kvita¹¹⁶, T. Kwan¹⁶⁹, D. Kyriazopoulos¹⁴⁰, A. La Rosa¹⁰², J.L. La Rosa Navarro^{26d}, L. La Rotonda^{39a,39b}, C. Lacasta¹⁶⁷, F. Lacava^{133a,133b}, J. Lacey³¹, H. Lacker¹⁷, D. Lacour⁸², V.R. Lacuesta¹⁶⁷, E. Ladygin⁶⁷, R. Lafaye⁵, B. Laforge⁸², T. Lagouri¹⁷⁶, S. Lai⁵⁶, S. Lammers⁶³, W. Lampl⁷, E. Lançon¹³⁷, U. Landgraf⁵⁰, M.P.J. Landon⁷⁸, V.S. Lang^{60a}, J.C. Lange¹³, A.J. Lankford¹⁶³, F. Lanni²⁷, K. Lantzsch²³, A. Lanza^{122a}, S. Laplace⁸², C. Lapoire³², J.F. Laporte¹³⁷, T. Lari^{93a}, F. Lasagni Manghi^{22a,22b}, M. Lassnig³², P. Laurelli⁴⁹, W. Lavrijssen¹⁶, A.T. Law¹³⁸, P. Laycock⁷⁶, T. Lazovich⁵⁹, M. Lazzaroni^{93a,93b}, B. Le⁹⁰, O. Le Dortz⁸², E. Le Guiriec⁸⁷, E.P. Le Quilleuc¹³⁷, M. LeBlanc¹⁶⁹, T. LeCompte⁶, F. Ledroit-Guillon⁵⁷, C.A. Lee²⁷, S.C. Lee¹⁵², L. Lee¹, G. Lefebvre⁸², M. Lefebvre¹⁶⁹, F. Legger¹⁰¹,

C. Leggett¹⁶, A. Lehan⁷⁶, G. Lehmann Miotto³², X. Lei⁷, W.A. Leight³¹, A. Leisos^{155,ab},
 A.G. Leister¹⁷⁶, M.A.L. Leite^{26d}, R. Leitner¹³⁰, D. Lellouch¹⁷², B. Lemmer⁵⁶, K.J.C. Leney⁸⁰, T. Lenz²³,
 B. Lenzi³², R. Leone⁷, S. Leone^{125a,125b}, C. Leonidopoulos⁴⁸, S. Leontsinis¹⁰, G. Lerner¹⁵⁰, C. Leroy⁹⁶,
 A.A.J. Lesage¹³⁷, C.G. Lester³⁰, M. Levchenko¹²⁴, J. Levêque⁵, D. Levin⁹¹, L.J. Levinson¹⁷²,
 M. Levy¹⁹, A.M. Leyko²³, M. Leyton⁴³, B. Li^{35b,o}, H. Li¹⁴⁹, H.L. Li³³, L. Li⁴⁷, L. Li^{35e}, Q. Li^{35a},
 S. Li⁴⁷, X. Li⁸⁶, Y. Li¹⁴², Z. Liang^{35a}, B. Liberti^{134a}, A. Liblong¹⁵⁹, P. Lichard³², K. Lie¹⁶⁶, J. Liebal²³,
 W. Liebig¹⁵, A. Limosani¹⁵¹, S.C. Lin^{152,ac}, T.H. Lin⁸⁵, B.E. Lindquist¹⁴⁹, A.E. Lionti⁵¹, E. Lipeles¹²³,
 A. Lipniacka¹⁵, M. Lisovyi^{60b}, T.M. Liss¹⁶⁶, A. Lister¹⁶⁸, A.M. Litke¹³⁸, B. Liu^{152,ad}, D. Liu¹⁵²,
 H. Liu⁹¹, H. Liu²⁷, J. Liu⁸⁷, J.B. Liu^{35b}, K. Liu⁸⁷, L. Liu¹⁶⁶, M. Liu⁴⁷, M. Liu^{35b}, Y.L. Liu^{35b}, Y. Liu^{35b},
 M. Livan^{122a,122b}, A. Lleres⁵⁷, J. Llorente Merino^{35a}, S.L. Lloyd⁷⁸, F. Lo Sterzo¹⁵², E. Lobodzinska⁴⁴,
 P. Loch⁷, W.S. Lockman¹³⁸, F.K. Loebinger⁸⁶, A.E. Loevschall-Jensen³⁸, K.M. Loew²⁵, A. Loginov¹⁷⁶,
 T. Lohse¹⁷, K. Lohwasser⁴⁴, M. Lokajicek¹²⁸, B.A. Long²⁴, J.D. Long¹⁶⁶, R.E. Long⁷⁴, L. Longo^{75a,75b},
 K.A.Looper¹¹², L. Lopes^{127a}, D. Lopez Mateos⁵⁹, B. Lopez Paredes¹⁴⁰, I. Lopez Paz¹³,
 A. Lopez Solis⁸², J. Lorenz¹⁰¹, N. Lorenzo Martinez⁶³, M. Losada²¹, P.J. Lösel¹⁰¹, X. Lou^{35a},
 A. Lounis¹¹⁸, J. Love⁶, P.A. Love⁷⁴, H. Lu^{62a}, N. Lu⁹¹, H.J. Lubatti¹³⁹, C. Luci^{133a,133b}, A. Lucotte⁵⁷,
 C. Luedtke⁵⁰, F. Luehring⁶³, W. Lukas⁶⁴, L. Luminari^{133a}, O. Lundberg^{147a,147b}, B. Lund-Jensen¹⁴⁸,
 D. Lynn²⁷, R. Lysak¹²⁸, E. Lytken⁸³, V. Lyubushkin⁶⁷, H. Ma²⁷, L.L. Ma^{35d}, Y. Ma^{35d}, G. Maccarrone⁴⁹,
 A. Macchiolo¹⁰², C.M. Macdonald¹⁴⁰, B. Maček⁷⁷, J. Machado Miguens^{123,127b}, D. Madaffari⁸⁷,
 R. Madar³⁶, H.J. Maddocks¹⁶⁵, W.F. Mader⁴⁶, A. Madsen⁴⁴, J. Maeda⁶⁹, S. Maeland¹⁵, T. Maeno²⁷,
 A. Maevskiy¹⁰⁰, E. Magradze⁵⁶, J. Mahlstedt¹⁰⁸, C. Maiani¹¹⁸, C. Maidantchik^{26a}, A.A. Maier¹⁰²,
 T. Maier¹⁰¹, A. Maio^{127a,127b,127d}, S. Majewski¹¹⁷, Y. Makida⁶⁸, N. Makovec¹¹⁸, B. Malaescu⁸²,
 Pa. Malecki⁴¹, V.P. Maleev¹²⁴, F. Malek⁵⁷, U. Mallik⁶⁵, D. Malon⁶, C. Malone¹⁴⁴, S. Maltezos¹⁰,
 S. Malyukov³², J. Mamuzic¹⁶⁷, G. Mancini⁴⁹, B. Mandelli³², L. Mandelli^{93a}, I. Mandić⁷⁷,
 J. Maneira^{127a,127b}, L. Manhaes de Andrade Filho^{26b}, J. Manjarres Ramos^{160b}, A. Mann¹⁰¹,
 B. Mansoulie¹³⁷, J.D. Mansour^{35a}, R. Mantifel⁸⁹, M. Mantoani⁵⁶, S. Manzoni^{93a,93b}, L. Mapelli³²,
 G. Marceca²⁹, L. March⁵¹, G. Marchiori⁸², M. Marcisovsky¹²⁸, M. Marjanovic¹⁴, D.E. Marley⁹¹,
 F. Marroquim^{26a}, S.P. Marsden⁸⁶, Z. Marshall¹⁶, S. Marti-Garcia¹⁶⁷, B. Martin⁹², T.A. Martin¹⁷⁰,
 V.J. Martin⁴⁸, B. Martin dit Latour¹⁵, M. Martinez^{13,r}, S. Martin-Haugh¹³², V.S. Martoiu^{28b},
 A.C. Martyniuk⁸⁰, M. Marx¹³⁹, A. Marzin³², L. Masetti⁸⁵, T. Mashimo¹⁵⁶, R. Mashinistov⁹⁷, J. Masik⁸⁶,
 A.L. Maslennikov^{110,c}, I. Massa^{22a,22b}, L. Massa^{22a,22b}, P. Mastrandrea⁵, A. Mastroberardino^{39a,39b},
 T. Masubuchi¹⁵⁶, P. Mättig¹⁷⁵, J. Mattmann⁸⁵, J. Maurer^{28b}, S.J. Maxfield⁷⁶, D.A. Maximov^{110,c},
 R. Mazini¹⁵², S.M. Mazza^{93a,93b}, N.C. Mc Fadden¹⁰⁶, G. Mc Goldrick¹⁵⁹, S.P. Mc Kee⁹¹, A. McCarn⁹¹,
 R.L. McCarthy¹⁴⁹, T.G. McCarthy³¹, L.I. McClymont⁸⁰, E.F. McDonald⁹⁰, K.W. McFarlane^{58,*},
 J.A. McFayden⁸⁰, G. Mchedlidze⁵⁶, S.J. McMahon¹³², R.A. McPherson^{169,l}, M. Medinnis⁴⁴,
 S. Meehan¹³⁹, S. Mehlhase¹⁰¹, A. Mehta⁷⁶, K. Meier^{60a}, C. Meineck¹⁰¹, B. Meirose⁴³, D. Melini¹⁶⁷,
 B.R. Mellado Garcia^{146c}, M. Melo^{145a}, F. Meloni¹⁸, A. Mengarelli^{22a,22b}, S. Menke¹⁰², E. Meoni¹⁶²,
 S. Mergelmeyer¹⁷, P. Mermod⁵¹, L. Merola^{105a,105b}, C. Meroni^{93a}, F.S. Merritt³³, A. Messina^{133a,133b},
 J. Metcalfe⁶, A.S. Mete¹⁶³, C. Meyer⁸⁵, C. Meyer¹²³, J.-P. Meyer¹³⁷, J. Meyer¹⁰⁸,
 H. Meyer Zu Theenhausen^{60a}, F. Miano¹⁵⁰, R.P. Middleton¹³², S. Miglioranzi^{52a,52b}, L. Mijović²³,
 G. Mikenberg¹⁷², M. Mikestikova¹²⁸, M. Mikuž⁷⁷, M. Milesi⁹⁰, A. Milic⁶⁴, D.W. Miller³³, C. Mills⁴⁸,
 A. Milov¹⁷², D.A. Milstead^{147a,147b}, A.A. Minaenko¹³¹, Y. Minami¹⁵⁶, I.A. Minashvili⁶⁷, A.I. Mincer¹¹¹,
 B. Mindur^{40a}, M. Mineev⁶⁷, Y. Ming¹⁷³, L.M. Mir¹³, K.P. Mistry¹²³, T. Mitani¹⁷¹, J. Mitrevski¹⁰¹,
 V.A. Mitsou¹⁶⁷, A. Miucci⁵¹, P.S. Miyagawa¹⁴⁰, J.U. Mjörnmark⁸³, T. Moa^{147a,147b}, K. Mochizuki⁹⁶,
 S. Mohapatra³⁷, S. Molander^{147a,147b}, R. Moles-Valls²³, R. Monden⁷⁰, M.C. Mondragon⁹², K. Möning⁴⁴,
 J. Monk³⁸, E. Monnier⁸⁷, A. Montalbano¹⁴⁹, J. Montejo Berlingen³², F. Monticelli⁷³, S. Monzani^{93a,93b},
 R.W. Moore³, N. Morange¹¹⁸, D. Moreno²¹, M. Moreno Llácer⁵⁶, P. Morettini^{52a}, D. Mori¹⁴³,
 T. Mori¹⁵⁶, M. Morii⁵⁹, M. Morinaga¹⁵⁶, V. Morisbak¹²⁰, S. Moritz⁸⁵, A.K. Morley¹⁵¹, G. Mornacchi³²,

J.D. Morris⁷⁸, S.S. Mortensen³⁸, L. Morvaj¹⁴⁹, M. Mosidze^{53b}, J. Moss¹⁴⁴, K. Motohashi¹⁵⁸,
 R. Mount¹⁴⁴, E. Mountricha²⁷, S.V. Mouraviev^{97,*}, E.J.W. Moyse⁸⁸, S. Muanza⁸⁷, R.D. Mudd¹⁹,
 F. Mueller¹⁰², J. Mueller¹²⁶, R.S.P. Mueller¹⁰¹, T. Mueller³⁰, D. Muenstermann⁷⁴, P. Mullen⁵⁵,
 G.A. Mullier¹⁸, F.J. Munoz Sanchez⁸⁶, J.A. Murillo Quijada¹⁹, W.J. Murray^{170,132}, H. Musheghyan⁵⁶,
 M. Muškinja⁷⁷, A.G. Myagkov^{131,ae}, M. Myska¹²⁹, B.P. Nachman¹⁴⁴, O. Nackenhorst⁵¹, K. Nagai¹²¹,
 R. Nagai^{68,z}, K. Nagano⁶⁸, Y. Nagasaka⁶¹, K. Nagata¹⁶¹, M. Nagel⁵⁰, E. Nagy⁸⁷, A.M. Nairz³²,
 Y. Nakahama³², K. Nakamura⁶⁸, T. Nakamura¹⁵⁶, I. Nakano¹¹³, H. Namasivayam⁴³,
 R.F. Naranjo Garcia⁴⁴, R. Narayan¹¹, D.I. Narrias Villar^{60a}, I. Naryshkin¹²⁴, T. Naumann⁴⁴,
 G. Navarro²¹, R. Nayyar⁷, H.A. Neal⁹¹, P.Yu. Nechaeva⁹⁷, T.J. Neep⁸⁶, P.D. Nef¹⁴⁴, A. Negri^{122a,122b},
 M. Negrini^{22a}, S. Nektarijevic¹⁰⁷, C. Nellist¹¹⁸, A. Nelson¹⁶³, S. Nemecek¹²⁸, P. Nemethy¹¹¹,
 A.A. Nepomuceno^{26a}, M. Nessi^{32,af}, M.S. Neubauer¹⁶⁶, M. Neumann¹⁷⁵, R.M. Neves¹¹¹, P. Nevski²⁷,
 P.R. Newman¹⁹, D.H. Nguyen⁶, T. Nguyen Manh⁹⁶, R.B. Nickerson¹²¹, R. Nicolaïdou¹³⁷, J. Nielsen¹³⁸,
 A. Nikiforov¹⁷, V. Nikolaenko^{131,ae}, I. Nikolic-Audit⁸², K. Nikolopoulos¹⁹, J.K. Nilsen¹²⁰, P. Nilsson²⁷,
 Y. Ninomiya¹⁵⁶, A. Nisati^{133a}, R. Nisius¹⁰², T. Nobe¹⁵⁶, L. Nodulman⁶, M. Nomachi¹¹⁹, I. Nomidis³¹,
 T. Nooney⁷⁸, S. Norberg¹¹⁴, M. Nordberg³², N. Norjoharuddeen¹²¹, O. Novgorodova⁴⁶, S. Nowak¹⁰²,
 M. Nozaki⁶⁸, L. Nozka¹¹⁶, K. Ntekas¹⁰, E. Nurse⁸⁰, F. Nuti⁹⁰, F. O'grady⁷, D.C. O'Neil¹⁴³,
 A.A. O'Rourke⁴⁴, V. O'Shea⁵⁵, F.G. Oakham^{31,d}, H. Oberlack¹⁰², T. Obermann²³, J. Ocariz⁸²,
 A. Ochi⁶⁹, I. Ochoa³⁷, J.P. Ochoa-Ricoux^{34a}, S. Oda⁷², S. Odaka⁶⁸, H. Ogren⁶³, A. Oh⁸⁶, S.H. Oh⁴⁷,
 C.C. Ohm¹⁶, H. Ohman¹⁶⁵, H. Oide³², H. Okawa¹⁶¹, Y. Okumura³³, T. Okuyama⁶⁸, A. Olariu^{28b},
 L.F. Oleiro Seabra^{127a}, S.A. Olivares Pino⁴⁸, D. Oliveira Damazio²⁷, A. Olszewski⁴¹, J. Olszowska⁴¹,
 A. Onofre^{127a,127e}, K. Onogi¹⁰⁴, P.U.E. Onyisi^{11,v}, M.J. Oreglia³³, Y. Oren¹⁵⁴, D. Orestano^{135a,135b},
 N. Orlando^{62b}, R.S. Orr¹⁵⁹, B. Osculati^{52a,52b}, R. Ospanov⁸⁶, G. Otero y Garzon²⁹, H. Otono⁷²,
 M. Ouchrif^{136d}, F. Ould-Saada¹²⁰, A. Ouraou¹³⁷, K.P. Oussoren¹⁰⁸, Q. Ouyang^{35a}, M. Owen⁵⁵,
 R.E. Owen¹⁹, V.E. Ozcan^{20a}, N. Ozturk⁸, K. Pachal¹⁴³, A. Pacheco Pages¹³, C. Padilla Aranda¹³,
 M. Pagáčová⁵⁰, S. Pagan Griso¹⁶, F. Paige²⁷, P. Pais⁸⁸, K. Pajchel¹²⁰, G. Palacino^{160b}, S. Palestini³²,
 M. Palka^{40b}, D. Pallin³⁶, A. Palma^{127a,127b}, E.St. Panagiotopoulou¹⁰, C.E. Pandini⁸²,
 J.G. Panduro Vazquez⁷⁹, P. Pani^{147a,147b}, S. Panitkin²⁷, D. Pantea^{28b}, L. Paolozzi⁵¹,
 Th.D. Papadopoulou¹⁰, K. Papageorgiou¹⁵⁵, A. Paramonov⁶, D. Paredes Hernandez¹⁷⁶, A.J. Parker⁷⁴,
 M.A. Parker³⁰, K.A. Parker¹⁴⁰, F. Parodi^{52a,52b}, J.A. Parsons³⁷, U. Parzefall⁵⁰, V.R. Pascuzzi¹⁵⁹,
 E. Pasqualucci^{133a}, S. Passaggio^{52a}, F. Pastore^{135a,135b,*}, Fr. Pastore⁷⁹, G. Pásztor^{31,ag}, S. Pataraia¹⁷⁵,
 J.R. Pater⁸⁶, T. Pauly³², J. Pearce¹⁶⁹, B. Pearson¹¹⁴, L.E. Pedersen³⁸, M. Pedersen¹²⁰,
 S. Pedraza Lopez¹⁶⁷, R. Pedro^{127a,127b}, S.V. Peleganchuk^{110,c}, D. Pelikan¹⁶⁵, O. Penc¹²⁸, C. Peng^{35a},
 H. Peng^{35b}, J. Penwell⁶³, B.S. Peralva^{26b}, M.M. Perego¹³⁷, D.V. Perepelitsa²⁷, E. Perez Codina^{160a},
 L. Perini^{93a,93b}, H. Pernegger³², S. Perrella^{105a,105b}, R. Peschke⁴⁴, V.D. Peshekhanov⁶⁷, K. Peters⁴⁴,
 R.F.Y. Peters⁸⁶, B.A. Petersen³², T.C. Petersen³⁸, E. Petit⁵⁷, A. Petridis¹, C. Petridou¹⁵⁵, P. Petroff¹¹⁸,
 E. Petrolo^{133a}, M. Petrov¹²¹, F. Petrucci^{135a,135b}, N.E. Pettersson⁸⁸, A. Peyaud¹³⁷, R. Pezoa^{34b},
 P.W. Phillips¹³², G. Piacquadio¹⁴⁴, E. Pianori¹⁷⁰, A. Picazio⁸⁸, E. Piccaro⁷⁸, M. Piccinini^{22a,22b},
 M.A. Pickering¹²¹, R. Piegala²⁹, J.E. Pilcher³³, A.D. Pilkinson⁸⁶, A.W.J. Pin⁸⁶,
 M. Pinamonti^{164a,164c,ah}, J.L. Pinfold³, A. Pingel³⁸, S. Pires⁸², H. Pirumov⁴⁴, M. Pitt¹⁷², L. Plazak^{145a},
 M.-A. Pleier²⁷, V. Pleskot⁸⁵, E. Plotnikova⁶⁷, P. Plucinski⁹², D. Pluth⁶⁶, R. Poettgen^{147a,147b},
 L. Poggioli¹¹⁸, D. Pohl²³, G. Polesello^{122a}, A. Poley⁴⁴, A. Pollicchio^{39a,39b}, R. Polifka¹⁵⁹, A. Polini^{22a},
 C.S. Pollard⁵⁵, V. Polychronakos²⁷, K. Pommès³², L. Pontecorvo^{133a}, B.G. Pope⁹², G.A. Popeneciu^{28c},
 D.S. Popovic¹⁴, A. Poppleton³², S. Pospisil¹²⁹, K. Potamianos¹⁶, I.N. Potrap⁶⁷, C.J. Potter³⁰,
 C.T. Potter¹¹⁷, G. Poulard³², J. Poveda³², V. Pozdnyakov⁶⁷, M.E. Pozo Astigarraga³², P. Pralavorio⁸⁷,
 A. Pranko¹⁶, S. Prell⁶⁶, D. Price⁸⁶, L.E. Price⁶, M. Primavera^{75a}, S. Prince⁸⁹, M. Proissl⁴⁸,
 K. Prokofiev^{62c}, F. Prokoshin^{34b}, S. Protopopescu²⁷, J. Proudfoot⁶, M. Przybycien^{40a}, D. Puddu^{135a,135b},
 D. Puldon¹⁴⁹, M. Purohit^{27,ai}, P. Puzo¹¹⁸, J. Qian⁹¹, G. Qin⁵⁵, Y. Qin⁸⁶, A. Quadt⁵⁶,

W.B. Quayle^{164a,164b}, M. Queitsch-Maitland⁸⁶, D. Quilty⁵⁵, S. Raddum¹²⁰, V. Radeka²⁷, V. Radescu^{60b}, S.K. Radhakrishnan¹⁴⁹, P. Radloff¹¹⁷, P. Rados⁹⁰, F. Ragusa^{93a,93b}, G. Rahal¹⁷⁸, J.A. Raine⁸⁶, S. Rajagopalan²⁷, M. Rammensee³², C. Rangel-Smith¹⁶⁵, M.G. Ratti^{93a,93b}, F. Rauscher¹⁰¹, S. Rave⁸⁵, T. Ravenscroft⁵⁵, I. Ravinovich¹⁷², M. Raymond³², A.L. Read¹²⁰, N.P. Readioff⁷⁶, M. Reale^{75a,75b}, D.M. Rebuzzi^{122a,122b}, A. Redelbach¹⁷⁴, G. Redlinger²⁷, R. Reece¹³⁸, K. Reeves⁴³, L. Rehnisch¹⁷, J. Reichert¹²³, H. Reisin²⁹, C. Rembser³², H. Ren^{35a}, M. Rescigno^{133a}, S. Resconi^{93a}, O.L. Rezanova^{110,c}, P. Reznicek¹³⁰, R. Rezvani⁹⁶, R. Richter¹⁰², S. Richter⁸⁰, E. Richter-Was^{40b}, O. Ricken²³, M. Ridel⁸², P. Rieck¹⁷, C.J. Riegel¹⁷⁵, J. Rieger⁵⁶, O. Rifki¹¹⁴, M. Rijssenbeek¹⁴⁹, A. Rimoldi^{122a,122b}, M. Rimoldi¹⁸, L. Rinaldi^{22a}, B. Ristić⁵¹, E. Ritsch³², I. Riu¹³, F. Rizatdinova¹¹⁵, E. Rizvi⁷⁸, C. Rizzi¹³, S.H. Robertson^{89,l}, A. Robichaud-Veronneau⁸⁹, D. Robinson³⁰, J.E.M. Robinson⁴⁴, A. Robson⁵⁵, C. Roda^{125a,125b}, Y. Rodina⁸⁷, A. Rodriguez Perez¹³, D. Rodriguez Rodriguez¹⁶⁷, S. Roe³², C.S. Rogan⁵⁹, O. Røhne¹²⁰, A. Romaniouk⁹⁹, M. Romano^{22a,22b}, S.M. Romano Saez³⁶, E. Romero Adam¹⁶⁷, N. Rompotis¹³⁹, M. Ronzani⁵⁰, L. Roos⁸², E. Ros¹⁶⁷, S. Rosati^{133a}, K. Rosbach⁵⁰, P. Rose¹³⁸, O. Rosenthal¹⁴², N.-A. Rosien⁵⁶, V. Rossetti^{147a,147b}, E. Rossi^{105a,105b}, L.P. Rossi^{52a}, J.H.N. Rosten³⁰, R. Rosten¹³⁹, M. Rotaru^{28b}, I. Roth¹⁷², J. Rothberg¹³⁹, D. Rousseau¹¹⁸, C.R. Royon¹³⁷, A. Rozanov⁸⁷, Y. Rozen¹⁵³, X. Ruan^{146c}, F. Rubbo¹⁴⁴, M.S. Rudolph¹⁵⁹, F. Rühr⁵⁰, A. Ruiz-Martinez³¹, Z. Rurikova⁵⁰, N.A. Rusakovich⁶⁷, A. Ruschke¹⁰¹, H.L. Russell¹³⁹, J.P. Rutherford⁷, N. Ruthmann³², Y.F. Ryabov¹²⁴, M. Rybar¹⁶⁶, G. Rybkin¹¹⁸, S. Ryu⁶, A. Ryzhov¹³¹, G.F. Rzehorz⁵⁶, A.F. Saavedra¹⁵¹, G. Sabato¹⁰⁸, S. Sacerdoti²⁹, H.F-W. Sadrozinski¹³⁸, R. Sadykov⁶⁷, F. Safai Tehrani^{133a}, P. Saha¹⁰⁹, M. Sahinsoy^{60a}, M. Saimpert¹³⁷, T. Saito¹⁵⁶, H. Sakamoto¹⁵⁶, Y. Sakurai¹⁷¹, G. Salamanna^{135a,135b}, A. Salamon^{134a,134b}, J.E. Salazar Loyola^{34b}, D. Salek¹⁰⁸, P.H. Sales De Bruin¹³⁹, D. Salihagic¹⁰², A. Salnikov¹⁴⁴, J. Salt¹⁶⁷, D. Salvatore^{39a,39b}, F. Salvatore¹⁵⁰, A. Salvucci^{62a}, A. Salzburger³², D. Sammel⁵⁰, D. Sampsonidis¹⁵⁵, A. Sanchez^{105a,105b}, J. Sánchez¹⁶⁷, V. Sanchez Martinez¹⁶⁷, H. Sandaker¹²⁰, R.L. Sandbach⁷⁸, H.G. Sander⁸⁵, M. Sandhoff¹⁷⁵, C. Sandoval²¹, R. Sandstroem¹⁰², D.P.C. Sankey¹³², M. Sannino^{52a,52b}, A. Sansoni⁴⁹, C. Santoni³⁶, R. Santonico^{134a,134b}, H. Santos^{127a}, I. Santoyo Castillo¹⁵⁰, K. Sapp¹²⁶, A. Sapronov⁶⁷, J.G. Saraiva^{127a,127d}, B. Sarrazin²³, O. Sasaki⁶⁸, Y. Sasaki¹⁵⁶, K. Sato¹⁶¹, G. Sauvage^{5,*}, E. Sauvan⁵, G. Savage⁷⁹, P. Savard^{159,d}, C. Sawyer¹³², L. Sawyer^{81,q}, J. Saxon³³, C. Sbarra^{22a}, A. Sbrizzi^{22a,22b}, T. Scanlon⁸⁰, D.A. Scannicchio¹⁶³, M. Scarcella¹⁵¹, V. Scarfone^{39a,39b}, J. Schaarschmidt¹⁷², P. Schacht¹⁰², B.M. Schachtner¹⁰¹, D. Schaefer³², R. Schaefer⁴⁴, J. Schaeffer⁸⁵, S. Schaepe²³, S. Schaetzl^{60b}, U. Schäfer⁸⁵, A.C. Schaffer¹¹⁸, D. Schaile¹⁰¹, R.D. Schamberger¹⁴⁹, V. Scharf^{60a}, V.A. Schegelsky¹²⁴, D. Scheirich¹³⁰, M. Schernau¹⁶³, C. Schiavi^{52a,52b}, S. Schier¹³⁸, C. Schillo⁵⁰, M. Schioppa^{39a,39b}, S. Schlenker³², K. Schmieden³², C. Schmitt⁸⁵, S. Schmitt⁴⁴, S. Schmitz⁸⁵, B. Schneider^{160a}, U. Schnoor⁵⁰, L. Schoeffel¹³⁷, A. Schoening^{60b}, B.D. Schoenrock⁹², E. Schopf²³, M. Schott⁸⁵, J. Schovancova⁸, S. Schramm⁵¹, M. Schreyer¹⁷⁴, N. Schuh⁸⁵, M.J. Schultens²³, H.-C. Schultz-Coulon^{60a}, H. Schulz¹⁷, M. Schumacher⁵⁰, B.A. Schumm¹³⁸, Ph. Schune¹³⁷, A. Schwartzman¹⁴⁴, T.A. Schwarz⁹¹, Ph. Schwegler¹⁰², H. Schweiger⁸⁶, Ph. Schwemling¹³⁷, R. Schwienhorst⁹², J. Schwindling¹³⁷, T. Schwindt²³, G. Sciolla²⁵, F. Scuri^{125a,125b}, F. Scutti⁹⁰, J. Searcy⁹¹, P. Seema²³, S.C. Seidel¹⁰⁶, A. Seiden¹³⁸, F. Seifert¹²⁹, J.M. Seixas^{26a}, G. Sekhniaidze^{105a}, K. Sekhon⁹¹, S.J. Sekula⁴², D.M. Seliverstov^{124,*}, N. Semprini-Cesari^{22a,22b}, C. Serfon¹²⁰, L. Serin¹¹⁸, L. Serkin^{164a,164b}, M. Sessa^{135a,135b}, R. Seuster¹⁶⁹, H. Severini¹¹⁴, T. Sfiligoj⁷⁷, F. Sforza³², A. Sfyrla⁵¹, E. Shabalina⁵⁶, N.W. Shaikh^{147a,147b}, L.Y. Shan^{35a}, R. Shang¹⁶⁶, J.T. Shank²⁴, M. Shapiro¹⁶, P.B. Shatalov⁹⁸, K. Shaw^{164a,164b}, S.M. Shaw⁸⁶, A. Shcherbakova^{147a,147b}, C.Y. Shehu¹⁵⁰, P. Sherwood⁸⁰, L. Shi^{152,aj}, S. Shimizu⁶⁹, C.O. Shimmin¹⁶³, M. Shimojima¹⁰³, M. Shiyakova^{67,ak}, A. Shmeleva⁹⁷, D. Shoaleh Saadi⁹⁶, M.J. Shochet³³, S. Shojaei^{93a,93b}, S. Shrestha¹¹², E. Shulga⁹⁹, M.A. Shupe⁷, P. Sicho¹²⁸, P.E. Sidebo¹⁴⁸, O. Sidiropoulou¹⁷⁴, D. Sidorov¹¹⁵, A. Sidoti^{22a,22b}, F. Siegert⁴⁶, Dj. Sijacki¹⁴, J. Silva^{127a,127d}, S.B. Silverstein^{147a}, V. Simak¹²⁹, O. Simard⁵, Lj. Simic¹⁴, S. Simion¹¹⁸, E. Simioni⁸⁵,

B. Simmons⁸⁰, D. Simon³⁶, M. Simon⁸⁵, P. Sinervo¹⁵⁹, N.B. Sinev¹¹⁷, M. Sioli^{22a,22b}, G. Siragusa¹⁷⁴, S.Yu. Sivoklokov¹⁰⁰, J. Sjölin^{147a,147b}, T.B. Sjursen¹⁵, M.B. Skinner⁷⁴, H.P. Skottowe⁵⁹, P. Skubic¹¹⁴, M. Slater¹⁹, T. Slavicek¹²⁹, M. Slawinska¹⁰⁸, K. Sliwa¹⁶², R. Slovak¹³⁰, V. Smakhtin¹⁷², B.H. Smart⁵, L. Smestad¹⁵, J. Smiesko^{145a}, S.Yu. Smirnov⁹⁹, Y. Smirnov⁹⁹, L.N. Smirnova^{100,al}, O. Smirnova⁸³, M.N.K. Smith³⁷, R.W. Smith³⁷, M. Smizanska⁷⁴, K. Smolek¹²⁹, A.A. Snesarev⁹⁷, S. Snyder²⁷, R. Sobie^{169,l}, F. Socher⁴⁶, A. Soffer¹⁵⁴, D.A. Soh¹⁵², G. Sokhrannyi⁷⁷, C.A. Solans Sanchez³², M. Solar¹²⁹, E.Yu. Soldatov⁹⁹, U. Soldevila¹⁶⁷, A.A. Solodkov¹³¹, A. Soloshenko⁶⁷, O.V. Solovyanov¹³¹, V. Solovyev¹²⁴, P. Sommer⁵⁰, H. Son¹⁶², H.Y. Song^{35b,am}, A. Sood¹⁶, A. Sopczak¹²⁹, V. Sopko¹²⁹, V. Sorin¹³, D. Sosa^{60b}, C.L. Sotiropoulou^{125a,125b}, R. Soualah^{164a,164c}, A.M. Soukharev^{110,c}, D. South⁴⁴, B.C. Sowden⁷⁹, S. Spagnolo^{75a,75b}, M. Spalla^{125a,125b}, M. Spangenberg¹⁷⁰, F. Spanò⁷⁹, D. Sperlich¹⁷, F. Spettel¹⁰², R. Spighi^{22a}, G. Spigo³², L.A. Spiller⁹⁰, M. Spousta¹³⁰, R.D. St. Denis^{55,*}, A. Stabile^{93a}, R. Stamen^{60a}, S. Stamm¹⁷, E. Stanecka⁴¹, R.W. Stanek⁶, C. Stanescu^{135a}, M. Stanescu-Bellu⁴⁴, M.M. Stanitzki⁴⁴, S. Stapnes¹²⁰, E.A. Starchenko¹³¹, G.H. Stark³³, J. Stark⁵⁷, P. Staroba¹²⁸, P. Starovoitov^{60a}, S. Stärz³², R. Staszewski⁴¹, P. Steinberg²⁷, B. Stelzer¹⁴³, H.J. Stelzer³², O. Stelzer-Chilton^{160a}, H. Stenzel⁵⁴, G.A. Stewart⁵⁵, J.A. Stillings²³, M.C. Stockton⁸⁹, M. Stoebe⁸⁹, G. Stoica^{28b}, P. Stolte⁵⁶, S. Stonjek¹⁰², A.R. Stradling⁸, A. Straessner⁴⁶, M.E. Stramaglia¹⁸, J. Strandberg¹⁴⁸, S. Strandberg^{147a,147b}, A. Strandlie¹²⁰, M. Strauss¹¹⁴, P. Strizenec^{145b}, R. Ströhmer¹⁷⁴, D.M. Strom¹¹⁷, R. Stroynowski⁴², A. Strubig¹⁰⁷, S.A. Stucci¹⁸, B. Stugu¹⁵, N.A. Styles⁴⁴, D. Su¹⁴⁴, J. Su¹²⁶, R. Subramaniam⁸¹, S. Suchek^{60a}, Y. Sugaya¹¹⁹, M. Suk¹²⁹, V.V. Sulin⁹⁷, S. Sultan soy^{4c}, T. Sumida⁷⁰, S. Sun⁵⁹, X. Sun^{35a}, J.E. Sundermann⁵⁰, K. Suruliz¹⁵⁰, G. Susinno^{39a,39b}, M.R. Sutton¹⁵⁰, S. Suzuki⁶⁸, M. Svatos¹²⁸, M. Swiatlowski³³, I. Sykora^{145a}, T. Sykora¹³⁰, D. Ta⁵⁰, C. Taccini^{135a,135b}, K. Tackmann⁴⁴, J. Taenzer¹⁵⁹, A. Taffard¹⁶³, R. Tafirout^{160a}, N. Taiblum¹⁵⁴, H. Takai²⁷, R. Takashima⁷¹, T. Takeshita¹⁴¹, Y. Takubo⁶⁸, M. Talby⁸⁷, A.A. Talyshев^{110,c}, K.G. Tan⁹⁰, J. Tanaka¹⁵⁶, R. Tanaka¹¹⁸, S. Tanaka⁶⁸, B.B. Tannenwald¹¹², S. Tapia Araya^{34b}, S. Tapprogge⁸⁵, S. Tarem¹⁵³, G.F. Tartarelli^{93a}, P. Tas¹³⁰, M. Tasevsky¹²⁸, T. Tashiro⁷⁰, E. Tassi^{39a,39b}, A. Tavares Delgado^{127a,127b}, Y. Tayalati^{136d}, A.C. Taylor¹⁰⁶, G.N. Taylor⁹⁰, P.T.E. Taylor⁹⁰, W. Taylor^{160b}, F.A. Teischinger³², P. Teixeira-Dias⁷⁹, K.K. Temming⁵⁰, D. Temple¹⁴³, H. Ten Kate³², P.K. Teng¹⁵², J.J. Teoh¹¹⁹, F. Tepel¹⁷⁵, S. Terada⁶⁸, K. Terashi¹⁵⁶, J. Terron⁸⁴, S. Terzo¹⁰², M. Testa⁴⁹, R.J. Teuscher^{159,l}, T. Theveneaux-Pelzer⁸⁷, J.P. Thomas¹⁹, J. Thomas-Wilske⁷⁹, E.N. Thompson³⁷, P.D. Thompson¹⁹, A.S. Thompson⁵⁵, L.A. Thomsen¹⁷⁶, E. Thomson¹²³, M. Thomson³⁰, M.J. Tibbetts¹⁶, R.E. Ticse Torres⁸⁷, V.O. Tikhomirov^{97,an}, Yu.A. Tikhonov^{110,c}, S. Timoshenko⁹⁹, P. Tipton¹⁷⁶, S. Tisserant⁸⁷, K. Todome¹⁵⁸, T. Todorov^{5,*}, S. Todorova-Nova¹³⁰, J. Tojo⁷², S. Tokár^{145a}, K. Tokushuku⁶⁸, E. Tolley⁵⁹, L. Tomlinson⁸⁶, M. Tomoto¹⁰⁴, L. Tompkins^{144,ao}, K. Toms¹⁰⁶, B. Tong⁵⁹, E. Torrence¹¹⁷, H. Torres¹⁴³, E. Torró Pastor¹³⁹, J. Toth^{87,ap}, F. Touchard⁸⁷, D.R. Tovey¹⁴⁰, T. Trefzger¹⁷⁴, A. Tricolí²⁷, I.M. Trigger^{160a}, S. Trincaz-Duvold⁸², M.F. Tripiana¹³, W. Trischuk¹⁵⁹, B. Trocmé⁵⁷, A. Trofymov⁴⁴, C. Troncon^{93a}, M. Trottier-McDonald¹⁶, M. Trovatelli¹⁶⁹, L. Truong^{164a,164c}, M. Trzebinski⁴¹, A. Trzupek⁴¹, J.C.-L. Tseng¹²¹, P.V. Tsiareshka⁹⁴, G. Tsipolitis¹⁰, N. Tsirintanis⁹, S. Tsiskaridze¹³, V. Tsiskaridze⁵⁰, E.G. Tskhadadze^{53a}, K.M. Tsui^{62a}, I.I. Tsukerman⁹⁸, V. Tsulaia¹⁶, S. Tsuno⁶⁸, D. Tsybychev¹⁴⁹, A. Tudorache^{28b}, V. Tudorache^{28b}, A.N. Tuna⁵⁹, S.A. Tupputi^{22a,22b}, S. Turchikhin^{100,al}, D. Turecek¹²⁹, D. Turgeman¹⁷², R. Turra^{93a,93b}, A.J. Turvey⁴², P.M. Tuts³⁷, M. Tyndel¹³², G. Ucchielli^{22a,22b}, I. Ueda¹⁵⁶, R. Ueno³¹, M. Ughetto^{147a,147b}, F. Ukegawa¹⁶¹, G. Unal³², A. Undrus²⁷, G. Unel¹⁶³, F.C. Ungaro⁹⁰, Y. Unno⁶⁸, C. Unverdorben¹⁰¹, J. Urban^{145b}, P. Urquijo⁹⁰, P. Urrejola⁸⁵, G. Usai⁸, A. Usanova⁶⁴, L. Vacavant⁸⁷, V. Vacek¹²⁹, B. Vachon⁸⁹, C. Valderanis¹⁰¹, E. Valdes Santurio^{147a,147b}, N. Valencic¹⁰⁸, S. Valentinetto^{22a,22b}, A. Valero¹⁶⁷, L. Valery¹³, S. Valkar¹³⁰, S. Vallecorsa⁵¹, J.A. Valls Ferrer¹⁶⁷, W. Van Den Wollenberg¹⁰⁸, P.C. Van Der Deijl¹⁰⁸, R. van der Geer¹⁰⁸, H. van der Graaf¹⁰⁸, N. van Eldik¹⁵³, P. van Gemmeren⁶, J. Van Nieuwkoop¹⁴³, I. van Vulpen¹⁰⁸, M.C. van Woerden³², M. Vanadia^{133a,133b}, W. Vandelli³²,

R. Vanguri¹²³, A. Vaniachine⁶, P. Vankov¹⁰⁸, G. Vardanyan¹⁷⁷, R. Vari^{133a}, E.W. Varnes⁷, T. Varol⁴², D. Varouchas⁸², A. Vartapetian⁸, K.E. Varvell¹⁵¹, J.G. Vasquez¹⁷⁶, F. Vazeille³⁶, T. Vazquez Schroeder⁸⁹, J. Veatch⁵⁶, L.M. Veloce¹⁵⁹, F. Veloso^{127a,127c}, S. Veneziano^{133a}, A. Ventura^{75a,75b}, M. Venturi¹⁶⁹, N. Venturi¹⁵⁹, A. Venturini²⁵, V. Vercesi^{122a}, M. Verducci^{133a,133b}, W. Verkerke¹⁰⁸, J.C. Vermeulen¹⁰⁸, A. Vest^{46,aq}, M.C. Vetterli^{143,d}, O. Viazlo⁸³, I. Vichou¹⁶⁶, T. Vickey¹⁴⁰, O.E. Vickey Boeriu¹⁴⁰, G.H.A. Viehhauser¹²¹, S. Viel¹⁶, L. Vigani¹²¹, R. Vigne⁶⁴, M. Villa^{22a,22b}, M. Villaplana Perez^{93a,93b}, E. Vilucchi⁴⁹, M.G. Vincter³¹, V.B. Vinogradov⁶⁷, C. Vittori^{22a,22b}, I. Vivarelli¹⁵⁰, S. Vlachos¹⁰, M. Vlasak¹²⁹, M. Vogel¹⁷⁵, P. Vokac¹²⁹, G. Volpi^{125a,125b}, M. Volpi⁹⁰, H. von der Schmitt¹⁰², E. von Toerne²³, V. Vorobel¹³⁰, K. Vorobev⁹⁹, M. Vos¹⁶⁷, R. Voss³², J.H. Vossebeld⁷⁶, N. Vranjes¹⁴, M. Vranjes Milosavljevic¹⁴, V. Vrba¹²⁸, M. Vreeswijk¹⁰⁸, R. Vuillermet³², I. Vukotic³³, Z. Vykydal¹²⁹, P. Wagner²³, W. Wagner¹⁷⁵, H. Wahlberg⁷³, S. Wahrmund⁴⁶, J. Wakabayashi¹⁰⁴, J. Walder⁷⁴, R. Walker¹⁰¹, W. Walkowiak¹⁴², V. Wallangen^{147a,147b}, C. Wang^{35c}, C. Wang^{35d,87}, F. Wang¹⁷³, H. Wang¹⁶, H. Wang⁴², J. Wang⁴⁴, J. Wang¹⁵¹, K. Wang⁸⁹, R. Wang⁶, S.M. Wang¹⁵², T. Wang²³, T. Wang³⁷, X. Wang¹⁷⁶, C. Wanotayaroj¹¹⁷, A. Warburton⁸⁹, C.P. Ward³⁰, D.R. Wardrope⁸⁰, A. Washbrook⁴⁸, P.M. Watkins¹⁹, A.T. Watson¹⁹, M.F. Watson¹⁹, G. Watts¹³⁹, S. Watts⁸⁶, B.M. Waugh⁸⁰, S. Webb⁸⁵, M.S. Weber¹⁸, S.W. Weber¹⁷⁴, J.S. Webster⁶, A.R. Weidberg¹²¹, B. Weinert⁶³, J. Weingarten⁵⁶, C. Weiser⁵⁰, H. Weits¹⁰⁸, P.S. Wells³², T. Wenaus²⁷, T. Wengler³², S. Wenig³², N. Wermes²³, M. Werner⁵⁰, P. Werner³², M. Wessels^{60a}, J. Wetter¹⁶², K. Whalen¹¹⁷, N.L. Whallon¹³⁹, A.M. Wharton⁷⁴, A. White⁸, M.J. White¹, R. White^{34b}, D. Whiteson¹⁶³, F.J. Wickens¹³², W. Wiedenmann¹⁷³, M. Wielers¹³², P. Wienemann²³, C. Wiglesworth³⁸, L.A.M. Wiik-Fuchs²³, A. Wildauer¹⁰², F. Wilk⁸⁶, H.G. Wilkens³², H.H. Williams¹²³, S. Williams¹⁰⁸, C. Willis⁹², S. Willocq⁸⁸, J.A. Wilson¹⁹, I. Wingerter-Seez⁵, F. Winkelmeier¹¹⁷, O.J. Winston¹⁵⁰, B.T. Winter²³, M. Wittgen¹⁴⁴, J. Wittkowski¹⁰¹, S.J. Wollstadt⁸⁵, M.W. Wolter⁴¹, H. Wolters^{127a,127c}, B.K. Wosiek⁴¹, J. Wotschack³², M.J. Woudstra⁸⁶, K.W. Wozniak⁴¹, M. Wu⁵⁷, M. Wu³³, S.L. Wu¹⁷³, X. Wu⁵¹, Y. Wu⁹¹, T.R. Wyatt⁸⁶, B.M. Wynne⁴⁸, S. Xella³⁸, D. Xu^{35a}, L. Xu²⁷, B. Yabsley¹⁵¹, S. Yacoob^{146a}, R. Yakabe⁶⁹, D. Yamaguchi¹⁵⁸, Y. Yamaguchi¹¹⁹, A. Yamamoto⁶⁸, S. Yamamoto¹⁵⁶, T. Yamanaka¹⁵⁶, K. Yamauchi¹⁰⁴, Y. Yamazaki⁶⁹, Z. Yan²⁴, H. Yang^{35e}, H. Yang¹⁷³, Y. Yang¹⁵², Z. Yang¹⁵, W-M. Yao¹⁶, Y.C. Yap⁸², Y. Yasu⁶⁸, E. Yatsenko⁵, K.H. Yau Wong²³, J. Ye⁴², S. Ye²⁷, I. Yeletskikh⁶⁷, A.L. Yen⁵⁹, E. Yildirim⁸⁵, K. Yorita¹⁷¹, R. Yoshida⁶, K. Yoshihara¹²³, C. Young¹⁴⁴, C.J.S. Young³², S. Youssef²⁴, D.R. Yu¹⁶, J. Yu⁸, J.M. Yu⁹¹, J. Yu⁶⁶, L. Yuan⁶⁹, S.P.Y. Yuen²³, I. Yusuff^{30,ar}, B. Zabinski⁴¹, R. Zaidan^{35d}, A.M. Zaitsev^{131,ae}, N. Zakharchuk⁴⁴, J. Zalieckas¹⁵, A. Zaman¹⁴⁹, S. Zambito⁵⁹, L. Zanello^{133a,133b}, D. Zanzi⁹⁰, C. Zeitnitz¹⁷⁵, M. Zeman¹²⁹, A. Zemla^{40a}, J.C. Zeng¹⁶⁶, Q. Zeng¹⁴⁴, K. Zengel²⁵, O. Zenin¹³¹, T. Ženiš^{145a}, D. Zerwas¹¹⁸, D. Zhang⁹¹, F. Zhang¹⁷³, G. Zhang^{35b,am}, H. Zhang^{35c}, J. Zhang⁶, L. Zhang⁵⁰, R. Zhang²³, R. Zhang^{35b,as}, X. Zhang^{35d}, Z. Zhang¹¹⁸, X. Zhao⁴², Y. Zhao^{35d}, Z. Zhao^{35b}, A. Zhemchugov⁶⁷, J. Zhong¹²¹, B. Zhou⁹¹, C. Zhou⁴⁷, L. Zhou³⁷, L. Zhou⁴², M. Zhou¹⁴⁹, N. Zhou^{35f}, C.G. Zhu^{35d}, H. Zhu^{35a}, J. Zhu⁹¹, Y. Zhu^{35b}, X. Zhuang^{35a}, K. Zhukov⁹⁷, A. Zibell¹⁷⁴, D. Ziemińska⁶³, N.I. Zimine⁶⁷, C. Zimmermann⁸⁵, S. Zimmermann⁵⁰, Z. Zinonos⁵⁶, M. Zinser⁸⁵, M. Ziolkowski¹⁴², L. Živković¹⁴, G. Zobernig¹⁷³, A. Zoccoli^{22a,22b}, M. zur Nedden¹⁷, G. Zurzolo^{105a,105b}, L. Zwalinski³².

¹ Department of Physics, University of Adelaide, Adelaide, Australia

² Physics Department, SUNY Albany, Albany NY, United States of America

³ Department of Physics, University of Alberta, Edmonton AB, Canada

⁴ ^(a) Department of Physics, Ankara University, Ankara; ^(b) Istanbul Aydin University, Istanbul; ^(c)

Division of Physics, TOBB University of Economics and Technology, Ankara, Turkey

⁵ LAPP, CNRS/IN2P3 and Université Savoie Mont Blanc, Annecy-le-Vieux, France

⁶ High Energy Physics Division, Argonne National Laboratory, Argonne IL, United States of America

- ⁷ Department of Physics, University of Arizona, Tucson AZ, United States of America
⁸ Department of Physics, The University of Texas at Arlington, Arlington TX, United States of America
⁹ Physics Department, University of Athens, Athens, Greece
¹⁰ Physics Department, National Technical University of Athens, Zografou, Greece
¹¹ Department of Physics, The University of Texas at Austin, Austin TX, United States of America
¹² Institute of Physics, Azerbaijan Academy of Sciences, Baku, Azerbaijan
¹³ Institut de Física d'Altes Energies (IFAE), The Barcelona Institute of Science and Technology, Barcelona, Spain, Spain
¹⁴ Institute of Physics, University of Belgrade, Belgrade, Serbia
¹⁵ Department for Physics and Technology, University of Bergen, Bergen, Norway
¹⁶ Physics Division, Lawrence Berkeley National Laboratory and University of California, Berkeley CA, United States of America
¹⁷ Department of Physics, Humboldt University, Berlin, Germany
¹⁸ Albert Einstein Center for Fundamental Physics and Laboratory for High Energy Physics, University of Bern, Bern, Switzerland
¹⁹ School of Physics and Astronomy, University of Birmingham, Birmingham, United Kingdom
²⁰ ^(a) Department of Physics, Bogazici University, Istanbul; ^(b) Department of Physics Engineering, Gaziantep University, Gaziantep; ^(d) Istanbul Bilgi University, Faculty of Engineering and Natural Sciences, Istanbul, Turkey; ^(e) Bahcesehir University, Faculty of Engineering and Natural Sciences, Istanbul, Turkey, Turkey
²¹ Centro de Investigaciones, Universidad Antonio Narino, Bogota, Colombia
²² ^(a) INFN Sezione di Bologna; ^(b) Dipartimento di Fisica e Astronomia, Università di Bologna, Bologna, Italy
²³ Physikalisches Institut, University of Bonn, Bonn, Germany
²⁴ Department of Physics, Boston University, Boston MA, United States of America
²⁵ Department of Physics, Brandeis University, Waltham MA, United States of America
²⁶ ^(a) Universidade Federal do Rio De Janeiro COPPE/EE/IF, Rio de Janeiro; ^(b) Electrical Circuits Department, Federal University of Juiz de Fora (UFJF), Juiz de Fora; ^(c) Federal University of Sao Joao del Rei (UFSJ), Sao Joao del Rei; ^(d) Instituto de Fisica, Universidade de Sao Paulo, Sao Paulo, Brazil
²⁷ Physics Department, Brookhaven National Laboratory, Upton NY, United States of America
²⁸ ^(a) Transilvania University of Brasov, Brasov, Romania; ^(b) National Institute of Physics and Nuclear Engineering, Bucharest; ^(c) National Institute for Research and Development of Isotopic and Molecular Technologies, Physics Department, Cluj Napoca; ^(d) University Politehnica Bucharest, Bucharest; ^(e) West University in Timisoara, Timisoara, Romania
²⁹ Departamento de Física, Universidad de Buenos Aires, Buenos Aires, Argentina
³⁰ Cavendish Laboratory, University of Cambridge, Cambridge, United Kingdom
³¹ Department of Physics, Carleton University, Ottawa ON, Canada
³² CERN, Geneva, Switzerland
³³ Enrico Fermi Institute, University of Chicago, Chicago IL, United States of America
³⁴ ^(a) Departamento de Física, Pontificia Universidad Católica de Chile, Santiago; ^(b) Departamento de Física, Universidad Técnica Federico Santa María, Valparaíso, Chile
³⁵ ^(a) Institute of High Energy Physics, Chinese Academy of Sciences, Beijing; ^(b) Department of Modern Physics, University of Science and Technology of China, Anhui; ^(c) Department of Physics, Nanjing University, Jiangsu; ^(d) School of Physics, Shandong University, Shandong; ^(e) Department of Physics and Astronomy, Shanghai Key Laboratory for Particle Physics and Cosmology, Shanghai Jiao Tong University, Shanghai; (also affiliated with PKU-CHEP); ^(f) Physics Department, Tsinghua University, Beijing 100084, China

- ³⁶ Laboratoire de Physique Corpusculaire, Clermont Université and Université Blaise Pascal and CNRS/IN2P3, Clermont-Ferrand, France
- ³⁷ Nevis Laboratory, Columbia University, Irvington NY, United States of America
- ³⁸ Niels Bohr Institute, University of Copenhagen, Kobenhavn, Denmark
- ³⁹ ^(a) INFN Gruppo Collegato di Cosenza, Laboratori Nazionali di Frascati; ^(b) Dipartimento di Fisica, Università della Calabria, Rende, Italy
- ⁴⁰ ^(a) AGH University of Science and Technology, Faculty of Physics and Applied Computer Science, Krakow; ^(b) Marian Smoluchowski Institute of Physics, Jagiellonian University, Krakow, Poland
- ⁴¹ Institute of Nuclear Physics Polish Academy of Sciences, Krakow, Poland
- ⁴² Physics Department, Southern Methodist University, Dallas TX, United States of America
- ⁴³ Physics Department, University of Texas at Dallas, Richardson TX, United States of America
- ⁴⁴ DESY, Hamburg and Zeuthen, Germany
- ⁴⁵ Institut für Experimentelle Physik IV, Technische Universität Dortmund, Dortmund, Germany
- ⁴⁶ Institut für Kern- und Teilchenphysik, Technische Universität Dresden, Dresden, Germany
- ⁴⁷ Department of Physics, Duke University, Durham NC, United States of America
- ⁴⁸ SUPA - School of Physics and Astronomy, University of Edinburgh, Edinburgh, United Kingdom
- ⁴⁹ INFN Laboratori Nazionali di Frascati, Frascati, Italy
- ⁵⁰ Fakultät für Mathematik und Physik, Albert-Ludwigs-Universität, Freiburg, Germany
- ⁵¹ Section de Physique, Université de Genève, Geneva, Switzerland
- ⁵² ^(a) INFN Sezione di Genova; ^(b) Dipartimento di Fisica, Università di Genova, Genova, Italy
- ⁵³ ^(a) E. Andronikashvili Institute of Physics, Iv. Javakhishvili Tbilisi State University, Tbilisi; ^(b) High Energy Physics Institute, Tbilisi State University, Tbilisi, Georgia
- ⁵⁴ II Physikalisches Institut, Justus-Liebig-Universität Giessen, Giessen, Germany
- ⁵⁵ SUPA - School of Physics and Astronomy, University of Glasgow, Glasgow, United Kingdom
- ⁵⁶ II Physikalisches Institut, Georg-August-Universität, Göttingen, Germany
- ⁵⁷ Laboratoire de Physique Subatomique et de Cosmologie, Université Grenoble-Alpes, CNRS/IN2P3, Grenoble, France
- ⁵⁸ Department of Physics, Hampton University, Hampton VA, United States of America
- ⁵⁹ Laboratory for Particle Physics and Cosmology, Harvard University, Cambridge MA, United States of America
- ⁶⁰ ^(a) Kirchhoff-Institut für Physik, Ruprecht-Karls-Universität Heidelberg, Heidelberg; ^(b) Physikalisches Institut, Ruprecht-Karls-Universität Heidelberg, Heidelberg; ^(c) ZITI Institut für technische Informatik, Ruprecht-Karls-Universität Heidelberg, Mannheim, Germany
- ⁶¹ Faculty of Applied Information Science, Hiroshima Institute of Technology, Hiroshima, Japan
- ⁶² ^(a) Department of Physics, The Chinese University of Hong Kong, Shatin, N.T., Hong Kong; ^(b) Department of Physics, The University of Hong Kong, Hong Kong; ^(c) Department of Physics, The Hong Kong University of Science and Technology, Clear Water Bay, Kowloon, Hong Kong, China
- ⁶³ Department of Physics, Indiana University, Bloomington IN, United States of America
- ⁶⁴ Institut für Astro- und Teilchenphysik, Leopold-Franzens-Universität, Innsbruck, Austria
- ⁶⁵ University of Iowa, Iowa City IA, United States of America
- ⁶⁶ Department of Physics and Astronomy, Iowa State University, Ames IA, United States of America
- ⁶⁷ Joint Institute for Nuclear Research, JINR Dubna, Dubna, Russia
- ⁶⁸ KEK, High Energy Accelerator Research Organization, Tsukuba, Japan
- ⁶⁹ Graduate School of Science, Kobe University, Kobe, Japan
- ⁷⁰ Faculty of Science, Kyoto University, Kyoto, Japan
- ⁷¹ Kyoto University of Education, Kyoto, Japan
- ⁷² Department of Physics, Kyushu University, Fukuoka, Japan

- ⁷³ Instituto de Física La Plata, Universidad Nacional de La Plata and CONICET, La Plata, Argentina
⁷⁴ Physics Department, Lancaster University, Lancaster, United Kingdom
⁷⁵ ^(a) INFN Sezione di Lecce; ^(b) Dipartimento di Matematica e Fisica, Università del Salento, Lecce, Italy
⁷⁶ Oliver Lodge Laboratory, University of Liverpool, Liverpool, United Kingdom
⁷⁷ Department of Physics, Jožef Stefan Institute and University of Ljubljana, Ljubljana, Slovenia
⁷⁸ School of Physics and Astronomy, Queen Mary University of London, London, United Kingdom
⁷⁹ Department of Physics, Royal Holloway University of London, Surrey, United Kingdom
⁸⁰ Department of Physics and Astronomy, University College London, London, United Kingdom
⁸¹ Louisiana Tech University, Ruston LA, United States of America
⁸² Laboratoire de Physique Nucléaire et de Hautes Energies, UPMC and Université Paris-Diderot and CNRS/IN2P3, Paris, France
⁸³ Fysiska institutionen, Lunds universitet, Lund, Sweden
⁸⁴ Departamento de Fisica Teorica C-15, Universidad Autonoma de Madrid, Madrid, Spain
⁸⁵ Institut für Physik, Universität Mainz, Mainz, Germany
⁸⁶ School of Physics and Astronomy, University of Manchester, Manchester, United Kingdom
⁸⁷ CPPM, Aix-Marseille Université and CNRS/IN2P3, Marseille, France
⁸⁸ Department of Physics, University of Massachusetts, Amherst MA, United States of America
⁸⁹ Department of Physics, McGill University, Montreal QC, Canada
⁹⁰ School of Physics, University of Melbourne, Victoria, Australia
⁹¹ Department of Physics, The University of Michigan, Ann Arbor MI, United States of America
⁹² Department of Physics and Astronomy, Michigan State University, East Lansing MI, United States of America
⁹³ ^(a) INFN Sezione di Milano; ^(b) Dipartimento di Fisica, Università di Milano, Milano, Italy
⁹⁴ B.I. Stepanov Institute of Physics, National Academy of Sciences of Belarus, Minsk, Republic of Belarus
⁹⁵ National Scientific and Educational Centre for Particle and High Energy Physics, Minsk, Republic of Belarus
⁹⁶ Group of Particle Physics, University of Montreal, Montreal QC, Canada
⁹⁷ P.N. Lebedev Physical Institute of the Russian Academy of Sciences, Moscow, Russia
⁹⁸ Institute for Theoretical and Experimental Physics (ITEP), Moscow, Russia
⁹⁹ National Research Nuclear University MEPhI, Moscow, Russia
¹⁰⁰ D.V. Skobeltsyn Institute of Nuclear Physics, M.V. Lomonosov Moscow State University, Moscow, Russia
¹⁰¹ Fakultät für Physik, Ludwig-Maximilians-Universität München, München, Germany
¹⁰² Max-Planck-Institut für Physik (Werner-Heisenberg-Institut), München, Germany
¹⁰³ Nagasaki Institute of Applied Science, Nagasaki, Japan
¹⁰⁴ Graduate School of Science and Kobayashi-Maskawa Institute, Nagoya University, Nagoya, Japan
¹⁰⁵ ^(a) INFN Sezione di Napoli; ^(b) Dipartimento di Fisica, Università di Napoli, Napoli, Italy
¹⁰⁶ Department of Physics and Astronomy, University of New Mexico, Albuquerque NM, United States of America
¹⁰⁷ Institute for Mathematics, Astrophysics and Particle Physics, Radboud University Nijmegen/Nikhef, Nijmegen, Netherlands
¹⁰⁸ Nikhef National Institute for Subatomic Physics and University of Amsterdam, Amsterdam, Netherlands
¹⁰⁹ Department of Physics, Northern Illinois University, DeKalb IL, United States of America
¹¹⁰ Budker Institute of Nuclear Physics, SB RAS, Novosibirsk, Russia

- ¹¹¹ Department of Physics, New York University, New York NY, United States of America
¹¹² Ohio State University, Columbus OH, United States of America
¹¹³ Faculty of Science, Okayama University, Okayama, Japan
¹¹⁴ Homer L. Dodge Department of Physics and Astronomy, University of Oklahoma, Norman OK, United States of America
¹¹⁵ Department of Physics, Oklahoma State University, Stillwater OK, United States of America
¹¹⁶ Palacký University, RCPTM, Olomouc, Czech Republic
¹¹⁷ Center for High Energy Physics, University of Oregon, Eugene OR, United States of America
¹¹⁸ LAL, Univ. Paris-Sud, CNRS/IN2P3, Université Paris-Saclay, Orsay, France
¹¹⁹ Graduate School of Science, Osaka University, Osaka, Japan
¹²⁰ Department of Physics, University of Oslo, Oslo, Norway
¹²¹ Department of Physics, Oxford University, Oxford, United Kingdom
¹²² ^(a) INFN Sezione di Pavia; ^(b) Dipartimento di Fisica, Università di Pavia, Pavia, Italy
¹²³ Department of Physics, University of Pennsylvania, Philadelphia PA, United States of America
¹²⁴ National Research Centre "Kurchatov Institute" B.P.Konstantinov Petersburg Nuclear Physics Institute, St. Petersburg, Russia
¹²⁵ ^(a) INFN Sezione di Pisa; ^(b) Dipartimento di Fisica E. Fermi, Università di Pisa, Pisa, Italy
¹²⁶ Department of Physics and Astronomy, University of Pittsburgh, Pittsburgh PA, United States of America
¹²⁷ ^(a) Laboratório de Instrumentação e Física Experimental de Partículas - LIP, Lisboa; ^(b) Faculdade de Ciências, Universidade de Lisboa, Lisboa; ^(c) Department of Physics, University of Coimbra, Coimbra; ^(d) Centro de Física Nuclear da Universidade de Lisboa, Lisboa; ^(e) Departamento de Física, Universidade do Minho, Braga; ^(f) Departamento de Física Teórica y del Cosmos and CAFPE, Universidad de Granada, Granada (Spain); ^(g) Dep Física and CEFITEC of Faculdade de Ciencias e Tecnologia, Universidade Nova de Lisboa, Caparica, Portugal
¹²⁸ Institute of Physics, Academy of Sciences of the Czech Republic, Praha, Czech Republic
¹²⁹ Czech Technical University in Prague, Praha, Czech Republic
¹³⁰ Faculty of Mathematics and Physics, Charles University in Prague, Praha, Czech Republic
¹³¹ State Research Center Institute for High Energy Physics (Protvino), NRC KI, Russia
¹³² Particle Physics Department, Rutherford Appleton Laboratory, Didcot, United Kingdom
¹³³ ^(a) INFN Sezione di Roma; ^(b) Dipartimento di Fisica, Sapienza Università di Roma, Roma, Italy
¹³⁴ ^(a) INFN Sezione di Roma Tor Vergata; ^(b) Dipartimento di Fisica, Università di Roma Tor Vergata, Roma, Italy
¹³⁵ ^(a) INFN Sezione di Roma Tre; ^(b) Dipartimento di Matematica e Fisica, Università Roma Tre, Roma, Italy
¹³⁶ ^(a) Faculté des Sciences Ain Chock, Réseau Universitaire de Physique des Hautes Energies - Université Hassan II, Casablanca; ^(b) Centre National de l'Energie des Sciences Techniques Nucléaires, Rabat; ^(c) Faculté des Sciences Semlalia, Université Cadi Ayyad, LPHEA-Marrakech; ^(d) Faculté des Sciences, Université Mohamed Premier and LPTPM, Oujda; ^(e) Faculté des sciences, Université Mohammed V, Rabat, Morocco
¹³⁷ DSM/IRFU (Institut de Recherches sur les Lois Fondamentales de l'Univers), CEA Saclay (Commissariat à l'Energie Atomique et aux Energies Alternatives), Gif-sur-Yvette, France
¹³⁸ Santa Cruz Institute for Particle Physics, University of California Santa Cruz, Santa Cruz CA, United States of America
¹³⁹ Department of Physics, University of Washington, Seattle WA, United States of America
¹⁴⁰ Department of Physics and Astronomy, University of Sheffield, Sheffield, United Kingdom
¹⁴¹ Department of Physics, Shinshu University, Nagano, Japan

- ¹⁴² Fachbereich Physik, Universität Siegen, Siegen, Germany
- ¹⁴³ Department of Physics, Simon Fraser University, Burnaby BC, Canada
- ¹⁴⁴ SLAC National Accelerator Laboratory, Stanford CA, United States of America
- ¹⁴⁵ ^(a) Faculty of Mathematics, Physics & Informatics, Comenius University, Bratislava; ^(b) Department of Subnuclear Physics, Institute of Experimental Physics of the Slovak Academy of Sciences, Kosice, Slovak Republic
- ¹⁴⁶ ^(a) Department of Physics, University of Cape Town, Cape Town; ^(b) Department of Physics, University of Johannesburg, Johannesburg; ^(c) School of Physics, University of the Witwatersrand, Johannesburg, South Africa
- ¹⁴⁷ ^(a) Department of Physics, Stockholm University; ^(b) The Oskar Klein Centre, Stockholm, Sweden
- ¹⁴⁸ Physics Department, Royal Institute of Technology, Stockholm, Sweden
- ¹⁴⁹ Departments of Physics & Astronomy and Chemistry, Stony Brook University, Stony Brook NY, United States of America
- ¹⁵⁰ Department of Physics and Astronomy, University of Sussex, Brighton, United Kingdom
- ¹⁵¹ School of Physics, University of Sydney, Sydney, Australia
- ¹⁵² Institute of Physics, Academia Sinica, Taipei, Taiwan
- ¹⁵³ Department of Physics, Technion: Israel Institute of Technology, Haifa, Israel
- ¹⁵⁴ Raymond and Beverly Sackler School of Physics and Astronomy, Tel Aviv University, Tel Aviv, Israel
- ¹⁵⁵ Department of Physics, Aristotle University of Thessaloniki, Thessaloniki, Greece
- ¹⁵⁶ International Center for Elementary Particle Physics and Department of Physics, The University of Tokyo, Tokyo, Japan
- ¹⁵⁷ Graduate School of Science and Technology, Tokyo Metropolitan University, Tokyo, Japan
- ¹⁵⁸ Department of Physics, Tokyo Institute of Technology, Tokyo, Japan
- ¹⁵⁹ Department of Physics, University of Toronto, Toronto ON, Canada
- ¹⁶⁰ ^(a) TRIUMF, Vancouver BC; ^(b) Department of Physics and Astronomy, York University, Toronto ON, Canada
- ¹⁶¹ Faculty of Pure and Applied Sciences, and Center for Integrated Research in Fundamental Science and Engineering, University of Tsukuba, Tsukuba, Japan
- ¹⁶² Department of Physics and Astronomy, Tufts University, Medford MA, United States of America
- ¹⁶³ Department of Physics and Astronomy, University of California Irvine, Irvine CA, United States of America
- ¹⁶⁴ ^(a) INFN Gruppo Collegato di Udine, Sezione di Trieste, Udine; ^(b) ICTP, Trieste; ^(c) Dipartimento di Chimica, Fisica e Ambiente, Università di Udine, Udine, Italy
- ¹⁶⁵ Department of Physics and Astronomy, University of Uppsala, Uppsala, Sweden
- ¹⁶⁶ Department of Physics, University of Illinois, Urbana IL, United States of America
- ¹⁶⁷ Instituto de Física Corpuscular (IFIC) and Departamento de Física Atomica, Molecular y Nuclear and Departamento de Ingeniería Electrónica and Instituto de Microelectrónica de Barcelona (IMB-CNM), University of Valencia and CSIC, Valencia, Spain
- ¹⁶⁸ Department of Physics, University of British Columbia, Vancouver BC, Canada
- ¹⁶⁹ Department of Physics and Astronomy, University of Victoria, Victoria BC, Canada
- ¹⁷⁰ Department of Physics, University of Warwick, Coventry, United Kingdom
- ¹⁷¹ Waseda University, Tokyo, Japan
- ¹⁷² Department of Particle Physics, The Weizmann Institute of Science, Rehovot, Israel
- ¹⁷³ Department of Physics, University of Wisconsin, Madison WI, United States of America
- ¹⁷⁴ Fakultät für Physik und Astronomie, Julius-Maximilians-Universität, Würzburg, Germany
- ¹⁷⁵ Fakultät für Mathematik und Naturwissenschaften, Fachgruppe Physik, Bergische Universität

Wuppertal, Wuppertal, Germany

¹⁷⁶ Department of Physics, Yale University, New Haven CT, United States of America

¹⁷⁷ Yerevan Physics Institute, Yerevan, Armenia

¹⁷⁸ Centre de Calcul de l’Institut National de Physique Nucléaire et de Physique des Particules (IN2P3), Villeurbanne, France

^a Also at Department of Physics, King’s College London, London, United Kingdom

^b Also at Institute of Physics, Azerbaijan Academy of Sciences, Baku, Azerbaijan

^c Also at Novosibirsk State University, Novosibirsk, Russia

^d Also at TRIUMF, Vancouver BC, Canada

^e Also at Department of Physics & Astronomy, University of Louisville, Louisville, KY, United States of America

^f Also at Department of Physics, California State University, Fresno CA, United States of America

^g Also at Department of Physics, University of Fribourg, Fribourg, Switzerland

^h Also at Departament de Fisica de la Universitat Autonoma de Barcelona, Barcelona, Spain

ⁱ Also at Departamento de Fisica e Astronomia, Faculdade de Ciencias, Universidade do Porto, Portugal

^j Also at Tomsk State University, Tomsk, Russia

^k Also at Universita di Napoli Parthenope, Napoli, Italy

^l Also at Institute of Particle Physics (IPP), Canada

^m Also at National Institute of Physics and Nuclear Engineering, Bucharest, Romania

ⁿ Also at Department of Physics, St. Petersburg State Polytechnical University, St. Petersburg, Russia

^o Also at Department of Physics, The University of Michigan, Ann Arbor MI, United States of America

^p Also at Centre for High Performance Computing, CSIR Campus, Rosebank, Cape Town, South Africa

^q Also at Louisiana Tech University, Ruston LA, United States of America

^r Also at Institutio Catalana de Recerca i Estudis Avancats, ICREA, Barcelona, Spain

^s Also at Graduate School of Science, Osaka University, Osaka, Japan

^t Also at Department of Physics, National Tsing Hua University, Taiwan

^u Also at Institute for Mathematics, Astrophysics and Particle Physics, Radboud University Nijmegen/Nikhef, Nijmegen, Netherlands

^v Also at Department of Physics, The University of Texas at Austin, Austin TX, United States of America

^w Also at Institute of Theoretical Physics, Ilia State University, Tbilisi, Georgia

^x Also at CERN, Geneva, Switzerland

^y Also at Georgian Technical University (GTU),Tbilisi, Georgia

^z Also at Ochadai Academic Production, Ochanomizu University, Tokyo, Japan

^{aa} Also at Manhattan College, New York NY, United States of America

^{ab} Also at Hellenic Open University, Patras, Greece

^{ac} Also at Academia Sinica Grid Computing, Institute of Physics, Academia Sinica, Taipei, Taiwan

^{ad} Also at School of Physics, Shandong University, Shandong, China

^{ae} Also at Moscow Institute of Physics and Technology State University, Dolgoprudny, Russia

^{af} Also at Section de Physique, Université de Genève, Geneva, Switzerland

^{ag} Also at Eotvos Lorand University, Budapest, Hungary

^{ah} Also at International School for Advanced Studies (SISSA), Trieste, Italy

^{ai} Also at Department of Physics and Astronomy, University of South Carolina, Columbia SC, United States of America

^{aj} Also at School of Physics and Engineering, Sun Yat-sen University, Guangzhou, China

^{ak} Also at Institute for Nuclear Research and Nuclear Energy (INRNE) of the Bulgarian Academy of Sciences, Sofia, Bulgaria

^{al} Also at Faculty of Physics, M.V.Lomonosov Moscow State University, Moscow, Russia

am Also at Institute of Physics, Academia Sinica, Taipei, Taiwan

an Also at National Research Nuclear University MEPhI, Moscow, Russia

ao Also at Department of Physics, Stanford University, Stanford CA, United States of America

ap Also at Institute for Particle and Nuclear Physics, Wigner Research Centre for Physics, Budapest, Hungary

aq Also at Flensburg University of Applied Sciences, Flensburg, Germany

ar Also at University of Malaya, Department of Physics, Kuala Lumpur, Malaysia

as Also at CPPM, Aix-Marseille Université and CNRS/IN2P3, Marseille, France

* Deceased